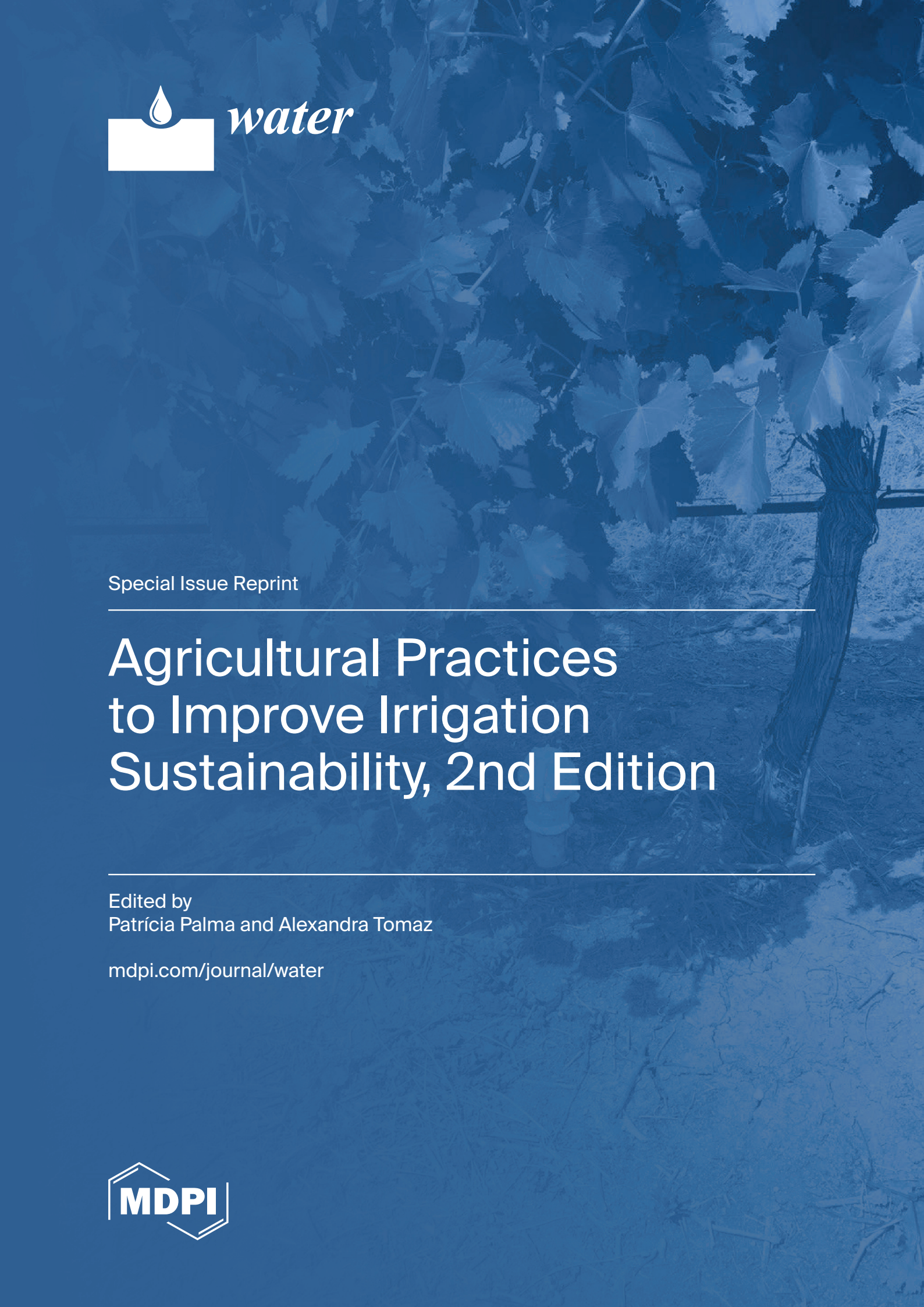


water

Special Issue Reprint

Agricultural Practices to Improve Irrigation Sustainability, 2nd Edition

Edited by
Patrícia Palma and Alexandra Tomaz

mdpi.com/journal/water

MDPI

Agricultural Practices to Improve Irrigation Sustainability, 2nd Edition

Agricultural Practices to Improve Irrigation Sustainability, 2nd Edition

Guest Editors

Patrícia Palma
Alexandra Tomaz

MDPI

Basel • Beijing • Wuhan • Barcelona • Belgrade • Novi Sad • Cluj • Manchester

Guest Editors

Patrícia Palma
Center for Sci-Tech Research in Earth System and Energy (CREATE)
Polytechnic Institute of Beja
Beja
Portugal

Alexandra Tomaz
Center for Sci-Tech Research in Earth System and Energy (CREATE)
Polytechnic Institute of Beja
Beja
Portugal

Editorial Office
MDPI AG
Grosspeteranlage 5
4052 Basel, Switzerland

This is a reprint of the Special Issue, published open access by the journal *Water* (ISSN 2073-4441), freely accessible at: https://www.mdpi.com/journal/water/special_issues/6SO3ZK81ZW.

For citation purposes, cite each article independently as indicated on the article page online and as indicated below:

Lastname, A.A.; Lastname, B.B. Article Title. *Journal Name* **Year**, *Volume Number*, Page Range.

ISBN 978-3-7258-7370-8 (Hbk)
ISBN 978-3-7258-7371-5 (PDF)
https://doi.org/10.3390/books978-3-7258-7371-5

Cover image courtesy of Alexandra Telo da Costa Trincalhetas Tomaz

© 2026 by the authors. Articles in this reprint are Open Access and distributed under the Creative Commons Attribution (CC BY) license. The reprint as a whole is distributed by MDPI under the terms and conditions of the Creative Commons Attribution-NonCommercial-NoDerivs (CC BY-NC-ND) license (https://creativecommons.org/licenses/by-nc-nd/4.0/).

Contents

About the Editors . . . . . **vii**

Patrícia Palma and Alexandra Tomaz
Agricultural Practices to Improve Irrigation Sustainability, 2nd Edition
Reprinted from: *Water* **2026**, *18*, 333, https://doi.org/10.3390/w18030333 . . . . . **1**

Simone Pietro Garofalo, Francesca Ardito, Nicola Sanitate, Gabriele De Carolis, Sergio Ruggieri, Vincenzo Giannico, et al.
Robustness of Actual Evapotranspiration Predicted by Random Forest Model Integrating Remote Sensing and Meteorological Information: Case of Watermelon (*Citrullus lanatus*, (Thunb.) Matsum. & Nakai, 1916)
Reprinted from: *Water* **2025**, *17*, 323, https://doi.org/10.3390/w17030323 . . . . . **5**

Zhijie Shan, Junwei Chen, Xiping Zhang, Zhuanyun Si, Ruochen Yi and Haiyan Fan
Optimizing Irrigation and Nitrogen Application for Greenhouse Tomato Using the DSSAT–CROPGRO–Tomato Model
Reprinted from: *Water* **2025**, *17*, 426, https://doi.org/10.3390/w17030426 . . . . . **23**

Simone Pietro Garofalo, Anna Francesca Modugno, Gabriele de Carolis and Pasquale Campi
Energy of Sorghum Biomass Under Deficit Irrigation Strategies in the Mediterranean Area
Reprinted from: *Water* **2025**, *17*, 578, https://doi.org/10.3390/w17040578 . . . . . **39**

Michael Scobie, David Freebairn, Shahbaz Mushtaq and Darrell Donahue
How Much Is Enough? Data Requirements for Practical Irrigation Decision-Making in Vietnamese Coffee Production
Reprinted from: *Water* **2025**, *17*, 646, https://doi.org/10.3390/w17050646 . . . . . **59**

Russell Poma-Chamana, Ricardo Flores-Marquez, Joel Cordova-Tadeo, Antony Quello, José Arapa-Quispe and Richard Solórzano-Acosta
Transformation of Terraces with Irrigation Systems: Profitability and Water Savings in Potato Crop (*Solanum tuberosum* L.)
Reprinted from: *Water* **2025**, *17*, 668, https://doi.org/10.3390/w17050668 . . . . . **77**

Alper Baydar, Yeşim Bozkurt Çolak, Cenk Küçükyumuk and Burak Dalkılıç
Evaluation of Hydraulic and Irrigation Performances of Drip Systems in Nectarine Orchards (*Prunus persica* var. *nucipersica*) in The Mediterranean Region
Reprinted from: *Water* **2025**, *17*, 758, https://doi.org/10.3390/w17050758 . . . . . **96**

Bhawana Gupta and John S. Rowan
Understanding Unsustainable Irrigation Practices in a Regionally Contested Large River Basin in Peninsular India Through the Lens of the Water–Energy–Food–Environment (WEFE) Nexus
Reprinted from: *Water* **2025**, *17*, 1644, https://doi.org/10.3390/w17111644 . . . . . **114**

Alexandra Tomaz, Adriana Catarino, Pedro Tomaz, Marta Fabião and Patrícia Palma
Patterns, Risks, and Forecasting of Irrigation Water Quality Under Drought Conditions in Mediterranean Regions
Reprinted from: *Water* **2025**, *17*, 1783, https://doi.org/10.3390/w17121783 . . . . . **137**

About the Editors

Patrícia Palma

Patrícia Palma is a full professor at the Polytechnic Institute of Beja. Currently, as a researcher, she is a member of the scientific committee of the Center for Scientific and Technological Research in Earth Systems and Energy (CREATE) and an associate researcher at the Geobiotec Research Unit. She develops her research career guided by the principle of deepening knowledge about environmental pollution and its possible consequences for environmental health. She has participated as a coordinator or researcher in several funded projects, particularly in relation to the development of ecotoxicological tools used to assess the impact of agricultural activities on heavily modified water bodies, the impact of organic waste use on the recovery of degraded soils, the environmental risk assessment of treated agro-industrial effluents, ecotoxicological tools to assess the environmental risk of pesticides, and the use of IoT to improve laboratory analyses. An active researcher with over 70 publications, she is also a dedicated academic advisor, having supervised 4 doctoral students, 17 master's students, and 28 postdoctoral researchers. She is a member of the Society of Toxicology and Environmental Chemistry, the Portuguese Association of Toxicology, and the Board of Directors of the Southern Regional Committee of the Water Resources Association.

Alexandra Tomaz

Alexandra Tomaz is an assistant professor at the School of Agriculture of the Polytechnic University of Beja (Portugal), an integrated researcher at the Center for Sci-Tech Research in Earth System and Energy (CREATE), and an associate researcher at the Geobiotec Research Unit. Her research focuses on soil and water conservation, sustainable irrigation management, and water use efficiency in Mediterranean agroecosystems. She has been involved in several national and European research projects addressing sustainable agricultural practices and water management under climate uncertainty. Her scientific output includes publications in international peer-reviewed journals and active collaboration within national and international research networks. Since 2022, she has been a Guest Editor of several Special Issues of *Water*, focusing on irrigation sustainability as well as soil and water quality in agricultural systems. Her work also places strong emphasis on knowledge transfer, including organizing scientific and technical events, co-authoring technical manuals on sustainable Mediterranean agroecosystem management, and contributing to professional and outreach publications. Through research, teaching, and science communication, she actively promotes sustainable soil and water management, particularly in Mediterranean European regions.

water

MDPI

Editorial

Agricultural Practices to Improve Irrigation Sustainability, 2nd Edition

Patrícia Palma [1,2,3,4] and Alexandra Tomaz [1,2,3,*]

[1] Instituto Politécnico de Beja, Escola Superior Agrária de Beja, Campus do Instituto Politécnico de Beja, 7800-295 Beja, Portugal; ppalma@ipbeja.pt
[2] Center for Sci-Tech Research in Earth System and Energy (CREATE), Instituto Politécnico de Beja, Campus do Instituto Politécnico de Beja, 7800-295 Beja, Portugal
[3] GeoBioTec, Nova School of Science and Technology, Campus da Caparica, 2829-516 Caparica, Portugal
[4] Águas Publicas do Alentejo, Grupo Águas de Portugal, Rua Dr. Aresta Branco nº 51, 7800-310 Beja, Portugal
* Correspondence: atomaz@ipbeja.pt

1. Introduction

Agriculture accounts for approximately 70% of global water usage [1,2]. Although the use of water in agriculture yields considerable gains in productivity, thereby contributing significantly to food production and security, the agricultural sector is increasingly required to justify its use of water and is under growing scrutiny [3–5]. To address water governance and ensure fair access to water across sectors and scales, efficient water management, and environmental protection, it is critical to safeguard the sustainability of irrigation agriculture [6,7].

In the last few decades, considerable efforts have been made to improve water-use efficiency (WUE) across different sectors. According to a recent publication by the Food and Agriculture Organization of the United Nations (FAO) [8], there was an increase of 23% in WUE (expressed in USD m^{-3}) between 2015 and 2022, indicating a positive outcome under Sustainable Development Goal (SDG) target 6.4.1—Change in WUE over time. Gains in agricultural water productivity have been achieved thanks to agronomic technological advancements, like higher efficiency irrigation methods, remote-sensing integration, or smart irrigation systems [9–11].

As stated by the FAO (2025) [1] "Future gains must come from smarter—not just increased—food production, by closing yield gaps, diversifying the selection of suitable and resilient crops, and applying locally adapted, resource-efficient practices suited to land, soil and water conditions. There is no single pathway—no one-size-fits-all solution."

Currently, the issue of sustainable irrigation involves making optimal decisions amid uncertainty. Climate change, resource degradation and availability, the water–energy–food–environment (WEFE) nexus, and institutional and political issues often constrain the advancement of agricultural systems [12–14].

The second edition of the Special Issue (SI) "Agricultural practices to improve irrigation sustainability", published in *Water* in 2025, builds upon the first edition published in 2024 [3] and expands the scope in irrigation research from classic studies at the field or agricultural plot scale to research on the most effective tools to support decision-making under uncertainty. To achieve these advances, decision-making must be supported by reliable data and tools that are simple enough for stakeholders to interpret and can effectively inform their decisions.

The contributions for this SI highlight this shift in research, comprising articles that address best practices at the plot level, with a focus on increasing efficiency; refocus

agricultural decision-making on data and model analysis; and expose and reflect on trade-offs and governance related to the WEFE nexus.

2. An Overview of the Contributions to the Special Issue

2.1. Field-Scale Practices

Contributions from Baydar et al., Poma-Chamana et al., and Garofalo et al. (contributions 1–3) focused on efficiency, performance, and adaptation at the farm scale. Baydar et al. (contribution 1) studied the hydraulic performance and theoretical efficiency in drip irrigation systems in Nectarine Orchards (*Prunus persica* var. *nucipersica*) in the Mediterranean Region. The drip systems' performance was evaluated using statistical uniformity and efficiency parameters, highlighting the need to train farmers to address low performance and increase profitability.

Poma-Chamana et al. (contribution 2) examined how water conservation and economic productivity can be achieved through the integration of deficit irrigation (DI) and structural erosion control measures in potato (*Solanum tuberosum* L.) production. Their results suggested that drip irrigation enhanced efficiency while maintaining yield and profitability in terraced crops.

Garofalo et al. (contribution 3) studied the potential of sorghum (*Sorghum bicolor* L. Moench) for bioethanol production under DI strategies. They found higher biomass and ethanol water productivity under moderate deficit irrigation, underscoring the importance of adjusting irrigation practices to specific environmental conditions to improve WUE and yield.

2.2. Data, Models, and Decision Support

The contributions from Shan et al., Garofalo et al., Tomaz et al., and Scobie et al. (contributions 4–7) demonstrated a shift from research at the field-scale to data-driven agricultural decision-making. Shan et al. (contribution 4) reported a study using the DSSAT–CROPGRO–Tomato model to optimize water-saving irrigation and nitrogen-use efficiency in greenhouse tomato cultivation in North China. Their results showed that the maximum tomato yield and water–nitrogen-use efficiency were achieved with irrigation volumes of 320–340 mm and nitrogen application rates of 360–400 kg·ha^{-1}.

Garofalo et al. (contribution 5) studied data-driven irrigation management in watermelon (*Citrullus lanatus*, (Thunb.) Matsum & Nakai, 1916). They estimated actual evapotranspiration (ETa) using machine learning (ML) algorithms (Random Forest, Elastic Net, and Support Vector Machine) based on measured data and remote sensing.

Tomaz et al. (contribution 6) researched the prediction of irrigation water quality under drought conditions using multivariate statistical tools and ML models. Random Forest regression and Gradient Boosting Machine algorithms were employed to predict water quality parameters from chemical and climatic variables, providing a promising framework for early warning and informed decision-making in the context of increasing drought vulnerability across Mediterranean agro-environments.

Scobie et al. (contribution 7) examined the basis for specifying minimum data requirements for irrigation decision-making among small-scale Vietnamese coffee farmers. They found that Low-Data models (LDMs) are best suited to more informed irrigation scheduling decisions, which have the potential to improve the likelihood of success for farmers.

2.3. Trade-Offs and Governance

Institutional conflicts and governance may limit the sustainability of agricultural water use, as reported by Gupta & Rowan (contribution 8). These authors employed a WEFE nexus analytical framework to examine the socio-political, economic, and environmental

https://doi.org/10.3390/w18030333

factors driving unsustainable irrigation practices in a river basin of Peninsular India. They integrated spatially explicit analysis using digitized irrigation census data, theoretical energy modelling, and crop water requirements simulations to assess groundwater use and energy consumption for irrigation, and to examine their links with governance and economic growth. The findings highlight the need for holistic, catchment-wide planning that is aligned with the SDGs.

3. Conclusions

This SI addresses the challenge of improving irrigation sustainability under uncertainty related to climate and energy, water availability (quantity and quality), environmental degradation, institutional conflicts, and governance complexity.

Three contributions (Baydar et al., Poma-Chamana et al., and Garofalo et al.) reported that water-use efficiency and productivity can be enhanced through improvements in irrigation system performance, deficit irrigation strategies, and the adaptation of management options to crops and environmental conditions. The growing role of data-driven approaches in irrigation management was highlighted by four contributions (Shan et al., Garofalo et al., Tomaz et al., and Scobie et al.). One of the contributions (Gupta and Rowan) emphasized the need for integrated, basin-scale planning aligned with the SDG, which is critical for the effectiveness of technical solutions and irrigation sustainability.

Sustainable irrigation relies on integrating complementary approaches. The articles published in this SI demonstrate the need for improved decision-making in irrigated agriculture, whether informed by field data, modelling, or forecasting using new digital tools.

Author Contributions: Conceptualization, P.P. and A.T.; writing—original draft preparation, P.P. and A.T.; writing—review and editing, P.P. and A.T.; funding acquisition, P.P. and A.T. All authors have read and agreed to the published version of the manuscript.

Funding: The work is funded by national funds through FCT—Fundação para a Ciência e Tecnologia, I.P., in the framework of the UID/06107/2025—Centro de Investigação em Ciência e Tecnologia para o Sistema Terra e Energia (CREATE) and the UID/04035/2025—GeoBioTec.

Conflicts of Interest: The authors declare that the research was conducted in the absence of any commercial or financial relationships that could be construed as a potential conflict of interest.

Abbreviations

The following abbreviations are used in this manuscript:

DI	Deficit Irrigation
ETa	Actual Evapotranspiration
FAO	Food and Agriculture Organization of the United Nations
LDM	Low-Data Model
ML	Machine Learning
SDG	Sustainable Development Goal
WEFE	Water–Energy–Food–Environment
WUE	Water-Use Efficiency

List of Contributions:

1. Baydar, A.; Bozkurt Çolak, Y.; Küçükyumuk, C.; Dalkılıç, B. Evaluation of Hydraulic and Irrigation Performances of Drip Systems in Nectarine Orchards (*Prunus iersica* var. *nucipersica*) in The Mediterranean Region. *Water* **2025**, *17*, 758. https://doi.org/10.3390/w17050758.
2. Poma-Chamana, R.; Flores-Marquez, R.; Cordova-Tadeo, J.; Quello, A.; Arapa-Quispe, J.; Solórzano-Acosta, R. Transformation of Terraces with Irrigation Systems: Profitability and Water Savings in Potato Crop (*Solanum tuberosum* L.). *Water* **2025**, *17*, 668. https://doi.org/10.3390/w17050668.

https://doi.org/10.3390/w18030333

3. Garofalo, S.P.; Modugno, A.F.; de Carolis, G.; Campi, P. Energy of Sorghum Biomass Under Deficit Irrigation Strategies in the Mediterranean Area. *Water* **2025**, *17*, 578. https://doi.org/10.3390/w17040578.
4. Shan, Z.; Chen, J.; Zhang, X.; Si, Z.; Yi, R.; Fan, H. Optimizing Irrigation and Nitrogen Application for Greenhouse Tomato Using the DSSAT–CROPGRO–Tomato Model. *Water* **2025**, *17*, 426. https://doi.org/10.3390/w17030426.
5. Garofalo, S.P.; Ardito, F.; Sanitate, N.; De Carolis, G.; Ruggieri, S.; Giannico, V.; Rana, G.; Ferrara, R.M. Robustness of Actual Evapotranspiration Predicted by Random Forest Model Integrating Remote Sensing and Meteorological Information: Case of Watermelon (*Citrullus lanatus*, (Thunb.) Matsum. & Nakai, 1916). *Water* **2025**, *17*, 323. https://doi.org/10.3390/w17030323.
6. Tomaz, A.; Catarino, A.; Tomaz, P.; Fabião, M.; Palma, P. Patterns, Risks, and Forecasting of Irrigation Water Quality Under Drought Conditions in Mediterranean Regions. *Water* **2025**, *17*, 1783. https://doi.org/10.3390/w17121783.
7. Scobie, M.; Freebairn, D.; Mushtaq, S.; Donahue, D. How Much Is Enough? Data Requirements for Practical Irrigation Decision-Making in Vietnamese Coffee Production. *Water* **2025**, *17*, 646. https://doi.org/10.3390/w17050646.
8. Gupta, B.; Rowan, J.S. Understanding Unsustainable Irrigation Practices in a Regionally Contested Large River Basin in Peninsular India Through the Lens of the Water–Energy–Food–Environment (WEFE) Nexus. *Water* **2025**, *17*, 1644. https://doi.org/10.3390/w17111644.

References

1. FAO. *The State of the World's Land and Water Resources for Food and Agriculture 2025. The Potential to Produce More and Better*; Food and Agriculture Organization of the United Nations: Rome, Italy, 2025.
2. UNESCO UN World Water Development Report. Statistics Water Demand and Use. Available online: https://www.unesco.org/reports/wwdr/en/2024/s (accessed on 12 December 2025).
3. Palma, P.; Tomaz, A. Agricultural Practices to Improve Irrigation Sustainability. *Water* **2024**, *16*, 817. [CrossRef]
4. Mehta, P.; Siebert, S.; Kummu, M.; Deng, Q.; Ali, T.; Marston, L.; Xie, W.; Davis, K.F. Half of Twenty-First Century Global Irrigation Expansion Has Been in Water-Stressed Regions. *Nat. Water* **2024**, *2*, 254–261. [CrossRef]
5. IPCC. *Global Warming of 1.5 °C: IPCC Special Report on Impacts of Global Warming of 1.5 °C above Pre-Industrial Levels in Context of Strengthening Response to Climate Change, Sustainable Development, and Efforts to Eradicate Poverty*; Cambridge University Press: Cambridge, UK, 2022.
6. Pereira, L.S. Water, Agriculture and Food: Challenges and Issues. *Water Resour. Manag.* **2017**, *31*, 2985–2999. [CrossRef]
7. Dorafshan, M.M.; Golmohammadi, M.H.; De Michele, C.; Eslamian, S. Water-Energy-Food-Ecosystem Nexus: Ecosystem as a Key Component for Achieving Sustainable Development Goals. In *Global Nexus Handbook*; 2026; pp. 271–289.
8. Hernandez Lagana, M.; Mejias Moreno, P. *AQUASTAT Water Data Snapshot 2025*; FAO: Rome, Italy, 2025.
9. Bwambale, E.; Abagale, F.K.; Anornu, G.K. Smart Irrigation Monitoring and Control Strategies for Improving Water Use Efficiency in Precision Agriculture: A Review. *Agric. Water Manag.* **2022**, *260*, 107324. [CrossRef]
10. Ali, A.; Hussain, T.; Zahid, A. Smart Irrigation Technologies and Prospects for Enhancing Water Use Efficiency for Sustainable Agriculture. *AgriEngineering* **2025**, *7*, 106. [CrossRef]
11. Zhu, X. Advances in Agricultural Irrigation Management and Technology. *Water* **2025**, *17*, 2591. [CrossRef]
12. *Implementing the Water–Energy–Food–Ecosystems Nexus and Achieving the Sustainable Development Goals*; Carmona-Moreno, C., Crestaz, E., Cimmarrusti, Y., Farinosi, F., Biedler, M., Amani, A., Mishra, A., Carmona-Gutierrez, A., Eds.; UNESCO, European Union and IWA Publishing: Paris, France, 2021.
13. Correa-Cano, M.E.; Salmoral, G.; Rey, D.; Knox, J.W.; Graves, A.; Melo, O.; Foster, W.; Naranjo, L.; Zegarra, E.; Johnson, C.; et al. A Novel Modelling Toolkit for Unpacking the Water-Energy-Food-Environment (WEFE) Nexus of Agricultural Development. *Renew. Sustain. Energy Rev.* **2022**, *159*, 112182. [CrossRef]
14. Lalawmpuii; Rai, P.K. Role of Water-Energy-Food Nexus in Environmental Management and Climate Action. *Energy Nexus* **2023**, *11*, 100230. [CrossRef]

Disclaimer/Publisher's Note: The statements, opinions and data contained in all publications are solely those of the individual author(s) and contributor(s) and not of MDPI and/or the editor(s). MDPI and/or the editor(s) disclaim responsibility for any injury to people or property resulting from any ideas, methods, instructions or products referred to in the content.

water

MDPI

Article

Robustness of Actual Evapotranspiration Predicted by Random Forest Model Integrating Remote Sensing and Meteorological Information: Case of Watermelon (*Citrullus lanatus*, (Thunb.) Matsum. & Nakai, 1916)

Simone Pietro Garofalo [1,*], Francesca Ardito [2], Nicola Sanitate [1], Gabriele De Carolis [1], Sergio Ruggieri [1], Vincenzo Giannico [2], Gianfranco Rana [1] and Rossana Monica Ferrara [1,*]

[1] Research Center for Agriculture and Environment, Council for Agricultural Research and Economics, via Celso Ulpiani, 5, 70126 Bari, Italy
[2] Department of Soil, Plant and Food Science, University of Bari Aldo Moro, 70126 Bari, Italy
* Correspondence: simone.garofalo@crea.gov.it (S.P.G.); rossana.ferrara@crea.gov.it (R.M.F.)

Abstract: Water scarcity, exacerbated by climate change and increasing agricultural water demands, highlights the necessity for efficient irrigation management. This study focused on estimating actual evapotranspiration (ETa) in watermelons under semi-arid Mediterranean conditions by integrating high-resolution satellite imagery and agro-meteorological data. Field experiments were conducted in Rutigliano, southern Italy, over a 2.80 ha area. ETa was measured with the eddy covariance (EC) technique and predicted using machine learning models. Multispectral reflectance data from Planet SuperDove satellites and local meteorological records were used as predictors. Partial least squares, the generalized linear model and three machine learning algorithms (Random Forest, Elastic Net, and Support Vector Machine) were evaluated. Random Forest yielded the highest predictive accuracy with an average R^2 of 0.74, RMSE of 0.577 mm, and MBE of 0.03 mm. Model interpretability was performed through permutation importance and SHAP, identifying the near-infrared and red spectral bands, average daily temperature, and relative humidity as key predictors. This integrated approach could provide a scalable, precise method for watermelon ETa estimation, supporting data-driven irrigation management and improving water use efficiency in Mediterranean horticultural systems.

Keywords: evapotranspiration; horticulture; planet; irrigation; satellite; machine learning; SHAP

1. Introduction

Water scarcity, exacerbated by climate change and demands for limited freshwater resources, has highlighted the importance of efficient irrigation management in modern agriculture [1]. In regions characterized by hot, dry summers and high evaporation demand—such as the Mediterranean basin—water management strategies are essential to support sustainable agricultural production [2,3]. In this context, accurately quantifying crop water consumption is a key step in optimizing irrigation scheduling and improving overall water use efficiency [4]. The evapotranspiration (ET) rate represents the amount of water transferred from soil and plant surfaces to the atmosphere [5]. Traditional methods used to measure the ET involve different techniques, such as lysimeters and eddy covariance (EC). Generally, lysimeters measure the amount of water lost through evapotranspiration by monitoring changes in soil moisture within a defined volume of soil; they

provide direct measurements of ET and are particularly suitable for small-scale studies [6,7]. However, lysimeters can be expensive to install and maintain, and their limited spatial representativeness may not capture the variability of large fields and agricultural contexts. The eddy covariance technique involves measuring vertical turbulent fluxes of water vapor (eddies) above the canopy to estimate ET; this method provides continuous, real-time data over larger areas [8–11]. Nonetheless, EC systems require complex instrumentation and specialized technical personnel, and they may be excessively expensive to be extensively applied by farmers at the field scale [12]. In practical field applications, a common approach involves calculating the reference evapotranspiration (ETo) using equations such as the Penman–Monteith equation and adjusting the ETo with crop-specific coefficients (Kcs) [13–15]. The Penman–Monteith equation, recommended by the Food and Agriculture Organization, integrates meteorological variables to provide a standardized measure of ETo for a hypothetical reference crop. Therefore, Kcs are applied to adjust the ETo considering crop-related traits (species, growth stage, management practices) and local conditions [13]. However, this last method, although widely spread and used, is highly inaccurate under mainly arid and semi-arid conditions [16].

Satellite methods have emerged as powerful alternatives for estimating ET and monitoring vegetation dynamics and surface energy balances, especially over large areas. Many of these approaches incorporate thermal infrared (TIR) bands to estimate land surface temperature (LST), a key parameter in models such as the Surface Energy Balance Algorithm for Land (SEBAL) and Mapping Evapotranspiration at High Resolution with Internalized Calibration (METRIC) [17,18]. These models calculate ET by dividing the energy available at the land surface into sensible and latent heat fluxes, using the LST derived from the TIR data to estimate the sensible heat flux and then deriving the latent heat flux as a residual [19,20]. Although TIR-based methods provide useful information on ET by capturing temperature-related changes in evapotranspiration, they may often be limited by the spatial and/or temporal resolution of the available satellite platforms [21,22]. For instance, the Landsat program and the Moderate Resolution Imaging Spectroradiometer (MODIS) aboard NASA's Terra and Aqua satellites provide TIR imagery with a spatial resolution of 100 m and 1 km^2, respectively [23,24]. Recent advances in remote sensing may offer possible alternatives to these methods. Spectral data from higher-resolution satellite platforms with a high frequency of revisit time (e.g., Sentinel, Planet) make it possible to monitor vegetation dynamics on multiple spatial and temporal scales, detecting key indicators of crop status, canopy structure, and leaf area development [25–29]. Also, integrating multispectral remote sensing observations and machine learning algorithms could improve ET monitoring [30]. Among these platforms, Sentinel-2 is a useful data source, as it offers advantages such as free accessibility and wide spectral coverage. However, compared to satellite platforms with daily acquisition (Planet), its 5-day acquisition frequency, combined with potential cloud cover, may limit the number of usable observations for crops with short growth cycles, such as watermelon, ultimately reducing the dataset available for model training.

Machine learning is a field of artificial intelligence that focuses on developing algorithms able to learn from data to make predictions without being directly programmed; through the identification of patterns within the data, machine learning models can perform several tasks, including classification, regression, and clustering [31]. Machine learning is becoming a powerful tool in modern agriculture, improving several aspects of crop management by analyzing data from different sources (e.g., data from proximal sensors, images from satellites and drones) to monitor plant physiological and nutritional status or plant pests, enabling timely intervention from farmers [32–36]. Moreover, machine learning

methods are turning out to be highly and suitably automatable to be employed in efficient precision agriculture applications [37].

This study aims to develop a predictive model for estimating ETa in watermelon crops by integrating high-resolution, multispectral satellite imagery from Planet constellation with local meteorological data under semi-arid conditions (southern Italy); we chose Planet data to take advantage of their high temporal resolution (daily acquisition), which allows for a sufficient number of observations despite cloudy days. Different models and machine learning algorithms have been compared, including Elastic Net, the generalized linear model, partial least squares, Random Forest, and Support Vector Machine, to identify the most robust one to predict watermelon ETa.

2. Materials and Methods

2.1. Crop Management and Field Data

The trial was conducted in 2023 at the experimental farm of the Council for Agricultural Research and Economics in Rutigliano, southern Italy (41°01′ N, 17°01′ E, 147 m a.s.l.). Watermelon (*Citrullus lanatus* (Thunb.) Matsum. & Nakai, 1916), cultivar Lion King, mulched by a biodegradable film (model PC 100 d8, BASF 67056 Ludwigshafen, Germany, 1 m width), was grown over an area of 2.80 ha, with a density of 3200 plants ha^{-1} (spacing: 2.70 m × 1.00 m) (Figure 1). From the transplanting (9 June), the irrigation was performed 3 times per week through drip lines with a flow rate of 2.10 L h^{-1} and drippers spaced at 0.60 m; the irrigation ended on 24 August. The marketable fruits were harvested between 28 and 31 August 2023. After harvesting, on 25 September 2023, the fresh plant residues, unharvested fruits, and the mulching film were chopped by a tractor shredder and plowed on 2 and 13 October 2023. During the growing season, the watermelon leaf area index (LAI, m^2 m^{-2}) was determined through a Licor 3100 (Li-COR Inc., Lincoln, NE, USA).

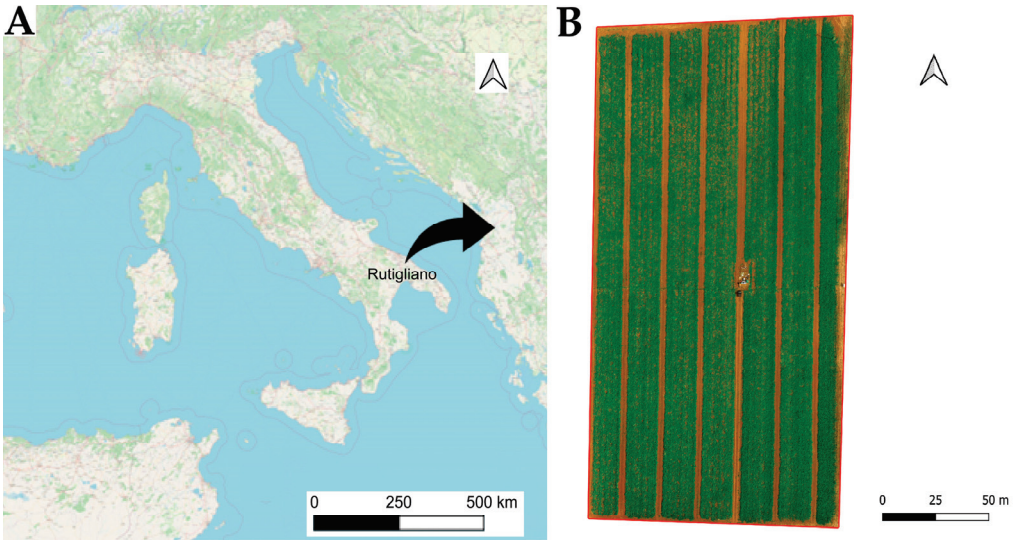


Figure 1. (**A**) Rutigliano, southern Italy (OpenStreetMap contributors); (**B**) aerial view of the experimental field where watermelon was cultivated in 2023.

The area's climate is typically Mediterranean, with hot and dry summers and mildly cold winters. The climate is CSa following the Köppen and Geiger classification [38]. The main rainfall occurs in autumn and winter (over the past thirty years, the average annual rainfall has been 622 mm); the average annual temperature is 16.5 °C and the hottest and coldest months are August and January, respectively [38]. The soil is classified as "Lithic Rhodoxeralf" and features a clay texture, stable structure, shallow profile (0.60–1.10 m), and rapid drainage due to an underlying cracked limestone subsoil parent material. Meteo-

rological data were collected using an automatic weather station equipped with standard sensors installed within the experimental farm.

2.2. Eddy Covariance Measurements

The eddy covariance (EC) method was employed for measuring the hourly fluxes of water vapor (H_2O), corresponding to actual evapotranspiration (ETa, mm) [39]. It is considered the most direct and least error-prone approach for long-term monitoring of H_2O fluxes at the field scale [8,40,41]. The EC method is based on the covariance between the instantaneous values of the vertical velocity component and the scalar concentration (H_2O), measured by a three-dimensional sonic anemometer (uSonic 3 Scientific, Metek GmbH, 25337 Elmshorn, Germany) and a fast response open-path infrared gas analyzer (LI-7500, Li-COR Inc., Lincoln, NE, USA), respectively. On 25 May 2023, the EC flux tower was established in the center of the field at 1.5 m above the soil surface, reaching a maximum of 1.75 m, following the growth of the crop. Micrometeorological data were recorded every 0.1 s (10 Hz) by the MeteoFlux software (Servizi Territorio, S.n.c., Cinisello Balsamo, Italy) (https://meteorflux.org/). The EddyPro® software (v7.0.9, LiCor, 68504 Lincoln, NE, USA) [42] was used for calculating the ETa fluxes. All details can be found in Ferrara et al. [43].

2.3. Satellite Images

In this work, high-resolution spectral images acquired by the SuperDove satellites were used (Planet Images©, 2023). SuperDove satellites are part of the PlanetScope constellation operated by Planet Labs PBC company; they acquire spectral images with a 3 m spatial resolution and eight bands with a spectral resolution from visible to red-edge and near-infrared [44]. The images were downloaded from the online tool Planet Explorer as orthorectified and atmospherically corrected TIFF files. Only cloud-free images were downloaded for the investigated period (from the transplanting on 9 June of the watermelon to the end of the growing cycle on 3 October), for a total of 68 images. Per each spectral band, the mean reflectance value of the watermelon field was calculated by averaging the reflectance value of the pixels within the field (Figure 1B). Images were processed in R environment (RStudio IDE, version 2024.04.2+764 for Windows) using the packages "sf" [45] and "raster" [46].

2.4. Data Processing and Machine Learning Analyses

In the pre-processing phase, the daily ETa data, obtained as an integral of hourly positive EC values, for the entire watermelon growth cycle were filtered to consider only those days on which cloud-free SuperDove images were available (0% cloudiness for the field area at the time of image acquisition). Consequently, the ETa measurements of days without corresponding cloud-free images were excluded from the dataset. The coefficient of variance (CV) has been calculated before and after data processing as the ratio of standard deviation and mean. For the remaining set of data, the mean reflectance values for each spectral band of the SuperDove images were matched to the corresponding daily ETa measurements. The resulting dataset was used to develop a machine learning model to predict the daily ETa of the watermelon (target) based on the following predictors: (i) reflectance values of the SuperDove spectral bands (see Table 1), (ii) the average daily temperature, and (iii) the average daily RH; the last two variables were acquired by a standard agro-meteorological station, installed in a reference grass field close to the experimental plot.

Table 1. The eight SuperDove spectral bands considered in the analyses with their central wavelength (nm) and range (full width at half maximum, fwhm).

Band	Central Wavelength (fwhm)
Coastal Blue	443 (20)
Blue	490 (50)
Green I	531 (36)
Green	565 (36)
Yellow	610 (20)
Red	665 (31)
Red Edge	705 (15)
NIR	865 (40)

For the prediction of watermelon ETa, partial least squares (PLS), the generalized linear model (GLM) and three machine learning algorithms—Elastic Net (ENet), Random Forest (RF), Support Vector Machine (SVM)—were evaluated and compared. In this study, we have excluded deep learning approaches (e.g., CNN) since they require a large amount of data in the training phase [47,48]. ENet is a regularized regression technique that aims to combine the L1 (Lasso) and L2 (Ridge) regularization methods to improve the predictive accuracy; integrating both L1 and L2 penalties, ENet can handle datasets with highly correlated predictors [49]. The GLM extends traditional linear regression by allowing the response variable to follow various distributions. It consists of three components: a random component specifying the distribution of the response variable, a linear predictor formed by a linear combination of explanatory variables, and a link function that relates the mean of the response variable to the linear predictor [50]. PLS models the relationship between data by projecting them on a new space of latent variables. PLS focuses on maximizing the covariance between the predictors and the target. By extracting the latent variables that capture the most significant information, PLS provides a robust framework for predictive modeling and data analysis [51]. RF operates by building multiple decision trees on random subsets of the data, thus averaging the results of each tree. The final prediction is obtained by averaging the outputs of all individual trees, which enhances predictive accuracy and reduces overfitting [52]. The versatility of RF in handling complex datasets has also been demonstrated in downscaling studies. For example, Agarwal et al. [53] applied RF to downscale GRACE-derived groundwater storage data to a resolution of 5 km in California's Central Valley. This highlights the potential of RF in modeling non-linear relationships and improving the applicability of satellite data in environmental and resource management at the local scale. SVM identifies the optimal hyperplane to separate the data points into distinct classes, maximizing the margin between them. Utilizing kernel functions, SVM can handle both linear and non-linear distributions of data [54]. All the analyses have been performed in Python environment (v. 3.11.5) and Spyder IDE (Spyder©, v. 5.4.3 for Windows) using the Scikit-Learn library (v. 1.5.2).

To enhance the performance of the models, it is essential to fine-tune their hyperparameters. In this study, we utilized the Optuna library (v. 4.0.0) for automatic hyperparameter optimization. Optuna explores the parameter space to identify the best performing setups. For each machine learning model, 100 optimization trials were conducted, utilizing Bayesian optimization with the Tree-structured Parzen Estimator (TPE) sampler [55]. The specific hyperparameters fine-tuned for each algorithm are reported in Table 2.

Table 2. Hyperparameters fine-tuned through Optuna per each machine learning algorithm used in this study.

Algorithm	Parameters
ENet	L1 ratio, alpha
GLM	link function
PLS	n_components
RF	n_estimators, max_depth, min_sample_leaf, max_features, min_sample_split
SVR	C, epsilon, gamma

To evaluate and compare the performance of the models, we performed a five-fold cross-validation repeated three times. This method involves dividing the dataset into five subsets, training the model on four subsets (80% of the dataset) and validating it on the remaining one (20% of the dataset). The process is performed five times, each time with a different subset serving as the validation set, ensuring that all data points are used for validation in the process. This approach is widely used for estimating the generalizability of the models [56]. Repeating the entire procedure three times with different partitions of the data enhances the reliability of performance estimates by reducing variability due to specific data partitions [57].

Model performances were compared by calculating the coefficient of determination (R^2), the root mean squared error (RMSE), and the mean bias error (MBE), based on the validation folds of the cross-validation.

The best performing model has been applied to model the daily trend of watermelon ETa. Predicted and observed ETa mean values have been compared through Student's *t*-test with a significance level set at $\alpha = 0.05$.

Machine Learning Explainability

Machine learning interpretability is increasingly recognized as a key aspect of building and using machine learning systems [58]. Three methods were used to explain model predictions in this study: permutation importance, SHapley Additive exPlanations (SHAP), and Local Interpretable Model-agnostic Explanations (LIME). Permutation importance measures the most influential features in a model's predictions. This involves training a model on the original dataset to create baseline performance and then randomizing values for one feature, interrupting its relationship with the target. Thus, the model is evaluated on this new dataset, and the importance of the feature is defined by the change in performance after permutation [59]. SHAP, on the other hand, draws on the Shapley value from cooperative game theory, which evaluates a player's contribution by looking at all possible coalitions [60]. In machine learning, SHAP calculates the influence of each feature on a model's predictions, offering clear and detailed insights into how individual features contribute to the outcomes [61]. LIME was introduced as a complementary and localized interpretability method to explain predictions on a specific instance. LIME approximates the model locally by creating perturbed samples around the instance to be explained and fitting an interpretable surrogate model (e.g., linear regression) highlighting the most influential features and their values for the prediction of that specific instance; in this study, LIME was applied to the instance where the model made its most accurate prediction [62].

3. Results

3.1. Weather Conditions

During the watermelon growing season, the highest average temperature was recorded on 27 July (34.1 °C), while the lowest was on 24 September (18.4 °C). The seasonal average

temperature was 23.8 °C. The highest maximum temperature was recorded on 24 July (41.8 °C), while the lowest minimum temperature was recorded on 11 October (12.8 °C). RH showed a fluctuating trend during the season, with the lowest values during the second half of July (22 and 25 July: 33.2% and 38.2%, respectively) (Figure 2a). The driest months were July and August; the cumulated rainfall up to the incorporation of the crop residuals was 94.2 mm. The cumulated irrigation water applied was 582.8 mm (Figure 2b).

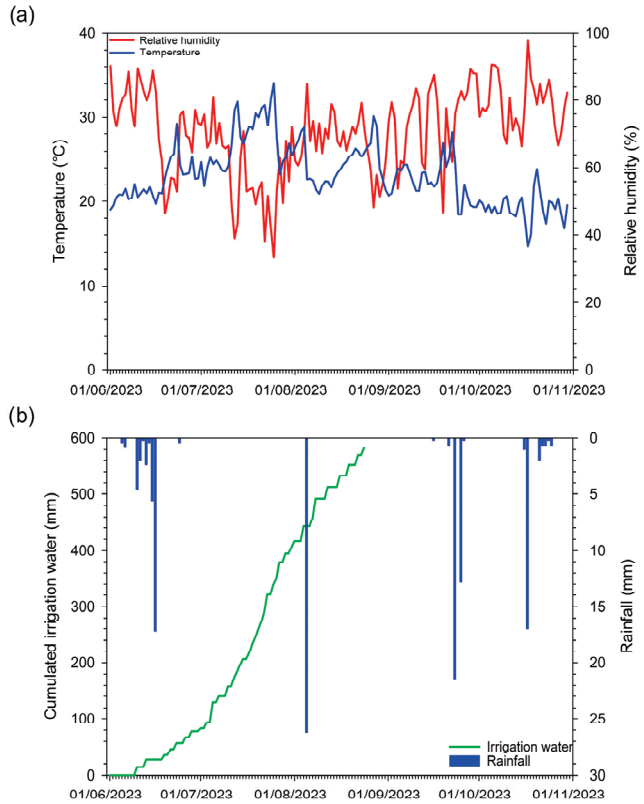


Figure 2. (**a**) Trend of mean temperature and relative humidity during the growing season; (**b**) daily rainfall and irrigation water applied during the growing season.

3.2. Measured Actual Evapotranspiration and Predictors

The full time series of the watermelon's ETa measured daily is shown in Figure 3, and the subset of ETa, coinciding with available satellite data, on clear days, is also indicated; this last subset effectively captures the most ETa variability (full time series CV = 0.509; subset time series CV = 0.455).

The ETa trend follows the typical evapotranspiration pattern of an irrigated crop under the Mediterranean climate, starting with relatively low values, indicating a moderate level of evapotranspiration in June (except for 14 June 2023, ETa = 4.6 mm). A progressive increase in ETa was observed until late July, with a peak on 25 July 2023 (5.5 mm). From the end of August, after the fruits' harvesting, ETa accounts only for the soil evaporative term, showing a steady decline (except for 21 September 2023 and 26 September 2023, ETa = 3.0 mm and 2.5 mm, respectively), reaching the lowest value (0.6 mm) on 10 October 2023.

Figure 4 shows the correlation matrix of the variables included in the analyses. The nir spectral band had the strongest positive correlation with ETa (r = 0.74), and the daily average temperature had a positive correlation (r = 0.57) as well. Other variables showed negative correlations with ETa, e.g., red and yellow spectral bands (r = −0.71 and r = −0.56, respectively). Coastal blue, blue, green, and green_I spectral bands were highly correlated with each other (r > 0.80). For instance, the correlation between coastal blue and blue was

0.89, and between green_I and green it was 0.95, suggesting multicollinearity between the predicting variables. Nir and red spectral bands showed a negative correlation ($r = -0.86$). Daily average temperature and daily RH also had a negative correlation ($r = -0.79$). In the Supplementary Materials (Table S1), we report the descriptive statistics of the variables included in the analyses.

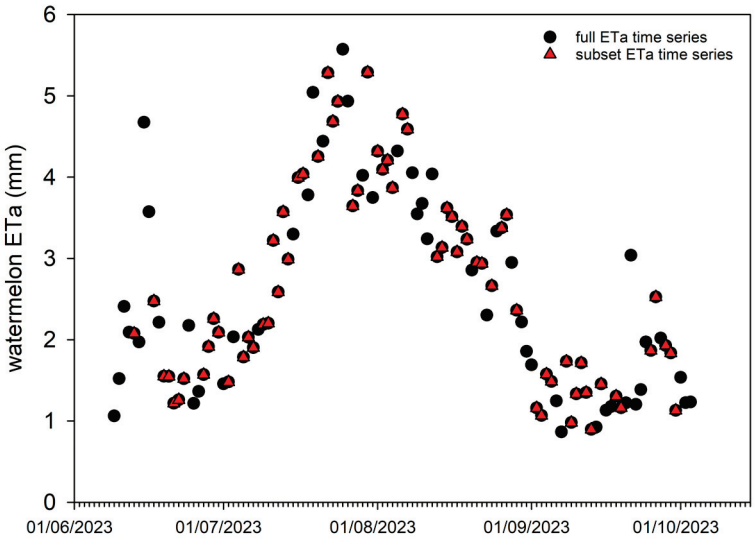


Figure 3. Comparison between the complete set of daily watermelon actual evapotranspiration data collected throughout the study season by eddy covariance method (black circles) and the subset corresponding to dates with available satellite imagery used in the analyses (red triangles).

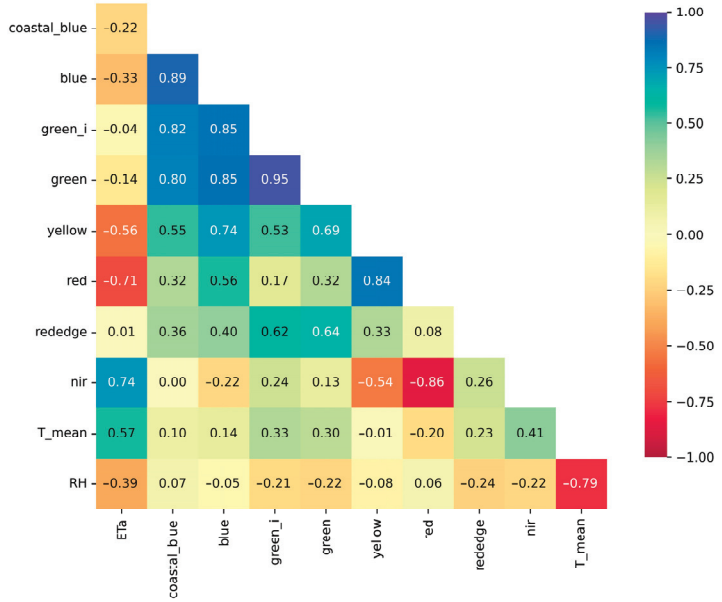


Figure 4. Heatmap of the correlation matrix among the dataset variables. The values within the cells represent Pearson correlation coefficients. ETa = actual evapotranspiration after pre-processing, T_mean = mean air temperature, RH = air relative humidity.

3.3. Models' Regression Performance

The results of the machine learning analysis (Table 3) indicate marked differences in the performance of the evaluated algorithms in predicting the watermelon ETa. In the Supplementary Materials (Figure S1), we show the scatterplot of the field-measured and predicted ETa per each model. Among the models, RF was found to be the best performing algorithm, resulting in an average R^2 of 0.747 ($\pm$0.076). This result is further

confirmed by the RMSE of 0.577 (±0.106) and the low MBE of 0.034 (±0.145). The scatter plot for RF shows a strong alignment of field-measured and predicted values, particularly in the middle range of ETa values, with only slight deviations for the extreme values. ENet was the second-best algorithm, with an R^2 of 0.684 (±0.142) and an RMSE of 0.666 mm (±0.693). However, the slightly higher RMSE and greater variability compared to RF suggest that ENet was less effective in modeling the inherent non-linear relationships within the data. The scatterplot of ENet predictions reflects this trait, showing greater dispersion, particularly at higher ETa values, which the model tends to underestimate. PLS performed similarly to ENet, with an R^2 of 0.631 (±0.197) and an RMSE of 0.673 mm (±0.139). The scatter plot for PLS shows a moderate fit of the predictions with the observed values, although it shows spread, especially for the high values of ETa. The GLM demonstrated a weaker performance compared to ENet and PLS, with an R^2 of 0.614 (±0.188) and an RMSE of 0.693 mm (±0.148). The scatterplot for GLM predictions highlights these limitations, showing a significant spread at lower ETa values. SVM, in contrast, performed poorly in predicting ETa. The model achieved a mean R^2 of 0.257 (±0.232) and had the highest RMSE. The scatterplot for SVM shows the weak fit of the predictions.

Table 3. Performance of the compared models across 3 repetitions of the 5-fold cross-validation (mean and standard deviation).

Algorithm	R^2	RMSE	MBE
ENet	0.684 (±0.142)	0.666 (±0.693)	0.005 (±0.137)
GLM	0.614 (±0.188)	0.693 (±0.148)	0.051 (±0.096)
PLS	0.631 (±0.197)	0.673 (±0.139)	0.044 (±0.101)
RF	0.747 (±0.076)	0.577 (±0.106)	0.034 (±0.145)
SVR	0.257 (±0.232)	0.984 (±0.170)	−0.034 (±0.250)

3.4. Predicted Watermelon Actual Evapotranspiration and Model Explainability

The RF model, found to be the best performing one among the others, has been applied to predict the daily watermelon ETa. The resulting predictions are shown in Figure 5, where they are also compared with the observed ETa values, and the trend of the field-measured LAI is also reported. From the beginning of the growing season in mid-June until the peak evapotranspiration period at the end of July, the RF model closely reflects the observed increases in ETa, corresponding to the vegetative and reproductive growth phases of the crop. However, slight deviations are evident on specific dates, corresponding to the peaks. In the second part of the growing cycle, the ETa predicted by the RF model fairly follows the decrease in the observed ETa until the end of September. Table 4 reports the cumulated and average daily ETa for the observed and predicted ETa; no statistically significant difference has been detected between the observed and predicted daily ETa (p = 0.64). In the Supplementary Materials (Figure S2), we report the boxplots showing the distribution of the observed and predicted ETa.

Table 4. Average observed and Random Forest-predicted watermelon evapotranspiration (ETa); the standard deviation is reported within the parentheses. Cumulated value of observed and Random Forest-predicted watermelon ETa. Observed ETa refers to the subset used for the machine learning analyses.

	Observed ETa	Predicted ETa
Average (mm day^{-1})	2.6 (±1.2)	2.6 (±1.0)
Cumulated (mm)	179	180

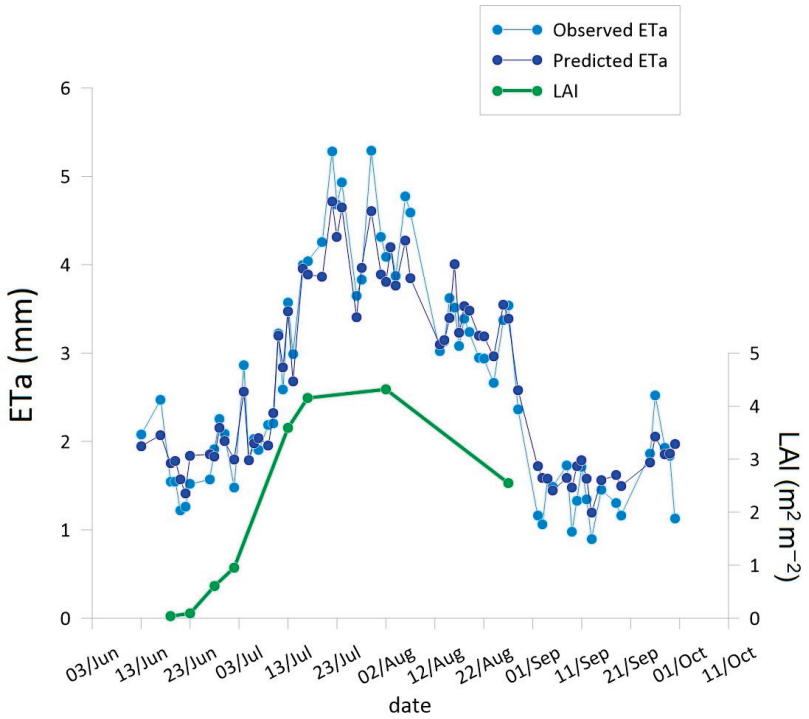


Figure 5. Trend of field-measured daily watermelon evapotranspiration (observed ETa) and the predicted watermelon ETa using the Random Forest-based model. The trend of watermelon leaf area index (LAI, m^2 m^{-2}).

The analysis of the feature importance, SHAP, and PDPs of the RF model provided insights into the contributions and impacts of the individual predictors in the prediction of the ETa of watermelon. According to the permutation-based features' importance, the Nir spectral band was the most important, with an average decrease in accuracy close to 0.4 when permuted. The red spectral band, daily average temperature, and yellow spectral band followed in importance (Figure 6). The SHAP summary graph quantifies the direction and magnitude of each feature's contribution to the model's predictions. Nir had the highest SHAP values, confirming the results of feature importance. Higher Nir values consistently contributed positively to ETa, while lower values had a negative impact on the model output. The red band shows an inverse relationship, with higher reflectance values reducing ETa predictions. The daily average temperature contributed positively to the prediction, with higher temperatures associated with higher ETa values. RH had a predominantly negative impact, reducing the Eta-predicted value as humidity increased. In the SHAP plot, the yellow reflectance exhibits a negative impact on ETa predictions. Higher values of yellow reflectance are associated with lower SHAP values, indicating that increased yellow reflectance reduces the predicted ETa (Figure 7). The LIME analysis provides localized insights by focusing on the most accurate prediction, identifying specific feature ranges contributing to its accuracy. Nir reflectance values between 0.33 and 0.43 and average temperature values above 26.66 °C had the greatest importance in the accuracy of the RF model. Similarly, the red, coastal blue and RH features showed positive but smaller contributions (Figure 8). PDPs provide insight into how each variable influences the expected ETa values while holding the other variables constant. The plot for the Nir spectral band shows a strong increase in ETa when Nir reflectance increases above 0.35. In contrast, the red spectral band reflectance shows an inverse relationship, with a strong decrease in ETa when the red reflectance rises above 0.11. The daily average temperature had a positive and almost linear relationship with ETa, particularly above 26 °C. As for RH, the graph shows a gradual decrease in ETa as relative humidity increases. The other spectral

bands, such as coastal blue, green, and blue, show flatter relationships with ETa, indicating their limited predictive power compared to the other predictors. In the Supplementary Materials, we report the PDPs illustrating the relationships between the predictors and watermelon actual evapotranspiration (Figure S3).

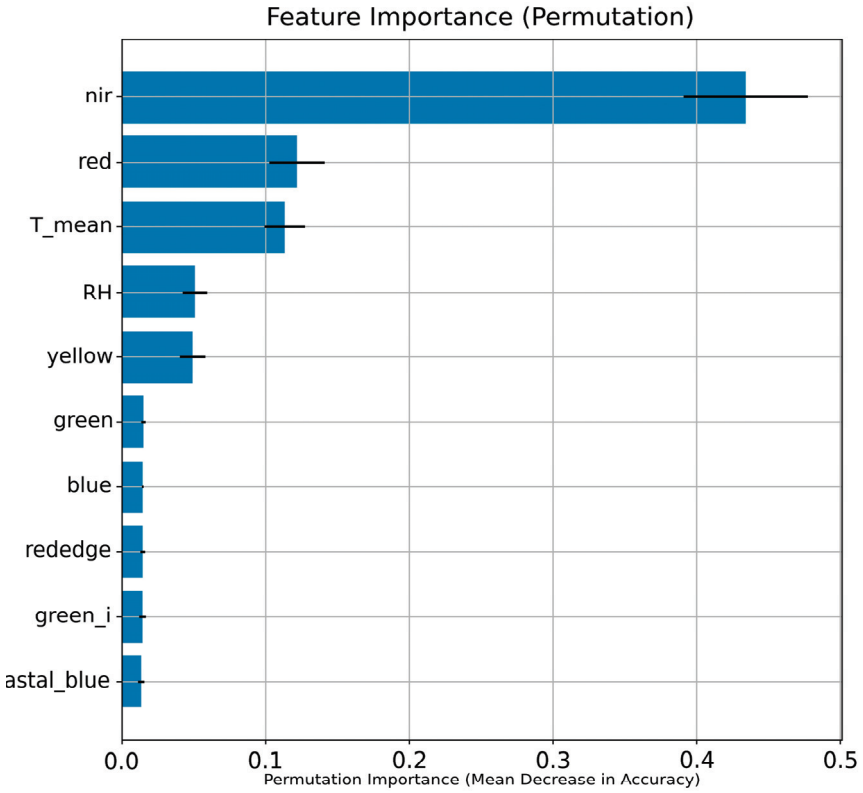


Figure 6. Permutation-based feature importance for the Random Forest model predicting watermelon actual evapotranspiration. Error bars indicate the standard deviation of feature importance across permutations.

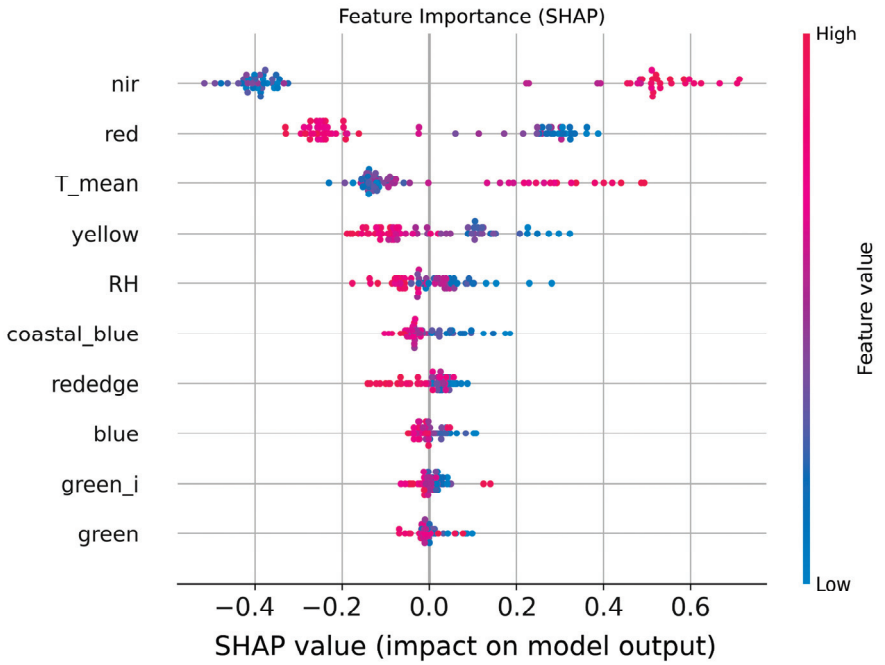


Figure 7. SHAP summary plot showing the impact of each feature on the Random Forest model's predictions for watermelon actual evapotranspiration.

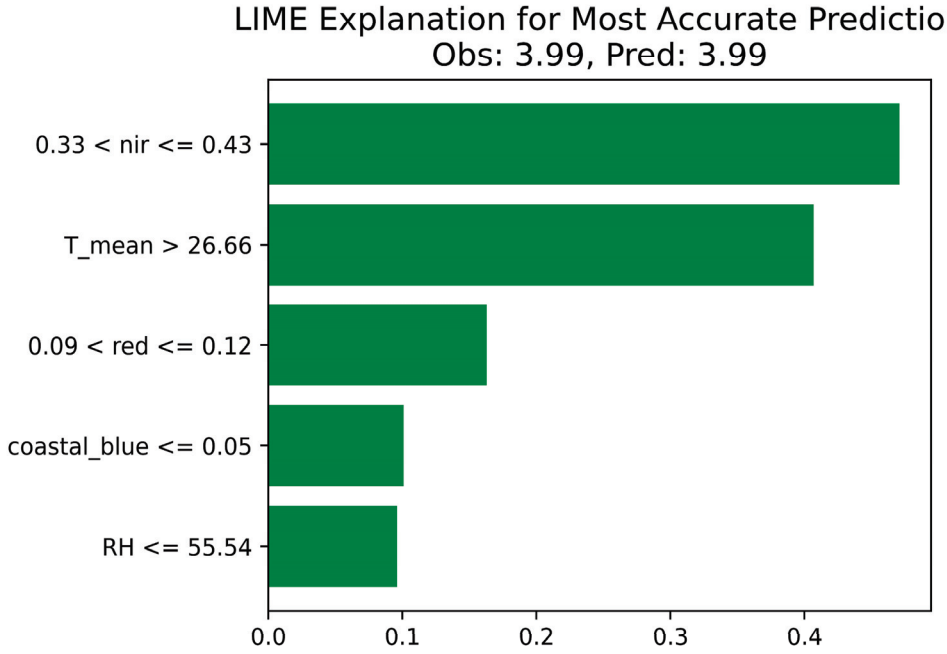


Figure 8. LIME explanation for the most accurate prediction. The bar plot highlights the contribution of specific feature ranges to the Random Forest prediction, showing their positive impact on model accuracy.

4. Discussion

In this study, the application of the RF algorithm to predict daily ETa in watermelon using Planet satellite imagery and meteorological information achieved the best result among the compared models. The performance of these models varies significantly, reflecting their methodological differences and suitability for modeling complex environmental processes [63]. The RF algorithm's capacity to handle multicollinearity among predictors is another significant advantage [64]; in our dataset, different spectral bands exhibited high correlations, which can be a challenge for multicollinearity-sensitive algorithms. RF addresses this problem by selecting random subsets of features during the construction of each tree, thus reducing the dominance of highly correlated variables and improving the robustness of the model [65,66]. These findings support the use of integrating machine learning techniques with remote sensing data for accurate estimation of ETa in horticultural crops (see, for example, the review by Ferreira et al. [67]). Interpretability is a key aspect of machine learning applications in environmental and agricultural sciences [68]. The permutation importance analysis found that the Nir spectral band was the most influential predictor, causing a significant decrease in model accuracy when permuted. This result is in line with the known sensitivity of the Nir band to vegetation biomass and water content, which are directly related to ETa [69–71]. The SHAP analysis provided a detailed overview of how each predictor impacted the model results. High values of Nir reflectance contributed positively to ETa predictions; on the contrary, higher reflectance values in the red band negatively affected ETa predictions, probably indicating areas of reduced chlorophyll content or plant stress, resulting in lower transpiration rates [72,73]. A high average daily temperature also had a positive effect on ETa, consistent with the physical processes that regulate evapotranspiration, where higher temperatures increase the vapor pressure deficit and drive transpiration [74]. Yellow band reflectance also negatively affected ETa predictions. High yellow band reflectance may be associated with some stress conditions or senescence of vegetation, resulting in reduced chlorophyll content and altered leaf pigment composition [75]. This may result in reduced photosynthetic activity and transpiration rates. SHAP values indicate that higher values of yellow reflectance contribute to lower ETa

predictions, consistent with this physiological understanding. Relative humidity showed a negative relationship with ETa in the RF model. Higher RH values corresponded to lower predicted ETa, as indicated by the negative SHAP values. This inverse relationship is physically explicit, as high humidity levels reduce the vapor pressure deficit between the leaf surfaces and the phyllosphere, thus decreasing the transpiration rate [76]. SHAP analysis confirmed that days with lower RH contributed positively to ETa predictions.

The presented results are the first related to the estimation of watermelon ETa in the Mediterranean environment by integrating high-resolution, high-frequency satellite data with agro-meteorological information. The use of satellite imagery has become increasingly important in precision agriculture, offering a noninvasive and scalable approach to monitor crop water use and status [28,35]. Traditional methods, such as lysimeters, while accurate, are limited by high costs and spatial limitations. The estimation of ET through remote sensing has generally been based on physical models involving thermal infrared (TIR) data. Furthermore, in addition to TIR data, crop-specific information is essential for an accurate estimation of ETa using models such as SEBAL and METRIC. This study focused on predicting ETa by training the models on data obtained by the eddy covariance technique, which is considered a micrometeorological standard approach for measuring fluxes of long-lived and inert gases [41] in the atmosphere and a reliable direct method to measure ETa [77,78]. Moreover, in the methodology proposed in this paper, the RF model was trained using agro-meteorological parameters and satellite band reflectance directly as predictors; the main advantage consists of the high frequency of Planet image acquisition, which can enable time-efficient monitoring of the crop ETa. This approach enables ETa to be estimated without relying on TIR data, overcoming the operational limitations of TIR-based models. In addition, the RF-based approach could offer further advantages besides overcoming the requirements of TIR data. By learning directly from different predictors, such as agro-meteorological parameters and spectral reflectance, it can capture complex, non-linear relationships that might be simplified too much when using traditional physical models. This flexibility reduces the need for rigid assumptions about surface properties or weather conditions and enables the model to adapt to different environmental and management contexts. Furthermore, enhancing the RF model would mainly require new input data rather than recalibrating multiple physical parameters, making this data-driven strategy easier to implement when frequent, high-resolution satellite imagery is available.

Through the method outlined in this work, growers and technicians could fine-tune irrigation schedules to match crop water demands, thereby improving water use efficiency and sustaining yields under increasingly variable weather conditions. The potential for remotely monitoring ETa at a high temporal frequency and at the field scale is not only useful for traditional full irrigation approaches but could also be particularly advantageous for the application of water-saving practices, such as deficit irrigation [79–83]. Since these strategies apply less water than total crop requirements, relying on remotely predicted ETa rather than Kc-approach calculations may reduce some sources of uncertainty—assumptions that are not valid in all agricultural environments or the need for some parameters that are difficult to measure consistently [16,84–86]. Nevertheless, some important limitations can be highlighted, e.g., the requirement for sufficiently frequent and cloud-free satellite imagery, the need for reliable ground-based measurements for calibration and validation, and the complexities associated with scaling this approach beyond individual test fields. Another key factor to consider is the cost of satellite data: while some platforms such as Sentinel provide imagery for free, dependence on high-resolution Planet imagery, which carries an associated cost, may limit wider adoption and accessibility to resource-limited regions or smaller farms. Furthermore, since this study was limited to a single field and a single growing season, the results could be influenced by the specific agro-environmental conditions

of the context. To increase the generalizability and robustness of the proposed modeling framework, future research should incorporate data from multiple fields extending to different agricultural contexts and to multiple growing seasons.

5. Conclusions

This study demonstrated the effectiveness of integrating high-resolution satellite images with meteorological data to accurately estimate effective daily evapotranspiration in watermelon crops under Mediterranean conditions. Direct measurements of evapotranspiration were performed using the eddy covariance technique, recognized for its accuracy in quantifying fluxes in agricultural environments. Among the machine learning models evaluated, the Random Forest algorithm showed the best performance. These results highlight the potential of combining remote sensing and machine learning techniques for accurate and non-invasive monitoring of water use in crops, offering valuable insights for optimizing irrigation practices and improving water management in agricultural systems. Future research should focus on integrating data from multiple fields, different crops, and growing seasons in various agro-environmental settings to improve the generalizability of the model.

Supplementary Materials: The following supporting information can be downloaded at: https://www.mdpi.com/article/10.3390/w17030323/s1, Figure S1: Scatterplot of the predicted and observed daily actual evapotranspiration (ETa) per each model optimized with Optuna. Figure S2: Boxplots showing the distribution of the observed and predicted watermelon actual evapotranspiration (ETa). The red and black lines within the boxes represent the mean and median values, respectively. Figure S3: Partial dependence plots illustrating the relationships between the predictors and watermelon actual evapotranspiration as modeled by the Random Forest algorithm. Table S1: Descriptive statistics of the target (ETa = actual evapotranspiration, after pre-processing) and the predictors included in the machine learning analyses (s.d. = standard deviation; AT = average temperature; RH = relative humidity) for all available data (n = 68).

Author Contributions: Conceptualization, S.P.G.; Data curation, S.P.G., N.S., G.D.C., S.R., G.R. and R.M.F.; Formal analysis, S.P.G., G.R. and R.M.F.; Investigation, S.P.G., S.R., G.R. and R.M.F.; Methodology, S.P.G., V.G., G.R. and R.M.F.; Resources, G.R. and R.M.F.; Software, S.P.G., G.R. and R.M.F.; Supervision, G.R. and R.M.F.; Validation, G.R. and R.M.F.; Visualization, S.P.G. and G.R.; Writing—original draft, S.P.G.; Writing—review and editing, F.A., V.G., G.R. and R.M.F. All authors have read and agreed to the published version of the manuscript.

Funding: This research was funded by the AgriDigit-Agromodelli project (DM n. 36502 20/12/2018), funded by the Italian Ministry of Agricultural, Food and Forestry Policies and Tourism (MIPAAFT).

Data Availability Statement: The original contributions presented in this study are included in the article/Supplementary Materials. Further inquiries can be directed to the corresponding authors.

Acknowledgments: The authors would like to express their gratitude to Planet Labs PBC for providing the satellite imagery used in this research through Planet's Education and Research Program.

Conflicts of Interest: The authors declare no conflicts of interest.

References

1. Alkhalidi, A.; Assaf, M.N.; Alkaylani, H.; Halaweh, G.; Salcedo, F.P. Integrated innovative technique to assess and priorities risks associated with drought: Impacts, measures/strategies, and actions, global study. *Int. J. Disaster Risk Reduct.* **2023**, *94*, 103800. [CrossRef]
2. Katerji, N.; Rana, G.; Ferrara, R.M. Actual evapotranspiration for a reference crop within measured and future changing climate periods in the Mediterranean region. *Theor. Appl. Climatol.* **2017**, *129*, 923–938. [CrossRef]
3. Maldera, F.; Garofalo, S.P.; Camposeo, S. Ecophysiological Recovery of Micropropagated Olive Cultivars: Field Research in an Irrigated Super-High-Density Orchard. *Agronomy* **2024**, *14*, 1560. [CrossRef]

4. Katerji, N.; Mastrorilli, M.; Rana, G. Water use efficiency of crops cultivated in Mediterranean region: Review and analysis. *Eur. J. Agron.* **2008**, *28*, 493–507. [CrossRef]
5. Rana, G.; Katerji, N. Measurement and estimation of actual evapotranspiration in the field under Mediterranean climate: A review. *Eur. J. Agron.* **2000**, *13*, 125–153. [CrossRef]
6. Kandra, B.; Tall, A.; Gomboš, M.; Pavelková, D. Quantification of Evapotranspiration by Calculations and Measurements Using a Lysimeter. *Water* **2023**, *15*, 373. [CrossRef]
7. Shi, W.; Zhang, X.; Xue, X.; Feng, F.; Zheng, W.; Chen, L. Analyzing Evapotranspiration in Greenhouses: A Lysimeter-Based Calculation and Evaluation Approach. *Agronomy* **2023**, *13*, 3059. [CrossRef]
8. Aubinet, M.; Vesala, T.; Papale, D. (Eds.) *Eddy Covariance: A Practical Guide to Measurement and Data Analysis*; Springer Science & Business Media: Dordrecht, The Netherlands, 2012.
9. Baldocchi, D.D. How eddy covariance flux measurements have contributed to our understanding of Global Change Biology. *Glob. Change Biol.* **2020**, *26*, 242–260. [CrossRef]
10. Fong, B.N.; Reba, M.L.; Teague, T.G.; Runkle, B.R.; Suvocarev, K. Eddy covariance measurements of carbon dioxide and water fluxes in US mid-south cotton production. *Agric. Ecosyst. Environ.* **2020**, *292*, 106813. [CrossRef]
11. Anapalli, S.S.; Pinnamaneni, S.R.; Reddy, K.N.; Singh, G. Eddy covariance quantification of corn water use and yield responses to irrigations on farm-scale fields. *Agron. J.* **2022**, *114*, 2445–2457. [CrossRef]
12. Rafi, Z.; Merlin, O.; Le Dantec, V.; Khabba, S.; Mordelet, P.; Er-Raki, S.; Ferrer, F. Partitioning evapotranspiration of a drip-irrigated wheat crop: Inter-comparing eddy covariance-, sap flow-, lysimeter-and FAO-based methods. *Agric. For. Meteorol.* **2019**, *265*, 310–326. [CrossRef]
13. Allen, R.G.; Pereira, L.S.; Raes, D.; Smith, M. Crop Evapotranspiration—Guidelines for Computing Crop Water Requirements—FAO Irrigation and Drainage Paper 56. 1998. Available online: https://www.fao.org/4/x0490e/x0490e00.htm (accessed on 14 September 2018).
14. Ndulue, E.; Ranjan, R.S. Performance of the FAO Penman-Monteith equation under limiting conditions and fourteen reference evapotranspiration models in southern Manitoba. *Theor. Appl. Climatol.* **2021**, *143*, 1285–1298. [CrossRef]
15. Meraz-Maldonado, N.; Flores-Magdaleno, H. Maize Evapotranspiration Estimation Using Penman-Monteith Equation and Modeling the Bulk Canopy Resistance. *Water* **2019**, *11*, 2650. [CrossRef]
16. Katerji, N.; Rana, G. FAO-56 methodology for determining water requirement of irrigated crops: Critical examination of the concepts, alternative proposals and validation in Mediterranean region. *Theor. Appl. Climatol.* **2013**, *116*, 515–536. [CrossRef]
17. Bastiaanssen, W.G.M.; Noordman, E.J.M.; Pelgrum, H.; Davids, G.; Thoreson, B.P.; Allen, R.G. SEBAL model with remotely sensed data to improve water-resources management under actual field conditions. *J. Irrig. Drain. Eng.* **2005**, *131*, 85–93. [CrossRef]
18. Allen, R.G.; Tasumi, M.; Trezza, R. Satellite-based energy balance for mapping evapotranspiration with internalized calibration (METRIC)—Model. *J. Irrig. Drain. Eng.* **2007**, *133*, 380–394. [CrossRef]
19. Derardja, B.; Khadra, R.; Abdelmoneim, A.A.A.; El-Shirbeny, M.A.; Valsamidis, T.; De Pasquale, V.; Deflorio, A.M.; Volden, E. Advancements in Remote Sensing for Evapotranspiration Estimation: A Comprehensive Review of Temperature-Based Models. *Remote Sens.* **2024**, *16*, 1927. [CrossRef]
20. Hendrickx, J.M.; Hong, S.H. Mapping sensible and latent heat fluxes in arid areas using optical imagery. In *Targets and Backgrounds XI: Characterization and Representation*; SPIE: Bellingham, WA, USA, 2005; Volume 5811, pp. 138–146.
21. Bhattarai, N.; Wagle, P. Recent Advances in Remote Sensing of Evapotranspiration. *Remote Sens.* **2021**, *13*, 4260. [CrossRef]
22. García-Santos, V.; Sánchez, J.M.; Cuxart, J. Evapotranspiration Acquired with Remote Sensing Thermal-Based Algorithms: A State-of-the-Art Review. *Remote Sens.* **2022**, *14*, 3440. [CrossRef]
23. Available online: https://www.usgs.gov/faqs/what-are-band-designations-landsat-satellites (accessed on 3 December 2024).
24. Available online: https://lpdaac.usgs.gov/data/get-started-data/collection-overview/missions/modis-overview/#modis-temporal-and-spatial-resolution (accessed on 3 December 2024).
25. Garofalo, S.P.; Modugno, A.F.; De Carolis, G.; Sanitate, N.; Negash Tesemma, M.; Scarascia-Mugnozza, G.; Tekle Tegegne, Y.; Campi, P. Explainable Artificial Intelligence to Predict the Water Status of Cotton (*Gossypium hirsutum* L., 1763) from Sentinel-2 Images in the Mediterranean Area. *Plants* **2024**, *13*, 3325. [CrossRef]
26. Bossung, C.; Schlerf, M.; Machwitz, M. Estimation of canopy nitrogen content in winter wheat from Sentinel-2 images for operational agricultural monitoring. *Precis. Agric.* **2022**, *23*, 2229–2252. [CrossRef]
27. Segarra, J.; Buchaillot, M.L.; Araus, J.L.; Kefauver, S.C. Remote Sensing for Precision Agriculture: Sentinel-2 Improved Features and Applications. *Agronomy* **2020**, *10*, 641. [CrossRef]
28. Helman, D.; Bahat, I.; Netzer, Y.; Ben-Gal, A.; Alchanatis, V.; Peeters, A.; Cohen, Y. Using Time Series of High-Resolution Planet Satellite Images to Monitor Grapevine Stem Water Potential in Commercial Vineyards. *Remote Sens.* **2018**, *10*, 1615. [CrossRef]
29. Breunig, F.M.; Galvão, L.S.; Dalagnol, R.; Dauve, C.E.; Parraga, A.; Santi, A.L.; Chen, S. Delineation of management zones in agricultural fields using cover–crop biomass estimates from PlanetScope data. *Int. J. Appl. Earth Obs. Geoinf.* **2020**, *85*, 102004. [CrossRef]

30. Costa, T.S.; Filgueiras, R.; dos Santos, R.A.; Cunha, F.F.d. Actual evapotranspiration by machine learning and remote sensing without the thermal spectrum. *PLoS ONE* **2023**, *18*, e0285535. [CrossRef]
31. Sharma, A.; Jain, A.; Gupta, P.; Chowdary, V. Machine learning applications for precision agriculture: A comprehensive review. *IEEE Access* **2021**, *9*, 4843–4873. [CrossRef]
32. Araújo, S.O.; Peres, R.S.; Ramalho, J.C.; Lidon, F.; Barata, J. Machine Learning Applications in Agriculture: Current Trends, Challenges, and Future Perspectives. *Agronomy* **2023**, *13*, 2976. [CrossRef]
33. Garofalo, S.P.; Giannico, V.; Lorente, B.; García, A.J.; Vivaldi, G.A.; Thameur, A.; Salcedo, F.P. Predicting carob tree physiological parameters under different irrigation systems using Random Forest and Planet satellite images. *Front. Plant Sci.* **2024**, *15*, 1302435. [CrossRef] [PubMed]
34. Liakos, K.G.; Busato, P.; Moshou, D.; Pearson, S.; Bochtis, D. Machine Learning in Agriculture: A Review. *Sensors* **2018**, *18*, 2674. [CrossRef]
35. Campi, P.; Modugno, A.F.; De Carolis, G.; Pedrero Salcedo, F.; Lorente, B.; Garofalo, S.P. A Machine Learning Approach to Monitor the Physiological and Water Status of an Irrigated Peach Orchard under Semi-Arid Conditions by Using Multispectral Satellite Data. *Water* **2024**, *16*, 2224. [CrossRef]
36. Barbedo, J.G.A. Detecting and Classifying Pests in Crops Using Proximal Images and Machine Learning: A Review. *AI* **2020**, *1*, 312–328. [CrossRef]
37. Patrício, D.I.; Rieder, R. Computer vision and artificial intelligence in precision agriculture for grain crops: A systematic review. *Comput. Electron. Agric.* **2018**, *153*, 69–81. [CrossRef]
38. Available online: https://en.climate-data.org/europa/italia/puglia/rutigliano-14028/ (accessed on 3 December 2024).
39. Lee, X.; Massman, W.; Law, B.E. Handbook of micrometeorology: A guide for surface flux measurement and analysis. In *Atmospheric and Oceanographic Sciences Library*; Springer: Dordrecht, The Netherlands, 2004.
40. Foken, T.; Aubinet, M.; Leuning, R. The eddy covariance method. In *Eddy Covariance: A Practical Guide to Measurement and Data Analysis*; Aubinet, M., Vesala, T., Papale, D., Eds.; Springer: Dordrecht, The Netherlands, 2012; pp. 1–19. [CrossRef]
41. Aubinet, M.; Grelle, A.; Ibrom, A.; Rannik, Ü.; Moncrieff, J.; Foken, T.; Kowalski, A.S.; Martin, P.H.; Berbigier, P.; Bernhofer, C.; et al. Estimates of the annual net carbon and water exchange of forests: The EUROFLUX methodology. *Adv. Ecol. Res.* **2000**, *30*, 113–175.
42. Eddy Covariance Software—EddyPro, FluxSuite, and Tovi | LI-COR Environmental. Available online: https://www.licor.com/products/eddy-covariance/eddypro (accessed on 3 December 2024).
43. Ferrara, R.M.; Azzolini, A.; Ciurlia, A.; De Carolis, G.; Mastrangelo, M.; Minorenti, V.; Montaghi, A.; Piarulli, M.; Ruggieri, S.; Vitti, C.; et al. Carbon and Water Balances in a Watermelon Crop Mulched with Biodegradable Films in Mediterranean Conditions at Extended Growth Season Scale. *Atmosphere* **2024**, *15*, 945. [CrossRef]
44. Available online: https://assets.planet.com/docs/Planet_PSScene_Imagery_Product_Spec_letter_screen.pdf (accessed on 3 December 2024).
45. Pebesma, E.; Bivand, R. *Spatial Data Science: With Applications in R*; Chapman and Hall/CRC: London, UK, 2023.
46. Hijmans, R.J.; Van Etten, J.; Mattiuzzi, M.; Sumner, M.; Greenberg, J.A.; Lamigueiro, O.P.; Shortridge, A. Raster Package in R. Version. 2013. Available online: https://cran.r-project.org/package=raster (accessed on 3 December 2024).
47. Barbedo, J.G.A. Impact of dataset size and variety on the effectiveness of deep learning and transfer learning for plant disease classification. *Comput. Electron. Agric.* **2018**, *153*, 46–53. [CrossRef]
48. Arafa, D.A.; Moustafa, H.E.D.; Ali, H.A.; Ali-Eldin, A.M.; Saraya, S.F. A deep learning framework for early diagnosis of Alzheimer's disease on MRI images. *Multimed. Tools Appl.* **2024**, *83*, 3767–3799. [CrossRef]
49. Zou, H.; Hastie, T. Regularization and Variable Selection Via the Elastic Net. *J. R. Stat. Soc. Ser. B Stat. Methodol.* **2005**, *67*, 301–320. [CrossRef]
50. Haberman, S.; Renshaw, A.E. Generalized Linear Models and Actuarial Science. *J. R. Stat. Soc. Ser. D (Stat.)* **1996**, *45*, 407–436. [CrossRef]
51. Guebel, D.V.; Torres, N.V. Partial Least-Squares Regression (PLSR). In *Encyclopedia of Systems Biology*; Dubitzky, W., Wolkenhauer, O., Cho, K.H., Yokota, H., Eds.; Springer: New York, NY, USA, 2013. [CrossRef]
52. Khan, M.A.; Memon, S.A.; Farooq, F.; Javed, M.F.; Aslam, F.; Alyousef, R. Compressive Strength of Fly-Ash-Based Geopolymer Concrete by Gene Expression Programming and Random Forest. *Adv. Civ. Eng.* **2021**, *2021*, 6618407. [CrossRef]
53. Agarwal, V.; Akyilmaz, O.; Shum, C.K.; Feng, W.; Yang, T.Y.; Forootan, E.; Uz, M. Machine learning based downscaling of GRACE-estimated groundwater in Central Valley, California. *Sci. Total Environ.* **2023**, *865*, 161138. [CrossRef]
54. Guido, R.; Ferrisi, S.; Lofaro, D.; Conforti, D. An Overview on the Advancements of Support Vector Machine Models in Healthcare Applications: A Review. *Information* **2024**, *15*, 235. [CrossRef]
55. Akiba, T.; Sano, S.; Yanase, T.; Ohta, T.; Koyama, M. Optuna: A Next-generation Hyperparameter Optimization Framework. In Proceedings of the 25th ACM SIGKDD International Conference on Knowledge Discovery & Data Mining (KDD '19), Anchorage, AK, USA, 4–8 August 2019; Association for Computing Machinery: New York, NY, USA, 2019; pp. 2623–2631. [CrossRef]

56. Oyedele, O. Determining the optimal number of folds to use in a K-fold cross-validation: A neural network classification experiment. *Res. Math.* **2023**, *10*, 2201015. [CrossRef]
57. Allgaier, J.; Pryss, R. Cross-Validation Visualized: A Narrative Guide to Advanced Methods. *Mach. Learn. Knowl. Extr.* **2024**, *6*, 1378–1388. [CrossRef]
58. Miller, T. Explanation in artificial intelligence: Insights from the social sciences. *Artif. Intell.* **2019**, *267*, 1–38. [CrossRef]
59. Strobl, C.; Boulesteix, A.L.; Kneib, T.; Augustin, T.; Zeileis, A. Conditional variable importance for random forests. *BMC Bioinform.* **2008**, *9*, 307. [CrossRef]
60. Shapley, L.S. 17. A Value for n-Person Games. In *Contributions to the Theory of Games (AM-28)*; Princeton University Press: Princeton, NJ, USA, 1953; pp. 307–318. [CrossRef]
61. Loi, C.L.; Wu, C.C.; Liang, Y.C. Prediction of Tropical Cyclogenesis Based on Machine Learning Methods and Its SHAP Interpretation. *J. Adv. Model. Earth Syst.* **2024**, *16*, e2023MS003637. [CrossRef]
62. Akkem, Y.; Biswas, S.K.; Varanasi, A. Streamlit-based enhancing crop recommendation systems with advanced explainable artificial intelligence for smart farming. *Neural Comput. Appl.* **2024**, *36*, 20011–20025. [CrossRef]
63. Vergni, L.; Todisco, F. A Random Forest Machine Learning Approach for the Identification and Quantification of Erosive Events. *Water* **2023**, *15*, 2225. [CrossRef]
64. Harrison, J.W.; Lucius, M.A.; Farrell, J.L.; Eichler, L.W.; Relyea, R.A. Prediction of stream nitrogen and phosphorus concentrations from high-frequency sensors using Random Forests Regression. *Sci. Total Environ.* **2021**, *763*, 143005. [CrossRef]
65. Lee, H.; Wang, J.; Leblon, B. Using Linear Regression, Random Forests, and Support Vector Machine with Unmanned Aerial Vehicle Multispectral Images to Predict Canopy Nitrogen Weight in Corn. *Remote Sens.* **2020**, *12*, 2071. [CrossRef]
66. Available online: https://scikit-learn.org/stable/modules/generated/sklearn.ensemble.RandomForestRegressor.html#sklearn.ensemble.RandomForestRegressor (accessed on 5 December 2024).
67. Ferreira, C.S.S.; Soares, P.R.; Guilherme, R.; Vitali, G.; Boulet, A.; Harrison, M.T.; Malamiri, H.; Duarte, A.C.; Kalantari, Z.; Ferreira, A.J.D. Sustainable Water Management in Horticulture: Problems, Premises, and Promises. *Horticulturae* **2024**, *10*, 951. [CrossRef]
68. Novielli, P.; Magarelli, M.; Romano, D.; de Trizio, L.; Di Bitonto, P.; Monaco, A.; Amoroso, N.; Stellacci, A.M.; Zoani, C.; Bellotti, R.; et al. Climate Change and Soil Health: Explainable Artificial Intelligence Reveals Microbiome Response to Warming. *Mach. Learn. Knowl. Extr.* **2024**, *6*, 1564–1578. [CrossRef]
69. Johnson, J.B. Rapid Prediction of Leaf Water Content in Eucalypt Leaves Using a Handheld NIRS Instrument. *Eng* **2023**, *4*, 1198–1209. [CrossRef]
70. Galleguillos, M.; Ulloa-Pino, J.; Munoz-Toro, N.; Perez-Quezada, J.F. Actual evapotranspiration and its relation with floristic composition and topographical features in an arid watershed. In Proceedings of the 2014 IEEE Geoscience and Remote Sensing Symposium, Quebec City, QC, Canada, 13–18 July 2014; pp. 3494–3497. [CrossRef]
71. Abbasi, N.; Nouri, H.; Didan, K.; Barreto-Muñoz, A.; Chavoshi Borujeni, S.; Opp, C.; Nagler, P.; Thenkabail, P.S.; Siebert, S. Mapping Vegetation Index-Derived Actual Evapotranspiration across Croplands Using the Google Earth Engine Platform. *Remote Sens.* **2023**, *15*, 1017. [CrossRef]
72. Li, H.; Lascano, R.J.; Barnes, E.M.; Booker, J.; Wilson, L.T.; Bronson, K.F.; Segarra, E. Multispectral Reflectance of Cotton Related to Plant Growth, Soil Water and Texture, and Site Elevation. *Agron. J.* **2001**, *93*, 1327–1337. [CrossRef]
73. Zahir, S.A.D.M.; Jamlos, M.F.; Omar, A.F.; Jamlos, M.A.; Mamat, R.; Muncan, J.; Tsenkova, R. Review–Plant nutritional status analysis employing the visible and near-infrared spectroscopy spectral sensor. *Spectrochim. Acta Part A Mol. Biomol. Spectrosc.* **2024**, *304*, 123273. [CrossRef]
74. Koehler, T.; Wankmüller, F.J.P.; Sadok, W.; Carminati, A. Transpiration response to soil drying versus increasing vapor pressure deficit in crops: Physical and physiological mechanisms and key plant traits. *J. Exp. Bot.* **2023**, *74*, 4789–4807. [CrossRef]
75. Adams, M.L.; Philpot, W.D.; Norvell, W.A. Yellowness index: An application of spectral second derivatives to estimate chlorosis of leaves in stressed vegetation. *Int. J. Remote Sens.* **1999**, *20*, 3663–3675. [CrossRef]
76. Gao, Y. Influencing factors for transpiration rate: A numerical simulation of an individual leaf system. *Therm. Sci. Eng. Prog.* **2022**, *27*, 101110. [CrossRef]
77. Ha, W.; Kolb, T.E.; Springer, A.E.; Dore, S.; O'Donnell, F.C.; Martinez Morales, R.; Koch, G.W. Evapotranspiration comparisons between eddy covariance measurements and meteorological and remote-sensing-based models in disturbed ponderosa pine forests. *Ecohydrology* **2015**, *8*, 1335–1350. [CrossRef]
78. Gao, G.; Zhang, X.; Yu, T.; Liu, B. Comparison of three evapotranspiration models with eddy covariance measurements for a *Populus euphratica* Oliv. forest in an arid region of northwestern China. *J. Arid. Land* **2016**, *8*, 146–156. [CrossRef]
79. Attia, A.; El-Hendawy, S.; Al-Suhaibani, N.; Alotaibi, M.; Tahir, M.U.; Kamal, K.Y. Evaluating deficit irrigation scheduling strategies to improve yield and water productivity of maize in arid environment using simulation. *Agric. Water Manag.* **2021**, *249*, 106812. [CrossRef]
80. Wang, Z.; Yu, S.; Zhang, H.; Lei, L.; Liang, C.; Chen, L.; Li, X. Deficit mulched drip irrigation improves yield, quality, and water use efficiency of watermelon in a desert oasis region. *Agric. Water Manag.* **2023**, *277*, 108103. [CrossRef]

81. Yavuz, D.; Seymen, M.; Yavuz, N.; Çoklar, H.; Ercan, M. Effects of water stress applied at various phenological stages on yield, quality, and water use efficiency of melon. *Agric. Water Manag.* **2021**, *246*, 106673. [CrossRef]
82. Pereira, L.S.; Paredes, P.; Jovanovic, N. Soil water balance models for determining crop water and irrigation requirements and irrigation scheduling focusing on the FAO56 method and the dual Kc approach. *Agric. Water Manag.* **2020**, *241*, 106357. [CrossRef]
83. Wu, R.; Liu, Y.; Xing, X. Evaluation of evapotranspiration deficit index for agricultural drought monitoring in North China. *J. Hydrol.* **2021**, *596*, 126057. [CrossRef]
84. Chen, L.-H.; Chen, J.; Chen, C. Effect of Environmental Measurement Uncertainty on Prediction of Evapotranspiration. *Atmosphere* **2018**, *9*, 400. [CrossRef]
85. Mata-González, R.; McLendon, T.; Martin, D.W. The Inappropriate Use of Crop Transpiration Coefficients (K_c) to Estimate Evapotranspiration in Arid Ecosystems: A Review. *Arid. Land Res. Manag.* **2005**, *19*, 285–295. [CrossRef]
86. Subedi, A.; Chávez, J.L. Crop evapotranspiration (ET) estimation models: A review and discussion of the applicability and limitations of ET methods. *J. Agric. Sci.* **2015**, *7*, 50. [CrossRef]

Disclaimer/Publisher's Note: The statements, opinions and data contained in all publications are solely those of the individual author(s) and contributor(s) and not of MDPI and/or the editor(s). MDPI and/or the editor(s) disclaim responsibility for any injury to people or property resulting from any ideas, methods, instructions or products referred to in the content.

water

MDPI

Article

Optimizing Irrigation and Nitrogen Application for Greenhouse Tomato Using the DSSAT–CROPGRO–Tomato Model

Zhijie Shan [1,2], Junwei Chen [1,3], Xiping Zhang [4], Zhuanyun Si [5,*], Ruochen Yi [1,3] and Haiyan Fan [1,*]

[1] Beijing Water Science and Technology Institute, Beijing 100048, China; shanzhj@iwhr.com (Z.S.); chenjunwei202204@163.com (J.C.); yiruochen1@163.com (R.Y.)
[2] State Key Laboratory of Simulation and Regulation of Water Cycle in River Basin, China Institute of Water Resources and Hydropower Research, Beijing 100048, China
[3] College of Water Conservancy Engineering, Tianjin Agricultural University, Tianjin 300392, China
[4] College of Urban and Rural Construction, Hebei Agricultural University, Baoding 071001, China; xpzhang1@hebau.edu.cn
[5] Institute of Farmland Irrigation, Chinese Academy of Agricultural Sciences/Key Laboratory of Crop Water Use and Regulation, Ministry of Agriculture and Rural Affairs, Xinxiang 453002, China
* Correspondence: sizhuanyun@caas.cn (Z.S.); fanhaiyan0402@163.com (H.F.)

Abstract: The aim of this study was to optimize water-saving and high-efficiency irrigation and nitrogen application scheduling for greenhouse tomato cultivation in North China. Using experimental data on water and nitrogen inputs, the DSSAT-GLUE parameter adjustment tool was employed to calibrate the genetic parameters of the DSSAT–CROPGRO–Tomato model. Simulations were conducted to assess greenhouse tomato growth, water use, and yield under varying water and nitrogen conditions. After calibration, the model showed average relative errors of 3.19% for the phenological stages, 3.33% for plant height, and 4.52% for yield dry weight, meeting accuracy standards. The results from the calibrated model indicated that increasing irrigation or nitrogen levels initially enhanced yield but led to diminishing returns beyond optimal ranges. The maximum tomato yield and water–nitrogen use efficiency were achieved with irrigation quotas between 320 and 340 mm and nitrogen applications between 360 and 400 kg·ha^{-1}. These findings provide a guideline for efficient water and nitrogen management for greenhouse tomatoes under drip irrigation conditions.

Keywords: DSSAT–CROPGRO–Tomato model; greenhouse; tomato; water and nitrogen management; yield; scenario simulation

1. Introduction

Tomato (*Solanum lycopersicum* L.) is among the most widely cultivated and popular vegetable crops globally [1], with China leading in terms of both the tomato planting area and total yield [2]. The manual adjustment of greenhouse environments to optimize tomato growth plays a crucial role in meeting the demands of climate variability and the increasing year-round need for high-quality produce. Water is essential to fertilizer efficiency, and fertilizer, in turn, is critical to enhancing water and soil productivity [3]. With modern agriculture advancing rapidly, irrigation and fertilizer application have become key strategies for ensuring high-quality and stable greenhouse crop yields. To maximize economic benefits, farmers often increase water and fertilizer application rates to boost yields. While this approach may provide short-term gains, excessive and unscientific inputs can increase production costs and reduce resource use efficiency. It can also increase the risk of greenhouse gas emissions, nitrate leaching, soil salinization, and pest and disease outbreaks. These issues hinder the sustainable and efficient development

of controlled environment agriculture [4]. Thus, establishing precise irrigation and nitrogen application systems is essential for promoting sustainable agricultural practices.

Considerable research on water-saving, high-yield irrigation methods for greenhouse tomatoes has been conducted both domestically and internationally, producing substantial insights [5–10]. However, due to differences in experimental objectives and regional conditions, these findings have some limitations. In recent years, combining field experiments with crop growth models has become a valuable approach for optimizing cultivation management. The DSSAT model is one of the most popular crop growth models globally [11–14]. The model integrates climate, soil, crop, and field management modules to simulate crop growth dynamics on a daily scale, providing quantitative insights into the relationships between crop growth and environmental factors [15]. The model's accuracy has been significantly increased after extensive improvements and regional validations [16–19]. DSSAT has been used by many researchers to optimize irrigation schedules for crops like winter wheat [20], tomato [21], and corn [22]. For instance, Si et al. [23] optimized irrigation and nitrogen application rates for winter wheat under drip irrigation conditions in North China using the DSSAT–CERES–Wheat model.

Efficient water and nitrogen management is vital for high-quality greenhouse tomato production amid increasing land and water scarcity and ongoing environmental degradation [24]. Therefore, the DSSAT–CROPGRO–Tomato model was used in this study to simulate the growth dynamics and resource use efficiency of tomatoes in various water and nitrogen application scenarios. The findings will offer technical support for optimizing irrigation and nitrogen schedules to promote high-quality, efficient tomato production in greenhouse environments.

2. Materials and Methods

2.1. Field Experiment

The experiment was conducted in a solar greenhouse in the Yongledian Experimental Base (N 39°20′, E 116°20′, altitude 12 m) in 2022. The average annual rainfall and potential evaporation in the area was 565 mm and 1140 mm, the average annual temperature was 11.5 °C, and the frost-free period was 185 days. The daily temperatures in the greenhouse during the experiment are shown in Figure 1. The soil texture of the experimental field was loamy (sand/silt/clay: 12.44%/44.37%/43.19%). The soil bulk weight was 1.40 $g \cdot cm^{-1}$, the saturated water content was 34.44 $cm^3 \cdot cm^{-3}$, the field water holding capacity was 29.96 $cm^3 \cdot cm^{-3}$, the soil electric conductivity was 36.0 $mS \cdot cm^{-1}$, the cation exchange capacity (CEC) was 11.3 $cmol \cdot kg^{-1}$, and the groundwater mineralization was 802.3 $mg \cdot L^{-1}$. The depth of the groundwater was more than 8 m. The physicochemical properties of the soil in the 0~60 cm soil layer are shown in Table 1.

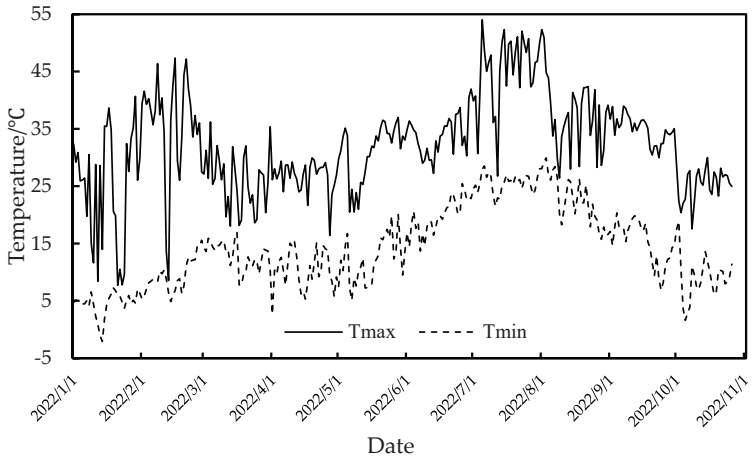


Figure 1. The air temperature in the greenhouse during the experiment.

Table 1. Physicochemical properties of the soil in the 0~60 cm soil layer.

Soil Layer (cm)	Ammonium N (mg·kg^{-1})	Nitrate-N (mg·kg^{-1})	Total Organic Carbon (g·kg^{-1})	Total Carbon (g·kg^{-1})	Total Nitrogen (g·kg^{-1})	pH	Soil Texture (%)		
							Sand <0.002 mm	Silt 0.002–0.02 mm	Clay 0.02–2 mm
0~10	86.043 ± 0.07	39.031 ± 0.09	14.19 ± 0.08	22.85 ± 0.16	1.72 ± 0.02	7.33 ± 0.02	11.64 ± 0.08	44.08 ± 0.07	44.28 ± 0.09
10~20	83.952 ± 0.08	15.497 ± 0.08	12.89 ± 0.07	17.66 ± 0.12	1.38 ± 0.03	7.99 ± 0.03	12.06 ± 0.07	43.39 ± 0.09	44.55 ± 0.11
20~30	31.413 ± 0.43	5.953 ± 0.10	5.03 ± 0.05	16.81 ± 0.08	1.00 ± 0.03	8.05 ± 0.05	13.33 ± 0.07	47.92 ± 0.07	38.75 ± 0.12
30~40	46.513 ± 0.02	13.34 ± 0.08	7.47 ± 0.08	16.94 ± 0.09	1.12 ± 0.02	7.99 ± 0.02	12.77 ± 0.08	43.5 ± 0.07	43.74 ± 0.08
40~60	22.559 ± 0.13	6.133 ± 0.07	3.56 ± 0.07	21.13 ± 0.06	0.76 ± 0.01	8.1 ± 0.03	12.38 ± 0.05	42.98 ± 0.06	44.64 ± 0.07

The tomato variety "Caomei 3" was used in the experiment, and the supplier was the Beijing Academy of Agriculture and Forestry Sciences. This variety is an infinite-growth, flavorful tomato. The plant is vigorous, with good comprehensive disease resistance. The fruit is a beautiful, deep pink color, and it has good properties of hardness, storage, and transportation resistance. Controlled water cultivation is favorable to enhance the sugar level and taste. The tomatoes were planted on 20 January 2022 and transplanted on 18 February 2022, with row spacing of 45 cm and plant spacing of 35 cm. The experiment was a two-factor split-plot design. The main block was the irrigation water treatment, and the irrigation water quota was set to the following three levels based on crop evapotranspiration (ET_C): 100% ET_C, 20 mm (I1); 85% ET_C, 17 mm (I2); and 70% ET_C, 14 mm (I3). Groundwater was used for irrigation, and each irrigation cycle lasted 7 days. In the secondary area, four levels of nitrogen fertilizer were applied: 220, 180, 160, and 140 kg·ha^{-1} (N1, N2, N3 and N4, respectively), and urea was used for fertilizer. The two factors were completely combined for a total of 12 treatments (Table 2). Each treatment was repeated 3 times for a total of 36 plots, with 0.5 m wide protective rows between each plot (Figure 2).

Table 2. Irrigation levels and nitrogen rates during tomato growth periods.

Treatment	Irrigation (mm)	Nitrogen Application (kg·ha^{-1})
I1N1	100% ET_C, 20	220
I1N2	100% ET_C, 20	180
I1N3	100% ET_C, 20	160
I1N4	100% ET_C, 20	140
I2N1	85% ET_C, 17	220
I2N2	85% ET_C, 17	180
I2N3	85% ET_C, 17	160
I2N4	85% ET_C, 17	140
I3N1	70% ET_C, 14	220
I3N2	70% ET_C, 14	180
I3N3	70% ET_C, 14	160
I3N4	70% ET_C, 14	140

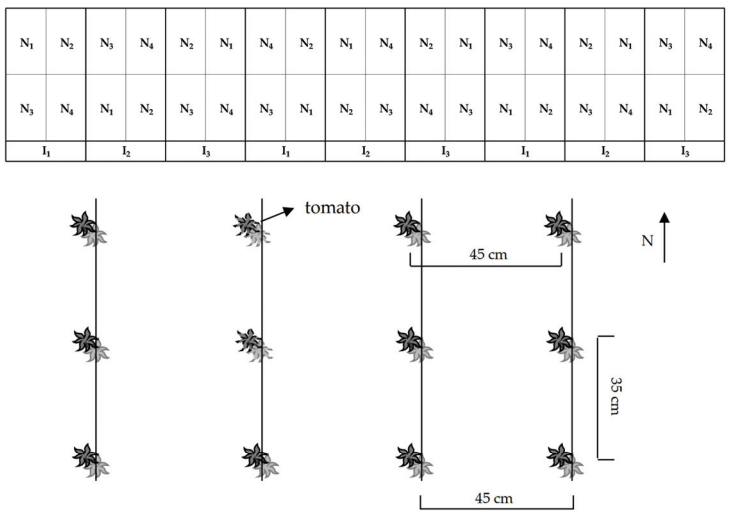


Figure 2. Layout of the experimental area.

2.2. DSSAT–CROPGRO–Tomato Model

The DSSAT model mainly includes soil water balance, nitrogen balance, phenological development, soil–plant atmosphere (SPAM), and growth development modules. The main function is to provide help with decision-making and support for the rational utilization of all types of resources in agricultural production [15,25]. The nitrogen balance module simulates nitrogen accumulation based on available nitrogen in the soil and nitrogen requirements of crops. The effective absorption of nitrogen from soil by crops depends on the concentration of available nitrogen in soil, the status of root development and the water table. Crop nitrogen requirements affect plant growth, nitrogen concentration in organs and critical nitrogen concentration [26,27]. The model incorporates atmospheric, plant, and soil data to calculate potential evapotranspiration, plant transpiration, soil evaporation, and root water uptake. There are two methods for calculating evapotranspiration in the model, the Penman–FAO method or the Priestley–Teller method, where the Priestley–Teller method only requires daily solar radiation and temperature. In this study, evapotranspiration was calculated using the Priestley–Teller method. Actual soil evaporation and plant transpiration were calculated by evapotranspiration [15,23]. The CROPGRO–Tomato model in the DSSAT system is used to simulate the physiological and growth dynamics of the tomato, such as leaf photosynthesis, plant respiration, dry matter accumulation and transformation, and plant response to environmental factors. The CROPGRO–Tomato model mainly includes data, simulation, analysis, and tool modules [15,28].

2.3. Model Parameters Rates

Crop variety parameters are often obtained using different parameter estimation methods. Among them, the Generalized Likelihood Uncertainty Estimation (GLUE) method has been made into a built-in parameter estimation program of the DSSAT model which can be used directly by users [29,30]. The measured indexes (phenological period, aboveground dry mass, dried fruit yield, and fresh fruit yield) in adequate water and nitrogen treatment (I1N1 and I1N2) from a field experiment in 2022 were used to determine the tomato genetic parameters required in the model in this study. First, a set of initial values required for model operation is set, and then a reliable set of genetic parameter combinations was obtained after 20,000 iterations by using the DSSAT-GLUE method (Table 3).

Table 3. Range and calibration value of genetic parameters in the model.

Parameters	Define	Realm	Calibration Value
EM-FL	Time between plant emergence and flower appearance (°C·d^{-1})	7~35	30.42
FL-SH	Time between first flower and first pod (°C·d^{-1})	1~9	3.833
FL-SD	Time between first flower and first seed (°C·d^{-1})	15~20	19.50
SD-PM	Time between first seed and physiological maturity (°C·d^{-1})	45~55	45.16
LFMAX	Maximum leaf photosynthesis rate at 30 C, 350 vpm CO_2, and high light (mg·m^{-2}·s^{-1}, in CO_2)	1~1.4	1.10
SLAVR	Specific leaf area of cultivar under standard growth conditions (cm^2·g^{-1})	300~380	380
XFRT	Maximum fraction of daily growth that is partitioned to seed + shell	0.65~0.85	0.744
SFDUR	Seed filling duration for pod cohort at standard growth conditions (°C·d^{-1})	23~27	26.03
PODUR	Time required for cultivar to reach final pod load under optimal conditions (°C·d^{-1})	40~65	57.12
THRSH	Threshing percentage. The maximum ratio of (seed/(seed + shell)) at maturity. Causes seed to stop growing as their dry weight increases until the shells are filled in a cohort.	7~10	8.50

Using the calibration parameters in Table 3, the model was evaluated under different water and nitrogen conditions (I1N3 treatment ~ I3N4 treatment in 2022), including the phenological period, average stem and leaf number, canopy height, and dry matter mass in

the ground and tomato yield. The simulated and measured values based on the calibrated CROPGRO–Tomato model are shown in Table 4.

Table 4. Calibration and validation results of the CROPGRO–Tomato model.

	Treatment	Anthesis Date (d)			Maturity Date (d)			Fruit Yield (kg·ha^{-1})			Aboveground Biomass (kg·ha^{-1})			Plant Height (m)		
		Sim	Mea	ARE	Sim	Mea	ARE	Sim	Mea	ARE	Sim	Mea	ARE	Sim	Mea	ARE
Model validation	I1N3	24	25	4	118	116	1.7	5532	5548	0.3	10,510	10,298	2.1	1.25	1.23	1.6
	I1N4	24	25	4	118	115	2.6	4979	4915	1.3	9710	9113	6.6	1.22	1.15	6.1
	I2N1	24	23	4.3	118	117	0.9	7083	7014	1	12,390	12,685	2.3	1.31	1.3	0.8
	I2N2	24	23	4.3	118	116	1.7	6025	6059	0.6	11,030	12,142	9.2	1.28	1.25	2.4
	I2N3	24	24	0	118	115	2.6	5399	5519	2.2	10,230	10,277	0.5	1.26	1.21	4.1
	I2N4	24	24	0	118	115	2.6	4931	4925	0.1	9540	9140	4.4	1.24	1.18	5.1
	I3N1	24	23	4.3	118	120	1.7	5685	6265	9.3	10,240	11,771	13	1.29	1.26	2.4
	I3N2	24	23	4.3	118	119	0.8	4888	5546	11.9	9230	10,334	10.7	1.26	1.22	3.3
	I3N3	24	22	9.1	118	121	2.5	4600	5046	8.8	8710	9313	6.5	1.25	1.21	3.3
	I3N4	24	22	9.1	118	122	3.3	4151	4598	9.7	8060	8664	7	1.24	1.19	4.2
	averages			4.34			2.04			4.52			6.23			3.33
	RMSE		1.18			2.57			345.37			786.02			0.04	
	nRMSE		5.06			2.18			6.23			7.58			3.57	

Notes: Sim, simulated value; Mea, measured value; ARE, absolute relative error, %. RMSE, root mean square error, %. nRMSE, normalized root mean square error, %.

In this study, a variety of statistical methods were selected as validation and evaluation indicators to evaluate the reliability of the model calibration and validation results, including absolute relative error (ARE), root mean square error (RMSE), and normalized root mean square error (nRMSE).

The absolute relative error (ARE) refers to the ratio of the absolute error caused by the simulation to the true value multiplied by 100%. The smaller the value of ARE, the higher the simulation accuracy of the model [31]. The calculation formula is as follows:

$$ARE = \frac{|S_i - O_i|}{O_i} \times 100\% \quad (1)$$

The root mean square error (RMSE) refers to the average difference between the simulated and actual values of a model. The calculation formula is as follows:

$$RMSE = \sqrt{\sum_{i=1}^{n} \frac{(S_i - O_i)^2}{n}} \quad (2)$$

The normalized root mean square error (nRMSE) measures the accuracy of a model by comparing simulated and observed values normalized to the mean of the observed data. The equation is as follows:

$$nRMSE = \frac{\sqrt{\sum_{i=1}^{n} \frac{(S_i - O_i)^2}{n}}}{\overline{O}} \times 100 \quad (3)$$

where O_i is the observed value at different growth stages; S_i is the simulated value; and $\overline{O}$ is the observed average value. When nRMSE < 10%, the analog value accuracy is very good; when 10% $\leq$ nRMSE $\leq$ 20%, the analog value accuracy is good; when 20% $\leq$ nRMSE $\leq$ 30%, the analog value accuracy is fair; and when nRMSE > 30%, the analog value accuracy is poor [20].

2.4. Irrigation and Nitrogen Management Scenario Setting

After calibration and validation, different levels of irrigation and nitrogen application were set up based on the CROPGRO–Tomato model to simulate the growth characteristics, yield, and water- and nitrogen-use efficiency of tomato. In this study, the total irrigation amount were set to 260, 280, 300, 320, 340, 360, 380, and 400 mm, a total of 8 levels.

Eight nitrogen application levels were set to 200, 240, 280, 320, 360, 400, 440, and 480 kg·ha^{-1}, and the two factors were completely combined to form 64 treatments (Table 5). According to the results of the field experiment, 20 irrigation periods and 4 nitrogen applications were set during the growth period, and the irrigation cycle was 7 days. The first nitrogen application was carried out at the time of tomato transplanting, the second nitrogen application was carried out when the diameter of the first tomato crop reached 1.5~2.5 cm, the third was performed when the diameter of the second fruit grew to 3 cm in size, and the fourth was conducted when the diameter of the third fruit grew to 3 cm in size.

Table 5. Different water and nitrogen application scenarios.

Scenario No.	Irrigation Amount (mm)	Nitrogen Application (kg·ha^{-1})	Scenario No.	Irrigation Amount (mm)	Nitrogen Application (kg·ha^{-1})
1	260	200	33	340	200
2	260	240	34	340	240
3	260	280	35	340	280
4	260	320	36	340	320
5	260	360	37	340	360
6	260	400	38	340	400
7	260	440	39	340	440
8	260	480	40	340	480
9	280	200	41	360	200
10	280	240	42	360	240
11	280	280	43	360	280
12	280	320	44	360	320
13	280	360	45	360	360
14	280	400	46	360	400
15	280	440	47	360	440
16	280	480	48	360	480
17	300	200	49	380	200
18	300	240	50	380	240
19	300	280	51	380	280
20	300	320	52	380	320
21	300	360	53	380	360
22	300	400	54	380	400
23	300	440	55	380	440
24	300	480	56	380	480
25	320	200	57	400	200
26	320	240	58	400	240
27	320	280	59	400	280
28	320	320	60	400	320
29	320	360	61	400	360
30	320	400	62	400	400
31	320	440	63	400	440
32	320	480	64	400	480

2.5. Measurement Items and Methods

2.5.1. Soil Moisture Content

The soil moisture content was measured using the soil drying method in layers (0–20, 20–40, 40–60, 60–80, and 80–100 cm) before planting, before and after irrigation, and after harvesting.

2.5.2. Dry Matter Accumulation

Tomato plants were sampled at harvest, and the plants were classified according to organs such as stems, leaves, and fruits. All organs were dried in an oven at 105 °C for 0.5 h, and then in an oven at 75 °C to constant weight. The dry weight of each organ was weighed separately.

2.5.3. Yield and Economic Benefit

Yield is calculated by multiplying the average yield per plant by planting density. Net income is obtained by subtracting total input from total income. The calculation formula is as follows:

$$Net\ income = (Y \times P) - (W \times C_1 + N \times C_2) - V \quad (4)$$

where Y (kg·ha^{-1}) is the simulated fruit yield, P is the fruit yield price (4.0 CNY·kg^{-1}), W is the irrigation water amount (m^3·ha^{-1}), C_1 and C_2 are the water and urea prices (5.0 CNY·m^{-3} and 2.5 CNY·kg^{-1}). V is the fixed inputs in production, including seeds, machinery, herbicides, pesticides, harvesting, and labor costs.

2.5.4. Assessment Criteria

The tomato water consumption (ET_C, mm), water-use efficiency (WUE, kg·m^{-3}), nitrogen partial factor productivity ($NPFP$, kg·kg^{-1}), harvest index (HI, kg·kg^{-1}), yield, and economics were used to assess the optimal water and nitrogen application schedule.

Based on the water balance equation, the water consumption for each treatment was calculated using Equation (5) [32]. The contribution of groundwater recharge to tomato water consumption was negligible (K = 0), given that the groundwater depth in the experimental area exceeded 8 m. Additionally, as the experiment was conducted in a greenhouse, there was no effective precipitation throughout the tomato growth period; thus, P_0 = 0. Field observations of soil moisture indicated that for irrigation levels below 20 mm, irrigation had minimal impact on soil moisture content below 60 cm depth, and there was no deep leakage (D = 0) [33]. Consequently, Equation (5) was simplified to Equation (6).

$$ET_C = P_0 + K + M - D + (W_0 - W_t) \quad (5)$$

$$ET_C = M + (W_0 - W_t) \quad (6)$$

where ET_C is tomato water consumption (mm); P_0 is precipitation (mm); K is the amount of groundwater recharge (mm); M is the irrigation depth (mm); D is the amount of water that seeps into the soil below 100 cm (mm); W_0 and W_t are the soil water storage (mm) at the beginning and end of the season, respectively.

The water-use efficiency was calculated using Equation (7):

$$WUE = Y/ET_C \quad (7)$$

where WUE denotes water-use efficiency (kg·m^{-3}) and Y denotes the fresh weight of the tomato yield (kg·ha^{-1}).

The nitrogen partial factor productivity was calculated using Equation (8):

$$NPFP = Y/N \quad (8)$$

where $NPFP$ represents the partial productivity of the nitrogen fertilizer (kg·kg^{-1}), and N is the total nitrogen application (kg·ha^{-1}) in the whole growth period of the greenhouse tomato.

The harvest index is the ratio of economic yield (seeds, fruits, etc.) to the aboveground biomass of a crop at harvest. It reflects the proportion of the crop's assimilated products distributed among the seeds and nutrient organs and the ability of a crop population to convert photosynthetically assimilated substances into economic products. The harvest index is an important indicator for evaluating the yield level of crop varieties and the effectiveness of cultivation. It was calculated using Formula (9):

$$HI = Y/BY \quad (9)$$

where HI represents the harvest index ($kg \cdot kg^{-1}$), and BY is the aboveground biomass ($kg \cdot ha^{-1}$).

3. Results

3.1. Calibration and Validation of CROPGRO–Tomato Model

3.1.1. Phenology

As can be seen from Table 4, water stress, nitrogen fertilizer stress, or their interaction can affect the flowering and maturity stages. Further analysis showed that the simulated values of the flowering and maturity stages subjected to the water and nitrogen stress treatment were different from the measured values. The ARE values for water and nitrogen stress treatment I3N4 were 9.1% and 3.3% at flowering and maturity, respectively. This treatment had higher ARE values than all other treatments. The absolute relative error (ARE) of simulated values and measured values at the flowering and maturity stages for different treatments ranged from 0 to 9.1% and 0.8% to 3.3%, respectively. The ARE of simulated values and measured values at the flowering stage was less than 5% in all treatments except for the I3N3 and I3N4 treatments, and the ARE of simulated values and measured values at the maturity stage was less than 3% in all treatments. The normalized root mean square error (nRMSE) values were 5.06% and 2.18% at anthesis and maturity, respectively, both less than 10%. This shows that the phenological period of greenhouse tomato can be simulated by using the fixed parameters.

3.1.2. Yield and Aboveground Biomass

The ARE values of tomato yield dry weight ranged from 0.10% to 11.9%, with an average value of 4.52%. The ARE values of aboveground dry matter mass ranged from 0.5% to 10.7%, with an average of 6.23%. By comparing the ARE values of each treatment, it was found that the ARE values of tomato yield dry weight with the I3N1, I3N2, I3N3, and I3N4 treatments were 9.3%, 11.9%, 8.8%, and 9.7%, respectively. The ARE values of the aboveground dry matter mass of the I1N4, I2N2, I3N1, I3N2, I3N3, and I3N4 treatments were 6.6%, 9.2%, 13%, 10.7%, 6.5%, and 7.0%, respectively. The simulated values of these treatments differed greatly from the measured values, mainly due to the effect of moisture. The yield simulation was better in the treatments with adequate water supply, while the ARE values of the yield of the water-stressed treatments were large, and the simulation was slightly poorer. The I3N4 treatment exhibited an especially severe water and nitrogen deficit. The unnatural deficit of water and nitrogen prevented the tomatoes from growing normally. This resulted in abnormal yield formation, which led to a large simulation error. The nRMSE values for tomato yield dry weight and aboveground dry matter mass were 6.23% and 7.58%, respectively, which were less than 10%. This indicates that the rate-set parameters simulated greenhouse tomato yield and aboveground biomass well.

3.1.3. Plant Height

As can be seen from Table 4, the ARE values of the plant height of each treatment ranged from 0.8% to 6.1%. The absolute value of relative error for most of the treatments was less than 5%. The nRMSE value of plant height was 3.57%, which was less than 10%.

This indicates that the model can better simulate the plant height growth of greenhouse tomato under different water and nitrogen supply conditions. It is shown based on the comparison of the ARE and nRMSE values of the indicators that the calibrated CROPGRO–Tomato model has a high simulation accuracy, and can be used to simulate the effects of different water and nitrogen treatments on tomato growth and yield formation indicators.

3.2. Optimization of Water and Nitrogen Schedule Based on the DSSAT–CROPGRO–Tomato Model

3.2.1. Influence of Water and Nitrogen Coupling on Water Consumption of Tomato in Greenhouse

The improved CROPGRO–Tomato model was used to simulate the water consumption of greenhouse tomatoes under varying water and nitrogen supply conditions. The simulation results (Figure 3) indicated that water consumption increased at higher irrigation levels. Specifically, when irrigation exceeded 320 mm, the nitrogen input did not significantly impact water consumption with the same irrigation quota. Conversely, when irrigation was below 340 mm, variations in nitrogen application rates substantially affected water consumption, with the differences becoming more pronounced as irrigation decreased. At an irrigation level of 400 mm, water consumption across all nitrogen treatments remained consistent at 371 mm. At an irrigation level of 320 mm, water consumption across nitrogen treatments ranged from 347 to 352 mm, and at 260 mm, it varied between 303 and 314 mm. Notably, under the same irrigation conditions, nitrogen supply changes had minimal impact on water consumption. Under the same nitrogen application rate, water consumption increased with the increase in irrigation levels. Further analysis revealed that with nitrogen rates between 200 and 480 kg·ha^{-1}, water consumption followed an upward trend as irrigation increased, ranging from 310 to 371 mm, with no significant differences across nitrogen groups.

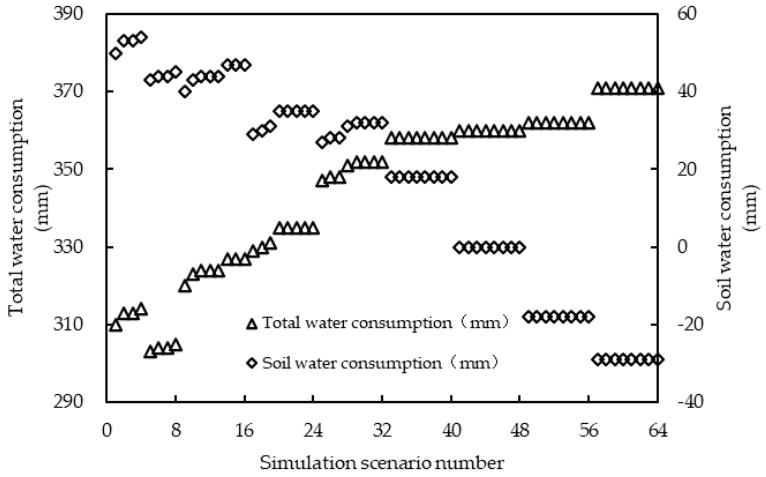


Figure 3. Effect of water–nitrogen coupling on water consumption of greenhouse tomatoes.

Soil water consumption, on the other hand, decreased as irrigation increased. When irrigation exceeded 340 mm, water consumption was predominantly from irrigation, and soil water storage remained consistent. When irrigation was below 320 mm, the proportion of soil water consumption relative to total water consumption increased as irrigation decreased. At an irrigation level of 260 mm, the proportion of soil water consumption across nitrogen treatments ranged from 14.75% to 17.20%, with an increasing trend in soil water consumption observed as nitrogen application rates rose, though differences among treatments were minimal. These findings underscore that irrigation levels are the primary factor influencing water consumption. Both total water consumption and soil

water consumption increased with the amount of nitrogen applied when irrigation was between 280 and 320 mm, but no deep leakage was observed.

3.2.2. Effect of Water–Nitrogen Coupling on Greenhouse Tomato Yield

The simulation results for greenhouse tomato yield under varying water and nitrogen supply conditions (Figure 4) showed an increasing trend with increasing irrigation levels. However, when irrigation exceeded 320 mm, the yield response to further irrigation began to plateau. Within the irrigation range of 260~400 mm, the tomato yield increased consistently with an increase in nitrogen application at the same irrigation level. In particular, when irrigation ranged from 320 to 340 mm, yields across nitrogen treatments were high and demonstrated a positive trend with additional nitrogen input. However, when nitrogen application exceeded 360 kg·ha^{-1}, further increases in nitrogen yielded only marginal gains in yield, indicating a diminishing response to nitrogen fertilization. Furthermore, as nitrogen application increased, the harvest index within the same irrigation treatments either stabilized or slightly declined once nitrogen levels surpassed 360 kg·ha^{-1}, even while maintaining high yield levels.

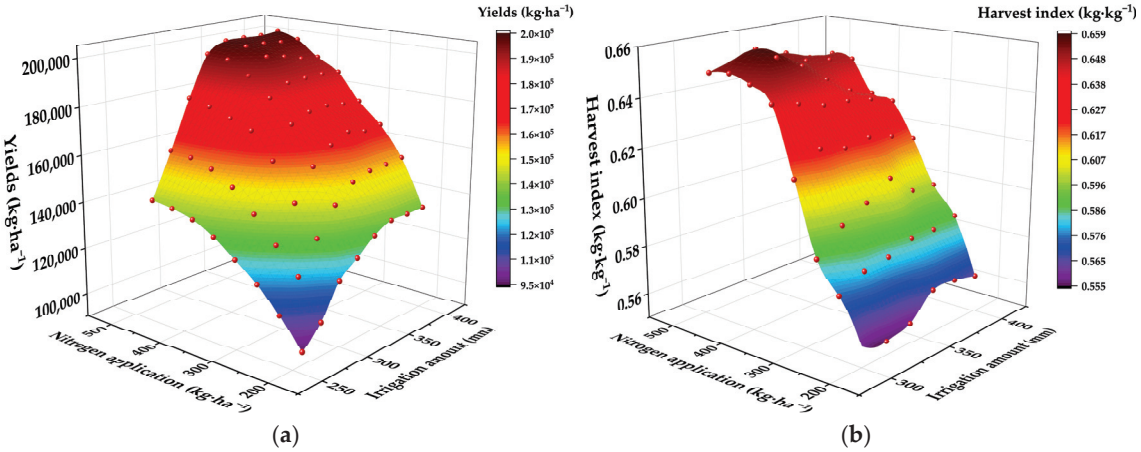


Figure 4. Effect of different water–nitrogen coupling schemes on yield (**a**) and harvest index (**b**) of greenhouse tomatoes.

3.2.3. Effect of Water–Nitrogen Coupling on Water- and Nitrogen-Use Efficiency of Greenhouse Tomatoes

Water-use efficiency (WUE) (Figure 5) and nitrogen partial factor productivity (NPFP) (Figure 6) were calculated based on the simulation results for greenhouse tomato yield and water consumption in various water–nitrogen coupling scenarios, using Equations (7) and (8). As shown in Figures 5 and 6, under the same irrigation conditions, WUE exhibited an increasing trend with an increase in nitrogen fertilizer input. However, when nitrogen input exceeded 360 kg·ha^{-1}, the rate of increase in WUE began to slow due to the synergistic effects of nitrogen fertilization. At a given nitrogen application level, when irrigation exceeded 320 mm, the positive effect of additional irrigation on WUE diminished. NPFP initially increased at higher irrigation levels under the same nitrogen conditions, then stabilized and eventually declined. Conversely, under a fixed irrigation level, NPFP decreased as nitrogen input increased.

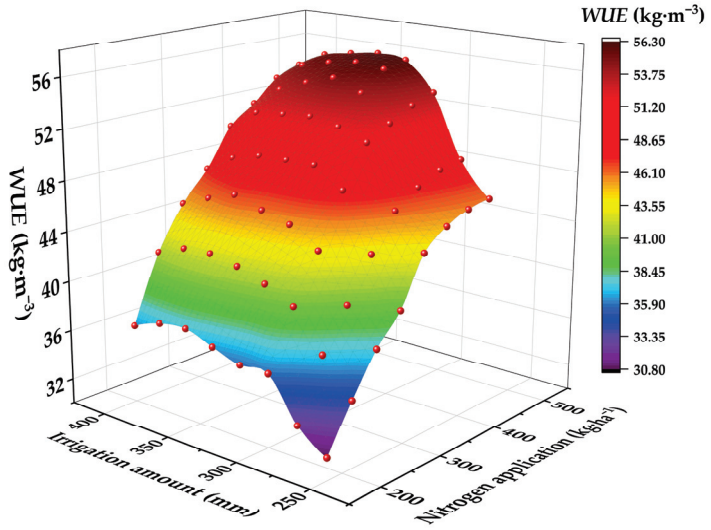


Figure 5. WUE of tomato in different water–nitrogen coupling scenarios.

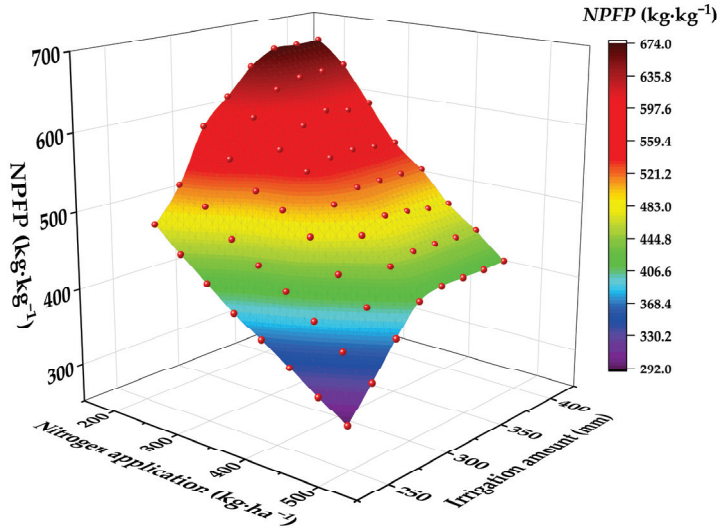


Figure 6. NPFP of tomato in different water–nitrogen coupling scenarios.

Scenarios 28~30 and 36~37 emerged as optimal water–nitrogen treatments under the experimental conditions considering economic yield, water-use efficiency, and nitrogen partial factor productivity, comprehensively. The recommended irrigation quota for greenhouse tomatoes is 320~340 mm, with a corresponding nitrogen application rate of 360~400 kg·ha^{-1}. These findings provide a robust theoretical basis for agricultural practices in this region, supporting high-yield, high-efficiency, and sustainable greenhouse tomato production.

3.3. Economic Benefit

Figure 7 shows the response of net income to irrigation and nitrogen fertilizer application. Net income increased with the increase in irrigation and nitrogen application, ranging from 352,833 CNY·ha^{-1} to 677,946.1 CNY·ha^{-1} across the 64 scenarios. The highest net income was obtained by the application with irrigation of 340 mm and nitrogen application of 400 kg·ha^{-1}. It should also be noted that excessive irrigation and nitrogen application can reduce water-use efficiency and nitrogen partial factor productivity of tomato. Therefore, the irrigation quota of 320~340 mm and the nitrogen fertilizer application rate of 360~400 kg·ha^{-1} are good choices for setting water levels and growing greenhouse tomatoes.

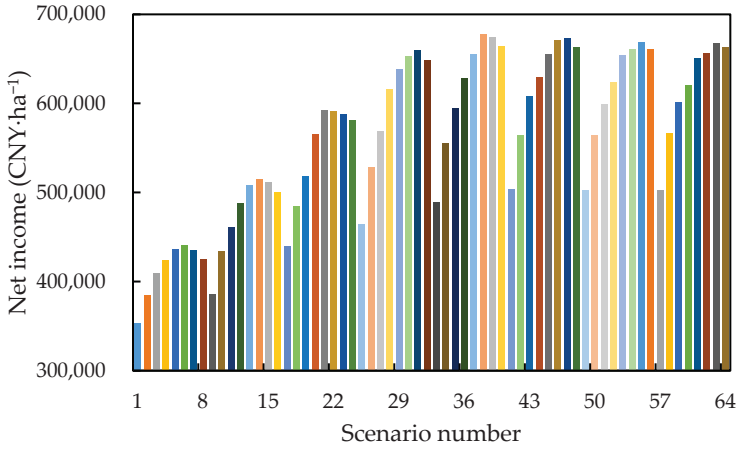


Figure 7. Economic analysis (net income) of tomato in different irrigation and nitrogen fertilizer application scenarios.

4. Discussion

4.1. Calibration and Validation of the CROPGRO–Tomato Model

Previous studies have shown that the DSSAT model can meet the needs of the various environmental and management interactions of different crops such as wheat [20], rice [31], corn [34], and cotton [35], such as the variety, climate impact, and the management of water and nitrogen coupling. Zhao et al. [21] used the DSSAT–CROPGRO–Tomato model simulation to determine a high-precision parameter estimation scheme for a greenhouse tomato trial, and the results showed that genetic parameter estimation using observations with adequate irrigation treatments could improve the simulation accuracy of the model. Through sensitivity analysis and uncertainty analysis of the genetic parameters of the DSSAT–CROPGRO–Tomato model, Li et al. concluded that the simulation accuracy of the high-irrigation treatment was higher than that of the low-irrigation treatment [29]. In this study, the DSSAT-GLUE method was used to calibrate the parameters of the CROPGRO–Tomato model to simulate the growth and yield of greenhouse tomato. The results showed that the model showed high accuracy in the simulation of tomato phenology. However, under water and nitrogen stress, especially with severe water stress, the simulation error of the model increases significantly, indicating that the application of the model under extreme conditions still needs further improvement. Li et al. [29] found that the simulation accuracy of the CROPGRO–Tomato model for simulating tomato growth and development in the higher soil moisture treatment was higher than that in the lower soil moisture treatment. Yao et al. [20] simulated the growth and development of winter wheat in water stress conditions using the DSSAT model, and the results showed that water stress would reduce the model simulation's accuracy. Similarly to the results of this study, the CROPGRO–Tomato model was used to simulate the flowering stage and ripening stage of tomato under different water and nitrogen supply conditions. The ARE values of plant height, tomato yield, and other indicators are mostly within 10% of the measured values, which is similar to the research results of Zhao [21] and Li [36]. It is further shown that the DSSAT–CROPGRO–Tomato model has good applicability, and the crop variety parameters determined in this study are scientifically reasonable and can be used to simulate the effects of different water and nitrogen supplies on the phenology, growth process, yield, and other indicators of greenhouse tomato.

The DSSAT model is widely used in water–nitrogen interaction analysis and crop growth simulation, but existing studies have shown that the model has certain limitations [14,20,37]. In the simulation of water–nitrogen interactions, the DSSAT model relies on a simplified nitrogen transformation equation, which fails to take into account

microbial activity and soil heterogeneity, resulting in a low simulation accuracy of nitrogen dynamics under complex soil and climate conditions [38]. In addition, the water–nitrogen interaction itself has significant nonlinear characteristics, especially under extreme moisture conditions. It is also difficult for the model to accurately capture the combined effects of water stress on crop growth and nitrogen uptake, which limits the applicability of DSSAT in the face of extreme climatic events, such as drought or floods. In addition, DSSAT often relies on more generalized crop variety parameters in crop growth simulation, failing to fully consider the variability of different varieties and agricultural management practices, resulting in insufficient accuracy of the model in practical applications. In regional-scale applications, the model's ability to handle spatial heterogeneity is weak, making it difficult to accurately reflect soil conditions and water and fertilizer management strategies in different plots [39]. To overcome these deficiencies, future research should be devoted to improving the model's simulation of nitrogen dynamics, strengthening the nonlinear description of the water–nitrogen coupling effect, and combining remote sensing technology and big data analysis to improve the model's applicability at the regional scale and under extreme climatic conditions. Meanwhile, the modeling of crop variety differences and diversity of agricultural management practices should be strengthened to improve the accuracy and reliability of DSSAT application in precision agriculture.

4.2. DSSAT–CROPGRO–Tomato Model Scenario Simulation

The application of crop models offers predictive insights and scientific guidance for agricultural production. Developing water-saving irrigation systems is a crucial strategy for maximizing water resource efficiency and reducing agricultural water demand [17]. In this study, calibrated DSSAT–CROPGRO–Tomato model was used to simulate the growth and yield indices of greenhouse tomato under different combinations of water and nitrogen. This allowed for analysis of the effects of differing water and nitrogen supplies on the tomato growth, yield, water consumption, water-use efficiency (WUE), and nitrogen partial factor productivity (NPFP). The results indicated that with an adequate water supply, optimal nitrogen input enhanced tomato growth and yield. However, under water stress or excessive nitrogen conditions, yield and water–nitrogen efficiency declined.

The study showed that tomato water consumption in greenhouses increased with irrigation volume. When irrigation exceeded 320 mm, nitrogen input had minimal effect on water consumption at the same irrigation level, consistent with findings by Lei et al. [40]. Under deficit irrigation conditions, tomato yield, WUE, and NPFP values increased with the increase in irrigation amount. When the amount of irrigation reaches a certain level, the growth of yield tends to flatten out or decline. Nitrogen application significantly improved tomato yield and WUE; an appropriate nitrogen level facilitated nutrient uptake, promoted root water absorption, increased net photosynthesis, and ultimately enhanced yield [41]. Li et al. [42] also observed that while increases in both irrigation and fertilizer levels significantly raised yield, excessive water or nitrogen application led to diminished yield, indicating that over- or under-application was suboptimal for tomato production. Other studies have shown that, at a given irrigation level, moderate fertilizer application enhances irrigation WUE, whereas excessive fertilizer lowers it [43]. Additionally, research has demonstrated that within a certain irrigation range, tomato yield rises significantly with irrigation, while WUE decreases markedly [44].

We also analyzed the economic benefits of greenhouse tomato considering the water consumption, yield, and water- and nitrogen-use efficiency. Ultimately, the DSSAT–CROPGRO–Tomato model simulations determined that the optimal irrigation level for greenhouse tomatoes in this region is 320~340 mm, and the corresponding nitrogen fertilizer application rate is 360~400 kg·ha^{-1}. These findings provide valuable technical support for the development of

high-quality and efficient irrigation and nitrogen application strategies for greenhouse tomato production. In future studies, we will explore the complex interactions of water and nitrogen in plant growth more deeply, in particular the effects on soil microbial activity, root growth, and plant nutrient uptake. This will help to better elucidate the growth mechanism of plants under different soil, water, and nitrogen conditions, and provide more reliable theoretical basis and technical support for agricultural production.

5. Conclusions

(1) The genetic parameters of greenhouse tomato in the experimental area in the CROPGRO–Tomato model according to DSSAT-GLUE are as follows: 30.42, 3.833, 19.50, 45.16, 1.10, 380, 0.744, 26.03, 57.12, and 8.50 for EM-FL, FL-SH, FL-SD, SD-PM, LFMAX, SLAVE, XFRT, SFDUR, PODUR, and THRSH, respectively.

(2) The CROPGRO–Tomato model performs well when simulating various growth indicators of greenhouse tomato, except the average stem and leaf number. The stem and leaf number are affected by field management measures, resulting in an average ARE of 13.84%. The ARE values of other growth indicators are less than 10%.

(3) Considering the economic yield of tomato, water, and nitrogen utilization efficiency, and other indicators, the optimal irrigation rate for greenhouse tomato in this region is 320~340 mm, and the nitrogen application rate is 360~400 kg·ha^{-1}.

Author Contributions: Conceptualization, Z.S. (Zhijie Shan); methodology, J.C. and Z.S. (Zhuanyun Si); investigation, J.C. and R.Y.; data curation, J.C., X.Z. and R.Y.; formal analysis, J.C. and X.Z.; writing—original draft preparation, J.C. and X.Z.; writing—editing, J.C. and Z.S. (Zhijie Shan); supervision, X.Z. and H.F.; project administration, X.Z. and H.F.; funding acquisition, Z.S. (Zhijie Shan) and Z.S. (Zhuanyun Si). All authors have read and agreed to the published version of the manuscript.

Funding: This work was supported by the National Key Research and Development Program of China (2023YFD1900802-01), the Major Science and Technology Projects of Ministry of Water Resources of the People's Republic of China (No. SKS-2022044), the Central Water Conservancy Development Fund Funded Project (11000023T000002098219), and the Central Public Interest Scientific Institution Basal Research Fund (Y2024QC19).

Data Availability Statement: The data are contained within the article.

Conflicts of Interest: The authors declare no conflicts of interest.

References

1. Jin, N.; Zhang, D.; Jin, L.; Wang, S.Y.; Yang, X.T.; Lei, Y.Z.; Meng, X.; Xu, Z.Q.; Sun, J.H.; Lyu, J.; et al. Controlling water deficiency as an abiotic stress factor to improve tomato nutritional and flavour quality. *Food Chem. X* **2023**, *19*, 100756. [CrossRef] [PubMed]
2. National Bureau of Statistics of China. *China Statistical Yearbook*; China Statistics Press: Beijing, China, 2022.
3. Dong, J.S.; Xue, Z.; Shen, X.J.; Yi, R.C.; Chen, J.W.; Li, Q.; Hou, X.F.; Miao, H.C. Effects of different water and nitrogen supply modes on peanut growth and water and nitrogen use efficiency under mulched drip irrigation in Xinjiang. *Plants* **2023**, *12*, 3368. [CrossRef]
4. Cheng, G.T.; Wang, Y.F.; Jiang, W.T.; Lin, J.S.; Feng, X.D.; Chang, H.F.; Qiao, H.X.; Liang, Y. Research progress on comprehensive preventive and control measures for soil obstacle in facility tomato. *China Veg.* **2023**, 16–24. [CrossRef]
5. Abdelghany, A.E.; Dou, Z.; Alashram, M.G.; Eltohamy, K.M.; Elrys, A.S.; Liu, X.; Wu, Y.; Cheng, M.; Fan, J.; Zhang, F. The joint application of biochar and nitrogen enhances fruit yield, quality and water-nitrogen productivity of water-stressed greenhouse tomato under drip fertigation. *Agric. Water Manag.* **2023**, *290*, 108605. [CrossRef]
6. Sun, Y.N.; Duan, L.B.; Zhong, H.Y.; Cai, H.J.; Xu, J.T.; Li, Z.J. Effects of irrigation-fertilization-aeration coupling on yield and quality of greenhouse tomatoes. *Agric. Water Manag.* **2024**, *299*, 108893. [CrossRef]
7. Wang, H.D.; Qu, Y.; Wen, Z.J.; Cheng, M.H.; Zhang, F.C.; Fan, J.L.; Yang, Q.L.; Liu, X.G.; Wang, X.K. Interactive effects of irrigation and N fertilization management on fruit yield, quality and water-N productivity of greenhouse cherry tomato. *Sci. Hortic.* **2024**, *328*, 112895. [CrossRef]

8. Wu, Y.; Si, W.; Yan, S.; Wu, L.; Zhao, W.; Zhang, J.; Zhang, F.; Fan, J. Water consumption, soil nitrate-nitrogen residue and fruit yield of drip-irrigated greenhouse tomato under various irrigation levels and fertilization practices. *Agric. Water Manag.* **2023**, *277*, 108092. [CrossRef]
9. Yu, H.Y.; Zhao, W.J.; Ding, L.; Zhou, C.Q.; Ma, H. Effects of coordinated regulation of water, nitrogen, and biochar on the yield and soil greenhouse gas emission intensity of greenhouse tomatoes. *J. Environ. Manag.* **2024**, *370*, 122801. [CrossRef] [PubMed]
10. Zhang, J.W.; Xiang, L.X.; Liu, Y.X.; Jing, D.; Zhang, L.L.; Liu, Y.; Li, W.Q.; Wang, X.Y.; Li, T.L.; Li, J.M. Optimizing irrigation schedules of greenhouse tomato based on a comprehensive evaluation model. *Agric. Water Manag.* **2024**, *295*, 108741. [CrossRef]
11. Ma, W.W.; Shi, J.C.; Jin, X.X.; Ning, S.R.; Li, S.; Tao, Y.Y.; Zhang, Y.N.; Liu, Y.; Lin, S.; Hu, P.C.; et al. Improved CERES-Rice model to simulate the growth of mulched dry rice. *Trans. China Soc. Agric. Eng.* **2017**, *33*, 115–123.
12. Corbeels, M.; Chirat, G.; Messad, S.; Thierfelder, C. Performance and sensitivity of the DSSAT crop growth model in simulating maize yield under conservation agriculture. *Eur. J. Agron.* **2016**, *76*, 41–53. [CrossRef]
13. Xu, N.; Dang, T.H. Prediction of nitrogen fertilizer effect of winter wheat based on DSSAT model: A case study of Weibei dry plateau in the gully area of the Loess Plateau. *J. Irrig. Drain.* **2017**, *36*, 147–154. [CrossRef]
14. Du, J.T.; Zhang, N.; Gong, K.N.; Du, M.Z.; Yang, Y.P.; Wang, X.P. Optimization of drip irrigation system of cotton under membrane in southern Xinjiang based on DSSAT model. *China J. Ecol.* **2021**, *40*, 3760–3768. [CrossRef]
15. Jones, J.W.; Hoogenboom, G.; Porter, C.H.; Boote, K.J.; Batchelor, W.D.; Hunt, L.A.; Wilkens, P.W.; Singh, U.; Gijsman, A.J.; Ritchie, J.T. The DSSAT cropping system model. *Eur. J. Agron.* **2003**, *18*, 235–265. [CrossRef]
16. Bhatia, V.S.; Singh, P.; Wani, S.P.; Chauhan, G.S.; Rao, A.V.R.K.; Mishra, A.K.; Srinivas, K. Analysis of potential yields and yield gaps of rainfed soybean in India using CROPGRO-Soybean model. *Agric. For. Meteorol.* **2008**, *148*, 1252–1265. [CrossRef]
17. Wang, P.Y.; Liu, J.R.; Zhang, T.Q.; Liu, X. Optimization of sugarcane deficit irrigation in Guangxi based on DSSAT model. *J. Irrig. Drain.* **2021**, *40*, 133–139. [CrossRef]
18. Li, Y.; Zhang, S.Y.; Liu, Q.Z.; Ji, Y.D.; Yao, N.; Song, X.Y. Effects of droughts and meteorology on spring wheat in western Loess Plateau based on DSSAT-CERES-Wheat model. *Trans. China Soc. Agric. Mach.* **2022**, *53*, 338–348.
19. Maldonado-Ibarra, I.; Rodríguez, G.R.; Castillo-Rosales, D. Determination of genetic coefficients of three springwheat varieties under a Mediterranean environment applying the DSSAT model. *Chil. J. Agric. Res.* **2015**, *75*, 418–424. [CrossRef]
20. Yao, N.; Zhou, Y.G.; Song, L.B.; Liu, J.; Li, Y.; Wu, S.F.; Feng, H.; He, J.Q. Parameter estimation and verification of DSSAT-CERES-Wheat model for simulation of growth and development of winter wheat under water stresses at different growth stages. *Trans. China Soc. Agric. Eng.* **2015**, *31*, 138–150.
21. Zhao, Z.L.; Li, B.; Feng, X.; Yao, M.Z.; Xie, Y.; Xing, J.W.; Li, C.X. Parameter estimation and verification of DSSAT-CROPGRO-Tomato model under different irrigation levels in greenhouse. *China J. Appl. Ecol.* **2018**, *29*, 2017–2027. [CrossRef]
22. Li, Z. The response of spring maize-soil system to different water-nitrogen management regimes and applicability research of DSSAT-CERES-Maize model in hetao irrigation district. Ph.D. Thesis, Inner Mongolia Agricultural University, Hohhot, China, 2017.
23. Si, Z.Y.; Zain, M.; Li, S.; Liu, J.M.; Liang, Y.P.; Gao, Y.; Duan, A.W. Optimizing nitrogen application for drip-irrigated winter wheat using the DSSAT-CERES-Wheat model. *Agric. Water Manag.* **2021**, *244*, 106592. [CrossRef]
24. Han, Y.J.; Han, T.H. China's wheat yield increase potential and realization path during the 14th five-year plan period. *Issues Agric. Econ.* **2021**, 38–46. [CrossRef]
25. Ritchie, J.T. International consortium for agricultural systems applications (ICASA): Establishment and purpose. *Agric. Syst.* **1995**, *49*, 329–335. [CrossRef]
26. Liu, H.; Yang, J.; Drury, C.F.; Reynolds, D.; Tan, C.S.; Bai, Y.; He, P.; Jin, J.; Hoogenboom, G. Using the DSSAT-CERES-Maize model to simulate crop yield and nitrogen cycling in fields under long-term continuous maize production. *Nutr. Cycl. Agroecosystems* **2011**, *89*, 313–328. [CrossRef]
27. DeJonge, K.C.; Ascough, J.C., II; Ahmadi, M.; Andales, A.A.; Arabi, M. Global sensitivity and uncertainty analysis of a dynamic agroecosystem model under different irrigation treatments. *Ecol. Model.* **2012**, *231*, 113–125. [CrossRef]
28. Rinaldi, M.; Ventrella, D.; Gagliano, C. Comparison of nitrogen and irrigation strategies in tomato using CROPGRO model. A case study from Southern Italy. *Agric. Water Manag.* **2007**, *87*, 91–105. [CrossRef]
29. Li, B.; Li, C.X.; Yao, M.Z.; Wei, X.G.; Bao, Z.R.; Sun, X.L. Sensitivity and uncertainty analysis for CROPGRO—Tomato model at different irrigation levels. *J. Shenyang Agric. Univ.* **2020**, *51*, 153–161.
30. He, J.; Jones, J.W.; Graham, W.D.; Dukes, M.D. Influence of likelihood function choice for estimating crop model parameters using the generalized likelihood uncertainty estimation method. *Agric. Syst.* **2010**, *103*, 256–264. [CrossRef]
31. Wang, B.; Yang, H.X.; Feng, J.; Guo, Z.Y.; Guo, Y.W. Rice genotype coefficient optimization of DSSAT based on PSO. *Trans. China Soc. Agric. Mach.* **2023**, *54*, 369–375.
32. Allen, R.G.; Pereira, L.S.; Raes, D.; Smith, M. *Crop Evapotranspiration-Guidelines for Computing Crop Water Requirements-FAO Irrigation and Drainage Paper 56*; FAO: Rome, Italy, 1998; p. 300.
33. Shen, X.J. Real-time irrigation forecasting technology for cotton with under-membrane drip irrigation. Master's Thesis, Shihezi University, Shihezi, China, 2008.

34. Liu, Y.; Guan, X.; Yang, M.; Ding, C.; Cui, J.; Huang, J.; Mei, F.; Wang, H.; Wang, T. Optimizing the summer maize irrigation schedule in North Henan Province based on the DSSAT model. *Acta Ecol. Sin.* **2019**, *39*, 5348–5358.
35. Wang, X.P.; Xin, L.; Du, J.T.; Li, M.F. Simulation of cotton growth and yield under film drip irrigation condition based on DSSAT model in Southern Xinjiang. *Trans. China Soc. Agric. Mach.* **2022**, *53*, 314–321.
36. Li, B.; Sun, X.L.; Yao, M.Z.; Bao, H.; Wang, J.H. Parameter estimation and verification of the DSSAT-CROPGRO-Tomato model under the condition of different amounts of straw returned to the field in the greenhouse. *China J. Ecol.* **2021**, *40*, 908–918. [CrossRef]
37. Mao, X.; Yang, J.L.; Zhu, X.H.; He, C.; Feng, H.; He, J.Q. Simulation accuracy of growth and development of winter rape (*Brassica napus* L.) in Guanzhong plain with different crop models. *Trans. China Soc. Agric. Mach.* **2019**, *50*, 306–314.
38. Li, Z.K.; Li, X.Y.; Zhou, S.; Yang, X.F.; Fu, Y.Y.; Miao, C.Y.; Wang, S.; Zhang, G.; Wu, X.C.; Yang, C.; et al. A comprehensive review on coupled processes and mechanisms of soil-vegetation-hydrology, and recent research advances. *Sci. China Earth Sci.* **2022**, *65*, 2083–2114. [CrossRef]
39. Meng, J.H.; Wang, Y.N.; Lin, Z.X.; Fang, H.T. Progress and perspective of crop growth models. *Trans. China Soc. Agric. Mach.* **2024**, *55*, 1–15+27.
40. Lei, C.X.; Li, W.H. Effects of water and nitrogen coupling under film drip irrigation on the water consumption intensity and nitrogen uptake and distribution of processing tomatoes. *J. Shihezi Univ.* **2021**, *39*, 54–61. [CrossRef]
41. Wang, H.B.; Cao, H.X.; Hao, S.X.; Pan, X.Y. Responses of plant nutrient and photosynthesis in greenhouse tomato to water-fertilizer coupling and their relationship with yield. *Sci. Agric. Sin.* **2019**, *52*, 1761–1771.
42. Li, J.M.; Pan, T.H.; Wang, L.H.; Du, Q.J.; Chang, Y.B.; Zhang, D.L.; Liu, Y. Effects of water-fertilizer coupling on tomato photosynthesis, yield and water use efficiency. *Trans. China Soc. Agric. Eng.* **2014**, *30*, 82–90.
43. Song, N.; Wang, F.; Yang, C.F.; Yang, K.J. Coupling effects of water and nitrogen on yield, quality and water use of potato with drip irrigation under plastic film mulch. *Trans. China Soc. Agric. Eng.* **2013**, *29*, 98–105.
44. Xing, Y.Y.; Zhang, F.C.; Zhang, Y.; Li, J.; Qiang, S.C.; Wu, L.F. Effect of irrigation and fertilizer coupling on greenhouse tomato yield, quality, water and nitrogen utilization under fertigation. *Sci. Agric. Sin.* **2015**, *48*, 713–726.

Disclaimer/Publisher's Note: The statements, opinions and data contained in all publications are solely those of the individual author(s) and contributor(s) and not of MDPI and/or the editor(s). MDPI and/or the editor(s) disclaim responsibility for any injury to people or property resulting from any ideas, methods, instructions or products referred to in the content.

water

MDPI

Article

Energy of Sorghum Biomass Under Deficit Irrigation Strategies in the Mediterranean Area

Simone Pietro Garofalo *, Anna Francesca Modugno, Gabriele de Carolis and Pasquale Campi

Research Center for Agriculture and Environment—Council for Agricultural Analysis and Economics (CREA-AA), Via Celso Ulpiani, 5, 70125 Bari, Italy
* Correspondence: simone.garofalo@crea.gov.it

Abstract: The growing demand for renewable energy sources and the need to optimize water use in agriculture, particularly in water-scarce regions, highlights the importance of growing species suitable for semi-arid areas, such as sorghum (*Sorghum bicolor* L. Moench). Deficit irrigation strategies allow water savings by optimizing water use efficiency. However, the potential of sorghum for bioethanol production with deficit irrigation strategies is still not well studied. This work investigates the impact of three irrigation strategies (full, deficit, and regulated deficit) on the biomass yield, ethanol production, and water use efficiency of sorghum ('KWS Bulldozer') in a semi-arid Mediterranean area (the Apulia region, Southeastern Italy) over three growing seasons (2013, 2014, and 2017); irrigation needs were calculated from crop evapotranspiration using standard crop coefficients and soil water content measurements. Harvested biomass was analyzed for cellulose and hemicellulose content, and ethanol production was estimated using conversion models. The full irrigation treatment resulted in the highest biomass and ethanol production in all seasons (22,633 kg $\times$ ha^{-1}, 28,367 kg $\times$ ha^{-1}, and 23,835 kg $\times$ ha^{-1}, in 2013, 2014, and 2017, respectively), highlighting the relationship between a full water supply and yield optimization. However, deficit irrigation showed a higher biomass and ethanol water productivity (10.93 kg $\times$ m^{-3} and 3.23 L $\times$ m^{-3}, respectively) than other treatments, suggesting that moderate irrigation strategies can effectively balance production and sustainable water use. The results suggest the importance of adjusting irrigation practices to specific environmental conditions to improve the efficiency and productivity of sorghum.

Keywords: energy production; biomass yield; deficit irrigation; water use efficiency; ethanol

1. Introduction

Socio-economic development and population growth strongly pressure food supply, water, and energy security. The production of energy crops must be studied and evaluated in terms of environmental impact to integrate them into sustainable agricultural development. As bioenergy carriers, they offer ecological advantages over fossil fuels by contributing to the reduction of greenhouse gases and acidifying emissions [1,2]. Biomass production through "dedicated" crops helps to meet global energy demand. Some controversial issues have been identified, such as the possible conflict between the goal of increasing plant biomass and food production and the need to limit environmental impacts [1,2]. From an economic perspective, replacing traditional crops with nonfood species represents a new opportunity for rural development when some food crops are no longer sustainable [3]. Beyond economic benefits, the introduction of nonfood crops such as sorghum could offer agronomic advantages in systems where continuous monoculture increases the risk of soil depletion and the spread of crop-specific diseases. As an

annual crop with high adaptability, sorghum could provide a sustainable alternative in such systems, contributing to more resilient agricultural practices. Although this study focuses on the agronomic potential of sorghum under water-limited conditions, its role in diversifying crop rotations and mitigating disease risks highlights additional benefits that deserve further exploration. Moreover, biomass crops allow in some cases the revaluation of marginal land by farmers [4]. In the scope of the project Future Crops for Food, Feed, Fiber, and Fuel (4F Crops) supported by the European Union, an environmental impact assessment study was developed and applied to the production of potential energy crops in Europe [1]. One of the main sources studied as energy is biomass maintained by "dedicated" sorghum crops. Sorghum (*Sorghum bicolor* L. Moench), a C4 species with a tropical origin, is grown as a summer crop; it is a drought-resistant crop due to a relatively lower water requirement than other energy crops [5–7]. Approximately 85% of global sorghum cultivation is concentrated in dry environments [8]. Its drought resistance is attributed to a dense and prolific root system that can extract soil water deep into the soil profile, its ability to maintain stomatal opening at low levels of potential leaf water through osmotic adaptation, and its ability to delay reproductive development [9–11]. The shorter duration of sorghum growth compared to other energy crops, such as corn, also contributes to its ability to escape drought. Sorghum is widely cultivated in many semi-arid areas of the world thanks to its ability to achieve sufficient production in rainfed or limited water conditions [12]. Moreover, in many parts of the world water scarcity is an increasingly important issue.

Climate change will cause higher temperatures, heat waves, and frequent dry periods, resulting in a higher evapotranspiration demand and difficulties in irrigation management [13,14]. Thus, different strategies need to be implemented to preserve and maximize water use efficiency, especially in arid and semi-arid areas, such as the Mediterranean basin [15]. To allow the cultivation of sorghum in regions with limited water resources, without compromising the yield of biomass and ethanol, it is necessary to know the response of the crop to variation in irrigation volumes [16], to develop sustainable strategies and increase water use efficiency (WUE). A promising management strategy to improve WUE is to apply water-saving practices, such as deficit irrigation (DI) and regulated deficit irrigation (RDI) [17,18]. These agronomical techniques attempt to optimize energy production, yield, and WUE by synchronizing the water use of crops with the reproductive stages of crops [15]. To this end, a study of the effects deriving from the application of DI and RDI on the production of biomass and energy could be important [19,20]. Deficit irrigation (DI) has been studied as a strategy to increase water productivity and is an approach that uniformly reduces the irrigation applied below the water needs of crops during the growing season [21,22]. RDI consists of an adequate water application during periods of critical growth such as sowing and flowering [23,24]. Therefore, irrigation deficit strategies must be tested under real conditions for biomass crops. This context of expanding energy crop cultivation, underscored by the critical balance between maximizing biomass production and preserving environmental integrity, sets sorghum research within a crucial area of inquiry [1]. The energy productivity of sorghum in the semi-arid climate of the Mediterranean area, with limited water resources, is still being studied. Developing suitable irrigation strategies by researching biomass production and energy yield under limited irrigation conditions is important for the Mediterranean basin [1,25]. Several research projects on sorghum yield have been carried out using deficit irrigation strategies. Limited studies have been reported on the effect of deficit irrigation strategies on ethanol production by sorghum. Pang et al. [26] showed that the level of deficit irrigation had a significant effect on reducing bioethanol yield.

This study aims to investigate the effects of three different irrigation strategies—full irrigation, deficit, and regulated deficit—on sorghum biomass productivity, water use efficiency, and estimated bioethanol production in a semi-arid Mediterranean area. The objective is to provide insights into the dynamics between water availability and yield, helping to develop sustainable irrigation strategies for bioenergy crops in water-scarce regions such as the Apulia region. Moreover, this study was carried out in the south of Italy, where there exists a great risk for agroecosystems due to *Xylella fastidiosa* subsp. Pauca (ST53). This quarantine bacterium, regulated by phytosanitary authorities to prevent its spread, has had a severe impact on agriculture, particularly affecting the region's extensive olive groves—while Sorghum bicolor is not considered a host plant [27]. In this context, introducing new crops is crucial to ensure the sustainability of the rural economy [28].

2. Materials and Methods

2.1. Experimental Site

The trial was carried out at the experimental farm of the Council for Agricultural Research and Economics located in Rutigliano, the Apulia region, Southeastern Italy (latitude: 40°, 59′ N; longitude: 17°, 01′ E; 166 m a.s.l). The climate of the area is Mediterranean, characterized by warm and dry summers and mild winters, and classified as CSa according to Köppen and Geiger. The minimum and maximum annual air temperatures are between 0 and 5 °C and 32 and 43 °C, respectively; the relative humidity ranges between 15% and 40%. The annual rainfall around the area is about 535 mm, concentrated mainly during the autumn–winter period and scarce during the spring and summer. The yearly average difference in the area between precipitation and reference evapotranspiration is about −560 mm; consequently, precipitation does not supply the water requirement of the crops from April to September, and most of the crops can be successfully cultivated only by supplying irrigation water [29].

Before the start of the experiment, soil sampling was performed to understand its main physical and chemical properties. Sampling was carried out at five separate locations within the experimental area to ensure an adequate representativeness of soil conditions [30]. The average clay, silt, and sand content were 32%, 36%, and 33%, respectively. The pH was 8.1, while the EC was 1.1 dS/m. The soil of the experimental site can be classified as clay loam (USDA classification) and Rhodoxeralf Lithic Ruptic (FAO classification). At 0.50 m of soil depth, the presence of apparent rock was detected, which could reduce the capacity of the roots to expand more deeply. The experimental area was predominantly flat, with an average slope of 1.6%.

2.2. Crop Management and Experimental Design

The study was carried out over three growing seasons (2013, 2014, and 2017). The sorghum hybrid used for the trial was the "KWS Bulldozer" (KWS SAAT SE & Co. KGaA, Einbeck, Germany), characterized by a medium-late vegetative cycle, a tolerance to bending, and a high yield in dry and green biomass [2].

Sorghum was sown at the beginning of June in 2013 and in mid-May in 2014 and 2017; the sowing density was 7 kg of seeds per hectare; harvest took place when the sorghum achieved the maximum dry matter yield or the second half of September over the three years. Each year, plots were fertilized before the sowing with 120 kg ha^{-1} of N and 90 kg ha^{-1} of P_2O_5 as diammonium phosphate. Weeds were controlled by herbicides before sowing and by hand-hoeing during the first part of the growing cycle.

An experimental design employing randomized complete blocks was utilized and replicated three times. The basic units of the experiment were plots of 80 square meters each, consisting of 22 plants $\times$ m^{-2}.

Three different irrigation strategies were applied:

- I100 (full irrigation), restoring 100% of the ETc. The irrigation was applied when ready water availability was exhausted (on average once per week) according to Allen et al.'s [31] methodology. In particular, the tabulated crop coefficients (Kcini = 0.15; Kcmed = 1.10; Kcend = 0.30) and a depletion fraction value of 0.50 were adopted. Corrections on Kcini (for precipitation events), Kcmed, and Kcend (for climatic conditions and crop height) were performed according to Allen et al.'s methodology.
- I50 (deficit irrigation), restoring 50% of the ETc from the beginning of the growing cycle to the harvesting.
- I100-0 (regulated deficit irrigation), restoring 100% of the ETc from the beginning of the growing cycle to the phase of the flag leaf being visible.

Cumulative irrigation water at a daily scale was calculated as follows:

$$\sum Irrigation_{(n)} = \sum_{i=1}^{n} IRRW_{(i)} \quad (1)$$

where $\sum Irrigation_{(n)}$ is the cumulative irrigation amount up to day n, and $IRRW_{(i)}$ is the irrigation water applied for day i.

2.3. Crop Evapotranspiration

Daily crop evapotranspiration (ETc(i), mm), at day i was estimated by the average of the water balance equation [32] for each season. Runoff and capillary rise are negligible because of the flat ground and the presence of a cracked rocky layer that limits the soil depth (0.50 m). The simplified equation for the soil water balance can be expressed, at a daily scale, as

$$ETc_{(i)} = P_{(i)} + I_{(i)} - Dr_{(i)} \pm \Delta SWC_{(i)} \quad (2)$$

where ETc(i) is crop water evapotranspiration (mm d-1); P(i), effective precipitation (mm d-1); I(i), irrigation (mm d-1); and Dr(i), drainage (mm d-1). Dr(i) was estimated as the amount of water exceeding the maximum water capacity in the entire soil profile. $\pm\Delta$SWC(i), is the difference in the volume of soil water content (SWC), between i and i-1 values, in the whole soil profile (mm d^{-1}) explored by the root system, measured by capacitive probes (10HS, Decagon Devices Inc., Pullman, WA, USA). They were inserted horizontally in the ground at a depth of 0.16 m and 0.33 m and connected to a data logger (Grillo MMS, Tecno.El, Formello (Rome), Italy). The output data for each depth was in m^3 m^{-3}.

So, the SWC(i) for the soil profile (0.5 m) was determined as an integral of the values measured for each depth, since a probe is supposed to detect the water content in a 0.25 m soil layer:

$$\int_0^{0.5} SWC(i) = SWc_{0.16}(m^3m^{-3})\cdot 0.25(m) + SWc_{0.3}3(m^3m^{-3})\cdot 0.25(m) \quad (3)$$

The approach used to measure daily ET was previously validated at the same experimental site by Mastrorilli et al. [33] in diverse soil water conditions by comparing on a daily scale the ET from Equation (1) and ET measured by the Bowen ratio method [34]. Differences within 10–15% were measured between the daily ET determined by the two independent methods [33].

The trends of the cumulative ETc at a daily scale were calculated as follows:

$$\sum ET_{C_{(n)}} = \Sigma_{i=1}^{n} ET_{C_{(i)}} \quad (4)$$

where $\sum ET_{C_{(n)}}$ is the cumulative evapotranspiration up to day n, and $ET_{C_{(i)}}$ is the daily (i) evapotranspiration.

2.4. Biomass Evaluation

During the three growing seasons, the leaf area index (LAI) and dry matter were determined for the sampled sorghum plants. The LAI was calculated by using an LAI-2000 Plant Canopy Analyzer (Li-COR Environmental, Lincoln, NE, USA), and dry matter was measured after drying the samples in an oven at 65 °C for 48 h. At the end of each growing season, the aboveground biomass production was determined for all the plants within 20 m^2 per plot. The biomass was harvested manually, and its weight was measured directly in the field using a portable scale. The neutral content of detergent fibers (aNDFom) was determined without sodium sulfite and with heat-stable amylase [35]. The determination of acid detergent fiber (ADFom) and acid-soluble lignin [lignin (sa)] was conducted through sequential analysis on the residue of aNDFom, with results reported after exclusively accounting for ash content, as described by Van Soest et al. [35]. Hemicellulose content was determined by subtracting the ADFom value from the aNDFom, and cellulose content was calculated by subtracting the lignin (sa) value from the ADFom. Both the hemicellulose and cellulose were determined sequentially on the same sample. The extraction and filtering processes were performed using an Ankom apparatus (Ankom220, Fairport, NY, USA).

2.5. Calculation and Statistical Analysis

A theoretical framework to estimate ethanol production from cellulose and hemicellulose was established as follows [2]. Ethanol production from cellulose and hemicellulose (l ha^{-1}) was obtained by multiplying the content of cellulose and hemicellulose in dry matter (%), the dry biomass (kg ha^{-1}), the sugar conversion factor (1.11 for cellulose and hemicellulose), the sugar process efficiency factor (0.85 for cellulose and hemicellulose), the ethanol conversion factor (0.51 for sugar), the ethanol process efficiency factor (0.85 for sugar), and the specific gravity of ethanol (790 g l^{-1}) [36]. Biomass water use efficiency (bWUE; kg × m^{-3}) and ethanol water use efficiency (ethWUE; l × m^{-3}) were calculated by dividing the biomass and the ethanol production by the ETc. bWUE represents the amount of biomass obtained by sorghum production using 1 m^3 of water; ethWUE represents the amount of ethanol obtained by sorghum production using 1 m^3 of water. Water productivity (WP) has been calculated for sorghum biomass (bWP) and estimated ethanol production (ethWP) by dividing them by the sum of the irrigation applied and rainfall [37].

Data were analyzed and represented using SigmaPlot (Systat Software Inc., Palo Alto, CA, USA, Version 14 for Windows). Tukey's post hoc test was used to test the mean differences after the Analysis of Variance (ANOVA), with a significance level set at 0.05. Figure 1 presents a flowchart of the study.

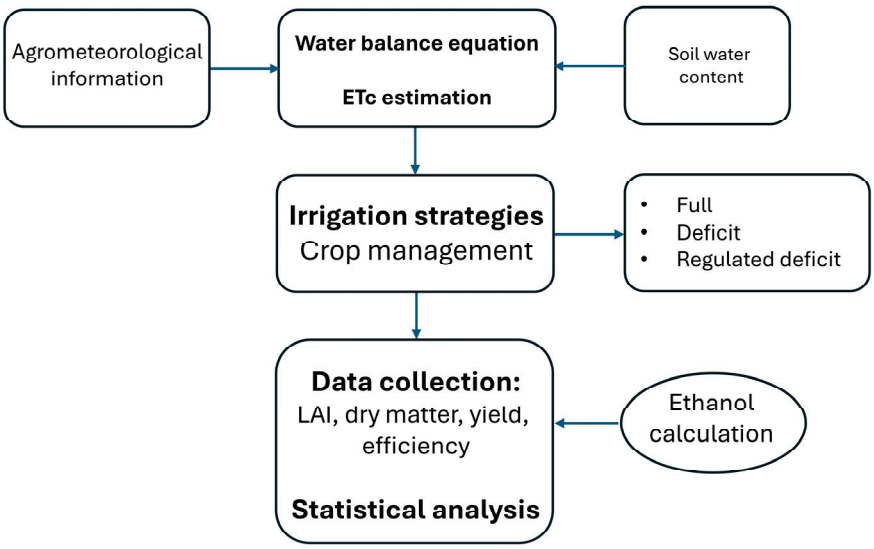


Figure 1. Flowchart of the research work.

3. Results

3.1. Agrometeorological Data

During the seasons of 2013, 2014, and 2017 (from 1 May to 30 September each year), air temperatures varied as follows: minimum temperatures ranged from 6 to 24 °C in 2013, 6 to 23 °C in 2014, and 6 to 26 °C in 2017; maximum temperatures ranged from 19 to 37 °C in 2013, 12 to 37 °C in 2014, and 17 to 39 °C in 2017 (Figure 2).

Temperature trends were similar during the three years of the study, and they did not differ from the standard of the site.

Seasonal rainfall was 91, 336, and 122 mm for 2013, 2014, and 2017, respectively (Table 1). Precipitation was distributed more homogeneously in the 2013 and 2014 seasons than in 2017, when a long period of scarce or null rainfall occurred between the end of May and mid-August (Figure 2).

Table 1. The amount of precipitation (P), reference evapotranspiration (ET0), crop evapotranspiration (ETc), and cumulated irrigation water applied (full irrigation, I100; deficit irrigation, I50; regulated deficit irrigation, I100-0) for the three years of the experiment.

	P (mm)	**ET0 (mm)**	**P-ET0 (mm)**
2013	91	496	−424
2014	336	486	−207
2017	122	568	−495
		ETc (mm)	
	I100-0	I100	I50
2013	439	329	289
2014	427	344	365
2017	504	362	335
		Irrigation water applied (mm)	
	I100-0	I100	I50
2013	310	155	160
2014	225	113	135
2017	404	202	217

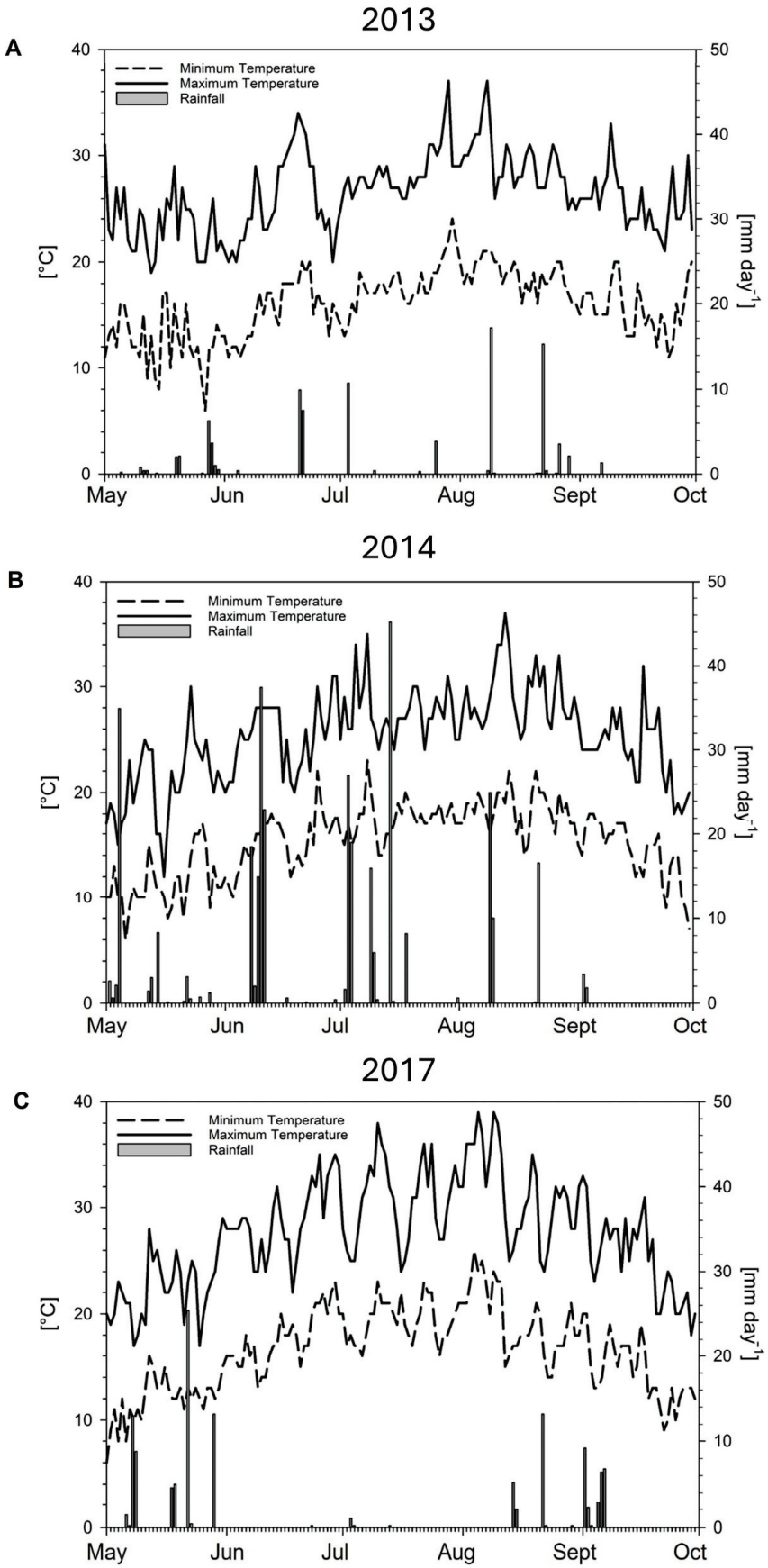


Figure 2. Weather conditions recorded at the experimental site during the three growing seasons ((**A**): 2013; (**B**): 2014; (**C**): 2017). The graphs show the daily maximum and minimum temperatures (°C, left *y*-axis) and daily rainfall (mm/day, right *y*-axis) from May to October of each year.

3.2. Soil Water Content, Crop Evapotranspiration, and Irrigation

The evolution in time of SWC (mm d^{-1}) into the whole profile showed a similar trend in the three seasons (Figure 3) for all treatments. In the I100 treatment, SWC values reached FC after each irrigation event, and they varied between the field capacity (FC) and the "Readily Available Water" (RAW) threshold. A seasonal RAW of 0.5 was obtained by threshold values (p = 0.50) derived from the guidelines provided in FAO Irrigation and Drainage Paper No. 56. The irrigation scheduling of IRR treatment allowed us to keep the water content values in the soil profile within the RAW threshold (174 mm) and to avoid water stress.

In the I50 and I100-0 treatments, SWC varied between the RAW threshold and wilting point (WP). It was lower in the second part of the cycle each year than the first, reaching or overpassing the wilting point of the soil, particularly during the 2013 and 2017 seasons and for the I100-0 treatment. During the 2014 season, the SWC trends for the deficit irrigation treatments (I50 and I100-0) were higher than the other seasons, probably due to the larger amount of precipitation. During the last part of the 2017 season, the SWC for the I100-0 treatment was lower than the wilting point (Figure 3).

During the seasons of the experiment, the seasonal ETc ranged from a minimum of 283 mm (2013, I100-0) to a maximum of 504 mm (2017, I100). Table 2 reports the seasonal ETc for each treatment. Figure 4 reports the trends of the ΣETc at a daily scale per treatment during the three growing seasons. The ΣETc of I100 was higher than the other treatment across all the seasons, in the second part of the cycle. The ΣETc of I50 was lower than I100-0 from the beginning until the end of the cycle only in the second year of the experiment.

Table 2. Impact of seasonal variation and irrigation treatments on sorghum cellulose, hemicellulose, biomass yield, estimated ethanol production, and water use efficiency (bWUE, ethWUE) and productivity (bWP, ethWP). Data are presented as mean values, with letters indicating significant differences between treatments and seasons. n.s. = not significant. *** = significant at $p < 0.001$.

Treatments		**Cellulose (%)**	**Hemicellulose (%)**	**Biomass (kg ha^{-1})**	**Ethanol (L ha^{-1})**	**bWUE (kg m-3)**	**ethWUE (L m^{-3})**	**bWP (kg m^{-3})**	**ethWP (L m^{-3})**
Season (S)	2013	32.5	24.9	13,300 c	3928 c	3.60 b	1.06 b	6.11 b	1.80 b
	2014	32.7	25.0	23,800 a	7035 a	6.26 a	1.85 a	15.94 a	4.71 a
	2017	32.9	24.9	15,700 b	5325 b	3.80 b	1.13 b	5.69 b	1.69 c
Irrigation water (I)	I100	32.8	24.8	24,944 a	7383 a	5.50 a	1.66 a	8.59 b	2.54 b
	I50	32.8	25.0	15,000 b	4444 b	4.34 b	1.38 b	10.93 a	3.23 a
	I100-0	32.5	25.0	12,888 c	3803 c	3.82 c	1.17 c	8.21 b	2.42 b
p	S	n.s.	n.s.	***	***	***	***	***	***
	I	n.s.	n.s.	***	***	***	***	***	***
	S x I	n.s.	n.s.	***	***	***	***	***	***

For each treatment, irrigation started on 7 June, 20 May, and 28 May in the 2013, 2014, and 2017 growing seasons, respectively. Table 2 shows the amount of irrigation water applied at a seasonal scale during the trial period. All the treatments received a higher amount of irrigation water during the 2017 season (Figure 5). Irrigation was interrupted for I100-0 on 27 July, 10 July, and 25 July in the 2013, 2014, and 2017 growing seasons, respectively. In the Supplementary Material, Table S1 shows the amount of water applied per each irrigation application.

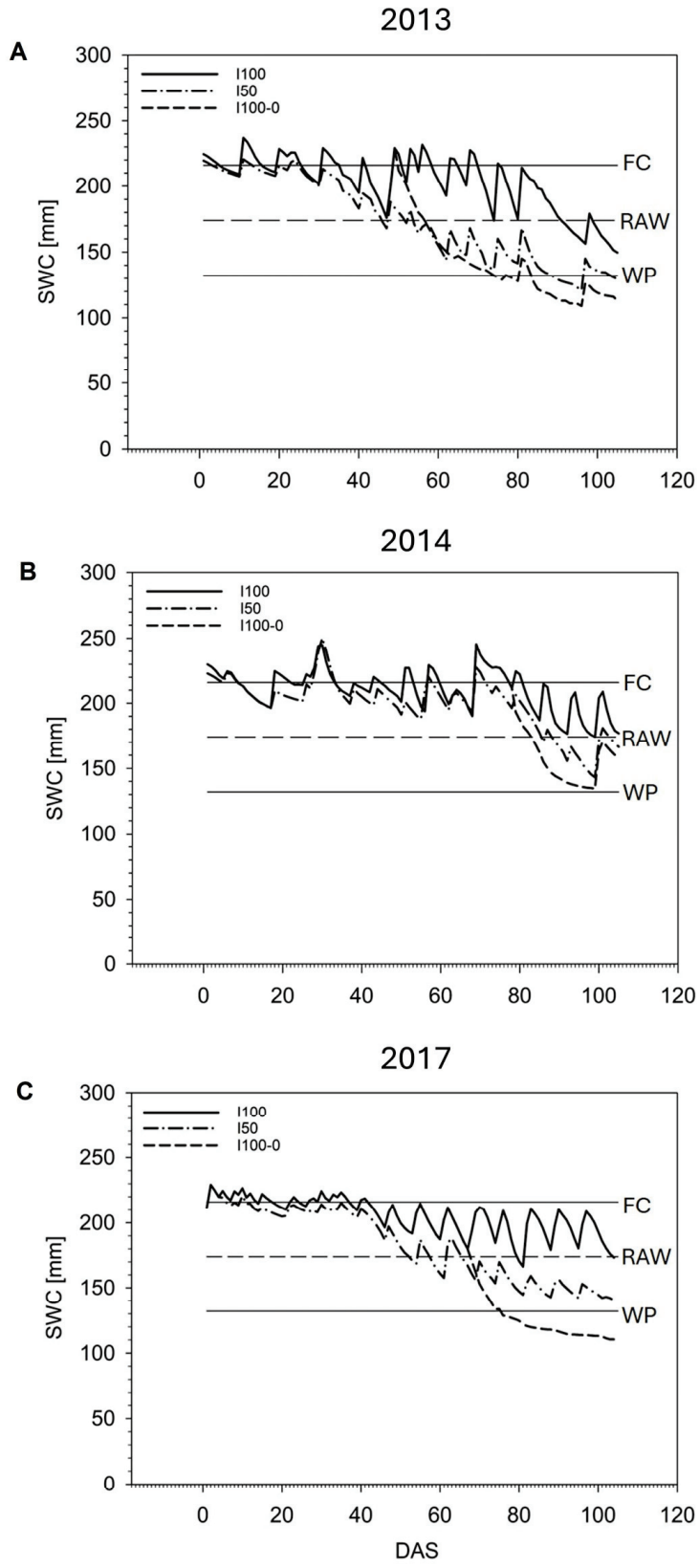


Figure 3. Daily variation in the soil water content (SWC), as the average of the SWC detected at 0.16 m and 0.33 m depths, for each treatment (full irrigation, I100; deficit irrigation, I50; regulated deficit irrigation, I100-0) during the three years of the trial (2013 (**A**); 2014 (**B**); 2017 (**C**)); FC, RAW, and WP indicate the field capacity, readily available water, and wilting point thresholds of the soil, respectively; DAS indicates days after sowing.

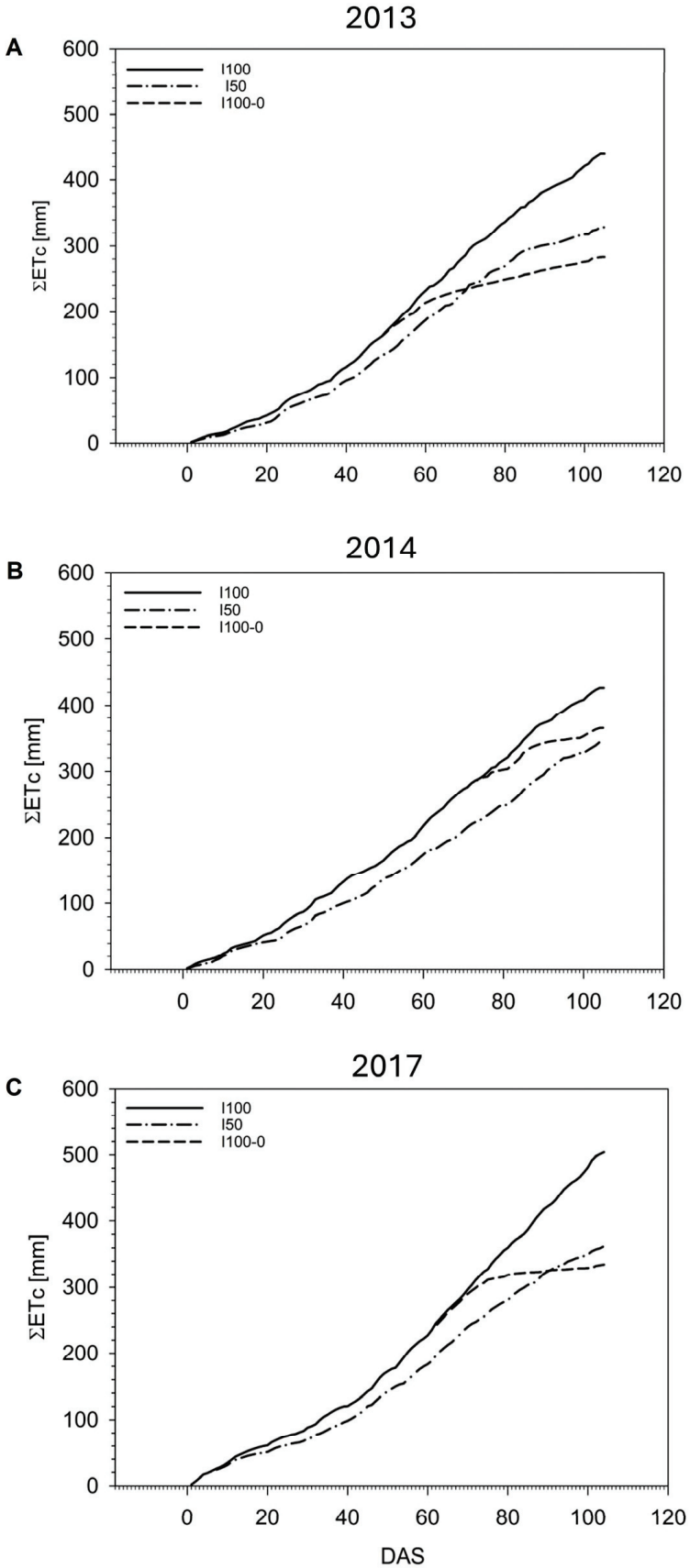


Figure 4. Daily trend of cumulative ETc (ΣETc) for each treatment (full irrigation, I100; deficit irrigation, I50; regulated deficit irrigation, I100-0) during the three years of the trial (2013 (**A**); 2014 (**B**); 2017 (**C**)); DAS indicates days after sowing.

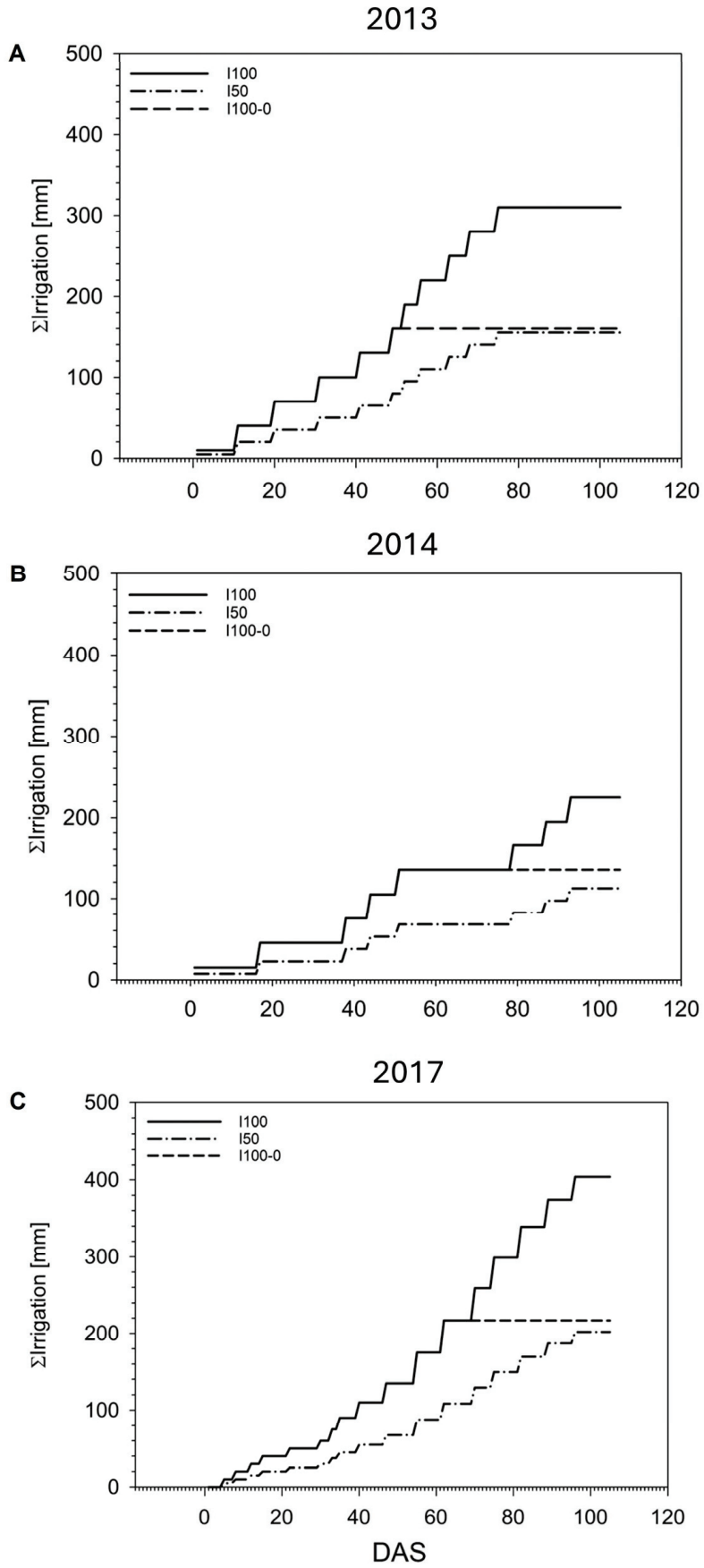


Figure 5. Daily trend of cumulative irrigation applied (ΣIrrigation) for each treatment (full irrigation, I100; deficit irrigation, I50; regulated deficit irrigation, I100-0) during the three years of the trial (2013 (**A**); 2014 (**B**); 2017 (**C**)); DAS indicates days after sowing.

3.3. LAI, Biomass, and Estimated Ethanol Production

The LAI of I100 was significantly higher than the other two deficit irrigation treatments at the end of each growth season (I100: 5.2 ± 0.28 m^2 m^{-2}; I50: 3.8 ± 0.34 m^2 m^{-2}; I100-0: 3.3 ± 0.23 m^2 m^{-2}). During the first year, I100 showed a significantly higher LAI than the other treatments since DAS 74.; there were no differences between the I50 and I100-0 LAIs. During the 2014 season, no difference in LAI was detected (except for the last day of measurement). At DAS 61 and 68 of the 2017 season, there were no differences between the LAIs of I100 and I50, but both were significantly different from I100-0; from DAS 75 until the end of the season, the I100 LAI was significantly higher than that of the other two treatments, and, in the same period, there were no statistically significant differences between the LAIs of I50 and I100-0 (Figure 6).

Every year, treatment I100 led to a statistically significant higher final production of sorghum biomass than the other treatments. I50 showed a higher biomass production in seasons 2013 and 2014 (Figure 7A,B). Table 2 reports the amount of sorghum biomass cellulose and hemicellulose produced and normalized per season and per irrigation treatment. Biomass production showed significant differences between the seasons: in 2013, there was the lowest production of biomass (13,300 kg ha^{-1}), and in 2014 the highest biomass production (23,800 kg ha^{-1}) was observed. No differences were observed in cellulose and hemicellulose percentage between treatments and across the seasons; cellulose and hemicellulose production was ~32% and ~25%, respectively, for all the treatments and seasons. Significant interactions between irrigation treatment and season were observed for biomass production, differently from cellulose and hemicellulose, for which the interaction was not significant.

The estimated ethanol production was significantly higher for I100 than I50 and I100-0 for all the growing seasons. A difference between I50 and I100-0 was detected only in 2014 (Figure 7C). Significant differences in ethanol production were observed across the seasons and treatments (Table 2): the highest production was obtained in 2014 (7035 L ha^{-1}), and the most productive treatment was I100 (7383 L ha^{-1}). The interaction between irrigation treatment and season was statistically significant for estimated ethanol production.

3.4. Water Use Efficiency and Water Productivity

Differences in biomass water use efficiency between I100 and I50 were observed in the 2013 and 2017 seasons (2013: I100, 5.14 kg m^{-3}, I50, 2.94 kg m^{-3}; 2017; I100, 4.72 kg m^{-3}, I50, 3.40 kg m^{-3}). No significant difference was observed between I100 and I50 during the 2014 season, while on the other hand, significant differences were observed between I50 (6.70 kg m^{-3}) and I100-0 (5.46 kg m^{-3}). The same patterns occurred for ethanol water use efficiency (Figure 7) in all seasons of the study. The results presented in Table 2 show significant differences in biomass yield, ethanol production, and water use efficiency in both seasons and irrigation treatments. The 2014 season recorded the highest values for biomass (23,800 kg ha^{-1}), ethanol production (7035 L ha^{-1}), and water productivity (bWP: 15.94 kg m^{-3}; ethWP: 4.71 L m^{-3}). Among the irrigation treatments, I50 consistently demonstrated the best balance between resource efficiency and productivity, achieving a higher ethanol water use efficiency (ethWUE: 1.38 L m^{-3}) and productivity (ethWP: 3.23 L m^{-3}) than I100-0. This indicates that a moderate water deficit can increase efficiency while maintaining acceptable biomass and ethanol yields. In contrast, full irrigation (I100) produced the highest absolute biomass (24,944 kg ha^{-1}) and ethanol yield (7383 L ha^{-1}), highlighting its potential under non-water-limiting conditions. These observations are further illustrated in Figure 8, which shows the relationship between water use efficiency (bWUE and ethWUE) and productivity (biomass and ethanol) for the different irrigation treatments across all seasons. The figure highlights the balance between efficiency and

productivity, with I50 as the most efficient treatment in terms of biomass and ethanol production per unit of water used.

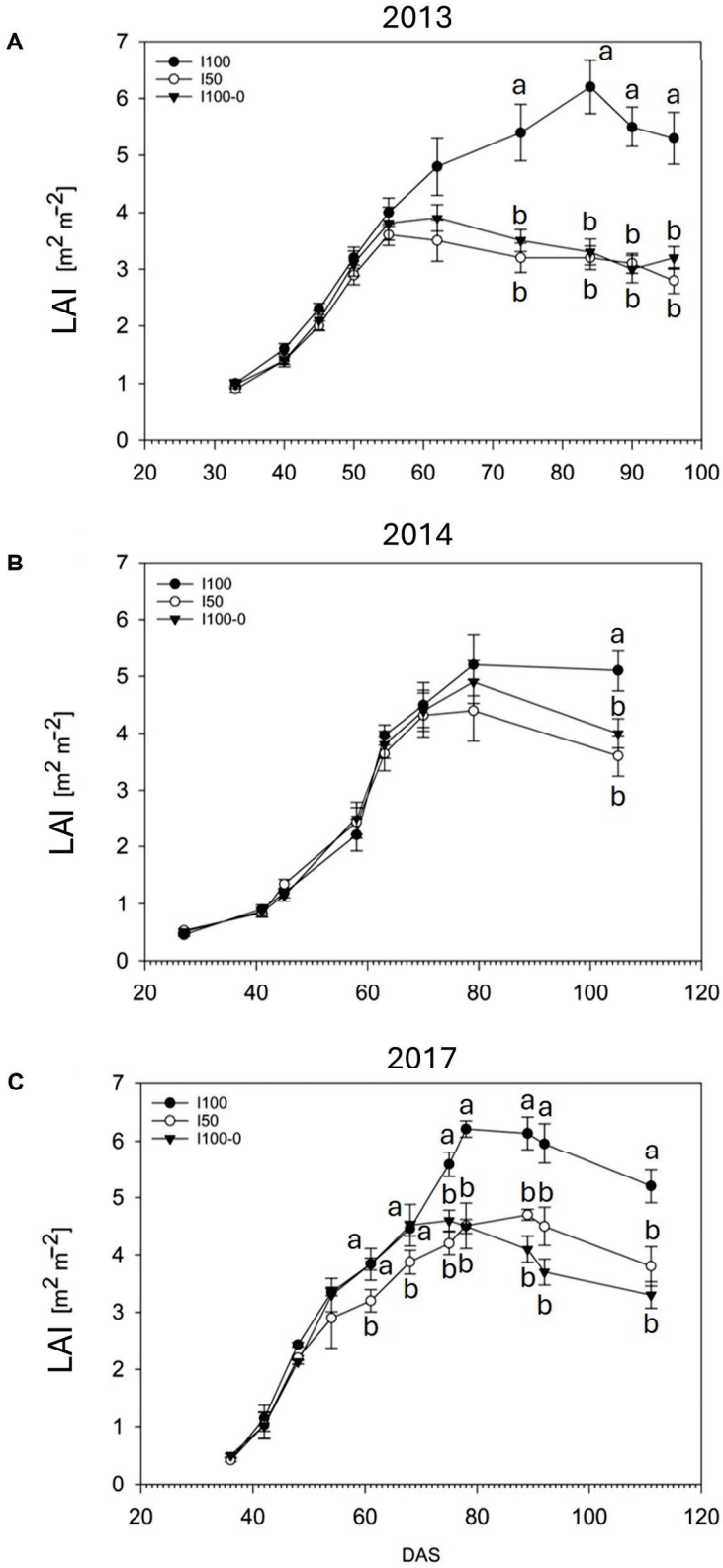


Figure 6. Trends in the mean and standard error of leaf area index (m^2 m^{-2}) for each treatment (full irrigation, I100; deficit irrigation, I50; regulated deficit irrigation, I100-0) during the three years of the trial (2013 (**A**); 2014 (**B**); 2017 (**C**)); DAS indicates days after sowing. Different letters indicate significant differences ($p < 0.05$).

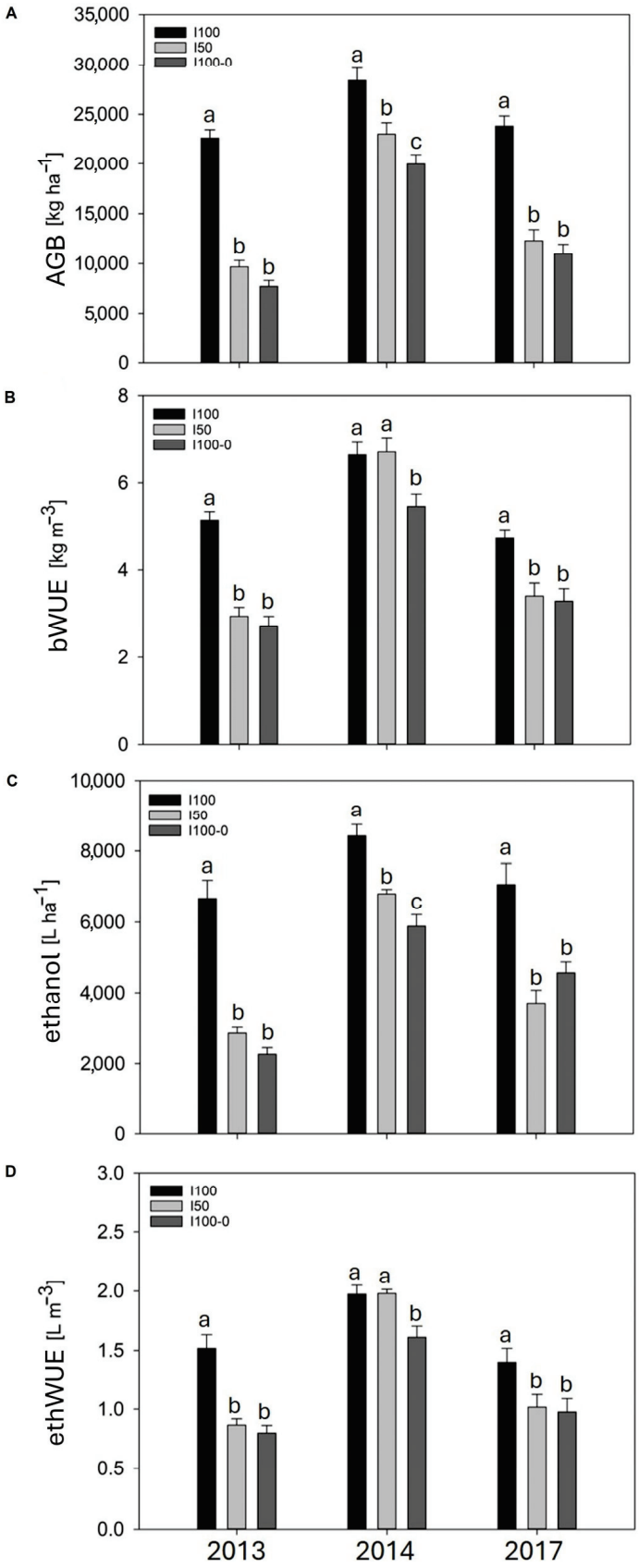


Figure 7. The amount of aboveground biomass ((**A**); kg ha^{-2}), biomass water use efficiency ((**B**); kg m^{-3}), the amount of calculated ethanol production ((**C**); L m^{-3}), and ethanol water use efficiency ((**D**); L m^{-3}) for each treatment (full irrigation, I100; deficit irrigation, I50; regulated deficit irrigation, I100-0) during the study period. Different letters indicate significant differences ($p < 0.05$).

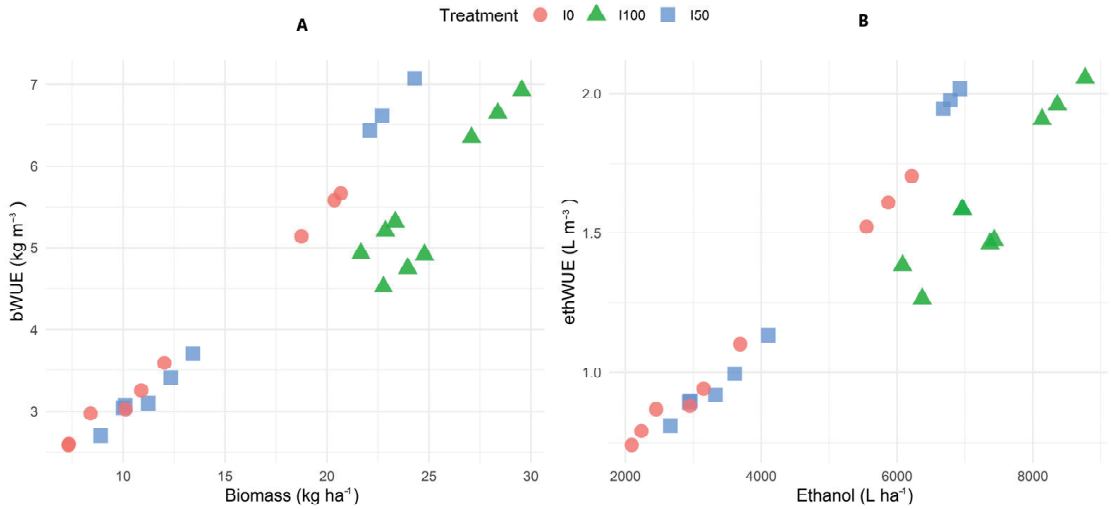


Figure 8. Relationship between water use efficiency and productivity for the three irrigation treatments (I0, I50, I100). (**A**) Biomass water use efficiency (bWUE) vs. biomass production. (**B**) Ethanol water use efficiency (ethWUE) vs. ethanol production.

4. Discussion

Sorghum is a crop that requires irrigation to achieve optimal growth and productivity; particularly, the biomass productivity and water use of energy sorghum are affected by irrigation levels [38]. In the present research, the results follow the pattern mentioned above. Sorghum irrigated replacing 100% of the ETc (I100) showed the highest final values of LAI and aboveground biomass; the latter parameter was higher for all the irrigation treatments during the second year of the experiment than the first and the third. This could be attributed to the high amount of precipitation that fell during the 2014 summer.

Few studies have investigated the effect of different irrigation levels on biomass composition. Enciso et al. [39] reported that the irrigation water amount did not cause differences in sorghum dry biomass composition, with no effects on biofuel quality. In this study, the irrigation level did not compromise the amount of cellulose and hemicellulose of sorghum during all the seasons of the trial, confirming the results of Enciso et al. [39]. In this research, the content of cellulose and hemicellulose was higher (~32% and ~25%, respectively, each year) than what was reported by Zhao et al. [40] in China (19–27% of cellulose and 16–23% of hemicellulose), confirming what already reported by Campi et al. [2], in a previous study that investigated the effect of irrigation with wastewater on sorghum biomass composition under Mediterranean conditions. On the other hand, they did not find a significant effect in terms of the season on the hemicellulose content, different from the present research. Fracasso et al. [41] evaluated the performance of different sorghum cultivars grown under rainfed and irrigated conditions in the north of Italy. The Bulldozer cultivar had lower values of cellulose content (between 24 and 27% of cellulose) than those of the present study but a similar hemicellulose content (~24%). Moreover, in their study, cellulose content was affected by irrigation water application. Taken together, these findings may suggest that the cultivation environment and climatic zones could significantly affect the cellulose content in sorghum. Considering that cellulose and hemicellulose are both sources of fermentable sugars that can be converted into biofuel, their high content in dry biomass is necessary to ensure sufficient ethanol production [42–45], and long-term studies seem to be required to assess the content of these sorghum biomass structural components in different cultivars in the Mediterranean basin and to identify adequate field practices to maximize their content in sorghum dry biomass.

Studies carried out on sorghum performance under different irrigation regimes, in the same region as the present research, are not so numerous; Maucieri et al. [46] studied sorghum biomass production in southern Italy with different levels of irrigation (0%, 33%, 66%, and 100% ETc) using treated urban wastewater. Their results indicate that the highest dry biomass yield was obtained with full irrigation (100% ETc), while reduced irrigation levels significantly reduced biomass accumulation. This is in line with our results, in which full irrigation provided the highest biomass yield, confirming the importance of providing an adequate water supply in Mediterranean climates. Similarly, Habyarimana et al. [47] evaluated the performance of 75 sorghum genotypes under both irrigated and rainfed conditions at three locations in Italy. They reported that irrigated sorghum achieved significantly higher dry biomass yields (33–51 t ha^{-1}) than rainfed conditions (20–29 t ha^{-1}). Their study also showed a significant interaction between genotype and location, suggesting that environmental variability plays an important role in biomass production. Our results confirm these findings, showing a marked reduction in biomass production under deficit irrigation conditions, emphasizing the need to adapt irrigation strategies to local climatic and soil conditions. Also, Garofalo and Rinaldi [7] conducted a trial in the same region as the current research on the effect of different irrigation levels on sorghum biomass water use efficiency. They reported that sorghum biomass had a high potential productivity of dry matter under Mediterranean conditions, whether or not water demands were adequately satisfied. In this study, the I100 treatment showed the highest level of bWUE in 2013 and 2017. In 2014, the bWUE of I100 and I50 were comparable; probably, the high amount of rainfall overturned the effect of irrigation water deprivation [48,49]. bWUE values were in line with the literature (between 2.89 kg m^{-3} and 3.75 kg m^{-3}) for the I50 and I100-0 treatments [50]; in contrast, I100 showed a notably higher bWUE. I100 and I100-0 showed comparable values of bWP (see Table 2), with no statistically significant differences. However, for bWUE (see Figure 7), I100 showed significantly higher values than I100-0, indicating greater efficiency in converting water to biomass under full irrigation; instead, I50 showed a higher water productivity, appearing as the most efficient treatment in terms of the use of water in sorghum cultivation. The relationships between biomass and bWUE, and between ethanol yield and ethWUE, further support these results. The I100 treatment achieved the highest bWUE values, particularly at the highest biomass yields (25–30 kg ha^{-1}) and also provided the highest ethanol yields (>6000 L ha^{-1}), along with the highest ethWUE values (>2 L m^{-3}). These results are consistent with the observation that full irrigation maximizes both biomass and ethanol productivity and water use efficiency. However, the I50 treatment emerged as a balanced alternative that can maintain substantial biomass (15–20 kg ha^{-1}) and ethanol (4000-6000 L ha^{-1}) yields, while maintaining the bWUE (5–6 kg m^{-3}) and ethWUE (1.5–2 L m^{-3}). This highlights that I50 is a sustainable strategy to optimize water use without drastically reducing productivity. In contrast, the I0 treatment produced the lowest values for both bWUE (3–4 kg m^{-3}) and ethWUE (<1.5 L m^{-3}), highlighting the important role of supplemental irrigation in improving productivity and efficiency. These results are in line with those of Aydinsakir et al. [25] and Pang et al. [26], who showed that moderate water deficits, as in the I50 treatment, can maintain acceptable bioethanol yields and water use efficiency. However, the highest productivity and efficiency is generally achieved with full irrigation (I100), highlighting the trade-off between water savings and maximum yields.

Sweet sorghum has a minor relevance in producing refined sugar when compared with other crops, such as sugar beet and sugarcane; nonetheless, it is a more efficient crop, since the input required to produce raw juice for ethanol yields is less than with those crops [51]. In this study, total ethanol production was higher for the I100 treatments each year than the other irrigation treatments, due to the higher amount of biomass produced,

since ethanol production, dry biomass, and LAI are strictly related [52]. Average ethanol production was higher in the 2014 season, due to the higher water amount received. These results are in line with Neto et al. [53], who found that when starch crops like sorghum and maize (*Zea mays* L., 1753) are fully watered they can allow for a higher ethanol production. Ethanol water indices followed biomass water indices trends, with a higher ethWP in 2014 than other seasons and a higher productivity performance by I50 than the other treatments.

5. Conclusions and Future Directions

This study highlighted significant outcomes regarding the effectiveness of irrigation strategies for energy sorghum cultivation, within a Mediterranean context, characterized by limited water resources. Full irrigation consistently led to the highest biomass production across the study period, underlining its effectiveness in maximizing yields in water-sufficient scenarios. In contrast, regulated deficit irrigation resulted in the lowest biomass yields among the three treatments. This highlighted the impact of water limitation on biomass productivity in energy sorghum. Although full irrigation offers the significant opportunity to increase biomass yields, under conditions of limited water availability, deficit irrigation offers less risk than regulated deficit irrigation, providing, compared to the latter, higher yields (of both biomass and calculated ethanol), as well as a higher water use efficiency and productivity. The irrigation level did not significantly alter the biomass composition in terms of cellulose and hemicellulose content, which are crucial for bioethanol production; this finding suggests that even under reduced water conditions, fermentable sugar content remained unaffected. Long-term field studies are necessary to assess cellulose and hemicellulose content in energy sorghum under different environmental conditions in the Mediterranean basin. The outcomes of this study could be useful for strategic irrigation planning in energy sorghum growing, especially in arid and semi-arid areas. The results point to the need to adapt irrigation practices to balance yield maximization and irrigation water preservation, depending on the specific aim of the farmer (biomass production or water use efficiency) and environmental conditions.

Future research should focus on optimizing irrigation strategies by integrating additional agronomic practices aimed at improving water retention and mitigating thermal stress. The use of soil amendments such as organic mulches and compost could enhance soil moisture conservation, improve plant water status, and sustain biomass productivity under limited water availability [54]. Additionally, the application of mineral-based protective coatings, such as reflective particle films, may help reduce canopy temperatures and improve photosynthetic efficiency, potentially enhancing crop resilience to heat and drought stress [55]. Investigating the combined effects of these techniques with different irrigation levels could provide valuable insights into sustainable sorghum production, particularly in arid and semi-arid environments.

Supplementary Materials: The following supporting information can be downloaded at: https://www.mdpi.com/article/10.3390/w17040578/s1, Table S1: Daily amount of rainfall and irrigation water applied during the three years of the experiment for each treatment (full irrigation, I100; deficit irrigation, I50; regulated deficit irrigation, I100-0).

Author Contributions: Conceptualization, S.P.G., A.F.M. and P.C.; Data curation, S.P.G., G.d.C., A.F.M. and P.C.; Formal analysis, S.P.G.; Investigation, S.P.G., A.F.M. and P.C.; Methodology, S.P.G., A.F.M. and P.C.; Project administration, P.C.; Resources, P.C.; Software, S.P.G. and P.C.; Supervision, P.C.; Visualization, S.P.G.; Writing—original draft, S.P.G. and P.C.; Writing—review and editing, A.F.M. and P.C. All authors have read and agreed to the published version of the manuscript.

Funding: This research received no external funding.

Data Availability Statement: The raw data supporting the conclusions of this article will be made available by the authors on request.

Conflicts of Interest: The authors declare no conflicts of interest.

References

1. Fernando, A.L.; Duarte, M.P.; Almeida, J.; Boléo, S.; Mendes, B. Environmental impact assessment of energy crops cultivation in Europe. *Biofuels Bioprod. Biorefining* **2010**, *4*, 594–604. [CrossRef]
2. Campi, P.; Navarro, A.; Domenico Palumbo, A.; Solimando, M.; Lonigro, A.; Mastrorilli, M. Productivity of energy sorghum irrigated with reclaimed wastewaters. *Ital. J. Agron.* **2014**, *9*, 115–119. [CrossRef]
3. McKendry, P. Energy production from biomass (part 1): Overview of biomass. *Bioresour. Technol.* **2002**, *83*, 37–46. [CrossRef] [PubMed]
4. Zema, D.A.; Bombino, G.; Andiloro, S.; Zimbone, S.M. Irrigation of energy crops with urban wastewater Effects on biomass yields, soils and heating values. *Agric. Water Manag.* **2012**, *115*, 55–65. [CrossRef]
5. Steduto, P.; Katerji, N.; Puertos-Molina, H.; Unlu, M.; Mastrorilli, M.; Rana, G. Water-use efficiency of sweet sorghum under water stress conditions:gas-exchange investigations at leaf and canopy scales. *Field Crops Res.* **1997**, *54*, 221–234. [CrossRef]
6. Mastrorilli, M.; Katerji, N.; Rana, G. Productivity water use efficiency of sweet sorghum as affected by soil water deficit occurring at different vegetative growth stages. *Eur. J. Agron.* **1999**, *11*, 207–215. [CrossRef]
7. Garofalo, P.; Rinaldi, M. Water-use efficiency of irrigated biomass sorghum in a Mediterranean environment. *Span. J. Agric. Res.* **2013**, *11*, 1153–1169. [CrossRef]
8. Assefa, Y.; Staggenborg, S.A.; Prasad, V.P. Grain sorghum water requirement and responses to drought stress: A review. *Crop Manag.* **2010**, *9*, 1–11. [CrossRef]
9. Singh, B.R.; Singh, D.P. Agronomic and physiological responses of sorghum, maize and pearl millet to irrigation. *Field Crops Res.* **1995**, *42*, 57–67. [CrossRef]
10. Girma, F.S.; Krieg, D.R. Osmotic Adjustment in Sorghum: I. *Mechanisms of Diurnal Osmotic Potential Changes, Plant Physiol.* **1992**, *99*, 577–582. [CrossRef]
11. Wright, G.C.; Smith, R.C.G.; McWilliam, J.R. Differences between two grain sorghum genotypes in adaptation to drought stress. I. Crop growth and yield responses. *Aust. J. Agric. Res.* **1983**, *34*, 615–626. [CrossRef]
12. Djanaguiraman, M.; Gowsiga, S.; Govindaraj, M.; Habyarimana, E.; Senthil, A.; Thavaprakaash, N.; Jeyakumar, P.; Kokilavani, J.; Chellammal, C. Impact of root architecture and transpiration rate on drought tolerance in stay-green sorghum. *Crop Sci.* **2024**, *64*, 2612–2629. [CrossRef]
13. Ajjur, S.B.; Al-Ghamdi, S.G. Evapotranspiration and water availability response to climate change in the Middle East and North Africa. *Clim. Change* **2021**, *166*, 28. [CrossRef]
14. Campi, P.; Modugno, A.F.; De Carolis, G.; Pedrero Salcedo, F.; Lorente, B.; Garofalo, S.P. A Machine Learning Approach to Monitor the Physiological and Water Status of an Irrigated Peach Orchard under Semi-Arid Conditions by Using Multispectral Satellite Data. *Water* **2024**, *16*, 2224. [CrossRef]
15. Garofalo, S.P.; Giannico, V.; Lorente, B.; García AJ, G.; Vivaldi, G.A.; Thameur, A.; Salcedo, F.P. Predicting carob tree physiological parameters under different irrigation systems using Random Forest and Planet satellite images. *Front. Plant Sci.* **2024**, *15*, 1302435. [CrossRef]
16. Alsanad, M.A.; Emara, E.I.R. Optimizing Bioethanol (C_2H_5OH) Yield of Sweet Sorghum Varieties in a Semi-Arid Environment: The Impact of Deheading and Deficit Irrigation. *Water* **2024**, *16*, 1456. [CrossRef]
17. Campi, P.; Gaeta, L.; Mastrorilli, M.; Losciale, P. Innovative soil management and micro-climate modulation for saving water in peach orchards. *Front. Plant Sci.* **2020**, *11*, 544947. [CrossRef]
18. Garofalo, S.P.; Intrigliolo, D.S.; Camposeo, S.; Alhajj Ali, S.; Tedone, L.; Lopriore, G.; De Mastro, G.; Vivaldi, G.A. Agronomic Responses of Grapevines to an Irrigation Scheduling Approach Based on Continuous Monitoring of Soil Water Content. *Agronomy* **2023**, *13*, 2821. [CrossRef]
19. Katerji, N.; Mastrorilli, M.; Rana, G. Water use efficiency of crops cultivated in the Mediterranean region: Review analysis. *Eur. J. Agron.* **2008**, *28*, 493–507. [CrossRef]
20. Kirda, C. *Deficit Irrigation Scheduling Based on Plant Growth Stages Showing Water Stress Tolerance*; FAO Corp: Rome, Italy, 2002; pp. 3–10. Available online: https://www.fao.org/3/y3655e/y3655e03.htm (accessed on 1 February 2025).
21. Consoli, S.; Stagno, F.; Roccuzzo, G.; Cirelli, G.L.; Intrigliolo, F. Sustainable management of limited water resources in a young orange orchard. *Agric. Water Manag.* **2014**, *132*, 60–68. [CrossRef]
22. Consoli, S.; Stagno, F.; Vanella, D.; Boaga, J.; Cassiani, G.; Roccuzzo, G. Partial root-zone drying irrigation in orange orchards: Effects on water use crop production characteristics. *Eur. J. Agron.* **2017**, *82*, 190–202. [CrossRef]

23. Jiao, F.; Ding, R.; Du, T.; Kang, J.; Tong, L.; Gao, J.; Shao, J. Multi-growth stage regulated deficit irrigation improves maize water productivity in an arid region of China. *Agric. Water Manag.* **2024**, *297*, 108827. [CrossRef]
24. Zeleke, K.; Nendel, C. Yield response and water productivity of soybean (*Glycine max* L.) to deficit irrigation and sowing time in south-eastern Australia. *Agric. Water Manag.* **2024**, *296*, 108815. [CrossRef]
25. Aydinsakir, K.; Buyuktas, D.; Dinç, N.; Erdurmus, C.; Bayram, E.; Bayir Yegin, A. Yield and bioethanol productivity of sorghum under surface and subsurface drip irrigation. *Agric. Water Manag.* **2021**, *243*, 106452. [CrossRef]
26. Pang, B.; Zhang, K.; Kisekka, I.; Bean, S.; Zhang, M.; Wang, D. Evaluating effects of deficit irrigation strategies on grain sorghum attributes and biofuel production. *J. Cereal Sci.* **2018**, *79*, 13–20. [CrossRef]
27. Specie Ospiti di Xylella Fastidiosa in Salento. Available online: http://www.infoxylella.it/specie-ospiti-xylella-fastidiosa (accessed on 1 February 2024).
28. Costanza, L.; Maldera, F.; Garofalo, S.P.; Vivaldi, G.A.; Camposeo, S. Ecological optima show the potential diffusion of minor tree crops in *Xylella fastidiosa* subsp. pauca-infected areas through a GIS-Based Approach. *Front. Agron.* **2024**, *6*, 1421627. [CrossRef]
29. Campi, P.; Mastrorilli, M.; Stellacci, A.M.; Modugno, F.; Palumbo, A.D. Increasing the effective use of water in green asparagus through deficit irrigation strategies. *Agric. Water Manag.* **2019**, *217*, 119–130. [CrossRef]
30. Barca, E.; De Benedetto, D.; Stellacci, A.M. Optimization of sampling design for soil total organic carbon assessment in the precision agriculture framework: Impact of different variogram models and potentiality of ground penetrating radar (GPR) covariate information. *Comput. Electron. Agric.* **2024**, *226*, 109470. [CrossRef]
31. Allen, R.G.; Pereira, L.S.; Raes, D.; Smith, M. *Crop Evapotranspiration-Guidelines for Computing Crop Water Requirements-FAO Irrigation And Drainage Paper 56*; Fao: Rome, Italy, 1998; Volume 300, p. D05109.
32. Lhomme, J.P.; Katerji, N. A simple modelling of crop water balance for agrometeorological application. *Ecol. Model.* **1991**, *57*, 11–25. [CrossRef]
33. Mastrorilli, M.; Katerji, N.; Rana, G.; Ben Nouna, B. Daily actual evapotranspiration measured with TDR technique in Mediterranean conditions. *Agric. Forest Meteor.* **1998**, *90*, 81–89. [CrossRef]
34. Rana, G.; Katerji, N. Operational model for direct determination of evapotranspiration for well watered crops in Mediterranean region. *Theor. Appl. Climatol.* **2009**, *97*, 243–253. [CrossRef]
35. Van Soest, P.J.; Robertson, J.B.; Lewis, B.A. Methods for Dietary Fiber, Neutral Detergent Fiber, and Nonstarch Polysaccharides in Relation to Animal Nutrition. *J. Dairy Sci.* **1991**, *74*, 3583–3597. [CrossRef] [PubMed]
36. The Japan Institute of Energy. *The Asian Biomass Handbook. A Guide for Biomass Production and Utilization*; The Japan Institute of Energy: Tokyo, Japan, 2008.
37. Fernández, J.E.; Alcon, F.; Diaz-Espejo, A.; Hernandez-Santana, V.; Cuevas, M.V. Water use indicators and economic analysis for on-farm irrigation decision: A case study of a super high density olive tree orchard. *Agric. Water Manag.* **2020**, *237*, 106074. [CrossRef]
38. Chavez, J.C.; Enciso, J.; Meki, M.N.; Jeong, J.; Singh, V.P. Simulation of energy sorghum under limited irrigation levels using the EPIC model. Trans. *ASABE* **2018**, *61*, 121–131. [CrossRef]
39. Enciso, J.; Jifon, J.; Ribera, L.; Zapata, S.D.; Ganjegunte, G.K. Yield, water use efficiency and economic analysis of energy sorghum in South Texas. *Biomass Bioenergy* **2015**, *81*, 339–344. [CrossRef]
40. Zhao, Y.L.; Dolat, A.; Steinberger, Y.; Wang, X.; Osman, A.; Xie, G.H. Biomass yield and changes in chemical composition of sweet sorghum cultivars grown for biofuel. *Field Crops Res.* **2009**, *111*, 55–64. [CrossRef]
41. Fracasso, A.; Perego, A.; Amaducci, S. Characterisation of ten commercial sorghum genotypes grown under water-limited conditions for bioenergy production in Mediterranean environment. *Ital. J. Agron.* **2017**, *12*, 302–314. [CrossRef]
42. Avanthi, A.; Kumar, S.; Sherpa, K.C.; Banerjee, R. Bioconversion of hemicelluloses of lignocellulosic biomass to ethanol: An attempt to utilize pentose sugars. *Biofuels* **2017**, *8*, 431–444. [CrossRef]
43. Alabdalall, A.H.; Almutari, A.A.; Aldakeel, S.A.; Albarrag, A.M.; Aldakheel, L.A.; Alsoufi, M.H.; Alfuraih, L.Y.; Elkomy, H.M. Bioethanol production from lignocellulosic biomass using Aspergillus niger and Aspergillus flavus hydrolysis enzymes through immobilized *S. cerevisiae*. *Energies* **2023**, *16*, 823. [CrossRef]
44. Propheter, J.L.; Staggenborg, S.A.; Wu, X.; Wang, D.J.A.J. Performance of annual and perennial biofuel crops: Yield during the first two years. *Agron. J.* **2010**, *102*, 806–814. [CrossRef]
45. Billa, E.; Koullas, D.P.; Monties, B.; Koukios, E.G. Structure and composition of sweet sorghum stalk components. *Ind. Crops Prod.* **1997**, *6*, 297–302. [CrossRef]
46. Maucieri, C.; Cavallaro, V.; Caruso, C.; Borin, M.; Milani, M.; Barbera, A.C. Sorghum biomass production for energy purpose using treated urban wastewater and different fertilization in a Mediterranean environment. *Agriculture* **2016**, *6*, 67. [CrossRef]
47. Habyarimana, E.; Laureti, D.; De Ninno, M.; Lorenzoni, C. Performances of biomass sorghum [*Sorghum bicolor* (L.) Moench] under different water regimes in Mediterranean region. *Ind. Crops Prod.* **2004**, *20*, 23–28. [CrossRef]
48. Akinseye, F.M.; Folorunsho, A.H.; Hakeem, A.; Agele, S.O. Impacts of rainfall and temperature on photoperiod insensitive sorghum cultivar: Model evaluation and sensitivity analysis. *J. Agrometeorol.* **2019**, *21*, 262–269. [CrossRef]

49. Hadebe, S.T.; Mabhaudhi, T.; Modi, A.T. Water use of sorghum (Sorghum bicolor, L. Moench) in response to varying planting dates evaluated under rainfed conditions. *Water SA* **2017**, *43*, 91–103. [CrossRef]
50. Farré, I.; Faci, J.M. Comparative response of maize (*Zea mays* L.) and sorghum (*Sorghum bicolor* L. Moench) to deficit irrigation in a Mediterranean environment. *Agric. Water Manag.* **2006**, *83*, 135–143. [CrossRef]
51. Whitfield, M.B.; Chinn, M.S.; Veal, M.W. Processing of materials derived from sweet sorghum for biobased products. *Ind. Crops Prod.* **2012**, *37*, 362–375. [CrossRef]
52. Tang, C.; Li, S.; Li, M.; Xie, G.H. Bioethanol potential of energy sorghum grown on marginal and arable lands. *Front. Plant Sci.* **2018**, *9*, 291348. [CrossRef]
53. Chaiben, M.; Robaina, A.D.; Peiter, M.X.; Rodrigues, S.A.; Flores, Y.R.; Bruning, J.; Silva, J.G.D.; Ferreira, L.D. Economic indicators for ethanol production from starch crops under different irrigation managements. *Rev. Bras. Eng. Agrícola E Ambient.* **2022**, *26*, 640–648. [CrossRef]
54. Abd El-Mageed, T.A.; El-Samnoudi, I.M.; Ibrahim, A.E.A.M.; Abd El Tawwab, A.R. Compost mulching modulates morphological physiological responses water use efficiency in sorghum (bicolor, *L. Moench*) under low moisture regime. *Agric. Water Manag.* **2018**, *208*, 431–439. [CrossRef]
55. Petoumenou, D.G. Enhancing Yield and Physiological Performance by Foliar Applications of Chemically Inert Mineral Particles in a Rainfed Vineyard under Mediterranean Conditions. *Plants* **2023**, *12*, 1444. [CrossRef]

Disclaimer/Publisher's Note: The statements, opinions and data contained in all publications are solely those of the individual author(s) and contributor(s) and not of MDPI and/or the editor(s). MDPI and/or the editor(s) disclaim responsibility for any injury to people or property resulting from any ideas, methods, instructions or products referred to in the content.

water

MDPI

Article

How Much Is Enough? Data Requirements for Practical Irrigation Decision-Making in Vietnamese Coffee Production

Michael Scobie [1,*], David Freebairn [1], Shahbaz Mushtaq [1] and Darrell Donahue [2]

[1] Centre for Applied Climate Sciences, University of Southern Queensland, Toowoomba, QLD 4350, Australia; david.freebairn@gmail.com (D.F.); shahbaz.mushtaq@unisq.edu.au (S.M.)
[2] Davis College of Agriculture, Natural Resources and Design, West Virginia State University, Morgantown, WV 26506, USA; darrell.donahue@mail.wvu.edu
* Correspondence: michael.scobie@unisq.edu.au; Tel.: +61-7-4631-1394

Abstract: In making irrigation decisions, farmers typically rely on local observation and experience, such as observing crops and neighbors' actions. Research has mainly focused on understanding crop water requirements to improve farming practices, but it is important to acknowledge that farmers have unique perspectives, access to diverse local "signals", and experience. The challenge is to strike a balance between complex technical assessments of field conditions (the science) and harnessing farmers' skills to manage their irrigation in ways that maximize yield and quality. This study established a basis for specifying minimum data requirements for pragmatic, but not necessarily perfect, irrigation decision-making for small-scale Vietnamese coffee farmers. This study focuses on three areas in Dak Lak province in the Central Highlands of Vietnam. To explore the role of monitoring in irrigation management, two contrasting monitoring systems were set up to collect soil, weather, and irrigation data. We also compared a variety of water balance models with different data requirements, with a focus on processes that used "passive data collection", i.e., farmers do not manually collect data, rather data can be accessed readily from external sources. In Vietnam, traditional hosepipe irrigation is applied where it is impractical to know the volume of applied water. The proposed Low Data Model (LDM) is suited to more informed irrigation scheduling decisions, which have potential to improve the likelihood of coffee growers adopting measurement-based decision-making. While researchers may seek a detailed daily sub-millimeter understanding of soil water dynamics, farmers require practical decision support if there is to be any adoption of improved methods. This study offers a simple and practical approach for irrigation scheduling rather than a model using numerically perfect data that is unachievable in the field. The work demonstrates that on-site rainfall data is essential. However, other data can be collected passively to reduce the burden of data collection on users. This approach may enhance the likelihood of model-based irrigation scheduling being adopted by coffee farmers in Vietnam.

Keywords: coffee; Vietnam; irrigation strategy; irrigation scheduling; dss; decision

1. Introduction

Vietnam is the world's leading Robusta coffee producer and the second-largest coffee producer in the world. Approximately 80 percent of the coffee is produced in the Central Highlands regions, with most of Vietnam's coffee produced by small land holders. Yields are among the highest in the world, with irrigation critical to Vietnam's success in maintaining a sustainable coffee industry. Without irrigation, coffee trees would struggle to survive the region's extended dry season, with most small farmers having access to

constructed wells, surface water, or groundwater for irrigation. Farmers face "agricultural droughts" when both groundwater and surface water flows are reduced and irrigation is not possible [1,2].

Irrigation from January to April is critical to achieving high yield. Approximately three-quarters of annual rainfall in the Central Highlands occurs in the monsoon season (June through September) with the remaining 8 months characterized by unreliable and small falls, insufficient to sustain a perennial crop such as coffee. While total annual rainfall (1800–3000 mm) appears sufficient for Robusta coffee [3], it does not occur at critical periods for maximum yields. Irrigation is required to offset the impacts of inter and intra-seasonal rainfall variability [4], but over-irrigation can be costly and reduce crop growth. Consequently, improved irrigation practices are necessary for the future success of the Vietnamese coffee industry, as resources become less reliable and area increases [5]. Previous studies have determined coffee crop water requirements of higher-grade Coffea arabica [6,7], with a few studies focused on the Coffea Canephora (Robusta) varieties that represent 30% of global production [8].

While irrigation is an essential part of coffee production, Amarasinghe, et al. [9] found coffee in Vietnam benefited from some induced water stress between January and April to boost flowering and pollination with higher and more uniform yields. Kath, et al. [10] provide evidence that there is a quantifiable response between irrigation and yield and that future work should investigate the relationships between irrigation, water stress, flowering, and yield. Clearly, there is a need to manage water supply to meet crop needs as well as constrain watering at critical growth stages.

Current irrigation of coffee in the Central Highlands involves hand-held hosepipes to individually bunded trees. Volumes applied vary with rainfall, antecedent moisture conditions, water availability, and farmers' opinions on crop needs. Visual performance of the crop and neighboring actions typically trigger irrigation as few farmers have on-farm water, soil, plant, or weather-sensing equipment to support data-driven decisions. Irrigation is generally based on experience and routines [11], with few other metrics used to assess benefit, making it difficult to compare alternative practices. A typical response of smallholders is to apply luxury water, estimated to be up to double crop needs [12]. While under-irrigating may carry risks of crop failure, over-irrigating is viewed by farmers as "insurance" for their high-yielding crops, yet this practice is clearly wasteful and may limit industry development when water supply becomes more limited under climate uncertainty [13].

Drip and micro-sprinkler irrigation systems are increasing in use [6] as they can apply small, measured volumes of water and are promoted as water and energy-saving with environmental and catchment-wide benefits. However, because of poor training or maintenance, irrigation systems are not always managed in a way that supports productivity and profit [14].

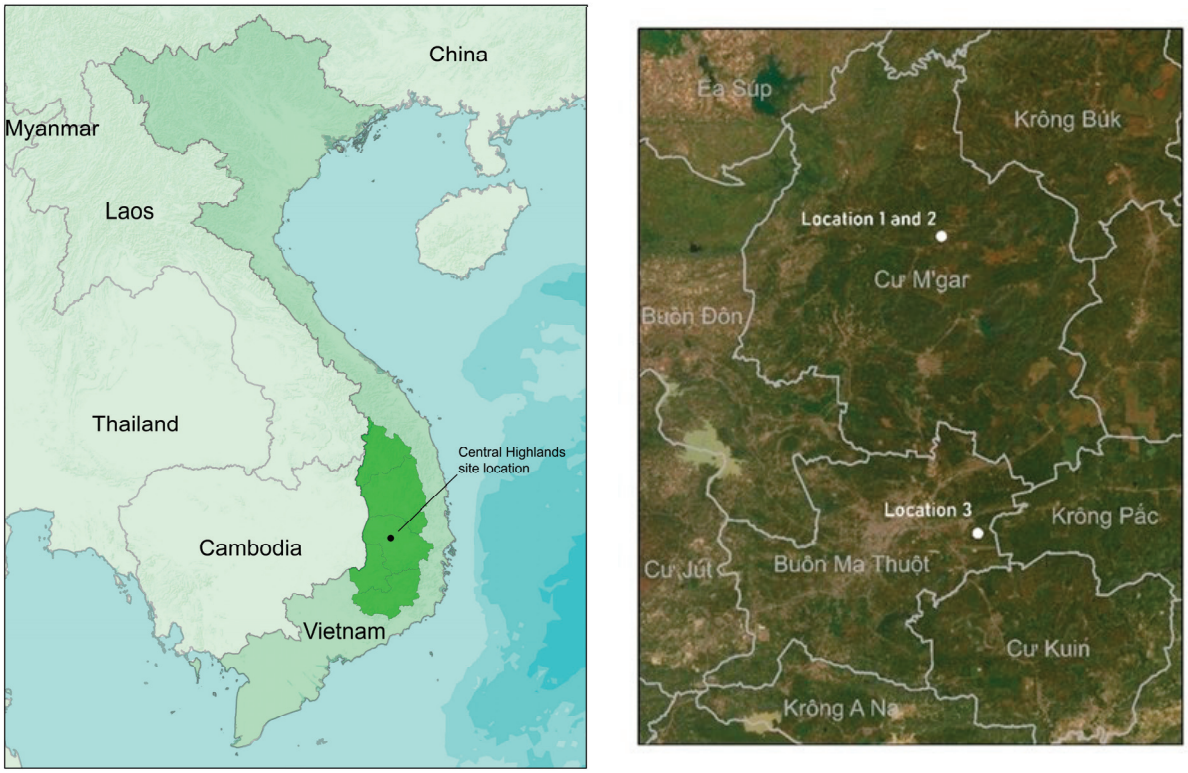
Recent unpublished data indicate that approximately 90% of coffee farmers in the Central Highlands use irrigation on their coffee farms at least once per season and 85% use irrigation twice or more each season. However, less than 2% of farmers use a quantitative method to determine volumes and timing of irrigation schedules. Farmers and their local service providers are generally making decisions based on set practices, with little attention to site-specific conditions that might improve water application volumes.

Computing power available in handheld devices now makes dependence on large computer systems redundant. Freely available remote sensing and synthetic weather data provide opportunities to develop irrigation tools for farmers that avoid some of the previous constraints to adoption. Even with the elimination of technical constraints, challenges remain on how best to present information to small-scale irrigators. For example,

can datasets be used in isolation or is local validation required? What are the minimum data requirements to make reasonable irrigation decisions, accounting for the relative inefficiency of traditional irrigation and the inherent error in volumes applied? Nguyen, et al. [15] propose a smart agriculture platform that utilizes LoRaWAN IoT, Big Data, Blockchain, and AI for improved decision-making for farmers who do not yet record any data. A commonsense beginning is needed in the design, analysis, and delivery of irrigation guidance information.

Industry Description

Coffee production in Vietnam's Central Highlands region is characterized by diverse topography, fertile soils, and favorable climatic conditions for a range of crops with potential for broad commercial agricultural development (Figure 1). The region is home to many of Vietnam's agricultural commodities and is the world's second-largest exporter of coffee and a top producer of pepper globally [16].



(**a**) (**b**)

Figure 1. (**a**) Location of Dak Lak Province in the Central Highlands of Vietnam and (**b**) the locations of the study sites in Dak Lak province in the Cu M'Gar and Buon Ma Thuot districts. Locations 1 and 2 were near Cu M'Gar, located at selected farms (farmer sites), and Location 3 was at a research station near Buon Ma Thuot.

The Central Highlands region accounts for 95 percent of Vietnam's coffee-growing area [17], with an annual production of approximately 1.68 million tonnes in an area of 683,800 ha [18]. It is estimated that more than 640,000 smallholdings are involved in coffee production (around 85% of the total coffee area) [19], most of which access irrigation for a portion of the growing season.

Coffee production in the Central Highlands has been expanding since the late 1990s. Between 1980 and 2000, the area cultivated under coffee in Vietnam increased 23-fold, with an 83-fold production increase [20] primarily due to expansion in the Central Highlands.

Soils and climate in the Central Highlands are ideal for irrigated coffee production, with most of the coffee grown in deep weathered Rhodic Ferrosols derived from basalt [21]. To achieve high yields, irrigation is required in the dry months to break bud dormancy [6,22] and to promote uniform flowering and fruit development. Due to the Asian monsoon impacting the Central Highlands (Figure 2), rainfall provides ~25% of potential crop evapotranspiration demand [9].

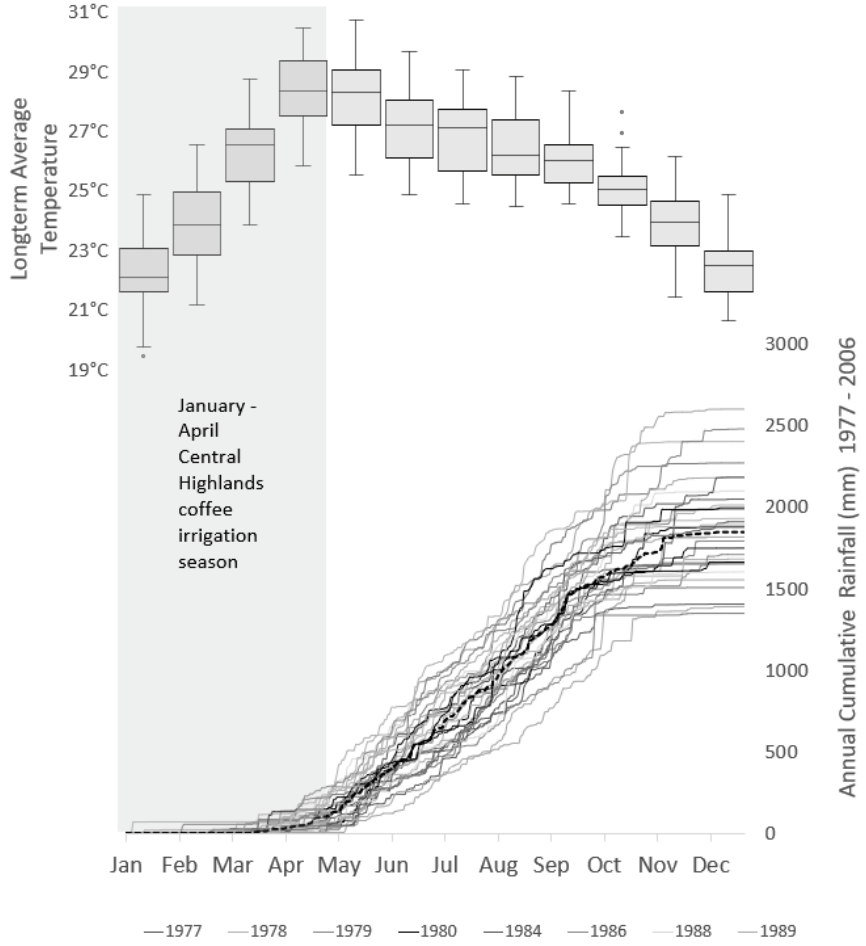


Figure 2. Long-term average monthly temperature (box and whisker) and accumulated annual rainfall (witches' hair plot) for Buon Ma Thuot (1977–2002). Each grey line indicates one year of accumulated rainfall data from January to December. The dotted line is the median accumulated rainfall. The grey section to the left is the typical irrigation season from January to April. This period is characterized by temperatures increasing to a peak in April, and by minimal accumulated rainfall (mean < 100 mm) during the period.

The extensive expansion of coffee areas and unsustainable irrigation practices threaten the Central Highlands' groundwater reserves through over-extraction [12,21]. Modelling undertaken by Truong, et al. [23] has shown that farmers' irrigation directly affects the depletion of the groundwater resources and fundamentally disrupts the regional hydrological cycle. Water supply is finite, and water use efficiency will determine the extent of future development. If irrigation can be optimized, the risk of water shortage is minimized, especially in drought years [1,24]. More efficient irrigation can conserve groundwater, reduce irrigation costs, and improve profitability of coffee farmers. Policy and regulation of the systems are key to ensuring long-term viability [25,26].

Government-funded extension of the Central Highlands coffee industry is a well-regarded source of agronomic information; however, less than 1% of farmers use the agency for irrigation scheduling advice. Using experience and data from three locations in Dak

Lak province in the Central Highlands of Vietnam and freely available climate data, we develop a physically based crop water-use model to achieve a balance between complexity of technical information, data access, and farmers' ability to action a decision. We compare complex and simpler water balance models to explore trade-offs between effort, reliability, and repeatability. We test the use of a tailored, fit-for-purpose, irrigation scheduling model, which can provide reasonable, measurement-based advice for farmers, with a minimal burden of cost, data collection, and analysis.

2. Materials and Methods

Three locations were selected in Dak Lak province of the Central Highlands for detailed monitoring in 2019 (Figure 1). The predominant soils at both the Cu M'Gar and Buon Ma Thuot sites are deep (>1000 mm), well-drained, uniformly textured ferrosols derived from basalt and are well suited to a variety of cropping systems including coffee, rubber, and cashew [27].

Datasets for atmospheric, soil, and water flow parameters were recorded for three sites over three irrigation seasons. The instrumentation supported a data-rich representation of crop water usage patterns during irrigation seasons. Data were recorded at 15-min intervals at all sites, with 2020 data sets used to calibrate models and 2021 and 2022 data applied for model validation.

2.1. Data Sets

Two on-site data collection systems were deployed: a high-end system from The Meter Group (Pullman, Washington, DC, USA); and a low-cost system from a local AgTech Start-up, MimosaTEK (Ho Chi Minh City, Vietnam). A comparison was made between the cost, quality, and reliability of the two systems.

2.1.1. Weather—Local

Both the Cu M'Gar and Buon Ma Thuot locations were equipped with two automatic weather stations. An Atmos 41 (The Meter Group) recorded air temperature, solar radiation, wind speed and direction, relative humidity, atmospheric pressure, and rainfall at 15-min time intervals. The second automatic weather station (MimosaTEK) recorded air temperature, illuminance (lux), wind speed and direction, relative humidity, and rainfall at 15-min intervals.

2.1.2. Weather—Remote Sensing

Remote-sensing platforms including NASA POWER data (https://power.larc.nasa.gov/, accessed on 15 February 2025) [28,29] are available with varying reliability across much of Southeast Asia. Satellite and model-based products provide reliable solar and meteorological data in Dak Lak Province, where historical and reliable measurements are not readily available. These data series are available on a 0.5° latitude by 0.5° longitude grid as a range of time series. Local meteorological datasets are available for Dak Lak province from 1981 (Figure 2).

2.1.3. Soil Moisture

Two independent soil moisture monitoring systems were installed at each site to ensure greater reliability and provide some redundancy capacity (Figure 3). Five Teros 12 water content sensors (The METER Group) were installed at each site at depths of −150 mm, −300 mm, −600 mm, −900 mm and −1200 mm. These sensors have a volume of influence of 1100 mL with a reported accuracy of ± 3% volumetric water content in mineral soils, an electrical conductivity of <8 dS/m, and a resolution of 0.001 m^3/m^3. (MeterGroup, 2023).

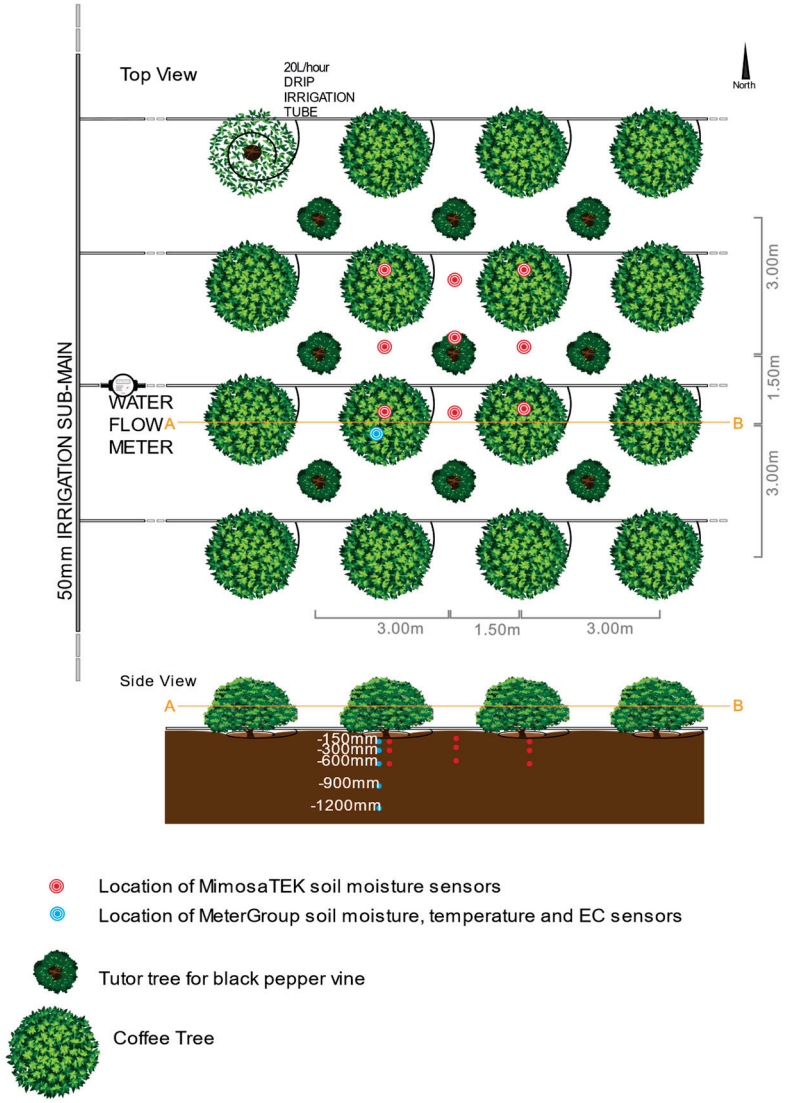


Figure 3. Systematic view of irrigation and soil water measurement instrumentation. Plant spacing between coffee trees is typically 3 m × 3 m. An opportunity or shade tree may be planted interspersed between the coffee at offset 3 m × 3 m spacing. The red targets show the location of the low-cost MimosaTEK sensors in an intensive grid pattern on the northern side of the tree line. The Meter Group sensors were installed near the southwest-most MimosaTEK sensor at the same depths to compare the sensing systems.

Lower-cost moisture sensing equipment (MimosaTEK) was also installed at the same depths. These sensors report apparent soil moisture content calculated using soil capacitance.

Soil samples were taken at each soil sensor location and depth at the time of sensor installation. Laboratory analysis of the volumetric water content [30] and the texture classification was undertaken and used to calibrate sensors and parameterize soils for modelling.

2.2. Approaches to Estimating Evapotranspiration

Crop water use estimations can be calculated using a range of methods involving measurements of one or more parameters in the soil–plant–atmosphere continuum. Allen, et al. [31] note that there have been many approaches to validation of evapotranspiration and crop water use estimates for coffee and other crops through calculation of atmospheric demand and undertaking a soil water balance. These studies aimed at defining reference evapotranspiration at daily or sub-daily scales. The ability to quantify irrigation inputs

with millimeter precision is beyond what a small-scale holder farmer can action using traditional hosepipe irrigation.

There are numerous methods for calculating reference crop evapotranspiration from meteorological data with varying input requirements and reliability. This study does not assess the relative performance of the range of methods; rather, two methods were chosen, the industry-standard FAO56 Penman–Monteith [31] and the Hargreaves method [32]. These two methods were then assessed with a range of input sources of varying accessibility and local reliability.

Penman–Monteith (P-M) (Equation (1)) was recognized as the standard by the International Commission for Irrigation and Drainage (ICID) and the World Meteorological Organization (WMO) in May 1990 [33]. The method is seen to overcome concerns with the previous Penman method and has been shown to represent crop water use reliably for a wide range of soil and environmental conditions. However, the application of P-M requires radiation, air temperature, air relative humidity, and wind speed data [31] at the local level, which is a limitation in many situations, with on-site equipment requirements.

$$ET_0 = \frac{0.408\Delta(R_n - G) + \gamma\left(\frac{900}{(T+273)}\right)u_2(e_s - e_a)}{\Delta + \gamma(1 + 0.34u_2)} \quad (1)$$

ET_0 = reference evapotranspiration (mm day^{-1}),
R_n = net radiation at the crop surface (MJ m^{-2} day^{-1}),
G = soil heat flux density (MJ m^{-2} day^{-1}),
T = mean daily air temperature at 2 m height (°C),
U_2 = wind speed at 2 m height (m s^{-1}),
e_s = saturation vapor pressure (kPa),
e_a = actual vapor pressure (kPa),
$e_s - e_a$ = saturation vapor pressure deficit (kPa),
Δ = slope vapor pressure curve (kPa °C^{-1}),
γ = psychrometric constant (kPa °C^{-1})

Many empirical methods use temperature as a primary input. Allen, Pereira, Raes, and Smith [31] note that the Hargreaves and Samani [32] method (Equation (2)) shows satisfactory results globally without significant local calibration. Input data requirements of the Hargreaves method are lower and simpler to collect.

$$ET_0 = 0.0023(T_{max} - T_{min})^{0.5}(T_{mean} + 17.8)0.408R_a \quad (2)$$

ET_0 = reference evapotranspiration (mm day^{-1}),
T_{max} = maximum daily air temperature (°C),
T_{min} = minimum daily air temperature (°C),
T_{mean} = mean daily air temperature (°C),
R_a = extra-terrestrial radiation (MJ m^{-2} day^{-1}),
Empirical Hargreaves Coefficient = 0.0023

This study calculated evapotranspiration using both the FAO56 Penman–Monteith and the Hargreaves Equations from two data types: on-site weather station; and synthetic satellite-based data from NASA POWER.

2.3. Modelling Crop Water Use and Soil Moisture Change

Soil moisture sensors in the top 600 mm were interrogated at 15-min time steps to better understand the soil water dynamics within a day and crop use characteristics through irrigation seasons. Numerous investigations into soil moisture monitoring have provided insight into the behavior of soil water under different situations. For example, D'Haeze,

Deckers, Raes, Phong, and Chanh [21] indicate that the active root zone of Robusta coffee is the surface 600 mm of soil, which is supported by our intensive monitoring data.

The FAO56 Penman–Monteith model was calibrated to minimize RMSE between the model and the observed data on the 2020 irrigation data set for all sites. The parameters shown in Table 1 were adjusted to conform with four phases of the measured soil moisture detailed above.

Table 1. Model rules to mimic simplified soil moisture trace phases.

Phase	Model Rule or Parameter
Dormancy	Reducing the crop coefficient for the period up to 15 February or before the first rainfall or irrigation to 0.3.
Non-stressed crop water use	Crop coefficients were taken from Allen, Pereira, Raes, and Smith [31] and Amarasinghe, Hoanh, D'Haeze, and Hung [9]
Increasing stress condition	Method from Allen, Pereira, Raes, and Smith [31]
Drainage above field capacity	If previous 5 days' irrigation plus rainfall exceeds 20 mm or soil moisture > field capacity, drain at saturated hydraulic conductivity rate from D'Haeze, Deckers, Raes, Phong, and Chanh [21] for Central Highland ferrosols

2.4. Simplified Models

A number of reduced data models were constructed using combinations of data sources and ET estimates. (Table 2). The impact of data source and model on irrigation decisions were then compared on the basis of their ability to replicate the irrigation decisions made by the FAO56 Penman–Monteith approach.

Table 2. Limited sources and options for atmospheric and rainfall data, evapotranspiration, crop coefficients, and stress coefficients to be used in combinations for modelling.

Parameter Group	Option	Data Detail
Atmospheric Data	A1	On-site Automatic Weather Station
	A2	NASA Power (daily data)
	A3	NASA Power (long-term average [1])
Rainfall Data	R1	On-site rain gauge (daily data)
	R2	NASA Power (daily data)
Evapotranspiration	E1	FAO56 Penman–Monteith
	E2	Hargreaves
	E3	Hargreaves corrected
Crop coefficients	C1	FAO56 method
	C2	Modified to accommodate dormancy
Stress coefficients	S1	FAO56 method
	S2	No accommodation for stress

Note: [1] Atmospheric data sets were downloaded from NASA POWER for all irrigation seasons from 1981–2021.

Observations from Allen, Pereira, Raes, and Smith [31] indicate that the Hargreaves Equation will tend to over predict ET_0 in regions of high humidity, including tropical climates. Therefore, the Hargreaves equation was adjusted to meet local conditions by undertaking a regression analysis as recommended by Allen, Pereira, Raes, and Smith [31].

Figure 4 shows the daily values of ETo (mm day^{-1}) calculated using the Hargreaves equation (grey) and the corrected Hargreaves (black), overlaying the FAO56 PM (green) daily values. Figure 4 indicates that the corrected Hargreaves tends to underpredict on

days with low FAO56 PM ETo, however, these underestimates are typically outside the irrigation season (January–April).

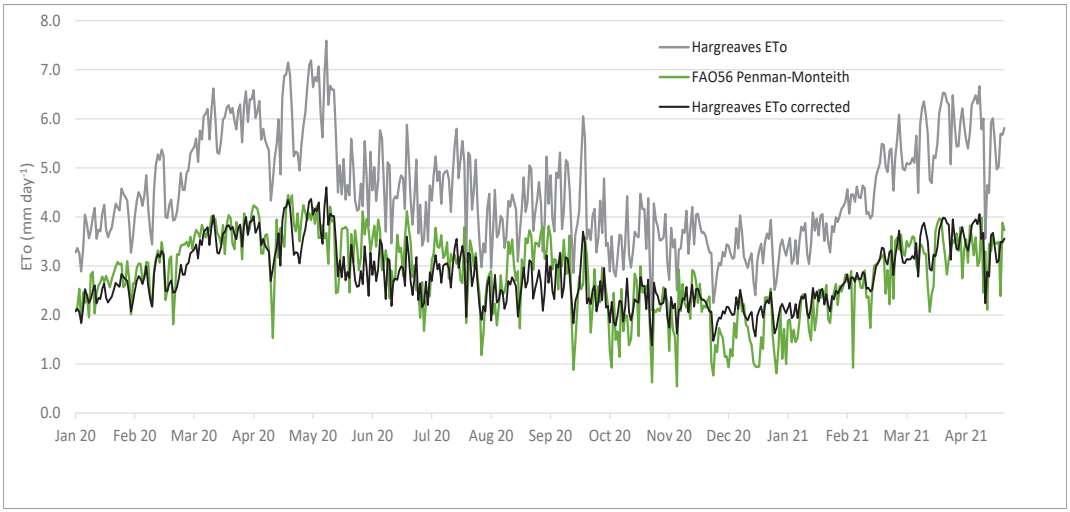


Figure 4. Estimated daily evapotranspiration rates (mm/day) showing variability in Hargreaves (grey), Hargreaves corrected (black), and FAO56 Penman–Monteith calculations (green).

Model Scenario Combinations

Seventy-two possible model/data scenarios are detailed in Table 2, but, for pragmatic purposes, these were limited to 10 practical combinations using options across 5 parameters including FAO56 Penman–Monteith.

Table 3 lists data and method combinations used for each model scenario, identified from the data sets (i) atmospheric data, (ii) rainfall data, (iii) reference evapotranspiration methods, (iv) crop coefficients, and (v) stress coefficients.

The FAO56 Penman–Monteith model (Figure 4) was calibrated against actual soil moisture at three sites and is taken as the reference water balance model. Irrigation was triggered with a refill point of 30% volumetric water content [21] and filled to field capacity with an application efficiency of 90%. Scenarios 2–10 used the same irrigation rules (Table 3).

Table 3. Model scenarios explored using a range of model and data detail (to be read in conjunction with Table 2).

Model Scenario	Atmospheric Data	Rainfall Data	Evapotranspiration Calculation	Crop Coefficients	Stress Coefficients
FAO56 Penman Monteith	A1	R1	E1	C1	S1
Model Scenario 2	A1	R1	E1	C2	S1
Model Scenario 3	A1	R1	E1	C1	S2
Model Scenario 4	A2	R2	E1	C1	S1
Model Scenario 5	A2	R1	E1	C1	S1
Model Scenario 6	A2	R1	E2	C1	S1
Model Scenario 7	A2	R1	E3	C1	S1
Model Scenario 8	A3	R1	E1	C1	S1
Model Scenario 9	A3	R1	E2	C1	S1
Model Scenario 10	A3	R1	E3	C1	S2

2.5. Modelling Irrigation Decision-Making

The aim was not to compare and/or contrast a range of models and their suitability for coffee growing systems, rather to determine whether a simple model with lower input requirements could provide a robust and practical irrigation guide to support farmers'

decision-making. Assessment of model options was based on number of irrigations, date, and timing between irrigations.

Traditional irrigation practice is to fill tree bunds two to four times during each irrigation season. Due to variation in soil texture and water holding capacity, traditional practices effectively refill the soil profile (field capacity), as surface ponding is an indicator of successful irrigation, as reported by farmers.

2.6. Statistical Methods

MAE, RMSE, and MAPE were used to describe each modelling scenario's performance against the measured soil moisture data sets for each of the model calibration runs. These indicators are defined as

$$MAE = \frac{1}{n}\sum_{t=1}^{n}|Me_t - Mo_{t,i}| \quad (3)$$

$$RMSE = \sqrt{\frac{1}{n}\sum_{t=1}^{n}(Me_t - Mo_{t,i})^2} \quad (4)$$

$$MAPE = \frac{1}{n}\sum_{t=1}^{n}\left|\frac{Me_t - Mo_{t,i}}{Me_t}\right| \times 100 \quad (5)$$

where

t = daily time step
n = number of days in the irrigation season
Me = measured soil moisture
Mo = modelled soil moisture
i = model scenario

3. Results and Discussion

3.1. Features of Soil Moisture Time Series Data

Without field calibration of sensors, the values on the y-axis of soil moisture curves can be misleading. Regardless, the shape and inflection points of curves provide insights into soil water dynamics.

Figure 5 illustrates volumetric soil moisture at Site 1 in Cu M'Gar. Label 1 shows a slow daily decline in soil moisture through winter when there is lower evapotranspiration, i.e., the coffee plant is in a semi-dormant state. Dormancy is broken by either the first irrigation or rainfall of the season, with increased crop water use (label 2) following, as the crop is actively transpiring under a "no-stress" condition. There is adequate, but not excessive, moisture available in the root zone.

The increasing stress condition (labelled 3 in Figure 5) shows a reduction in the moisture extraction rate as the crop depletes stored soil moisture from the most readily available soil water with increasing crop water stress.

The rapid decline in soil moisture (after rain or irrigation) (label 4 on Figure 5) indicates drainage of water through the soil profile (water in excess of the field capacity), which would add to a drainage term in systems water balance.

"Best Practice" Model (FAO56)

Daily crop water use was derived using the FAO56 Penman–Monteith model with ETo estimated by applying crop coefficients (Kc) to various stages of the crop growth cycle using daily data from the on-site weather station. Default crop coefficients were taken from Allen, Pereira, Raes, and Smith [31] and Amarasinghe, Hoanh, D'Haeze, and Hung [9]. These were adjusted to account for crop dormancy before the first rainfall or irrigation of

each season. Daily rainfall and irrigation values were inputs to the water balance. Due to the irrigation season typically having low rainfall, run-on, run-off, and deep percolation were ignored.

Figure 6 shows the calibrated model and measured soil moisture at Site 1 between 1 January and 30 April 2020.

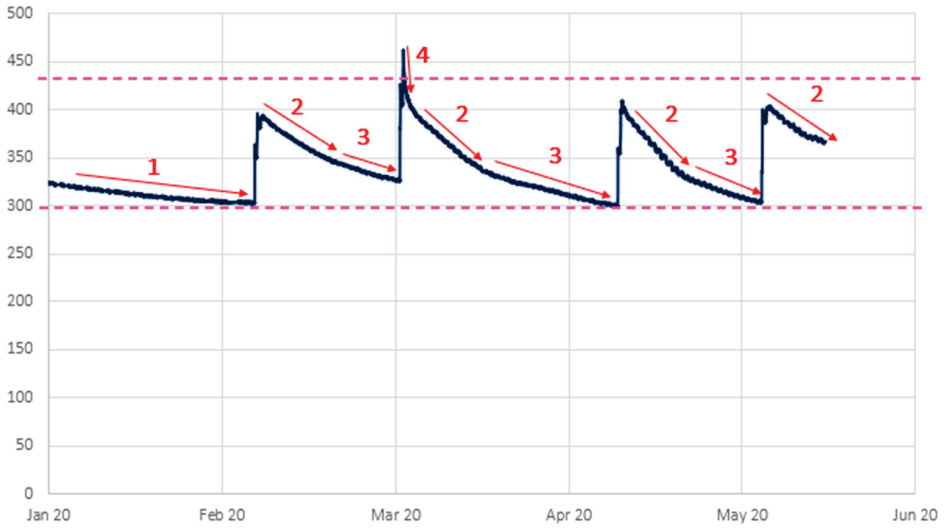


Figure 5. Fifteen-minute soil moisture trace of the surface 600 mm of soil showing phases of soil moisture depletion. The shape of the trace provides some insight into the availability and state of the water in the soil profile.

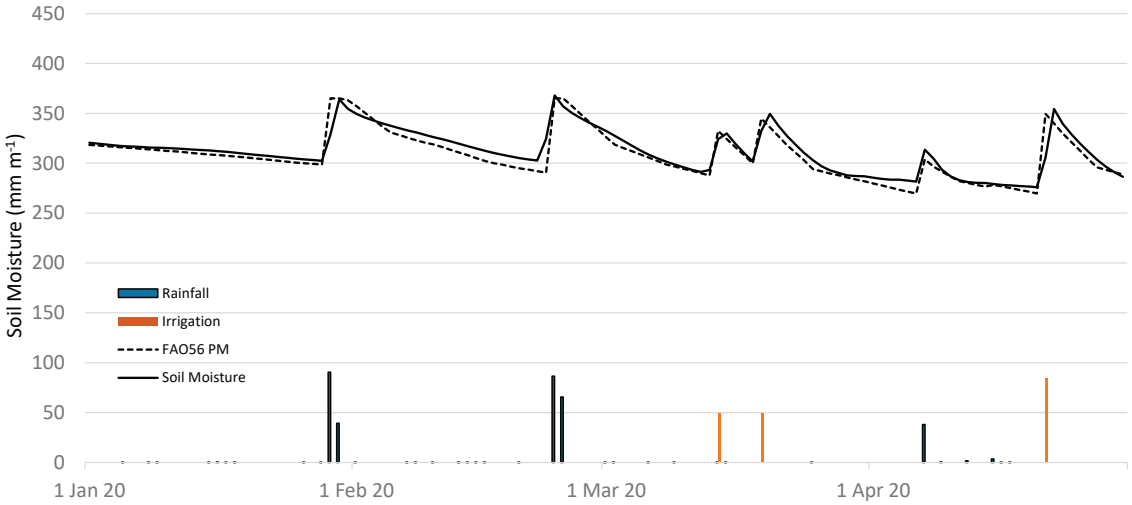


Figure 6. Measured soil water in top 600 mm of ferrosol soil at Site 1 (solid line) and FAO56 PM modelled soil moisture (dotted line). Blue vertical bars represent timing and volume of rainfall events and orange vertical bars represent timing and volume of irrigation events.

3.2. Model Scenario Selection

Each of the nine model scenarios (2–10) shown in Table 3 were calibrated against measured soil moisture at three sites through the 2020 irrigation season (January–April 2020). The objective functions to compare models were Root Mean Squared Error (RMSE), Mean Absolute Error (MAE), and Mean Absolute Percentage Errors (MAPE) for daily soil moisture.

3.3. Model Calibration

Each of the model scenarios described in Table 3 was calibrated using the irrigation season data set from 2020 through adjustment of the coefficients presented in Table 4.

Table 4. Calibration results: MAE (mm/m volumetric soil moisture), RMSE (mm/m volumetric soil moisture), and MAPE (%) of the calibration of FAO56 model and nine simpler model scenarios against actual soil moisture measurement in the top 600 mm of the soil profile for 2020.

Model Scenario	Site 1 2021			Site 2 2021			Site 3 2021		
	MAE	**RMSE**	**MAPE**	**MAE**	**RMSE**	**MAPE**	**MAE**	**RMSE**	**MAPE**
FAO56 Penman–Monteith	6.1	8.6	1.9	4.6	8.0	1.5	5.7	8.6	2.1
Model 2	10.2	13.4	3.3	7.7	10.0	2.5	5.4	8.4	1.9
Model 3	18.8	28.0	6.2	7.7	13.4	2.6	36.0	55.4	13.5
Model 4	22.6	32.0	7.0	40.4	52.4	12.3	27.1	33.3	9.8
Model 5	15.6	20.0	5.2	26.6	33.8	8.9	10.0	11.6	3.8
Model 6	81.4	117.9	27.1	64.1	96.5	21.6	91.2	127.0	34.1
Model 7	5.1	7.8	1.6	6.6	9.7	2.1	6.1	8.9	2.2
Model 8	15.2	19.7	5.0	25.9	32.9	8.6	9.9	11.5	3.8
Model 9	29.7	34.5	9.7	49.6	63.3	16.4	16.7	22.2	6.1
Model 10	10.7	14.2	3.5	6.8	10.3	2.2	10.0	14.4	3.7

The PM FAO56 model did not outperform all models at each site. Model Scenario 7 had a lower MAE, RMSE, and MAPE at Site 1. However, PM FAO56 errors were consistently lower (MAE average 4.6–6.5 mm/m, RMSE average 8.0–8.6 mm/m, MAPE average 1.5–2.1%) across the whole data set.

Three models that used on-site rainfall showed low MAE, RMSE, and MAPE:

- Model 2 (PM FAO56 with crop coefficients adjusted to allow for winter dormancy);
- Model 7 (daily NASA POWER data with adjusted Hargreaves equation, on-site rainfall);
- Model 10 (long-term average NASA POWER data with adjusted Hargreaves equation, on-site rainfall).

These three models were used in model validation.

3.4. Model Validation

Calibrated models using data from 2020 and observations from the three sites (2021) were used to test four models (Table 5) for the 2021 data set.

Table 5. Validation results: MAE (mm/m volumetric soil moisture), RMSE (mm/m volumetric soil moisture), and MAPE (%) of the validation of FAO56 model and three simpler model scenarios against actual soil moisture measurement in the top 600 mm of the soil profile.

Model Scenario	Site 1 2021			Site 2 2021			Site 3 2021		
	MAE	**RMSE**	**MAPE**	**MAE**	**RMSE**	**MAPE**	**MAE**	**RMSE**	**MAPE**
FAO56 Penman–Monteith	5.6	7.4	1.7	8.2	11.8	8.9	8.9	13.8	3.1
(Model 2) FAO56 w/dormancy	29.5	38.4	9.0	29.6	35.9	9.3	18.1	21.0	6.3
(Model 7) Hargreaves daily NASA temperature	6.5	8.9	1.9	8.0	11.4	2.4	6.9	9.5	2.4
(Model 10) Hargreaves average NASA temperature	6.9	9.0	2.0	9.6	13.3	3.0	8.5	13.0	2.9

The FAO56 reference model had lower MAE, RMSE, and MAPE indices of prediction compared to Model 7 and at Sites 1 and 2; however, results were higher than Model 10

(MAE average 6.9–9.6 mm/m, RMSE average 9.0–13.3 mm/m, MAPE average 2.0–3.0%) at Site 3 (Table 5).

The poor performance of Model 2 (PM FAO56 with crop coefficients adjusted to allow for winter dormancy) is the result of the long dormancy and the extended period between rainfall events, where the model was not reset by irrigation or rainfall refilling the soil moisture profile and errors in the evapotranspiration (Table 5).

Model 7 (daily NASA POWER data with adjusted Hargreaves equation, on-site rainfall) was the most reliable predictor across all sites in both the calibration (MAE average 5.1–6.1 mm/m, RMSE average 7.8–9.7 mm/m, MAPE average 1.6–2.2%) and validation phases (MAE average 6.5–8.0 mm, RMSE average 8.9–11.4 mm, MAPE average 1.9–2.4%). Model Scenario 7 was accepted as having similar reliability to the PM FAO56 model.

Model 7, referred to as the Low Data Model (LDM), was taken through to the next analysis to understand how it would determine irrigation schedules based on a longer-term historic data set.

3.5. Long-Term Analyses

To assess the decision-making skill of the LDM, a series of historical data sets were analyzed. These data sets were not collected on-site; instead, they were generated synthetically using data sourced from NASA POWER for the locations of the study sites. The following sections show the analysis of this data using the models described above.

Historically, irrigation volumes applied have been based on the amount of water required to fill a bund around each tree. If this deficit-controlled approach is maintained, there is little scope to control irrigation amounts [21,31]. Therefore, the measure of agreement between models was similarity in irrigation timing recommendations between FAO56 and the LDM.

Figure 7 presents an example of two seasons of scheduled irrigation using historic rainfall and a soil moisture deficit of 60 mm. Models were in close agreement in 2007 (1–4 days difference and total of four irrigations for both models). However, in 2008, the models were in lesser agreement, with greater differences between the irrigation dates of first, second, and third irrigations and the LDM scheduling an additional (fourth) irrigation.

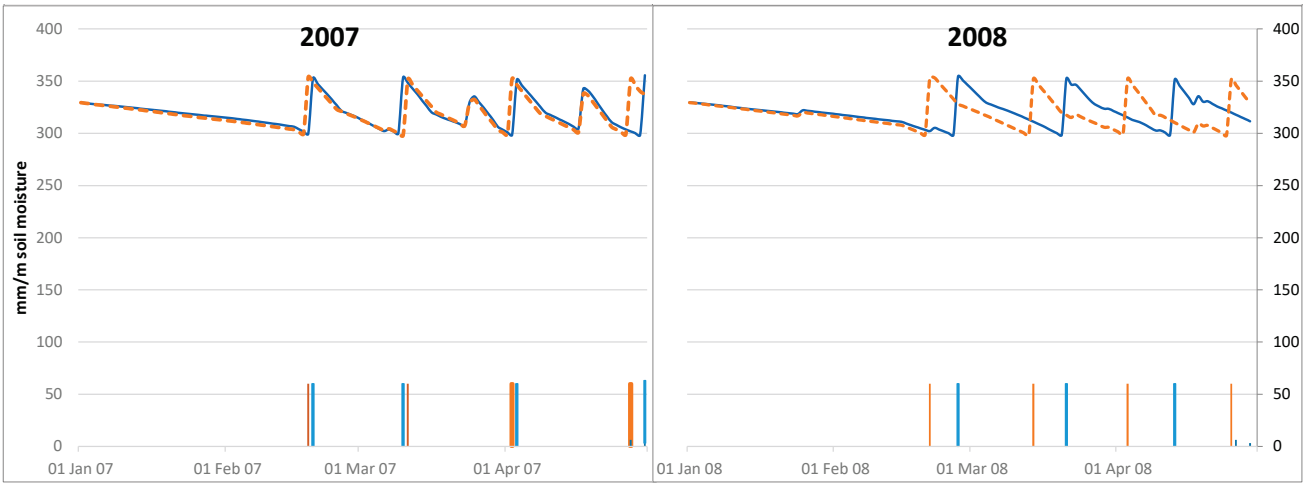


Figure 7. Soil moisture traces estimated using FAO56 P-M (blue trace and bars) and LDM (orange dotted trace and bars) for historic data sets from the 2007 and 2008 irrigation seasons. The timing and volume of rainfall events impact the performance of the LDM.

Table 6 shows the number of irrigations and volume applied recommended by the PM FAO56 and LDM between 2005 and 2018 using on-site rainfall and synthetic weather variables from NASA POWER data sets. To explore how each approach performs across

season types, each year/season was categorized into dry seasons (years with in-season rainfall in the lower quartile of years); average seasons (years with in-season rainfall within the interquartile range); and wet seasons (years with in-season rainfall in the upper quartile of the data set).

In each dry season, the LDM applied one more irrigation. The exception was 2008, which followed the trend of an average rainfall season applying less than PM FAO56. The average number of irrigations (PM FAO56 = 3.7, LDM = 3.6) and the total volumes applied (PM FAO56 = 222 mm and LDM = 214 mm) across all seasons modelled were similar.

Table 6 shows that Model Scenario 7 performs similarly to the FAO56 PM model in wet years, underpredicting by just one irrigation in one year out of four (2018), and with good agreement in the remaining three wet years.

In average rainfall irrigation seasons, the LDM underpredicts in three out of the six years, but only by one irrigation each year, with good agreement in the other three years.

In dry irrigation seasons, the LDM predicts greater irrigation requirements with respect to FAO56 PM in three out of four years and predicts less irrigation required in the remaining dry year.

Rainfall sufficient to refill the soil profile acts as a model reset, removing the accumulated differences in soil water that develop in prolonged dry conditions without irrigation.

Table 6 shows the number and depth of irrigation recommendations from both models between 2005 and 2018; however, the timing of these irrigations is equally important to the soil water balance to ensure that soil water is available to meet crop demand. The Low Data Model predicts the first irrigation of the season within 7 days of the FAO56 PM model (median = 2.2 days late, interquartile range = 2.8 days). Agreement between models diverges for subsequent irrigations; the second irrigation is 3.8 days later, the third 4.3 days later, and the fourth irrigation 3.6 days. Based on the irrigation system capacity and cycle times for coffee farmers in the Central Highlands, it is expected that a 7-day window for irrigation advice is adequate (Should I irrigate this week?). Therefore, it is expected that the LDM is adequate for at least the first two irrigations of the season. Further, a 7-day window for advice will capture 77.6% of the irrigation decisions determined over the analysis period (Figure 8).

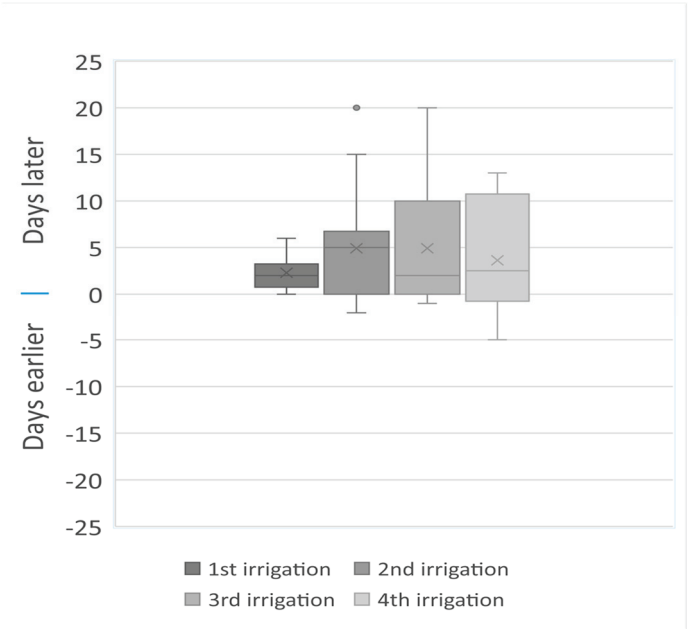


Figure 8. Differences in timing of irrigation recommendation using Low Data Model compared to FAO56 (PM model). Blue bars indicate a 7-day window before and after irrigation dates as modelled using PM FAO56. Dot above the whisker in the 2nd irrigation is an outlier.

Table 6. Comparison of FAO56 PM and the LDM annual irrigation events and water applied (mm) for a 14-year period (2005–2018).

		FAO56 Penman–Monteith			Low Data Model	
		Total Rainfall January–April (mm)	**Irrigations Applied (count)**	**Equivalent Depth of Irrigation Applied (mm)**	**Irrigations Applied (count)**	**Equivalent Depth of Irrigation Applied (mm)**
Dry seasons (lower quartile of in-season rainfall)	2015	8.2	4	240	5	300
	2005	9.4	4	240	5	300
	2006	21.1	4	240	5	300
	2008	32.0	4	240	3	180
Average seasons (interquartile range of in-season rainfall)	2011	32.5	4	240	3	180
	2017	66.0	4	240	3	180
	2006	83.4	4	240	4	240
	2007	89.6	4	240	4	240
	2010	93.9	4	240	4	240
	2009	101.3	4	240	3	180
Wet seasons (upper quartile of in-season rainfall)	2013	19.6	3	180	3	180
	2018	186.0	4	240	3	180
	2014	165.1	3	180	3	180
	2012	249.6	2	120	2	120
Average		89.8	3.7	222	3.6	214

4. Discussion

4.1. Sensitivity

Irrigation refill point (RP) is a key parameter in irrigation scheduling models. A generic refill point value is often taken as halfway between the field capacity and the permanent wilting point [31] on ferrosol soils. D'Haeze, Deckers, Raes, Phong, and Chanh [21] used a volumetric soil moisture of 30% or 300 mm/m. The calibration parameters here have RMSEs of 11.7 mm/m (wet), 13.1 mm/m (average), and 14.9 mm/m (dry seasons).

If the RP is increased to 330 mm/m, RMSE decreases to 7.4 mm/m, 7.8 mm/m, and 8.3 mm/m 1 for wet, average, and dry seasons, respectively; however, the number of irrigations increases to an average of 13.2 per season for the FAO56 PM model and 12.3 per season for the LDM, though this would be unrealistic for farmers as irrigating almost every week is inefficient [34], requires more time, and results in increased costs. Reducing the refill point by 10% (to 270 mm/m) has a lesser effect on the model agreement, increasing the RMSE to 13.3 mm/m in wet seasons, 17.9 mm/m in average rainfall seasons, and 16.0 mm/m in dry seasons. This affects the number of irrigations, which reduces to an average of 1.7 per season for the FAO56 PM model and 1.6 per season for Model Scenario 7. This is unrealistic, as the first irrigation is not recommended until the first week of March in most cases, which is very unlikely in practice.

All models are sensitive to the quality of rainfall inputs, indicating that, in the calibration phase, synthetic rainfall data from satellite observations did not reflect the actual rainfall on site and therefore created significant error in the water balance when compared with actual soil moisture.

Both models have a simplified rainfall routine and do not account for initial losses from surface run-off, but do account for drainage of excess water through the profile, which is reasonable considering the saturated hydraulic conductivity reported by D'Haeze,

Deckers, Raes, Phong, and Chanh [21] and grower experience with low rainfall and low run-off during the irrigation season.

4.2. Implications for Coffee Farmers

Optimal irrigation scheduling maintains adequate water supply in the rootzone to meet daily crop demand. Excess water in the rootzone may create problems associated with water logging and does not leave capacity to take opportunity of incoming moisture from rainfall. Crops that spend time at either end of the soil moisture spectrum are likely to experience yield penalties. This study tests a model that requires little active data collection from a farmer to generate an acceptable starting point for irrigation scheduling. Such a model is well suited to translation into a mobile decision support tool that farmers could access to aid in irrigation scheduling decisions to maximize production.

Kandulu and Connor [35] note that large-scale investments in irrigation may not be as cost-effective as small-scale localized investments. A simple tool that required little effort to set up and use could be promoted by coffee traders and buyers as a discussion starter and to ensure that more objective decisions were being made with respect to irrigation scheduling. Zheng, Ma, Boansi, and Owusu [34] conclude that promotion and adoption of water management technologies reduce water use, but may also support improvements in the performance of other farming practices. Improved irrigation scheduling, including more site-specific information, can contribute to improved productivity and profitability in a more environmentally sustainable cropping system.

5. Conclusions

Local and reliable rainfall data are a prerequisite of any irrigation scheduling approach as synthetic data underrepresented actual rainfall, which has a large impact on the water balance that drives irrigation decision advice for all models.

This study has shown that, while synthetic temperature data sets are available, site-specific calibration is important when using the Low Data Model with the Hargreaves equation to generate ETo estimates based on daily temperature alone.

A calibrated Low Data Model was able predict the first two irrigations in the coffee growing season to within 7 days of the industry standard FAO56 PM model and provides an acceptable decision point for Central Highland coffee farmers that generally use the traditional method of a hosepipe filling a bund around each tree.

All models tested are sensitive to soil water holding capacity data and irrigation refill trigger values. Therefore, soil texture analysis and understanding water holding capacity must be understood at a site level.

The Low Data Model also performs better in high and average rainfall years than in low rainfall years due to the resetting of the soil moisture balance on each rainfall event that refills the soil profile. This approach can be used by farmers to optimize their water use efficiency by understanding the seasonal variability in the daily water requirement of the crop.

Author Contributions: Conceptualization, M.S. and S.M.; methodology, M.S. and D.F.; modelling, M.S.; validation, M.S. and D.F.; formal analysis, M.S. and D.D.; investigation, M.S. and S.M.; resources, S.M.; data curation, M.S.; writing—original draft preparation, M.S., D.F. and S.M.; writing—review and editing, D.F., S.M. and D.D.; funding acquisition, S.M. All authors have read and agreed to the published version of the manuscript.

Funding: This research was funded by the Federal Ministry for the Environment, Nature Conservation and Nuclear Safety—International Climate Initiative (IKI). The APC was funded by the University of Southern Queensland.

Data Availability Statement: Data sets available on request.

Acknowledgments: We thank the coffee farmers of the Vietnamese Central Highlands and the ECOM Agroindustrial Corporation for providing access to sites for this research.

Conflicts of Interest: The authors declare no conflict of interest. The funders had no role in the design of the study; in the collection, analyses, or interpretation of data; in the writing of the manuscript; or in the decision to publish the results.

References

1. Le, T.; Sun, C.; Choy, S.; Kuleshov, Y. Regional drought risk assessment in the Central Highlands and the South of Vietnam. *Geomat. Nat. Hazards Risk* **2021**, *12*, 3140–3159. [CrossRef]
2. Stojanovic, M.; Liberato, M.L.R.; Sorí, R.; Vázquez, M.; Phan-Van, T.; Duongvan, H.; Cong, T.H.; Nguyen, P.N.B.; Nieto, R.; Gimeno, L. Trends and extremes of drought episodes in vietnam sub-regions during 1980–2017 at different timescales. *Water* **2020**, *12*, 813. [CrossRef]
3. Byrareddy, V.; Kouadio, L.; Mushtaq, S.; Stone, R. Sustainable Production of Robusta Coffee under a Changing Climate: A 10-Year Monitoring of Fertilizer Management in Coffee Farms in Vietnam and Indonesia. *Agronomy* **2019**, *9*, 499. [CrossRef]
4. Marsh, A. *Diversification by Smallholder Farmers: Vietnam Robusta Coffee*; Food and Agriculture Organisation: Rome, Italy, 2007.
5. Byrareddy, V.; Kouadio, L.; Mushtaq, S.; Kath, J.; Stone, R. Coping with drought: Lessons learned from robusta coffee growers in Vietnam. *Clim. Serv.* **2021**, *22*, 100229. [CrossRef]
6. Carr, M.K.V. The water relations and irrigation requirements of coffee. *Exp. Agric.* **2001**, *37*, 1–36. [CrossRef]
7. Gutiérrez, M.V.; Meinzer, F.C. Estimating water use and irrigation requirements of coffee in Hawaii. *J. Am. Soc. Hortic. Sci.* **1994**, *119*, 652–657. [CrossRef]
8. Bunn, C.; Laderach, P.; Rivera, O.O.; Kirschke, D. A bitter cup: Climate change profile of global production of Arabica and Robusta coffee. *Clim. Chang.* **2015**, *129*, 89–101. [CrossRef]
9. Amarasinghe, U.A.; Hoanh, C.T.; D'Haeze, D.; Hung, T.Q. Toward sustainable coffee production in Vietnam: More coffee with less water. *Agric. Syst.* **2015**, *136*, 96–105. [CrossRef]
10. Kath, J.; Byrareddy, V.M.; Reardon-Smith, K.; Mushtaq, S. Early flowering changes robusta coffee yield responses to climate stress and management. *Sci. Total Environ.* **2023**, *856*, 158836. [CrossRef] [PubMed]
11. Albert, M.; Bergez, J.E.; Couture, S.; Faivre, R.; Willaume, M. Decision-making process factors explain some of the heterogeneity of irrigation practices among maize farmers in southwestern France. *Water* **2021**, *13*, 3504. [CrossRef]
12. Byrareddy, V.; Kouadio, L.; Kath, J.; Mushtaq, S.; Rafiei, V.; Scobie, M.; Stone, R. Win-win: Improved irrigation management saves water and increases yield for robusta coffee farms in Vietnam. *Agric. Water Manag.* **2020**, *241*, 106350. [CrossRef]
13. Alejo, L.A.; Alejandro, A.S. Changes in Irrigation Planning and Development Parameters Due to Climate Change. *Water Resour. Manag.* **2022**, *36*, 1711–1726. [CrossRef]
14. Lamm, F.R.; Bordovsky, J.P.; Schwankl, L.J.; Grabow, G.L.; Enciso-Medina, J.; Peters, R.T.; Colaizzi, P.D.; Trooien, T.P.; Porter, D.O. Subsurface Drip Irrigation: Status of the Technology in 2010. *Trans. ASABE* **2012**, *55*, 483–491. [CrossRef]
15. Nguyen, V.D.; Pham, T.C.; Le, C.H.; Huynh, T.T.; Le, T.H.; Packianather, M. An Innovative and Smart Agriculture Platform for Improving the Coffee Value Chain and Supply Chain. In *Studies in Computational Intelligence*; Springer Science and Business Media Deutschland GmbH: Berlin/Heidelberg, Germany, 2023; Volume 1068, pp. 185–197.
16. Van Hiep, N. *A Review of Evidence of Recent Climate Change in the Central Highlands of Vietnam*; Coffee & Climate: Hamburg, Germany, 2013.
17. IDH. Sustainable Trade Initiative. Available online: https://www.idhsustainabletrade.com/initiative/central-highlands-vietnam/ (accessed on 23 March 2017).
18. General Statistics Office. *Statistical Yearbook of Viet Nam*; General Statistics Office: Hanoi, Vietnam, 2019.
19. ICO. *International Coffee Organization, Country Coffee Profile: Vietnam*; International Coffee Council: Nairobi, Kenya, 2019.
20. Rios, A.R.; Shively, G.E. Farm size, irrigation infrastructure, and the efficiency of coffee production in vietnam. *For. Trees Livelihoods* **2006**, *16*, 397–412. [CrossRef]
21. D'Haeze, D.; Deckers, J.; Raes, D.; Phong, T.A.; Chanh, N.D.M. Over-irrigation of Coffea canephora in the Central Highlands of Vietnam revisited: Simulation of soil moisture dynamics in Rhodic Ferralsols. *Agric. Water Manag.* **2003**, *63*, 185–202. [CrossRef]
22. Kath, J.; Craparo, A.; Fong, Y.; Byrareddy, V.; Davis, A.P.; King, R.; Nguyen-Huy, T.; van Asten, P.J.A.; Marcussen, T.; Mushtaq, S.; et al. Vapour pressure deficit determines critical thresholds for global coffee production under climate change. *Nat. Food* **2022**, *3*, 871–880. [CrossRef]
23. Truong, N.C.Q.; Khoi, D.N.; Nguyen, H.Q.; Kondoh, A. Impact of Forest Conversion to Agriculture on Hydrologic Regime in the Large Basin in Vietnam. *Water* **2022**, *14*, 854. [CrossRef]

24. Pham, Y.; Reardon-Smith, K.; Mushtaq, S.; Deo, R.C. Feedback modelling of the impacts of drought: A case study in coffee production systems in Viet Nam. *Clim. Risk Manag.* **2020**, *30*, 100255. [CrossRef]
25. Tran, T.A.; Pittock, J.; Tuan, L.A. Adaptive co-management in the Vietnamese Mekong Delta: Examining the interface between flood management and adaptation. *Int. J. Water Resour. Dev.* **2019**, *35*, 326–342. [CrossRef]
26. Tran, T.A.; Tuan, L.A. Policy transfer into flood management in the Vietnamese Mekong Delta: A North Vam Nao study. *Int. J. Water Resour. Dev.* **2020**, *36*, 106–126. [CrossRef]
27. Hoang, V.; Nguyen, A. PGI Buon Ma Thuot Coffee in Vietnam. In *Sustainability of European Food Quality Schemes*; Arfini, F., Bellassen, V., Eds.; Springer International Publishing: Cham, Switzerland, 2019; pp. 265–285. [CrossRef]
28. Kheyruri, Y.; Sharafati, A. Spatiotemporal assessment of the NASA POWER satellite precipitation product over different regions of Iran. *Pure Appl. Geophys.* **2022**, *179*, 3427–3439. [CrossRef]
29. Sparks, A.H. nasapower: A NASA POWER global meteorology, surface solar energy and climatology data client for R. *J. Open Source Softw.* **2018**, *3*, 1035. [CrossRef]
30. Gardner, W.H. Water content. In *Methods of Soil Analysis: Part 1 Physical and Mineralogical Methods, 5.1*, 2nd ed.; Klute, A., Ed.; American Society of Agronomy, Inc.; American Society of Agronomy, Inc.: Madison, WI, USA, 1986; Volume 5, pp. 493–544.
31. Allen, R.; Pereira, L.; Raes, D.; Smith, M. *FAO Irrigation and Drainage Paper No. 56*; FAO—Food and Agriculture Organization of the United Nations: Rome, Italy, 1998; pp. 26–40.
32. Hargreaves, G.H.; Samani, Z.A. Estimating Potential Evapotranspiration. *J. Irrig. Drain. Div.* **1982**, *108*, 225–230. [CrossRef]
33. Smith, M. The application of climatic data for planning and management of sustainable rainfed and irrigated crop production. *Agric. For. Meteorol.* **2000**, *103*, 99–108. [CrossRef]
34. Zheng, H.; Ma, W.; Boansi, D.; Owusu, V. Farmers' perceptions, adoption and impacts of integrated water management technology under changing climate. *Int. J. Water Resour. Dev.* **2023**, *40*, 425–447. [CrossRef]
35. Kandulu, J.M.; Connor, J.D. Improving the effectiveness of aid_ an evaluation of prospective Mekong irrigation investments. *Int. J. Water Resour. Dev.* **2017**, *33*, 270–291. [CrossRef]

Disclaimer/Publisher's Note: The statements, opinions and data contained in all publications are solely those of the individual author(s) and contributor(s) and not of MDPI and/or the editor(s). MDPI and/or the editor(s) disclaim responsibility for any injury to people or property resulting from any ideas, methods, instructions or products referred to in the content.

water

MDPI

Article

Transformation of Terraces with Irrigation Systems: Profitability and Water Savings in Potato Crop (*Solanum tuberosum* L.)

Russell Poma-Chamana [1], Ricardo Flores-Marquez [2], Joel Cordova-Tadeo [1], Antony Quello [1], José Arapa-Quispe [3] and Richard Solórzano-Acosta [2,4,*]

[1] Dirección de Supervisión y Monitoreo en las Estaciones Experimentales Agrarias, Instituto Nacional de Innovación Agraria (INIA), Campamento Autodema, Arequipa 04102, Peru; rpomac7@gmail.com (R.P.-C.); jcordovatadeo@gmail.com (J.C.-T.); aquello@inia.gob.pe (A.Q.)
[2] Dirección de Supervisión y Monitoreo en las Estaciones Experimentales Agrarias, Instituto Nacional de Innovación Agraria (INIA), Av. La Molina N° 1981, Lima 15024, Peru; ricardo.floresm29@gmail.com
[3] Facultad de Ingeniería Agrícola, Universidad Nacional Agraria La Molina (UNALM), Lima 15024, Peru; jarapa@lamolina.edu.pe
[4] Facultad de Ciencias Ambientales, Universidad Científica del Sur (UCSUR), Lima 15067, Peru
* Correspondence: investigacion_labsaf@inia.gob.pe

Abstract: In recent decades, climate change has intensified the challenges in agriculture, increasing the incidence of water and heat stress during critical stages of the crop cycle. It includes the exacerbation of the seasonality of rainfall and temperature. This significantly affects their development and yield. In addition, climate change has reduced irrigation water availability, highlighting the need to evaluate joint strategies to increase water productivity. These strategies include the implementation of irrigation systems, the use of terraces, and the application of deficit irrigation (DI). In this context, the present research aims to evaluate the irrigation water productivity (WP_{irri}) and the economic water productivity (EWP) of the combined use of DI through a pressurized irrigation system in terraces of the southern highlands of Peru for a potato crop. The treatments included L0: traditional surface irrigation with irrigation depth equivalent to 100% ETc, L1: drip irrigation with irrigation depth equivalent to 100% ETc, L2: drip irrigation with DI at 75% ETc, and L3: drip irrigation with DI at 50% ETc. The DI treatments (L2 and L3) were implemented by forming stolons (60 DAS). As a result, L2 allows saving irrigation water of 3930 m^3 ha^{-1} compared to L0 and 1164 m^3 ha^{-1} compared to L1. It means a WP_{irri} of 6.15 ± 0.35 kg m^{-3} allowing a commercial yield (CY: 27.15 ± 1.47 t ha^{-1}) statistically similar to L1 (WPirri: 5.45 ± 0.34 kg m^{-3}; CY: 30.14 ± 1.83 t ha^{-1}) and higher than the traditional surface irrigation (WP_{irri}: 2.63 ± 0.23 kg m^{-3}; CY: 21.62 ± 1.99 t ha^{-1}). This water saving meant a net income of 3097.04 ± 435.52 USD ha^{-1} for L2, close to L1 (4421.12 ± 724.24 USD ha^{-1}), and much higher than L0 (1664.50 ± 834.24 USD ha^{-1}). The results suggest that using drip irrigation systems in terraced crops optimizes water savings, maintains yields and profitability, and could promote the modernization of terraces in rural environments.

Keywords: deficit irrigation; water productivity; terraces; economic water productivity

1. Introduction

Potato (*Solanum tuberosum* L.), a native species from the high Andean region of South America [1], is currently produced in various latitudes, and it is considered the fourth most produced staple product in the world [2,3]. Its nutritional characteristics and widespread consumption are why it is considered an important crop that underpins food security in several countries [2]. In 2022, Peru produced more than 6 million tons of potatoes,

covering 1.61% of the world's production volume and establishing itself as the leading potato producer in Latin America [4]. Although an estimate of 4000 varieties can be found in Peru [5], most of the commercial production prioritizes conventionally bred white-fleshed cultivars and native yellow-fleshed varieties [6], reaching 61.9% of the cropping area of this country [7]. In a complementary and small-scale manner, the cultivation of native colored-fleshed potatoes has been developed, standing out for its high biodiversity but weak connection to the national and regional market [8]. Historically, these varieties have been grown and preserved in family and subsistence farming systems, forming an essential part of the Andean population's diet [3]. In recent years, their nutritional, aesthetic, and cultural potential has been unlocked, stimulating the growth of their demand and price in the market [6]. However, on a small scale, technological and institutional limitations persist. This situation has prevented the offer from meeting the demand for this product. Apart from that, the environmental vulnerabilities of dryland agriculture have not been properly reduced (climate, edaphic, and topography risks) [6].

In response to terrain challenges, Andean settlers developed technological alternatives such as constructing terraces (called 'Andenes' in pre-Hispanic cultures) [9]. These allowed the expansion of cropping areas in hillside environments, reducing the effects of erosive processes and generating microclimates, which helped cultivated species adapt to higher areas [10]. However, changes in demographic and climate patterns since colonial times led to the abandonment and lack of maintenance of vast terraced areas in the Andes [10]. It was estimated that Peru could have around 500 thousand hectares of terraces. Around 259 thousand ha are used, cultivating mainly alfalfa, starchy corn, and potatoes [11]. Production occurs mostly between November and May following the rainy season [3]. In cases where water is available for irrigation, it is complementarily applied by surface irrigation techniques [12].

The current context of climate change determines the exacerbation of seasonal patterns such as extreme precipitation events and reaching historical high and low temperatures. For the southern part of Peru, a decrease in annual precipitation volumes is expected, with more intense rains and shorter wet seasons [13]. This would aggravate the vulnerability of dryland agricultural systems to water erosion during the wet season [14] and to water stress during dry periods [15]. Given this, terrace use can be considered a local adaptive measure to improve water productivity by allowing the preservation of biodiversity in different altitudes and improving the ecosystem services that promote erosion control [16]. These interventions must be conceived and developed considering a basin management approach to guarantee their articulation with the whole hydrological system [11]. Therefore, utilizing irrigation patterns that enhance productivity and employing water distribution techniques to minimize unused water in terraces could alleviate demographic pressure in areas with physical vulnerabilities [16], ensuring the ongoing use and maintenance of terraces.

The sustainable management of resources implies their rational use in a manner that ensures the conservation of the associated ecosystems. In this context, the sustainable use of water resources in agriculture involves achieving higher crop yields while minimizing water usage, thereby positively impacting the farmer's economic outcomes. Consequently, Water Productivity ($kg \cdot m^{-3}$) and Economic Water Productivity (EWP, $USD \cdot m^{-3}$) are crucial indicators for evaluating the sustainability of agricultural water use [17]. These metrics facilitate improved planning in water-scarce regions by highlighting the relationship between output and resource use. Therefore, their analysis must account for the spatial and temporal variability of water availability, particularly in environments where irrigation is the primary factor influencing crop yield [18]. In response to these challenges, various technologies have been developed to enhance the management of irrigation systems, including the conveyance, distribution, and application of water, as well as optimizing the

timing and frequency of irrigation. Thus, pressurized irrigation systems are presented as a reliable alternative to improve water productivity [19–21]. It allows the conduction of water without losses due to evaporation or infiltration, the application of water in a localized manner in the root zone of the crop, work with fertigation, reducing losses due to surface runoff, and the control of application volumes [22].

However, among the main limitations are the costs of the initial investment required, management and operation costs, etc. [23]. In addition, research and methodological proposals have been developed around water-saving strategies to control irrigation times, such as deficit irrigation (DI) [24]. DI applies water during crop growth stages that are most susceptible to water stress. Shifting the focus to reducing or omitting irrigation during non-critical growth stages provided that rainfall supplies the minimum water requirements [24]. Implementing deficit irrigation can bring potential reductions in crop yield, but this can be offset by increased water productivity, thus allowing a potential increase in irrigated crop areas [25]. Operationally, its application may incur increased operating costs linked to the management of the irrigation system or investment costs linked to the automation of the irrigation system [26]. Therefore, it is necessary to conduct performance evaluations of these technologies, including the optimization of irrigation depths and the farmer's profitability, which implies market considerations in terms of commercial yields and operating costs [18].

Although extensive literature supports the benefits of using deficit irrigation through the management of pressurized irrigation systems, it is necessary to evaluate the technical-economic viability of its implementation at the local level [22]. In addition, to ensure the success of these technologies, it is crucial to implement farmer-oriented training and technology transfer programs focused on the design, operation, and maintenance of irrigation systems and efficient management of water and nutrients [27]. This would allow validating the adaptability of these technologies to the production of promising crops in terms of their market demand and their importance for food security. In this sense, the objective of the research is to evaluate the effect of the joint use of deficit irrigation applied through a pressurized drip irrigation system implemented on a terrace system for the cultivation of native potatoes, considering water productivity and economic profitability.

2. Materials and Methods

2.1. Study Area

The research was developed at the Cuyay Experimental Center of the National Institute of Agrarian Innovation (INIA) located in the Cuyay hamlet, Chuquibamba district, Condesuyos province, Arequipa region, Peru. The experimental plot was installed at 15°50′0.3″ S, 72°37′5.2″ W, at 2800 m above sea level (Figure 1). The study area has an average annual rainfall of 199.1 mm. Most precipitation events occur between January and March (179.9 mm accumulated), while the rest of the year is dry and cold. Minimum temperatures vary between 4.4 °C and 7.8 °C, and maximum temperatures range between 21.8 °C and 22.4 °C. Historical averages were calculated from data from the Chuquibamba meteorological station (15°50′45.65″ S, 72°39′2.32″ W, 2859 m.a.s.l.) of the National Meteorological and Hydrological Service of Peru (SENAMHI). To obtain daily meteorological records during the research (September 2023–March 2024), a Davis Vantage Pro 2 meteorological station (15°49′58.80″ S, 72°37′47.42″ W) was installed adjacent to the experimental plot (Figure 2). The geography of the study area is rugged, so agriculture is mainly developed on terraces with shallow soils. The terraces of Chuquibamba usually have widths between 3–7 m and lengths of up to 50 m, managed with surface irrigation or dry land systems depending on water availability. The predominant crops are corn, potato, alfalfa, barley, quinoa, squash, and kiwicha. It is not known precisely when and by

whom they were built; however, they could be an inheritance of the Huari culture from the beginning of the Middle Horizon (615–695 AD) and perfected or reused by the Incas during the late stage of the Late Intermediate Period (1200–1400 AD) [28]. Today, the locals use them frequently as part of their agricultural practices, and their maintenance is part of local cultural work.

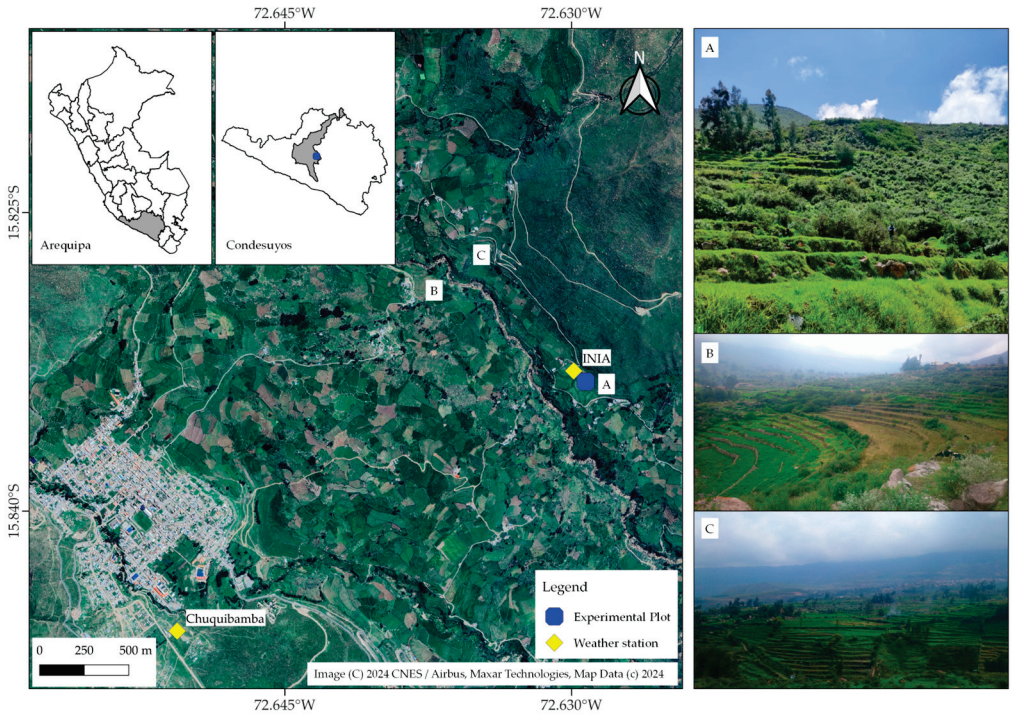


Figure 1. Study area in Condesuyos Province, Arequipa region, Peru. Some photographs from around the experimental plot are on the right side (A, B, C).

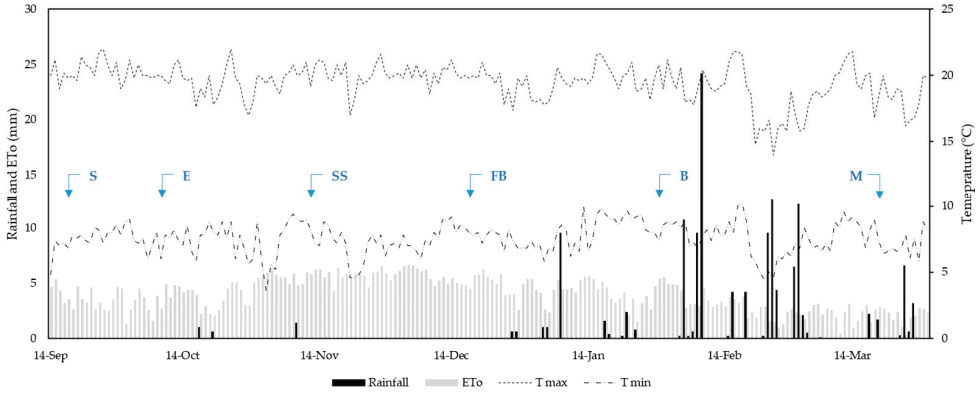


Figure 2. Daily meteorological parameters obtained during the potato season. Phenological stages are represented: sowing (S), emergency (E), side shoots (SS), floral button (FB), bloom (B), and maturity (M). ETo: potential evapotranspiration. Tmax: maximum temperature. Tmin: minimum temperature.

2.2. Experimental Design

A split-plot design with a 3 × 4 factorial arrangement was used. The main plot was defined by the location of terraces (A1: upper platform; A2: middle platform; A3: lower platform) and the subplot by different irrigation treatments based on crop evapotranspiration (ETc) (L0: surface irrigation with irrigation depth equivalent to 100% ETc; L1: drip irrigation with irrigation depth equivalent to 100% ETc; L2: drip irrigation with irrigation depth equivalent to 75% ETc; L3: drip irrigation with irrigation depth equivalent to 50% ETc). The design included 3 blocks comprising 36 experimental units (Figure 3). Each

experimental unit had an area of 7.68 m^2 (2.4 m × 3.2 m). The planting spacing was 0.95 m between furrows and 0.25 m between plants [29] (plant density 42,105 plants·ha^{-1}).

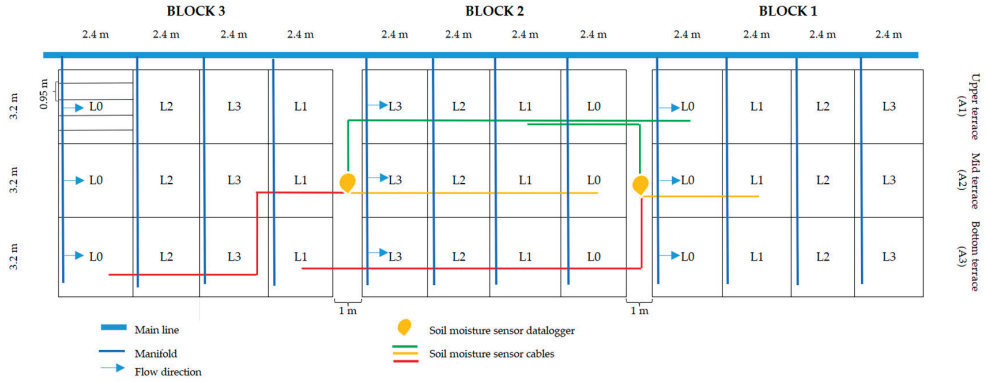


Figure 3. Layout of experimental units. L0, L1, L2, and L3: levels of the irrigation treatment applied.

2.3. Physical, Hydraulic, and Chemical Characteristics of Soils

Before installation, composite samples of the topsoil layer from each platform were collected at a depth of 0.30 m, where approximately 85% of the root length is concentrated [30,31]. The samples were entered into the Soil, Water, and Foliar Laboratory (LABSAF)—INIA Arequipa for physical and chemical characterization: texture [32], pH [33], electrical conductivity [34], organic matter (OM) [32], total N [35], available P [32], available K^+ [36], exchangeable cations (Ca^{+2}, Mg^{+2}, Na^+) [32], carbonates [32]. Additionally, undisturbed samples were extracted in metal core samplers (0.034 m length, 0.061 m diameter, 100 cm^3 sample volume) to calculate the soil bulk density by the cylinder method [37] at LABSAF-INIA and the water constants (i.e., field capacity (FC) and permanent wilting point (PWP)) at the Water and Soil Laboratory of the Faculty of Agricultural Engineering of the Universidad Nacional Agraria La Molina using the Richards pressure plate equipment [38]. The results of the soil characterization are shown in Table S1.

2.4. Conducting the Experimental Plot

The experimental plot was installed between September 2023 and March 2024 following the cropping calendar of local producers. Before its implementation, a drip irrigation system was installed, and an existing 300 m^3 geomembrane reservoir was given maintenance. The height difference between the reservoir and the entrance to the experimental field was 20 m. The main line was sized at 50 mm HDPE-SDR 21-PE 100, and the manifold (within each experimental unit) at 32 mm HDPE-SDR 21-PE 100. At the entrance to the field, a fertigation system via a Venturi-type injector $\frac{1}{2}$" (Hydro Environment, Tlalnepantla, Mexico) was implemented for pressurized irrigation treatments. Plots with the treatment of surface irrigation received basal fertilization. The valve manifolds were independent for each experimental unit, considering a manual control valve, air valves, and manometric control points. Two driplines were installed per crop row using Eolos 16 mm nominal diameter class 5000 with drippers of nominal flow rate 2.2 L·h^{-1} (nominal pressure 100 kPa) spaced every 0.20 m (Rivulis Irrigation, Ltd., Inofyta, Greece). The surface irrigation treatment units had a manual control valve that discharged directly into the upper platform inlet.

The land was left fallow for 4 years, plowed, turned over, and furrowed using tractor-powered implements. All subsequent agricultural work was carried out manually. After plowing, seeds of *Solanum tuberosum* L. cv. Imilla negra were sown. Based on the physical and chemical characterization of the soil (Table S1), the fertilizer application rate was calculated: 120–80–10 kg·ha^{-1} of N–P–K using ammonium nitrate, monoammonium phosphate, and potassium nitrate applied weekly via fertirrigation from the beginning of the branching stage for the treatments with pressurized irrigation. In the units with

surface irrigation, soil application was carried out by distributing 60% of the fertilizer at sowing and the remaining 40% in the hilling (75 days after sowing (DAS). Pest and disease management included two applications (64 DAS and 75 DAS) of cymoxanil + mancozeb to control *Phytophthora infestans*, *Alternaria solani*, and *Rhizoctonia solani*; and three applications (73 DAS, 85 DAS, and 99 DAS) of methomyl and alpha-cypermethrin to control *Russelliana solanicola* and *Premnotrypes* spp. Manual harvest was performed at 187 DAS.

2.5. Irrigation Management

The first irrigation was applied immediately after sowing. Subsequently, irrigation was applied every 7 days at 100% ETc until 60 DAS. From this point on, the irrigation rates (LR) were applied according to the distribution of proposed treatments, maintaining the weekly irrigation frequency (L0: surface irrigation with irrigation depth equivalent to 100% ETc; L1: drip irrigation with irrigation depth equivalent to 100% ETc; L2: drip irrigation with irrigation depth equivalent to 75% ETc; L3: drip irrigation with irrigation depth equivalent to 50% ETc). The Irrigation Depth (ID) was calculated according to the soil water balance formula proposed by Allen et al. [39].

$$ID = ETc - Pe \quad (1)$$

$$ETc = ETo \times Kc \quad (2)$$

where ETc is the crop evapotranspiration (mm), Pe is the effective precipitation (mm), ETo is the reference crop evapotranspiration (mm), and Kc is the crop coefficient. Pe was calculated according to the USDA methodology [40]. The ETo value was calculated with the Penman-Monteith equation modified by FAO [39] from the climatic data recorded by the meteorological station installed in the surroundings of the experimental plot. The Kc varied according to the development of the potato crop, as stated by Doorenbos and Kassam [41]. After the beginning of the rainy season, approximately at 168 DAS until the harvest at 187 DAS, the crop water requirement was covered by rainfall, so the restricted layer treatments could not be applied. Six soil moisture sensors (ZL6 Basic data logger with soil moisture sensors Teros-10; METER Group, Munich, Germany) were installed at 0.30 and 0.60 m depth in the surface irrigation plots (L0) and 100% ET drip irrigation plots (L1) to monitor moisture content, as shown in Figure 2.

2.6. Determination of Biometric Variables and Performance Components

Plant height (cm) was measured every 7 days from the beginning of flowering (75 DAS), for which four representative plants were selected per experimental unit. Using a 3.5 m measuring tape, the height from the neck to the apex of the plant's stem was measured. Additionally, during the harvest, four representative plants were selected per experimental unit from which the root depth (cm), fresh weight (g), and dry weight (g) of the aerial and root parts were measured using an oven (75 °C until a stable weight was observed). The four previously selected plants were used to determine the yield components. The number of tubers per plant was counted, and tuber yield was categorized according to traditional local criteria based on tuber weight. First category (C1, tuber weight > 81 g), second category (C2, tuber weight between 41–80 g), and third category (C3, tuber weight < 40 g). The yield of each category was quantified and expressed in tons per hectare ($t \cdot ha^{-1}$). Commercial yield (CY) ($t \cdot ha^{-1}$) was calculated from the sum of the accumulated weights of C1 and C2. According to local practices, third-category tubers were used for personal consumption and/or feed for small animals. Tuber dry weight (g) was used to calculate the percentage of dry matter. The Harvest Index (HI) was also calculated (defined as the ratio

between the fresh weight of tubers and the total fresh weight at harvest). An electronic balance was used to weigh the samples (Type: Electronic precision balance 5000 g, 0.01 g XingYun JA 5000C).

2.7. Water Productivity

The water productivity is an indicator that relates the actual yield achieved and the water use to produce it [17]. The water use can be based on the total used water (which includes rainfall and irrigation) or the water applied only by irrigation. Based on Pereira et al. [42], we calculated the Water Productivity (WP_{irri}, kg m^{-3}) and the Irrigation Water Productivity (WP, kg m^{-3}) for each treatment:

$$WP = \frac{Y_a}{TWU} \quad (3)$$

$$WP_{irri} = \frac{Y_a}{IWU} \quad (4)$$

Y_a is the actual crop's commercial yield (kg·ha^{-1}), IWU (m^3 ha^{-1}) is the irrigation water used throughout the entire campaign, and TWU (m^3 ha^{-1}) refers to the total water use, including the rainfall throughout the phenological development of the crop.

2.8. Profitability of Cultivation

The cost of production and the profitability rate for the different proposed treatments were examined, considering the data from the local agricultural market in the province of Chuquibamba, Arequipa. The profitability rate, defined as the amount of money received after covering the production costs [43], was calculated based on the net income and the total cost:

$$\text{Profitability} = (NI/TC) \quad (5)$$

$$NI = TI - TC \quad (6)$$

where NI represents Net Income, TI is Total Income, and TC is Total Cost. Total cost (TC) was determined by summing all production costs incurred throughout the crop cycle [44]:

$$TC = DC + IC \quad (7)$$

where DC represents direct costs (i.e., machine hours or labor for land preparation, seed tuber, planting tasks, cultural tasks, reservoir and irrigation system maintenance, laying of irrigation lines, irrigation management, fertilization, phytosanitary control, harvest, land rental, mobility, and unforeseen events); and IC, indirect costs included financial expenses only (13.3% DC). Our analysis did not include the costs of installing irrigation infrastructure or equipment depreciation. However, costs associated with maintaining a pre-existing irrigation system were included (i.e., reservoir maintenance, network cleaning, and drip line laying). Regarding units with surface irrigation, the cost of aqueduct cleaning was assumed.

Total income (TI) for each experimental unit was calculated by multiplying the yield of each category of marketable potato tubers by their respective local market price at the time of harvest:

$$TI = \sum_{i=1}^{n} (R_i \times P_i) \quad (8)$$

where R_i is the yield of marketable potato tubers of category i, P_i is the local market price for category i at harvest, and n is the number of marketable potato tubers of category i.

The local market price for C1 was 1.6 PEN·kg^{-1} (0.421 USD), and for C2, 1.00 PEN·kg^{-1} (0.263 USD). All monetary values were collected in the Peruvian national currency, the Sol (PEN); however, they were reported in USD (1 USD = 3.8 PEN). The local cost of daily wages for heavy work (i.e., reservoir cleaning and planting), generally performed by men, was 90 PEN·day^{-1}. For other tasks, which both men and women can perform, the daily wage was 80 PEN·day^{-1}. The hourly rental price for a 96 HP tractor was 150 PEN·h^{-1}. The calculated values were extrapolated to the value of PEN per ha^{-1}.

2.9. Economic Water Productivity

Observing the WP under an economic perspective, the Economic Water Productivity (EWP) relates the monetary value of the achieved yield and the water used [42]. Based on [17], we calculate the economic water productivity (EWP, USD m^{-3}):

$$\mathrm{EWP} = \frac{\mathrm{NI}}{\mathrm{IWU}} \tag{9}$$

where NI represents Net Income (reported in USD·ha^{-1}), and IWU (m^3 ha^{-1}) is the irrigation water used throughout the entire campaign.

2.10. Statistical Analysis

The Analysis of variance (ANOVA) was performed using InfoStat (version 2020) [45] to evaluate the main effects and significance of the interaction. The Tukey test ($\alpha = 0.05$) was applied to compare means between the factor levels. The Shapiro–Wilk test (normality) and Bartlett's test (homoscedasticity) corroborated the model's assumptions.

3. Results

3.1. Effect on Biometric Characteristics of Potato

Except for plant height, the biometric parameters evaluated showed significant differences for the main effect of the irrigation factor but not for the platform factor or the interaction. Thus, the fresh weight of the aerial part of the L0, L1, and L2 treatments presented values statistically higher than the L3 treatment, without presenting significant differences between them, but with a higher average for L1 (Figure 4). However, it was observed that L2 stood out with a higher average dry aerial biomass, followed by the treatments with irrigation equivalent to 100% ETc (L0 and L1) and widely differentiated from L3. No significant differences were observed regarding root depth.

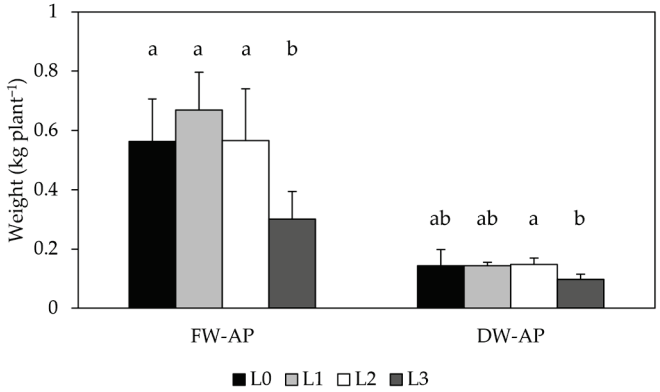


Figure 4. Potato aerial part weights at harvest. FW-AP: fresh weight of the aerial part. DW-AP: dry weight of the aerial part. L0, L1, L2, and L3: levels of the irrigation treatment applied. Different letters in each testing parameter represent statistical significance among groups at $p < 0.05$ for the Tukey test.

On the other hand, taller plants were observed for the upper and middle platforms compared to the lower platforms. In addition, the L1 treatment, with the highest theoretical water application efficiency, presented taller plants with values similar to L0. Consecutively, the decrease in irrigation depths was reflected in a decrease in the average height of the crop (Figure 5).

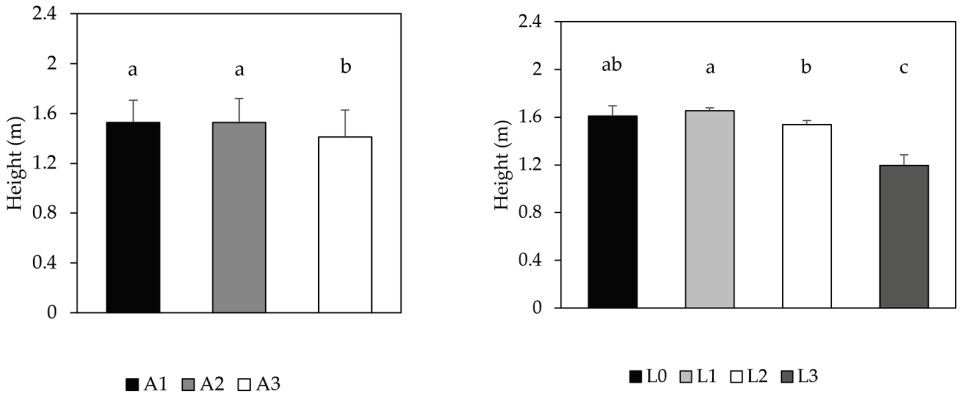


Figure 5. Plant height at harvest. (**a**) Analysis by platform. (**b**) Analysis by irrigation treatment applied. L0, L1, L2, and L3: levels of the irrigation treatment applied. A1, A2, and A3 are upper, middle, and lower platforms, respectively. Different letters in each testing parameter represent statistical significance among groups at $p < 0.05$ for the Tukey test.

3.2. Effect on Potato Yield

Statistical significance was observed only for the irrigation factor. The highest fresh yields were achieved with drip irrigation at 100% ETc and 75% ETc (Figure 6). Although 100% ETc was applied in L0, the fresh yield was lower than with reduced irrigation depth applied by drip (L2). However, these differences were not maintained when analyzing dry weights of the harvested tubers, and no statistical differences were observed in the number of tubers per plant according to treatment. After categorizing the tubers by weight (Table 1), it was observed that the effect of irrigation was statistically different only in the first category (C1), where L1 stood out with the highest values. The 75% ETc irrigation treatment achieved yields similar to those of the control (L0) despite requiring a lower volume of water. For the second category (C2), a tendency to obtain higher yields was observed with reduced depth irrigation but applied in a localized manner (L2). The third category (C3) presents higher values related to irrigation with a higher total volume of water applied to the field. Thus, the commercial yield of L1 is significantly higher than the other treatments. Furthermore, a non-significant trend of L2 values lower than L1 and higher than L0 was observed. The L3 treatment achieved commercial yields around 50% of the best treatment.

Table 1. Potato yields according to commercial categorization.

Treatments	C1 (t ha $^{-1}$)	C2 (t ha $^{-1}$)	C3 (t ha $^{-1}$)	Y (t ha $^{-1}$)	CY (t ha $^{-1}$)
L0	11.12 ± 2.05 ^{bc}	10.51 ± 0.74 ^{a}	10.99 ± 1.76 ^{a}	32.61 ± 1.82 ^{ab}	21.62 ± 1.99 ^{bc}
L1	18.04 ± 1.84 ^{a}	12.1 ± 1.31 ^{a}	9.88 ± 0.90 ^{a}	40.02 ± 2.01 ^{a}	30.14 ± 1.83 ^{a}
L2	14.64 ± 0.69 ^{ab}	12.51 ± 1.34 ^{a}	11.05 ± 1.38 ^{a}	38.2 ± 2.40 ^{a}	27.15 ± 1.47 ^{ab}
L3	5.66 ± 0.79 ^{c}	11.33 ± 1.17 ^{a}	8.66 ± 0.64 ^{a}	25.66 ± 1.58 ^{b}	16.99 ± 1.48 ^{c}

C1: first category (tuber weight > 81 g); C2: second category (tuber weight 41–80 g); C3: third category (tuber weight < 40 g); Y: total yield; CY: commercial yield (C1 + C2). L0, L1, L2, and L3: levels of the irrigation treatment applied. Different letters in each testing parameter represent statistical significance among groups at $p < 0.05$ for the Tukey Test.

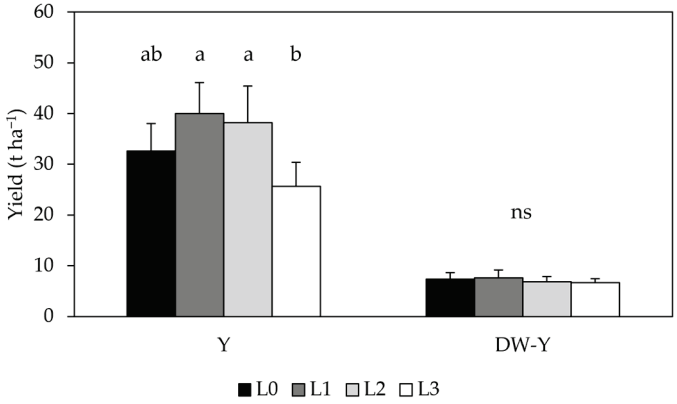


Figure 6. Fresh and dry potato yields according to irrigation treatment. Y: fresh yield. DW-Y: dry yield. L0, L1, L2, and L3: levels of the irrigation treatment applied. ns: indicates not significant ($p > 0.05$); different letters in each testing parameter represent statistical significance among groups at $p < 0.05$ for the Tukey test.

3.3. Crop Water Productivity

Drip irrigation treatments generated savings in water consumption compared to surface irrigation treatment (L0, 8296.5 $m^3 \cdot ha^{-1}$) of 33%, 47%, and 61% for L1 (5531.0 $m^3 \cdot ha^{-1}$), L2 (4366.7 $m^3 \cdot ha^{-1}$), and L3 (3202.5 $m^3 \cdot ha^{-1}$), respectively. Additionally, deficit irrigation treatments achieved additional savings compared to full irrigation (L1), reaching 22% and 44% water reductions for treatments L2 and L3, respectively. In this sense, the treatments where irrigation was applied through drip systems presented the highest Irrigation Water Productivity (WP_{irri}), highlighting the tendency to obtain a better result with a reduced depth of 75% ETc (L2, 6.15 ± 0.35 kg·m^{-3}) over a more (L3: 50% ETc, 5.41 ± 0.41 kg·m^{-3}) or less (L1: 100% ETc, 5.45 ± 0.34 kg·m^{-3}) restrictive management (Figure 7). The Water Productivity (WP) displayed a similar pattern, with treatments using drip irrigation (L1, L2, L3) outperforming the gravity irrigation treatment (L0, 2.36 ± 0.21 0.34 kg·m^{-3}). No significant differences were found between the WP of L1 (4.66 ± 0.29 kg·m^{-3}), L2 (5.06 ± 0.22 kg·m^{-3}), and L3 (4.18 ± 0.32 kg·m^{-3}), with L2 maintaining the highest water productivity. The accumulated rainfall (939 $m^3 \cdot ha^{-1}$) represented a larger proportion of the total water used by the deficit irrigation treatments (L2: 17.7%; L3: 22.7%). In this regard, the difference between WP and WP_{irri} was greatest for L3 and L2. The numerical data are also presented in Table S2.

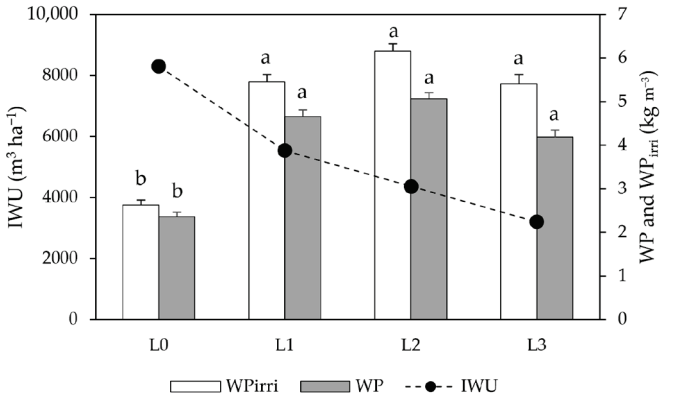


Figure 7. Applied irrigation water and water productivity per treatment. L0, L1, L2, and L3: levels of the applied irrigation treatment. WP: water productivity. WP_{irri}: irrigation water productivity. IWU: irrigation water use. L0, L1, L2, and L3: levels of the irrigation treatment applied. Different letters above each water productivity represent statistical significance among groups for the same parameter at $p < 0.05$ for the Tukey test.

3.4. Crop Economic Profitability

The profitability results (Table 2) during tuber harvest varied between the irrigation systems implemented, where L1 was statistically different from L0. Regarding deficit irrigation, it was found that 75% drip irrigation (L2) showed no significant difference with full drip irrigation (L1); however, these treatments are superior to 50% deficit drip irrigation (L3). The latter generated a loss of invested capital.

Table 2. Profitability indices, production cost components, revenues, and economic water productivity.

Parameters		L0	L1	L2	L3
Costs for agronomic management *	USD·ha^{-1}	3784.21	3763.16	3763.16	3763.16
Irrigation system conditioning	USD·ha^{-1}	0.00	507.89	507.89	507.89
Sprinkler and others related.	USD·ha^{-1}	500.79	500.79	500.79	500.79
Others **	USD·ha^{-1}	816.62	840.96	840.96	840.96
Financial expenses ***	USD·ha^{-1}	678.52	746.50	746.50	746.50
Total Cost	USD·ha^{-1}	5780.13	6359.31	6359.31	6359.31
C1 Income	USD·ha^{-1}	4680.11 ± 863.74 ^{bc}	7595.92 ± 776.25 ^{a}	6164.54 ± 292.29 ^{ab}	2384.59 ± 334.00 ^{c}
C2 Admission	USD·ha^{-1}	2764.53 ± 194.68 ^{a}	3184.51 ± 345.46 ^{a}	3291.80 ± 368.13 ^{a}	2981.79 ± 308.53 ^{a}
Total income	USD·ha^{-1}	7444.64 ± 834.24 ^{bc}	10,780.43 ± 724.24 ^{a}	9456.34 ± 435.52 ^{ab}	5366.38 ± 475.25 ^{c}
Net Income	USD·ha^{-1}	1664.50 ± 834.24 ^{b}	4421.12 ± 724.24 ^{a}	3097.04 ± 435.52 ^{ab}	−992.93 ± 475.25 ^{c}
Net Profitability	dimensionless	0.29 ± 0.14 ^{b}	0.70 ± 011 ^{a}	0.49 ± 0.07 ^{ab}	−0.16 ± 0.07 ^{c}
Economic Water Productivity	USD m^{-3}	0.20 ± 0.10 ^{b}	0.8 ± 0.13 ^{a}	0.71 ± 0.10 ^{a}	−0.31 ± 0.15 ^{c}

Note(s): * Includes land preparation, seed tuber, sowing, cultural work, fertilization, phytosanitary control, and harvest. ** Includes land rental, contingencies, and transportation. *** Capital interest (13.3% of incurred costs). C1 and C2: first and second commercial categories of tubers respectively. L0, L1, L2, and L3: levels of the irrigation treatment applied. Different letters in each testing parameter represent statistical significance among groups at $p < 0.05$ for the Tukey Test.

4. Discussion

Potato cultivation is susceptible to water stress, so its biometric development can be easily affected and expressed in yield losses depending on the cultivar [46,47]. Therefore, the use of deficit irrigation management allows for the evaluation of restriction thresholds to improve the efficiency of resource use. Thus, the results show that reducing the irrigation depth to 75% of the ETc (L2) from the beginning of the formation of stolons did not significantly affect the commercial yield or the WP of the *Solanum tuberosum* cv. Imilla negra crop. This result suggests that the level of induced water stress did not cause critical alterations in crop development [48] since only the height of the plant decreased directly to the reduction of the applied volume of water. In this sense, plant height is reaffirmed as a good indicator of water stress in sensitive stages of development where stomatal closure and inhibition of biochemical processes determine the growth of potato plants [49]. Thus, possible variations in the uniformity of discharge from uncompensated emitters and/or the inherent unevenness of application in surface irrigation systems could have affected the average height of the lower platform (A3). Results similar to those described for the main effect of the irrigation factor were reported when applying reduced irrigation depths up to 75% throughout the crop cycle [50]. However, it has been reported that the application of deficit irrigation plans focused on specific phenological stages can obtain higher WP depending on the agroecological conditions of the environment and the variety evaluated [49,51]. For our case study, the results show that the application of deficit irrigation at 75% ETc from the start of stolon formation is expressed in a slight tendency to reduce commercial yield that is not significant. In this line, it has been reported that certain potato varieties can maintain tuber formation under certain water stress conditions [52]. This is a good indicator of the capacity of the cultivar to maintain its aerial biomass under water stress conditions [53]. Regarding the above, the aerial biomass did not show significant differences between the treatments at 100% ETc and 75% ETc and suggests a

moderate degree of resistance to water stress by the cv. Imilla negra. However, the reduction of irrigation by 50% of the ETc (L3) from the start of stolon formation had a negative effect on biometric parameters such as the fresh weight of the aerial part of the plant, plant height, commercial yield, and total yield. This suggests an irrigation management threshold of around 75% ETc, below which water stress limited key processes in potato development, such as stolon formation, tuberization, and tuber filling, which could have significantly impacted final production [48]. Previous studies corroborate similar results regarding yield losses under 50% deficit irrigation throughout the crop cycle [50,51,54]. In this sense, it is confirmed that irrigation water is one of the most important factors in producing fresh potato tubers [55]. On the other hand, it is worth mentioning that the L3 treatment did not present a significant difference in dry yield compared to the other treatments (Figure 5). This implies a high percentage of dry matter for L3 (dry matter: 26%), which depended on the total irrigation depth [56] and, therefore, a potential alternative for irrigation management if the objective of the crop is the industrialization of potato flour [57–60].

In recent years, various studies have been developed concerning the effect of water stress on the yield and development of tubers [46]. However, as far as we have been able to review, there is limited literature regarding research developed on terraces [61,62]. Furthermore, there is much less information on terraces in the Andes or the application of deficit irrigation management on terraces for potato cultivation. In this sense, similar experiences have been identified in Himalayan terraces [63], where deficit irrigation improved tomato crop yields and the consequent WP compared to traditional management. For the present study, it was observed that the location of the terraces did not determine significant variations in yield, which could be linked to the fact that the topographic variation between the terraces is not sufficient to determine variable microclimates that end up influencing crop growth [64]. This suggests the need to conduct field trials considering the variation in typical microclimates of larger terrace systems.

WP and WP_{irri} exhibited similar values for L0, where rainfall contributed only 10.2% of the total water incorporated into the system throughout the season. This highlights irrigation as a key factor in achieving yield. Such behavior is typical of regions with arid or semi-arid climates [17]. The observed pattern is likely associated with the low efficiency of gravity irrigation and the relatively low rainfall volume (939 m^3 ha^{-1}) compared to the historical average for the rainy season (1799 m^3 ha^{-1}). This further underscores the intrinsic relationship between WP and the spatial-temporal characteristics of the studied environment, such as environmental conditions and water availability during the agricultural season [17].

In accordance with Pereira et al. [42] and Niu et al. [65], WP and WP_{irri} generally increased as the applied irrigation depth decreased. However, this trend was reversed for the most restrictive irrigation treatment (L3). This observation supports the idea that irrigating at 75% of crop evapotranspiration (ETc) may represent a potential threshold for water use efficiency. Furthermore, the observed increase in agricultural productivity, despite a reduction in irrigation water use (IWU), can be attributed to physiological response mechanisms such as partial stomatal closure, which reduces water consumption without affecting photosynthesis, and the redistribution of moisture across the soil profile, which reduces the exposure of evaporative surfaces [51].

WP and WP_{irri} among treatments with drip irrigation did not show significant differences, although there was a tendency for higher WP_{irri} in the drip irrigation (DI) treatment at 75% ETc. This could suggest that the crop is potentially able to adapt to local conditions, making efficient use of rainfall and thereby mitigating water stress situations. On the other hand, the lack of significant improvements in water savings with DI could limit the utility of WP as a relevant indicator for decision-making [42]. This may negatively affect the

adoption of DI techniques by smallholders, as their implementation requires additional investment [42], and the benefits may not be readily apparent in regions with surplus irrigation water supply and/or low water tariffs [17]. This premise underscores the importance of conducting economic analyses that demonstrate the benefits of technical proposals.

Adopting pressurized irrigation systems depends on the specific characteristics of each region (i.e., cultural, economic, geographic, and water availability characteristics) [66]. For the present research, drip irrigation systems positively affected the commercial yield and WP_{irri} of native potatoes grown on terraces, achieving a water saving of 33% compared to surface irrigation. These results coincide with previous studies that report higher yields and water productivity with drip irrigation, attributed to a homogeneous distribution of water, greater precision in the applied volume, and reduced evapotranspiration [67–69]. In addition, the use of fertigation would have reduced the leaching of nutrients compared to furrow irrigation, facilitating their absorption by the roots [70]. Soil moisture sensors confirmed that drip irrigation (L1) concentrated more moisture in the first 30 cm of soil, while surface irrigation distributed water at both depth strata (0–0.30 m and 0.30–0.60 m). However, potato roots developed mainly in the first 0.30 m, which limits the use of moisture concentrated at greater depth. Given the benefits mentioned above, drip irrigation exceeded the net profitability of surface irrigation, with an additional 0.41 USD being earned for each USD invested. However, if the implementation costs of drip irrigation are included, the profitability may not exceed that of surface irrigation. This is due to the high implementation cost of the rural location, the rugged geography, and the expenses associated with reservoir construction, equipment, accessories, and specialized labor [23]. Only the recurrent costs of conditioning the irrigation system have been considered in the research; those expenses after installation are based on the useful life of the accessories (e.g., drip tapes). The cost of preventive maintenance recommended for reservoirs and water conduction routes has also been incorporated. The latter involves local cultural practices linked to water resource management, such as channel cleaning and communal water rate payments [71]. In the case of terraces in the Peruvian Andes, irrigation water is limited but cheap (e.g., in the study area, the water rate depends on the cultivated area and is barely 10 USD ha^{-1} $year^{-1}$). Faced with this, Taylor and Zilberman [72] indicate that the adoption of drip irrigation will be more viable when the cost of water or the harvested product is high, so low water rates could contribute to limitations on the adoption of this type of technology in rural environments. To this can be added the limited evidence of using drip irrigation systems in terraces [63,73] despite various studies evaluating their adaptability for managing various crops in different soil and climate conditions [74–76]. On the other hand, the cost of land rental has been considered to reflect the local reality, where the fragmentation of rural properties motivates the need to rent land for agricultural production. From the economic point of view, no statistically significant differences were identified when comparing the irrigation plan at 75% Etc. (L2) with the irrigation plan at 100% Etc. (L1). This is based on the fact that the yields were similar, and the water savings (21%) were not reflected in monetary savings since the local water rate depends on the cultivated area instead of the volume used. In this sense, Shock et al. [77] conclude that in areas where water is not a limiting factor, the profitability of deficit irrigation does not show significant improvements. However, in regions with water scarcity, this practice can generate considerable economic increases [24,60]. Therefore, it is essential to promote public investment in technologies that improve the productivity of small farmers' crops and contribute to environmental and social sustainability [78]. To do so, it is essential to generate investment in basic infrastructure (e.g., reservoirs, filters, and main pipelines) that allows reducing implementation costs and improving the accessibility and adoption of new technologies adapted to local socioeconomic and cultural conditions. [79].

Another important approach is to make digital technologies for irrigation management more accessible to farmers. Enhancing the availability and accessibility of information can play a crucial role in promoting and organizing awareness programs on the efficient use of water resources. This, in turn, could facilitate the adoption of more efficient irrigation systems, such as micro-irrigation. In this context, the use of Irrigation Advisory Services (IAS) and Decision Support Systems (DSS) in agriculture helps to present management recommendations in a more comprehensible manner by 'translating' soil and climatic data into actionable guidelines that farmers can use to make informed decisions [80]. Additionally, the integration of remote sensing data and predictive climate models further enhances the potential for reducing data collection costs while providing results that are more aligned with real-world conditions [80,81]. Successful initiatives, such as CIMIS, BlueLeaf, and CoAgMet, leverage data from weather stations, while Manna Irrigation and IrriSAT rely solely on remote sensing data [81,82]. These initiatives help bridge the gap between scientific technical knowledge and its practical application by farmers, enabling optimized irrigation planning regardless of the irrigation system in use. However, several factors must be considered, including internet accessibility in rural areas, digital illiteracy, the costs of disseminating these technologies, and the investment required for their development. In this context, institutional support from the state plays a critical role in validating results in complex environments, such as the Andes, and in implementing participatory strategies that facilitate the adoption of these technologies.

Based on the above, the 75% ETc deficit irrigation treatment applied through drip irrigation (L2) achieved higher water yields compared to the other treatments (Figure 8). Although the WP_{irri} values of L2 were not statistically different from those of drip irrigation at 100% ETc (L1), L2 maintained a similar Economic Water Productivity (EWP) while reducing irrigation water use by 22%. This indicates the technical and economic feasibility of the proposed approach. In contrast, traditional gravity irrigation exhibited WP_{irri} and EWP values significantly lower than those of L1 and L2, associated with higher water consumption and lower yields. Finally, L3 was found to be economically unviable.

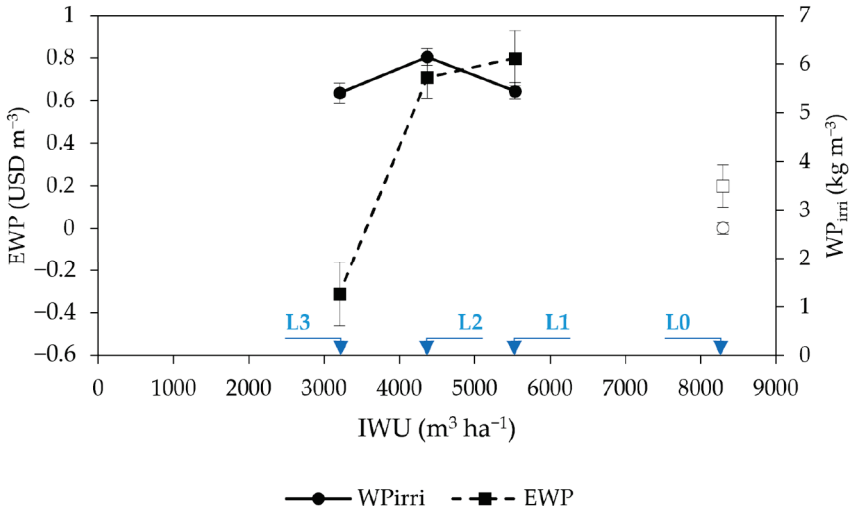


Figure 8. Economic Water Productivity (EWP) and Irrigation Water Productivity (WP_{irri}) as a function of Irrigation Water Use (IWU) for the evaluated treatments. Treatments L0, L1, L2, and L3 are represented in relation to their respective IWUs. The values filled with black represent the drip irrigation treatments, while the values filled with white correspond to the gravity irrigation treatment.

This study has potential limitations that constrained our understanding of the processes associated with deficit irrigation on terraces. Due to budgetary constraints, certain aspects were not implemented. For instance, the installation of soil moisture sensors in all

treatments would have allowed for better monitoring of water behavior in the soil, both within and outside the Readily Available Water (RAW) thresholds. Additionally, to obtain a more comprehensive understanding of water stress, it would have been beneficial to include physiological indicators of water stress response, such as stomatal conductance and photosynthetic rate [83]. Furthermore, as discussed earlier, WP is influenced by the spatial and temporal characteristics of the environment and the season, suggesting that extending the research to include additional campaigns and new study areas would be valuable. Despite these limitations, this study provides an initial approximation of the combined use of drip irrigation (DI) technologies on platforms and presents an economic analysis of their application.

5. Conclusions

This research contributes to developing innovative strategies for sustainable water use in terraced systems, combining traditional practices, such as agricultural terrace use, with modern technologies, such as deficit irrigation practices and pressurized irrigation use. This represents a comprehensive approach that fosters the conservation of ancestral agricultural heritage while responding to the demands of water productivity and economic sustainability in rural contexts. The study introduces the evaluation of deficit irrigation at 75% ETc applied through pressurized irrigation systems on terraces, which is not only an underexplored interaction but also integrates water sustainability principles with the recovery of ancestral agricultural systems, especially in regions where water availability is limited but not necessarily expensive. This combination demonstrates that it is possible to modernize local traditional practices without losing their cultural and ecological essence.

The implementation of deficit irrigation at 75% ETc on terraces (L2) allows for the saving of 3930 $m^3 \cdot ha^{-1}$ of irrigation water compared to traditional surface irrigation (L0) and 1164 $m^3 \cdot ha^{-1}$ compared to drip irrigation at 100% ETc (L1). This results in a WP_{irri} of 6.15 ± 0.35 $kg \cdot m^{-3}$, with a commercial yield (CY) of 27.15 ± 1.47 $t \cdot ha^{-1}$, statistically similar to L1 (WP_{irri}: 5.45 ± 0.34 $kg \cdot m^{-3}$; CY: 30.14 ± 1.83 $t \cdot ha^{-1}$), and higher than traditional surface irrigation (WP_{irri}: 2.63 ± 0.23 $kg \cdot m^{-3}$; CY: 21.62 ± 1.99 $t \cdot ha^{-1}$). Economically, this water saving corresponds to a net income of 3097.04 ± 435.52 $USD \cdot ha^{-1}$ for L2, which is comparable to L1 (4421.12 ± 724.24 $USD \cdot ha^{-1}$) and much higher than traditional surface irrigation (1664.50 ± 834.24 $USD \cdot ha^{-1}$). Moreover, this strategy contributes to the preservation and revitalization of agricultural terraces, promotes efficient resource management in rural areas, and strengthens food security in the southern highlands of Peru. However, it also underscores the need to promote public investment in basic infrastructure that reduces implementation costs, improves access to technologies suitable for local conditions, supports validation efforts, and fosters the adoption of digital technologies that reduce management costs and bridge the gap between technical-scientific knowledge and its field application. In all cases, it is crucial to continue developing research focused on smallholder and family farming as a means of building resilience to climate change and achieving Sustainable Development Goal (SDG) 2 (Zero Hunger) and SDG 1 (No Poverty) [84].

Supplementary Materials: The following supporting information can be downloaded at: https://www.mdpi.com/article/10.3390/w17050668/s1, Table S1: Physical and chemical soil parameters; Table S2: Irrigation water use and water productivities per treatment.

Author Contributions: R.P.-C., formal analysis, investigation, writing—original draft preparation. R.F.-M., Conceptualization, Methodology, Formal analysis, Investigation, Writing—original draft preparation. J.C.-T., Investigation. A.Q., Methodology, Investigation. J.A.-Q., Supervision. R.S.-A., Supervision. All authors have read and agreed to the published version of the manuscript.

Funding: This research was funded by the INIA project CUI 2487112 "Mejoramiento de los servicios de investigación y transferencia tecnológica en el manejo y recuperación de suelos agrícolas degradados y aguas para riego en la pequeña y mediana agricultura en los departamentos de Lima, Áncash, San Martín, Cajamarca, Lambayeque, Junín, Ayacucho, Arequipa, Puno y Ucayali".

Data Availability Statement: The data presented in this study are available on request from the corresponding author.

Conflicts of Interest: The authors declare no conflicts of interest.

References

1. Pan, Z.; Fan, D.; Jiang, R.; Abbasi, N.; Song, D.; Zou, G.; Wei, D.; He, P.; He, W. Improving Potato Productivity and Mitigating Nitrogen Losses Using Enhanced-Efficiency Fertilizers: A Global Meta-Analysis. *Agric. Ecosyst. Environ.* **2023**, *348*, 108416. [CrossRef]
2. Birch, P.R.J.; Bryan, G.; Fenton, B.; Gilroy, E.M.; Hein, I.; Jones, J.T.; Prashar, A.; Taylor, M.A.; Torrance, L.; Toth, I.K. Crops That Feed the World 8: Potato: Are the Trends of Increased Global Production Sustainable? *Food Secur.* **2012**, *4*, 477–508. [CrossRef]
3. De Haan, S.; Rodriguez, F. Potato Origin and Production. In *Advances in Potato Chemistry and Technology*; Elsevier: Amsterdam, The Netherlands, 2016; pp. 1–32. ISBN 978-0-12-800002-1.
4. FAO. *FAOSTAT: Food and Agriculture Data (Production/Crops and Livestock Products)*; FAO: Rome, Italy, 2023; Available online: https://www.fao.org/faostat/en/#data/QCL (accessed on 12 December 2024).
5. Thiele, G.; Devaux, A. Adding Value to Local Knowledge and Biodiversity of Andean Potato Farmers: The Papa Andina Project. In *Innovation for Development: The Papa Andina Experience*; Devaux, A., Ordinola, M., Horton, D., Eds.; International Potato Center: Lima, Peru, 2011; pp. 37–39, ISBN 978-92-9060-410-5.
6. Devaux, A.; Hareau, G.; Ordinola, M.; Andrade-Piedra, J.; Thiele, G. Native Potatoes: From Forgotten Crop to Culinary Boom and Market Innovation. *Choices* **2021**, *35*, 1–7. [CrossRef]
7. Pradel, W.; Hareau, G.; Quintanilla, L.; Suárez, V. *Adopcion e Impacto de Variedades Mejoradas de Papa En El Peru: Resultado de Una Encuesta a Nivel Nacional (2013)*; International Potato Center: Lima, Peru, 2017. [CrossRef]
8. Ordinola, M.; Devaux, A.; Manrique, K.; Fonseca, C.; Thomann, A. Strengthening Competitiveness of the Potato Market Chain: An Experience in Peru. In *Innovation for Development: The Papa Andina Experience*; Devaux, A., Ordinola, M., Horton, D., Eds.; International Potato Center: Lima, Peru, 2011; pp. 151–160. ISBN 978-92-9060-410-5.
9. Erickson, C.L. the Domesticated Landscapes of the Andes. In *The Andean World*; Seligmann, L.J., Fine-Dare, K.S., Eds.; Routledge: New York, NY, USA, 2018; pp. 29–43. [CrossRef]
10. Lane, K. Water Technology in the Andes. In *Encyclopaedia of the History of Science, Technology, and Medicine in Non-Western Cultures*; Selin, H., Ed.; Springer: Dordrecht, The Netherlands, 2014; pp. 1–24. ISBN 978-94-007-3934-5. [CrossRef]
11. Agrorural Andenes Para La Vida. *Inventario y Caracterización de Andenes En Los Andes Tropicales Del Perú*, 1st ed.; Agrorural: Lima, Perú, 2021; ISBN 978-612-4121-35-7.
12. INEI. *Encuesta Nacional Agropecuaria 2022 Principales Resultados: Pequeñas y Medianas Unidades Agropecuarias 2014–2019 y 2021–2022*; Instituto Nacional de Estadística e Informática: Lima, Peru, 2023.
13. Moya Álvarez, A.; Ortega León, J.M.; Jurado Pacheco, X. Evaluación Del Modelo Climático Global MIROC5 y Estimaciones de Temperatura y Precipitaciones Para Las Zonas Sur y Norte Del Perú. *Apunt. De Cienc. Soc.* **2015**, *5*, 188–195. [CrossRef]
14. Bibi, F.; Rahman, A. An Overview of Climate Change Impacts on Agriculture and Their Mitigation Strategies. *Agriculture* **2023**, *13*, 1508. [CrossRef]
15. Varotto, M.; Bonardi, L.; Tarolli, P. (Eds.) *World Terraced Landscapes: History, Environment, Quality of Life*; Environmental History; Springer: Cham, Switzerland, 2019; Volume 9, ISBN 978-3-319-96814-8. [CrossRef]
16. Willems, B.; Leyva-Molina, W.-M.; Taboada-Hermoza, R.; Bonnesoeur, V.; Román, F.; Ochoa-Tocachi, B.F.; Buytaert, W.; Walsh, D. Impactos de Andenes y Terrazas En El Agua y Los Suelos: ¿Qué Sabemos? In *Resumen de políticas, Proyecto "Infraestructura Natural para la Seguridad Hídrica"*; Forest Trends: Lima, Peru, 2021.
17. Çetin, O.; Kara, A. Assesment of Water Productivity Using Different Drip Irrigation Systems for Cotton. *Agric. Water Manag.* **2019**, *223*, 105693. [CrossRef]
18. Autovino, D.; Provenzano, G.; Monserrat, J.; Cots, L.; Barragán, J. Determining Optimal Seasonal Irrigation Depth Based on Field Irrigation Uniformity and Economic Evaluations: Application for Onion Crop. *J. Irrig. Drain. Eng.* **2016**, *142*, 04016037. [CrossRef]
19. Martínez, R.; Ruiz Carrascal, D.; Andrade, M.; Blacutt, L.; Pabón, D.; Jaimes, E.; León, G.; Villacís, M.; Quintana, J.; Montealegre, E.; et al. *Síntesis Del Clima de Los Andes Tropicales*; Cambio Climático y Biodiversidad en los Andes Tropicales; IAI-SCOPE: Buenos Aires, Argentina, 2012; pp. 117–130. Available online: https://www.iai.int/admin/site/sites/default/files/libro_completo.pdf (accessed on 20 February 2025).

20. Kumar, S.; Asrey, R.; Mandal, G.; Singh, R. Microsprinkler, Drip and Furrow Irrigation for Potato (*Solanum tuberosum*) Cultivation in a Semi-Arid Environment. *Indian J. Agric. Sci.* **2009**, *79*, 165–169.
21. Ibragimov, N.; Evett, S.R.; Esanbekov, Y.; Kamilov, B.S.; Mirzaev, L.; Lamers, J.P.A. Water Use Efficiency of Irrigated Cotton in Uzbekistan under Drip and Furrow Irrigation. *Agric. Water Manag.* **2007**, *90*, 112–120. [CrossRef]
22. Bansal, G.; Mahajan, A.; Verma, A.; Bandhu Singh, D. A Review on Materialistic Approach to Drip Irrigation System. *Mater. Today Proc.* **2021**, *46*, 10712–10717. [CrossRef]
23. Narayanamoorthy, A. Potential for Drip and Sprinkler Irrigation in India. In *Draft Prepared for the IWMI-CPWF Project on 'Strategic Analysis of National River Linking Project of India*; Gokhale Institute of Politics and Economics: Pune, India, 2006.
24. Geerts, S.; Raes, D. Deficit Irrigation as an On-Farm Strategy to Maximize Crop Water Productivity in Dry Areas. *Agric. Water Manag.* **2009**, *96*, 1275–1284. [CrossRef]
25. Kiziloglu, F.M.; Sahin, U.; Tunc, T.; Diler, S. The Effect of Deficit Irrigation on Potato Evapotranspiration and Tuber Yield under Cool Season and Semiarid Climatic Conditions. *J. Agron.* **2006**, *5*, 284–288.
26. Yang, P.; Wu, L.; Cheng, M.; Fan, J.; Li, S.; Wang, H.; Qian, L. Review on Drip Irrigation: Impact on Crop Yield, Quality, and Water Productivity in China. *Water* **2023**, *15*, 1733. [CrossRef]
27. Xiuling, D.; Qian, L.; Lipeng, L.; Sarkar, A. The Impact of Technical Training on Farmers Adopting Water-Saving Irrigation Technology: An Empirical Evidence from China. *Agriculture* **2023**, *13*, 956. [CrossRef]
28. Kemp, R.; Branch, N.; Silva, B.; Meddens, F.; Williams, A.; Kendall, A.; Vivanco, C. Pedosedimentary, Cultural and Environmental Significance of Paleosols within Pre-Hispanic Agricultural Terraces in the Southern Peruvian Andes. *Quat. Int.* **2006**, *158*, 13–22. [CrossRef]
29. Cahuana Quispe, R.; Arcos Pineda, J. *Variedades Nativas y Mejoradas de Papa En Puno*; Estación Experimental Illpa-Puno: Lima, Peru, 2002.
30. Joshi, M.; Fogelman, E.; Belausov, E.; Ginzberg, I. Potato Root System Development and Factors That Determine Its Architecture. *J. Plant Physiol.* **2016**, *205*, 113–123. [CrossRef]
31. Opena, G.B.; Porter, G.A. Soil Management and Supplemental Irrigation Effects on Potato: II. Root Growth. *Agron. J.* **1999**, *91*, 426–431. [CrossRef]
32. *NOM-021-RECNAT-2000*; Norma Oficial Mexicana Que Establece Las Especificaciones de Fertilidad, Salinidad y Clasificación de Suelos. Estudios, Muestreo y Análisis. SEMARNAT: Mexico City, Mexico, 2002.
33. *USEPA METHOD 9045D*; Soil and Waste pH. U.S. Environmental Protection Agency: Washington, DC, USA, 2004.
34. *ISO 11265:1994*; Soil Quality—Determination of the Specific Electrical Conductivity. International Organization for Standardization: Geneva, Switzerland, 1994.
35. *ISO 11261:1995*; Soil Quality—Determination of Total Nitrogen—Modified Kjeldahl Method. International Organization for Standardization: Geneva, Switzerland, 1995.
36. Bazán Tapia, R. *Manual de Procedimientos de Los Análisis de Suelos y Agua Con Fines de Riego*; Instituto Nacional de Innovación Agraria—INIA: Lima, Perú, 2017.
37. *ISO 11272:2017*; Soil Quality—Determination of Dry Bulk Density. International Organization for Standardization: Geneva, Switzerland, 2017.
38. Richards, L.A. A Pressure-Membrane Extraction Apparatus for Soil Solutions. *Soil Sci.* **1941**, *51*, 377–386. [CrossRef]
39. Allen, R.G.; Pereira, L.S.; Raes, D.; Smith, M. *Crop Evapotranspiration: Guidelines for Computing Crop Water Requirements-FAO Irrigation and Drainage Paper 56*; FAO, Food and Agriculture Organization of the United Nations: Rome, Italy, 1998; Volume 300, ISBN 92-5-104219-5.
40. Smith, M. *CROPWAT: A Computer Program for Irrigation Planning and Management*; Food and Agriculture Organization of the United Nations: Rome, Italy, 1992; p. 126.
41. Doorenbos, J.; Kassam, A.H. Yield Response to Water. In *Irrigation and Drainage Paper 33*; Food and Agriculture Organization of the United Nations: Rome, Italy, 1979.
42. Pereira, L.S.; Cordery, I.; Iacovides, I. Improved Indicators of Water Use Performance and Productivity for Sustainable Water Conservation and Saving. *Agric. Water Manag.* **2012**, *108*, 39–51. [CrossRef]
43. Brealey, R.A.; Myers, S.C.; Allen, F. *Principles of Corporate Finance*, 11th ed.; McGraw-Hill Irwin: New York, NY, USA, 2014; ISBN 978-0-07-803476-3.
44. Grozo Benavente, J.L. *Costos de Producción Para Actividad: Agricultura, Ganadería, Caza y Silvicultura En Base a La Encuesta Nacional Agraria (ENA-2018)*; Instituto Nacional de Estadística e Informática (INEI): Lima, Perú, 2021.
45. Di Rienzo, J.A.; Casanoves, F.; Balzarini, M.G.; Gonzalez, L.; Tablada, M.; Robledo, C.W. InfoStat 2020; Centro de Transferencia InfoStat, Facultad de Ciencias Agropecuarias, Universidad Nacional de Córdoba: Córdoba, Argentina. Available online: http://www.infostat.com.ar (accessed on 20 February 2025).
46. Nasir, M.W.; Toth, Z. Effect of Drought Stress on Potato Production: A Review. *Agronomy* **2022**, *12*, 635. [CrossRef]

47. Romero, A.P.; Alarcón, A.; Valbuena, R.I.; Galeano, C.H. Physiological Assessment of Water Stress in Potato Using Spectral Information. *Front. Plant Sci.* **2017**, *8*, 1608. [CrossRef]
48. Lal, M.K.; Tiwari, R.K.; Kumar, A.; Dey, A.; Kumar, R.; Kumar, D.; Jaiswal, A.; Changan, S.S.; Raigond, P.; Dutt, S.; et al. Mechanistic Concept of Physiological, Biochemical, and Molecular Responses of the Potato Crop to Heat and Drought Stress. *Plants* **2022**, *11*, 2857. [CrossRef] [PubMed]
49. Teshome, A.W.; Wosenie, M.D.; Addis, H.K. Effects of Deficit Irrigation on Potato Yield and Water Productivity in Northern Ethiopia. *PLOS Water* **2024**, *3*, e0000266. [CrossRef]
50. Ayas, S. The Effects of Different Regimes on Potato (*Solanum tuberosum* L. Hermes) Yield and Quality Characteristics under Unheated Greenhouse Conditions. *Bulg. J. Agric. Sci.* **2013**, *19*, 87–95.
51. Badr, M.A.; El-Tohamy, W.A.; Salman, S.R.; Gruda, N. Yield and Water Use Relationships of Potato under Different Timing and Severity of Water Stress. *Agric. Water Manag.* **2022**, *271*, 107793. [CrossRef]
52. Lefèvre, I.; Ziebel, J.; Guignard, C.; Hausman, J.-F.; Gutiérrez Rosales, R.O.; Bonierbale, M.; Hoffmann, L.; Schafleitner, R.; Evers, D. Drought Impacts Mineral Contents in Andean Potato Cultivars. *J. Agron. Crop Sci.* **2012**, *198*, 196–206. [CrossRef]
53. Schafleitner, R.; Gutierrez, R.; Espino, R.; Gaudin, A.; Pérez, J.; Martínez, M.; Domínguez, A.; Tincopa, L.; Alvarado, C.; Numberto, G.; et al. Field Screening for Variation of Drought Tolerance in Solanum Tuberosum L. by Agronomical, Physiological and Genetic Analysis. *Potato Res.* **2007**, *50*, 71–85. [CrossRef]
54. Mamani Laura, I. Evaluación del Comportamiento del Cultivo de Papa Bajo Condiciones de Riego Deficitario con Tres Láminas de Agua en la Comunidad Barco Belén, Municipio de Achacachi. Bachelor's Thesis, Universidad Mayor de San Andrés, La Paz, Bolivia, 2017.
55. Ferreira, T.C.; Gonçalves, D.A. Crop-Yield/Water-Use Production Functions of Potatoes (*Solanum tuberosum*, L.) Grown under Differential Nitrogen and Irrigation Treatments in a Hot, Dry Climate. *Agric. Water Manag.* **2007**, *90*, 45–55. [CrossRef]
56. Ierna, A.; Mauromicale, G. Tuber Yield and Irrigation Water Productivity in Early Potatoes as Affected by Irrigation Regime. *Agric. Water Manag.* **2012**, *115*, 276–284. [CrossRef]
57. Liu, S.; Wang, Y.; Guo, A.; Zhou, C.; Li, H. Analysis on Quality Properties of Different Varieties of Potato Flour. *Sci. Technol. Food Ind.* **2022**, *43*, 59–66. [CrossRef]
58. Whitney, K.; Simsek, S. Potato Flour as a Functional Ingredient in Bread: Evaluation of Bread Quality and Starch Characteristics. *Int. J. Food Sci. Tech.* **2020**, *55*, 3639–3649. [CrossRef]
59. Zhang, Y.; Yuan, X.; Liu, Q. Physical and Thermal Studies of Extruded Bio-Plastics Based on Potato Flour and Starch. *J. Biobased Mater. Bioenergy* **2015**, *9*, 236–243. [CrossRef]
60. Karam, F.; Amacha, N.; Fahed, S.; EL Asmar, T.; Domínguez, A. Response of Potato to Full and Deficit Irrigation under Semiarid Climate: Agronomic and Economic Implications. *Agric. Water Manag.* **2014**, *142*, 144–151. [CrossRef]
61. Liang, K.; Qi, J.; Liu, E.Y.; Jiang, Y.; Li, S.; Meng, F.-R. Estimated Potential Impacts of Soil and Water Conservation Terraces on Potato Yields under Different Climate Conditions. *J. Soil Water Conserv.* **2019**, *74*, 225–234. [CrossRef]
62. Liu, X.; He, B.; Li, Z.; Zhang, J.; Wang, L.; Wang, Z. Influence of Land Terracing on Agricultural and Ecological Environment in the Loess Plateau Regions of China. *Env. Earth Sci.* **2011**, *62*, 797–807. [CrossRef]
63. Kumar, A.; Kwatra, J.; Sharma, H.C.; Singh, A.K. Feasibility Study of Gravity-Fed Drip Irrigation System on Hilly Terrace Land in Mid-Himalayan Regions. *Indian J. Soil Conserv.* **2012**, *40*, 202–206.
64. Earls, J.C.; Cervantes, G. Chapter 8. Inka Cosmology in Moray: Astronomy, Agriculture, and Pilgrimage. In *the Inka Empire*; Shimada, I., Ed.; University of Texas Press: Austin, TX, USA, 2015; pp. 121–148. ISBN 978-1-4773-0392-4.
65. Niu, Y.; Zhang, K.; Khan, K.S.; Fudjoe, S.K.; Li, L.; Wang, L.; Luo, Z. Deficit Irrigation as an Effective Way to Increase Potato Water Use Efficiency in Northern China: A Meta-Analysis. *Agronomy* **2024**, *14*, 1533. [CrossRef]
66. García-Salazar, J.A.; Bautista-Mayorga, F.; Reyes-Santiago, E. Factors Conditioning the Adoption Rate of Technified Irrigation Systems in Mexico. *Agron. Mesoam.* **2023**, *34*, 51202. [CrossRef]
67. Akram, M.M.; Asif, M.; Rasheed, S.; Rafique, M.A. Effect of Drip and Furrow Irrigation on Yield, Water Productivity and Economics of Potato (*Solanum tuberosum* L.) Grown under Semiarid Conditions. *Sci. Lett.* **2020**, *8*, 48–54. [CrossRef]
68. Si, J.; Wang, L.; Zhang, K.; Li, L.; Fudjoe, S.K.; Luo, Z. Irrigation as an Effective Way to Increase Potato Yields in Northern China: A Meta-Analysis. *Agronomy* **2024**, *14*, 448. [CrossRef]
69. Haghighati-Boroujeni, B. Evaluating the Effects of Deficit Irrigation Strategies on Potato (*Solanum tuberosum* L.) Yield, Tuber Quality and Water Use Efficiency. *Res. Crop. Ecophysiol.* **2021**, *16*, 46–63.
70. Janat, M. Efficiency of Nitrogen Fertilizer for Potato under Fertigation Utilizing a Nitrogen Tracer Technique. *Commun. Soil Sci. Plant Anal.* **2007**, *38*, 2401–2422. [CrossRef]
71. Sánchez Dávila, M.E. Comprender la agricultura en los Andes Peruanos: Religión en la comunidad de Yanque (Caylloma, Arequipa). *Revista Antropologías del Sur.* **2017**, *7*, 235–256.
72. Taylor, R.; Zilberman, D. Diffusion of Drip Irrigation: The Case of California. *Appl. Econ. Perspect. Policy* **2017**, *39*, 16–40. [CrossRef]

73. Bhatnagar, P.; Srivastava, R. Gravity-Fed Drip Irrigation System for Hilly Terraces of the Northwest Himalayas. *Irrig. Sci.* **2003**, *21*, 151–157. [CrossRef]
74. Carroll, J.L.; Orr, S.T.; Benedict, C.A.; DeVetter, L.W.; Bryla, D.R. Feasibility of Using Pulse Drip Irrigation for Increasing Growth, Yield, and Water Productivity of Red Raspberry. *horts* **2024**, *59*, 332–339. [CrossRef]
75. Messaoudi, F.; Ben Nouna, B.; Chebil, A.; Ounaies, F.; Ben Alaya, A. Water Productivity and Economic Feasibility of Drip Irrigation System Investment in Tomato Cultivation: Case of Northeastern Tunisia. *Irrig. Drain.* **2024**, ird.3066. [CrossRef]
76. Rho, H.; Gray, J.; Paetzold, L.; Xue, Q.; Rush, C. Evaluation of Surface Drip Irrigation Systems Focusing on Water-Use Efficiency in High-Value Vegetable Production in the Semi-Arid, Windy Region of the Texas High Plains. *Hortic. Sci. Technol.* **2023**, *41*, 125–143. [CrossRef]
77. Shock, C.C.; Feibert, E.B.G.; Saunders, L.D. Potato Yield and Quality Response to Deficit Irrigation. *HortScience* **1998**, *33*, 655–659. [CrossRef]
78. Chapagain, T.; Raizada, M.N. Agronomic Challenges and Opportunities for Smallholder Terrace Agriculture in Developing Countries. *Front. Plant Sci.* **2017**, *8*, 331. [CrossRef]
79. Misquitta, K.; Birkenholtz, T. Drip Irrigation as a Socio-Technical Configuration: Policy Design and Technological Choice in Western India. *Water Int.* **2021**, *46*, 112–129. [CrossRef]
80. Bonfante, A.; Monaco, E.; Manna, P.; De Mascellis, R.; Basile, A.; Buonanno, M.; Cantilena, G.; Esposito, A.; Tedeschi, A.; De Michele, C.; et al. LCIS DSS—An Irrigation Supporting System for Water Use Efficiency Improvement in Precision Agriculture: A Maize Case Study. *Agric. Syst.* **2019**, *176*, 102646. [CrossRef]
81. Xing, Y.; Wang, X. Precision Agriculture and Water Conservation Strategies for Sustainable Crop Production in Arid Regions. *Plants* **2024**, *13*, 3184. [CrossRef] [PubMed]
82. Koliopanos, C.; Tsirogiannis, I.; Malamos, N. Challenges of Estimation Precision of Irrigation Water Management Parameters Based on Data from Reference Agrometeorological Stations. In Proceedings of the of the 7th International Electronic Conference on Water Sciences (ECWS-7), Online, 15–30 March 2023; p. 82.
83. Chai, Q.; Gan, Y.; Zhao, C.; Xu, H.-L.; Waskom, R.M.; Niu, Y.; Siddique, K.H.M. Regulated Deficit Irrigation for Crop Production under Drought Stress. A Review. *Agron. Sustain. Dev.* **2016**, *36*, 3. [CrossRef]
84. FAO. *Climate Change and Food Security: Risks and Responses*; Food and Agriculture Organization of the United Nations: Rome, Italy, 2015; ISBN 978-92-5-108998-9.

Disclaimer/Publisher's Note: The statements, opinions and data contained in all publications are solely those of the individual author(s) and contributor(s) and not of MDPI and/or the editor(s). MDPI and/or the editor(s) disclaim responsibility for any injury to people or property resulting from any ideas, methods, instructions or products referred to in the content.

water

MDPI

Article

Evaluation of Hydraulic and Irrigation Performances of Drip Systems in Nectarine Orchards (*Prunus persica* var. *nucipersica*) in The Mediterranean Region

Alper Baydar [1,*], Yeşim Bozkurt Çolak [2], Cenk Küçükyumuk [3] and Burak Dalkılıç [2]

[1] Department of Biosystem Engineering, Faculty of Agriculture, Siirt University, 56100 Siirt, Türkiye
[2] Department of Biosystem Engineering, Faculty of Agriculture, Malatya Turgut Özal University, 44210 Malatya, Türkiye; yesim.colak@ozal.edu.tr (Y.B.Ç.); burak.dalkilic@ozal.edu.tr (B.D.)
[3] Department of Park and Gardening Plants, Vocational Training School, İzmir Demokrasi University, 35140 İzmir, Türkiye; cenk.kucukyumuk@idu.edu.tr
* Correspondence: alper.baydar@siirt.edu.tr

Abstract: This study focused on evaluating the performance of the drip irrigation systems installed in 18 different nectarines (*Prunus persica* var. *nucipersica*) orchards in the Tarsus Plain in the Mediterranean region from 2017 through 2018. The performance of the drip systems was evaluated based on parameters like average emitter discharge (Qavg), Christiansen uniformity coefficient (CU), distribution uniformity (DU), emission uniformity (EU), and system application efficiency (Ea). The results indicated that the CU varied between 81 and 98%; DU changed from 82 to 97%; EU 61–92%; absolute emission uniformity (EUa) ranged between 93 and 98%; statistical uniformity (Us) changed from 85 to 97%; application efficiency of low-quarter (AELQ) varied between 45 and 97%; potential application efficiency of low-quarter (PELQ) ranged between 55 and 83%; system application efficiency (Ea) changed from 56 to 96%; storage efficiency (Es) fluctuated between 45 and 97%; and pressure variation (Pv) 17–81% and emitter flow variations (qv) of 2–36% were determined. Although the CU, DU, and EU values were acceptable, the variations in emitter flow rates and pressures were not acceptable. The results revealed that the lower performances might be attributed to physical clogging and/or lack of system design and application practices by the farmers. It is recommended that the farmers receive appropriate training on the operation and management of drip irrigation systems.

Keywords: emitter flow variation; pressure variation; distribution uniformity; application efficiency; emission uniformity

1. Introduction

As one of the most important precision irrigation technologies, microirrigation is used worldwide because it can supply water and fertilizer to the crop root zone in a highly controlled way and greatly improves irrigation water productivity [1]. Drip irrigation has the greatest potential for efficient water and fertilizer usage. To minimize irrigation and fertilization costs, drip irrigation is important to maximize nutrient intake while using a minimum amount of water and fertilizer. The drip irrigation system comprises a pressurized pipeline with an inline or an online emitter. The proper hydraulic design of lateral drip systems usually requires precise assessment of the total head loss represented by friction loss along the pipe and the emitter and the local loss due to the emitter's connection [2]. Irrigation modernization plans are mainly focused on improving infrastructure, providing adequate irrigation system designs but paying no attention to farmer management

skills [3]. Users are prone to operating systems at a lower pressure than designed, which significantly reduces the irrigation system's uniformity. Obviously, these drip irrigation systems have difficulty meeting the requirements of precision irrigation [1]. However, to be efficiently applied, irrigation water must be uniformly applied. That is, with each irrigation, approximately the same amount of water must be applied to all of the irrigated plants. If irrigation is not uniformly applied, some areas will receive too much water, and others will receive too little. As a result, plant growth will also be non-uniform, and water will be wasted where too much is applied. Uniformity is especially important when the irrigation system is used to apply chemicals along with the irrigation water because the chemicals will only be applied as uniformly as the irrigation water. The successful performance of a drip irrigation system depends on the physical and hydraulic characteristics of the drip tubing. The best and most desirable feature of drip irrigation is that it makes the uniform distribution of water possible, which is one of the most important parameters in the design, management, and adoption of this system [4]. Ideally, a well-designed system applies nearly equal amounts of water to each plant, maintaining uniformity while meeting its water requirements and being economically feasible.

The uniformity of water distribution is one of the important parameters in determining the efficiency of the design of drip irrigation systems. Clogging for a long period of time has been a major obstacle in the development of drip irrigation. Emitter clogging can reduce the uniformity of the irrigation system, especially when fertilizer (fertigation) is applied. Therefore, proper assessment to select an appropriate emitter is necessary to prevent clogging [5]. The emitter's hydraulic properties include the effects of emitter design, water quality, water temperature, and other factors on emitter flow rate. Factors such as emitter plugging and wear of emitter components will affect water distribution as emitters age.

Proper design ensures high potential efficiency that is achieved through adequate management [6]. The uniformity parameters are the main criteria for designing an efficient drip irrigation system [7]. The variation in water distribution by emitters may occur due to pressure changes, manufacturing variations, emitter sensitivity to clogging, temperature effects, and other factors [8].

Drip irrigation has made tremendous strides in the past four decades, and it has become the modern standard for efficient irrigation practices for water conservation and optimal plant responses. Microirrigation is an extremely flexible set of technologies that can be economically used on almost every crop, soil type, and climatic zone, but it requires a high level of management [9]. Obtaining the expected benefit from drip irrigation depends on projects designed and managed carefully by trained specialists as well as careful running of the drip irrigation. The system should be carried out and processed as suggested in the project. The initial investment costs of drip irrigation are high, and carrying out drip irrigation requires significant amounts of data and skill. Therefore, farmers should be informed about the management of drip irrigation systems, and they should be made conscious of these system. Thus, the systems should be used more effectively and efficiently.

It is stated that system evaluation techniques can be used to determine the system's potential for more economical and efficient operation by revealing irrigation performance under current operating conditions [10]. Such studies are important in deciding whether to continue with current implementations or whether business adjustments can be made. Parameters that affect the system, such as system water application efficiency (Ea), lower quarter potential, and actual application efficiencies (PELQ and AELQ) to evaluate the irrigation performance of systems have been developed by researchers [11]. PELQ and AELQ indicate whether the system is properly operated and display operating errors.

The hydraulic performance of a drip irrigation system is indicated by water distribution uniformity, which is measured by the uniformity coefficient, emission uniformity, coefficient of variation, and coefficient of manufacturing variation [12]. The efficiency of a drip irrigation system depends on the uniformity of the water distribution, which can be evaluated by measuring the flow rate in each emitter [13]. The different measurements for the hydraulic performance of drip irrigation systems are very useful for the effective design and operation of the system [14]. The determination of the total head loss in a drip irrigation system is very important to ensure the system operates with sufficient pressure. The average operating pressure head for the emitter, distribution of uniformity, and head loss between lateral and manifold will arise as a result of the optimal economic impact [15]. Bralts et al. [16] stated that theoretically, the compensating drip emitter discharge should not show any variation under different pressure heads. Even if pressure head should be only observed in non-pressure-compensating emitters, a properly designed pressure-compensating drip emitter will behave like a non-pressure-compensating emitter if the pressure variation limits exceed certain predefined limits provided by the manufacturers [17].

The use of microirrigation is rapidly increasing around the world, and it is expected to continue to be a viable irrigation method for agricultural production in the foreseeable future. With increasing demand on limited water resources and the need to minimize the environmental consequences of irrigation, microirrigation technology will undoubtedly play an even more important role in the future [9]. The use of drip systems has increased since the early 2000s, converting surface irrigation systems to drip through a national subsidy system by the Turkish Government. Therefore, through this subsidy program, many farmers in Tarsus Plain located in the eastern Mediterranean region of Turkey have also converted their system to a drip system. Tarsus Plain has an important place in our country's agricultural activities. In 2017, 106,674 tons of products were obtained from 7252 ha of nectarine orchards. In particular, nectarine plants have started to be preferred extensively by the producers in the region [18].

The objectives of this study are to evaluate the performance of drip irrigation systems in the young nectarine orchards in the Tarsus Plain located in the Eastern Mediterranean region of Türkiye. The performance evaluation of the drip systems was based on both the hydraulic performance criteria such as distribution uniformity, emission uniformity, Christiansen uniformity coefficient, pressure variation, flow rate variation, statistical uniformity coefficient, and irrigation management performance criteria such as application efficiency, potential application efficiency of the low quarter, actual application efficiency of the low quarter, and storage efficiency under the grower's operation conditions. The performance parameters of the drip systems tested are compared with the standards set by the American Society of Agricultural and Biological Engineers (ASABE) [19].

2. Materials and Methods

2.1. Experimental Site and Soil

This research was carried out between 2017 and 2018 in eighteen nectarine orchards in Tarsus, located in the Eastern Mediterranean region of Türkiye. The elevation of Tarsus is 12 m above sea level, and a typical Mediterranean climate prevails in the region. The average annual temperature in the region is 18.2 °C. According to long-term historical measurements (1965–2018), the average relative humidity is 70.2% and the annual evaporation is 1478 mm. The average annual rainfall is 630 mm, mostly distributed from September to May, with a high inter-annual variability. The long-term historical average climate characteristics of this study are given in Table 1 [20].

This study was carried out on 18 selected nectarine orchards irrigated with a drip system in the Tarsus Plain. The nectarine orchard size ranged from 1.1 ha to 9.0 ha, and the age of the orchards varied from 1 to 9 years. In the orchards, trees were planted with 3 m row spacing and 5 m in the rows.

Table 1. Long-term monthly mean climatic data for the nectarine orchards in Tarsus Plain (Turkish State Meteorological Service, 2019).

Months	February	March	April	May	June	July
Tmin °C	6.9	9.2	12.9	16.8	20.9	24.0
Tmax °C	15.5	18.1	21.6	24.9	28.1	30.7
Tmean °C	11.1	13.8	17.5	21.3	25.0	27.8
Sunshine time (h)	5.6	6.8	7.6	8.5	9.8	10.0
Number of rainy days	9.2	7.6	6.6	5.1	2.2	0.9
Monthly precipitation (mm)	85.1	55.2	34.7	23.4	9.0	6.8

Note: Tmax: maximum air temperature; Tmin: minimum air temperature; Tmean: mean air temperature.

The soils in the selected orchards were examined by taking gravimetric soil samples at four locations in each orchard, and the following analyses were carried out to determine water holding capacity, texture class, soil salinity, bulk density, organic matter content, lime amounts, and pH. In addition, double-ring infiltrometer tests were carried out to determine the infiltration rate of the soils. The soil analysis in the laboratory revealed that soil water content at field capacity varied between 7.50 and 35.43%, wilting point values ranged from 5.35 to 27.12%, and bulk density values changed between 1.27 and 1.60 g cm^{-3}. Soil infiltration rates (I) varied from 6.1 to 21.4 mm h^{-1}, and soil salinity values (EC) fluctuated between 0.398 and 6.10 dS m^{-1}. Organic matter contents ranged from 0.46 to 1.50%, lime amounts ranged between 7.37 and 34.32%, and pH values varied between 7.64 and 8.26. The soil textures were clay-loam in orchards P1 and P2, sandy-loam in orchards P7, P10, and P11, and clay in the other orchards. The physical and chemical properties of the soils of the selected orchards are given in Table 2.

Table 2. Physical and chemical properties of the soils in the selected nectarine orchards.

Orchard No.	Soil Depth cm	BD g cm^{-3}	FC % Pw	WP % Pw	Particle Size Distribution (%) Sand	Clay	Silt	Texture Class	I mm h^{-1}	pH	EC dS m^{-1}
1	0–30	1.38	26.86	17.57	33.9	29.5	36.7	CL	8.2	7.92	0.598
	30–60	1.27	27.53	18.18	31.7	31.6	36.8	CL		8.05	0.755
	60–90	1.33	32.17	22.07	29.1	38.1	32.8	CL		7.84	1.098
P2	0–30	1.40	27.13	17.88	27.2	31.7	41.1	CL	8.6	7.93	0.480
	30–60	1.43	25.93	17.60	31.5	29.6	38.9	CL		8	0.398
	60–90	1.44	27.25	18.43	29.4	31.6	38.9	CL		7.73	1.010
P3	0–30	1.33	32.43	26.57	6.3	70.1	23.6	C	6.5	7.84	4.240
	30–60	1.39	32.88	27.12	6.0	70.3	23.7	C		7.8	7.550
	60–90	1.35	33.53	24.16	13.5	54.6	31.9	C		7.82	4.240
P4	0–30	1.30	32.15	25.54	9.8	69.4	20.8	C	6.3	7.74	3.660
	30–60	1.32	32.12	26.44	7.6	67.3	25.1	C		7.85	4.680
	60–90	1.34	32.23	26.90	5.8	67.0	27.2	C		7.88	6.190
P5	0–30	1.36	30.81	20.17	22.4	40.1	37.5	C	7.9	7.72	0.795
	30–60	1.47	29.85	18.27	24.8	35.8	39.4	CL		7.74	0.792
	60–90	1.41	31.17	19.32	18.4	37.9	43.7	SiCL		7.71	0.977
P6	0–30	1.38	29.63	19.90	20.2	44.3	35.5	C	8.2	7.91	0.552
	30–60	1.37	30.62	20.68	22.1	40.2	37.6	C		7.88	0.626
	60–90	1.44	29.79	19.60	24.5	35.9	39.6	CL		7.9	0.634
P7	0–30	1.52	8.98	6.95	79.6	10.2	10.2	SL	18.4	7.48	0.629
	30–60	1.55	7.73	5.55	83.7	8.1	8.1	LS		7.38	0.603
	60–90	1.60	8.23	5.82	83.7	8.2	8.2	LS		7.47	0.589
P8	0–30	1.33	32.87	23.63	3.2	60.3	36.5	C	6.5	8.00	0.878
	30–60	1.39	32.91	25.04	11.4	54.1	34.5	C		7.98	1.311
	60–90	1.35	33.19	24.42	9.9	51.6	38.5	C		7.91	0.831
P9	0–30	1.33	32.04	24.14	13.2	53.1	33.7	C	6.4	7.64	0.678
	30–60	1.39	31.40	25.37	23.8	55.2	21.0	C		8.1	0.656
	60–90	1.35	32.47	25.38	15.4	57.3	27.3	C		8.26	0.945

Table 2. *Cont.*

Orchard No.	Soil Depth cm	BD g cm^{-3}	FC % Pw	WP % Pw	Particle Size Distribution (%) Sand	Clay	Silt	Texture Class	I mm h^{-1}	pH	EC dS m^{-1}
P10	0–30	1.52	8.92	6.89	79.0	10.5	10.5	SL	19.6	7.45	0.633
	30–60	1.55	7.65	5.70	83.4	8.2	8.4	LS		7.33	0.608
	60–90	1.60	8.29	6.00	83.1	8.3	8.6	LS		7.44	0.594
P11	0–30	1.51	9.01	7.04	79.2	10.5	10.3	SL	21.4	7.40	0.638
	30–60	1.57	7.50	6.50	83.4	8.5	8.1	LS		7.39	0.615
	60–90	1.60	8.40	5.35	83.2	8.4	8.4	LS		7.46	0.590
P12	0–30	1.36	29.56	21.04	16.7	48.6	34.7	C	6.7	8.06	0.607
	30–60	1.43	32.52	23.79	11.4	57.7	30.8	SiC		8.02	0.756
	60–90	1.40	30.07	21.59	1.6	57.2	41.2	C		8.07	0.554
P13	0–30	1.32	33.05	23.90	11.6	56.1	32.3	C	6.4	7.98	0.666
	30–60	1.40	34.09	23.56	15.7	56.2	28	C		8.12	0.602
	60–90	1.42	35.27	23.70	13.6	56.2	30.2	C		8.14	0.674
P14	0–30	1.34	33.56	24.97	11.9	72.7	15.4	C	6.8	8.32	0.894
	30–60	1.44	33.82	25.35	9.8	74.9	15.4	C		8.46	1.295
	60–90	1.41	34.43	25.15	5.5	74.7	19.7	C		8.50	1.980
P15	0–30	1.35	33.00	23.70	11.6	56.1	32.3	C	7.1	7.96	0.680
	30–60	1.41	35.45	23.78	15.7	56.2	28	C		8.10	0.615
	60–90	1.40	33.56	23.60	13.6	56.2	30.2	C		8.12	0.680
P16	0–30	1.32	32.56	24.97	11.9	72.7	15.4	C	7	8.30	0.900
	30–60	1.41	32.82	24.35	9.8	74.9	15.4	C		8.40	1.300
	60–90	1.42	35.43	25.15	5.5	74.7	19.7	C		8.46	1.983
P17	0–30	1.34	27.61	19.37	19.4	19.4	44.0	C	6.4	8.01	0.504
	30–60	1.44	28.12	19.82	14.6	14.6	44.3	SiC		7.96	0.466
	60–90	1.41	29.35	21.48	12.2	12.2	44.5	SiC		7.91	0.684
P18	0–30	1.40	32.11	22.99	19.8	44.5	35.7	C	6.1	7.68	0.574
	30–60	1.40	32.11	21.69	19.7	44.6	35.7	C		7.83	0.502
	60–90	1.42	31.61	21.01	21.7	44.7	33.6	C		7.87	0.598

Note: FC, field capacity; WP, permanent wilting point; BD, bulk density; I, infiltration rate; EC, soil electrical conductivity; C, clay; CL, clay loam; SiCL, silty clay loam; SL, sandy loam; LS, loamy sand; SiC, silty clay.

2.2. General Properties of Drip Irrigation in Nectarine Orchards

The drip systems installed in the 18 nectarine orchards were inspected visually from the control unit to the laterals. On the control unit, the filter types, pressure gauges, and fertilizer tanks were inspected. Then, the mainline pipe material, length, and diameter; the manifold material, length, and diameter; and the lateral line length and emitter spacing were also examined. In the tarsus area where the nectarine orchards are located, the land slopes are below 1%. In the nectarine orchard with the longest lateral line (P9, 191 m), the differences in elevation between the beginning and end of the line is 1 m.

The general characteristics of the drip irrigation systems in the nectarine orchards are given in Table A1. The sizes of these orchards vary between 1.1 and 9.0 ha, the planting spacing of fruit trees (tree row spacing × tree spacing in rows) is 5 × 3 m and the tree ages are between 1 and 9 years. The system filters consist of hydrocyclone, media filters, disk filters, and their combinations. The farmers supply water from the deep wells using hydrocyclone and disk filters, while they obtain water from open channel systems utilizing media filters as primary filters along with disk filters. PE and PVC pipes are used in the main pipe and manifold pipelines. The manifold pipe diameters vary between 50 and 90 mm, the main pipe diameters are 75–140 mm, the manifold line lengths vary between 50 and 385 m, and the main pipe lengths change from 100 to 487 m. Lateral pipe diameters of 16 and 20 mm were used on the systems, and the lateral lengths varied between 50 and 191 m. Fertilizer tanks existed on the drip systems tested. However, only a few growers used them for fertigation, while the others used conventional fertilizer applications.

Inline emitters with 2 L h^{-1} discharge rates are commonly used for irrigation of orchards in the project area. Some of them were pressure-compensating, and some of them

were non-pressure-compensating emitters on their systems. About 10% of the orchards tested and measurements taken used non-compensating emitters, while 90% used pressure-compensating emitters.

2.3. Measurements and Analysis in the Field

Measurements and observations in the selected orchards were carried out in the irrigation system sub-units to represent the production area. The evaluation tests were carried out in one sub-unit to obtain the performance criteria. Some performance criteria, such as uniformity (application uniformity, distribution uniformity, statistical uniformity, emission uniformity, emitter discharge coefficient of variation due to hydraulics, change in hydraulics on manifold and laterals, etc.), irrigation efficiencies (maximum application depth, application efficiency, potential and actual application efficiencies in the low quarter, etc.), wetting patterns of the system, etc., were measured or estimated, analyzed, and evaluated using the mentioned measurement values. Emitter flow and pressure variation along the lateral line in selected irrigation subunits in each orchard were measured. How these measurements were made is explained in the following paragraphs.

2.4. Hydraulic Performance Parameters

2.4.1. Emitter Flow and Pressure Measurements

The emitter flow rate and pressure measurements in the trial orchards were carried out using the method given by Merriam and Keller [10]. By measuring the emitter flow rates and emitter pressures, the average, minimum, and maximum emitter flow rates and average emitter pressures were determined. Evaluations were made by comparing the values specified by ASABE [19]. Four different lateral pipelines were selected: the first one was at the beginning of the manifold, the second one was at 1/3 distance from the beginning of the manifold, the third one was at 2/3 distance, and the fourth one was at the end of the manifold. On each lateral pipeline, 4 drippers were selected. The first one was at the beginning of the lateral, the second one was at 1/3 the distance from the lateral entrance, the third one was at 2/3 distance, and the fourth one was at the end of the lateral.

Emitter pressure measurements were measured using a glycerin pressure gauge with a scale of 0–600 kPa at the point where the water flows from the dripper to the atmosphere.

Emitter flow rates were determined volumetrically using shallow plastic containers under the emitters in the tested laterals for 5 min durations. Thus, flow measurements were made on at least 16 drippers in each lateral and at least 64 drippers in each drip system. Mean emitter flow rates were determined using Equation (1), and average emitter pressures were determined using Equation (2).

$$qavg = \frac{1}{n}\sum_{i=1}^{n} \times q_i \quad (1)$$

In this equation, *qavg* is the average emitter flow rate, L h^{-1}; qi is the emitter flow rate of the i-th emitter, L h^{-1}; and n is the number of emitters.

$$Pavg = \frac{1}{n}\sum_{i=1}^{n} \times P_i \quad (2)$$

where *Pavg* is the average emitter pressure, kPa; Pi is the pressure at the i-th emitter, kPa; and n is the number of emitters.

Pressure Variations in Laterals (Pv)

Pressure measurements were made at the inlets and outlets of the selected subdomains, as well as 4 laterals on each subdomain (at the inlet of the manifold and lateral, 1/3, 2/3,

and the end) using pressure gauges. Emitter flow rates and pressure measurements were made at the selected laterals. Pressure measurements were made at the inlet, 1/3 and 2/3 away from the inlet, and at the end of the lateral. The pressure variations were estimated using Equation (3).

$$P_v = (P_{inlet} - P_{outlet}) \div P_{inlet} \quad (3)$$

where Pv is the manifold or lateral pressure variation, %; P_{inlet} is the sub main or lateral inlet pressure (kPa); and P_{outlet} is the sub main or lateral outlet pressure (kPa). In drip irrigation system design, the maximum pressure variation allowed is 20% [10].

Emitter Flow Variation (qv)

Emitter flow variations in the laterals were calculated using Equation (4) [6].

$$q_v = [(q_{max} - q_{min})/q_{max}] \times 100 \quad (4)$$

where qv is the emitter flow variation, %; q_{max} is the maximum emitter flow rate, L h^{-1}; and q_{min} is the minimum emitter flow rate, L h^{-1}. The general standards for qv values are as follows: 10% or less is desired; 10% to 20% is acceptable; and above 25% is not acceptable based on the ASABE guidelines [19].

Coefficient of Variation (Cv) of the Emitter Flow

The manufacturing variation coefficient is a measure of the flow variation of a randomly selected emitter that has been manufactured by a producer in a certain model and size, has never been used, or has not been worn. The estimated producer modification coefficient must belong to a new emitter operating at a constant temperature and operating pressure. The manufacturing variation coefficient was determined using Equation (5), and it was evaluated according to the ASABE guidelines [19].

$$Cv = \frac{S_d}{qavg} \quad (5)$$

Here, Cv is the manufacturing coefficient of variation; Sd is the standard deviation of emitter flow rates, L h^{-1}; and $qavg$ is the average emitter flow rate, L h^{-1}. The guidelines for classifying the manufacturing coefficient of variation are specified by ASABE [19].

Christiansen Uniformity Coefficient (CU)

The Christiansen uniformity coefficient (CU) gives information regarding how efficiently water is distributed in the field. CU is calculated using Equation (6) [21]:

$$CU = 100.0 - 80.0\frac{s_d}{q_{avg}} \quad (6)$$

where Sd is the standard deviation of the emitter flow rates, L h^{-1}; and $qavg$ is the average emitter flow rate, L h^{-1}. The guidelines for classifying the Christiansen uniformity coefficient (CU) are shown in Table 3 [19].

Table 3. Classification of the performance criteria for different uniformity expressions [19].

Classification	*Cv* (%)	*CU* (%)	*DU* (%)	*EU* (%)	*Us* (%)
Excellent	<5	>90	>85	≥94	>90
Good	5–7	80–90	70–85	81–87	80–90
Fair	7–11	70–80	60–70	68–75	70–80
Low	11–15	60–70	50–60	56–62	60–70
Unacceptable	>15	<60	<50	≤50	<60

Distribution Uniformity (DU)

Distribution uniformity (*DU*) is another index of application uniformity. Distribution homogeneity (*DU*) is the ratio of the average amount of water in the 1/4 of the land receiving the least water to the average amount of water retained in the entire area. The dripper uniformity values are a strong indicator that all the drippers in the area provide nearly identical flow rates, ensuring an even distribution of water across the whole area. The distribution homogeneity (*DU*) was calculated using Equation (7), and it was evaluated according to Merriam and Keller [10].

$$DU = 100 \times \frac{q_{lq}}{q_{avg}} \tag{7}$$

In this equation, *DU* is the distribution homogeneity, %; *qlq* is the lower quarter average emitter flow rate, L h^{-1}; and *qavg* is the average emitter flow rate, L h^{-1}.

Emitter Flow Uniformity (EU)

For the emitter flow uniformity, ref. [21] presented a design method to determine irrigation depth and interval, system capacity, emitter flow characteristics and uniformity, and hydraulic design considerations. Furthermore, they developed two formulas to estimate the design emission uniformity for drip irrigation systems; these formulas are expressed as follows in Equation (8), and it was evaluated according to Table 3 [19].

$$EU = \left[1 - 1.27\frac{Cv}{N^{0.5}}\right] \times \frac{q_{min}}{q_{avg}} \tag{8}$$

Here, EU represents the dripper flow emission (output) uniformity, %; *N* is the evaluated number of emitters for each plant; *Cv* is the coefficient of variation; *qmin* is the minimum emitter flow rate, L h^{-1}; and *qavg* average emitter flow rate, L h^{-1}.

Statistical Uniformity (Us)

Statistical uniformity (Us) was calculated using the equation given below according to the principles given by Bralts and Kesner [16].

$$Us = 100 \times (1 - C_v) = 100\left(1 - \frac{S_d}{q_{avg}}\right) \tag{9}$$

In the equation, *Cv* is the coefficient of variation; Sd is the standard deviation of emitter flow rates, L h^{-1}; and *qavg* is the average emitter flow rate, L h^{-1}. Statistical uniformity was evaluated according to ASABE [19] based on the classification criterion presented in Table 3.

2.4.2. Irrigation Management Performance Parameters

Irrigation performance was evaluated for the farmers' operation conditions in the selected nectarine orchards in one irrigation application for each orchard, since the farmers apply fixed irrigation scheduling (weekly water application and durations set by growers). The following criteria were evaluated for irrigation management.

Wetting Percentage (P)

The wetting percentage (P) was determined using Equation (10) by measuring the wetted area in the field, taking into account the tree row spacing and tree spacing. The

wetted area was estimated about 15 cm below the soil surface under an emitter following irrigation in the selected nectarine orchards.

$$P = 100 \times \left(\frac{A_w}{S_s S_a} \right) \quad (10)$$

Here, P is the wetting percentage, %; Aw is the wetted area, m^2; Ss is the tree row spacing, m; and Sa: is the tree spacing, m.

Storage Efficiency (Es)

Storage efficiency is a criterion for irrigation efficiency determined by sufficient water application until the moisture deficit in the plant root zone reaches the field capacity. In the calculations, the equation given by James [22] was used.

$$E_s = 100 \times \frac{S_{rz}}{SMD} \quad (11)$$

In this equation, *Es* is the storage efficiency, %; *Srz* is the amount of water stored in the root zone (or depth of soil to be wetted) during irrigation, mm; and *SMD* is the amount of water deficit in the root zone before irrigation (the amount of water required to bring the available moisture to the field capacity), mm. SWD was determined via gravimetric soil sampling at three depths (0–30; 30–60; and 60–90 cm) one day before the date of scheduled irrigation.

Water Application Efficiency (Ea)

The application efficiency (*Ea*) of an irrigation system is defined as the percentage of total water applied accumulated in the plant root zone. When the plant root zone is fully irrigated according to the required water volume, the water application efficiency (*Ea*) ASAE [23] is calculated using Equation (12).

$$E_a = 100 \times \frac{Vs}{V_a} \quad (12)$$

In this equation, *Ea* is the water application efficiency, %; V_s is the required (water stored in the root zone) irrigation water, m^3; and V_a is the total amount of water applied in the wetted area, m^3.

Potential Application Efficiency of the Low Quarter (PELQ)

The potential application efficiency in the low quarter (PELQ) was calculated using the approach given by Meriam and Keller [10].

$$PELQ = 0.9 \times EU \quad (13)$$

In this equation, *PELQ* is the potential application in the low quarter and *EU* is emitter flow uniformity, %.

Actual Application Efficiency of the Low Quarter (AELQ)

AELQ is used as an indicator of the efficiency of drip irrigation systems and how much of the applied water is stored in the root zone and is available for plants. The actual application efficiency of the low quarter (AELQ) is calculated using the approach given by Meriam and Keller [10]:

$$AELQ = 100 \times \frac{SMD}{d} \quad (14)$$

where *AELQ* is the actual application efficiency of the low quarter, %; *SMD* is the soil moisture deficit in the rootzone, mm; and *d* is the average water depth applied through the emitters, mm.

2.5. Water Sources

Water was supplied from deep wells in seven of the orchards and from open-channel irrigation networks in 10 orchards for the performance evaluation study. Water samples were taken for each orchard, and water quality was analyzed in the laboratory. Information regarding the water quality of the canal water and well waters (EC and pH values) is presented in Table A1. In general, both water resources had good quality for irrigation, but they were rich in CO_3 and HCO_3, which causes emitter clogging in the drip systems.

3. Results

3.1. Evaluation of Hydraulic Performance Criteria

Lateral pressure variations (Pv) fluctuated between 17 and 81% and emitter flow variations ranged from 2 to 36%, as shown in Table 4. In drip irrigation design, the maximum pressure variation allowed, as stated by Evans et al. [9], is 20%. The lateral pressure variations in the tested plots remained above 20% in most of the 18 orchards except in P5, P6, and P16. The lateral lengths varied between 50 and 191 m in all the orchards. Orchard P9 had the longest lateral length of 191 m, while orchard P1 had the shortest lateral length of 50 m.

Table 4. Obtained drip system performance parameter values and yield for the selected nectarine orchards.

Orchard No.	q_{avg}	P_{avg}	q_v	P_v	C_v	*CU*	*DU*	*EU*	*Us*	E_s	E_a	*PELQ*	*AELQ*	Wetting Percentage
	L h^{-1}	kPa	%	%	%	%	%	%	%	%	%	%	%	%
P1	2.2	80	5	35	8	83	80	76	92	67	52	68	67	35
P2	2.2	130	2	36	3	82	80	75	97	45	74	67	45	33
P3	2.2	170	6	38	7	85	75	81	93	65	56	73	65	37
P4	2.3	120	5	30	8	88	79	78	92	55	66	70	55	37
P5	2.5	100	2	18	8	93	88	76	92	63	56	68	63	35
P6	2.8	170	6	19	9	86	82	81	91	52	71	73	52	37
P7	2.4	120	3	24	11	89	86	74	89	69	62	67	69	22
P8	1.8	90	19	39	15	81	80	61	85	50	74	55	50	37
P9	2.1	110	6	35	4	85	80	85	96	60	61	77	60	37
P10	2.3	80	19	27	10	80	76	78	90	85	71	70	85	20
P11	2.3	160	5.0	24	8	88	84	80	92	87	79	72	87	18
P12	1.5	80	36	26	15	78	76	63	85	49	76	57	49	37
P13	2.5	90	30	74	9	72	66	75	91	55	67	68	55	37
P14	2.1	150	2	31	4	95	90	89	96	86	71	80	86	30
P15	2.5	130	25	81	12	70	67	63	88	58	60	57	58	35
P16	2.2	170	8	17	5	86	80	87	95	79	40	78	79	32
P17	2.3	210	5	22	11	91	87	70	89	56	57	63	56	32
P18	2.9	150	3	23	4	94	90	88	96	76	68	79	76	37

The emitter flow variations observed in the tested drip systems were usually at acceptable levels. The general standards for emitter flow variation (*qv*) values are as follows: 10% or less, desired; 10% to 20%, acceptable; and above 25%, not acceptable [4,23]. The emitter flow variation remained between 10 and 20%, within acceptable limits, in orchards P8 and P10. However, flow variations above 25% were observed in orchards P12, P13, and P15 which were unacceptable. The average emitter flow rates (q_{avg}) measured in the drip systems varied between 1.5 and 2.9 L h^{-1}, and the mean operating pressures (P_{avg}) changed between 110 and 350 kPa, as shown in Table A1.

The coefficient of variation of the emitter flows (*Cv*) for the tested drip systems varied between 3 and 15%, and their classifications were made according to ASABE guidelines [19], as shown in Table A1. The calculated performance values and the classification evaluation of select performance criteria for the selected nectarine orchards are given in Tables 3 and 5, respectively. In the classification of the emitter flow rate change coefficient (*Cv*), point source emitters with *Cv* < 5% are classified as excellent; *Cv* = 5–7% are good; *Cv* = 7–11% are medium; *Cv* = 11–15% are low; and *CV* > 15% are unacceptable according to ASABE guidelines [20]. It is understood that emitter flow rate variation coefficients are excellent in five orchards (P2, P9, P14, P16, P18), good in P3, medium in nine orchards, and low in three orchards (P8, P12, P15). The research results revealed that the *Cv* values were classified as excellent and medium in general, thus considering the magnitude of *Cv* values as acceptable for the drip systems tested.

Table 5. Classification of performance criteria for the drip systems in selected nectarine orchards.

Orchard No	Classification Parameters					
	C_V	*CU*	*DU*	*EU*	*Us*	Yield (t ha^{-1})
P1	Fair	Good	Good	Fair	Excellent	45.02
P2	Excellent	Good	Good	Good	Excellent	46.49
P3	Fair	Good	Good	Fair	Excellent	44.71
P4	Fair	Good	Good	Fair	Excellent	43.55
P5	Fair	Excellent	Excellent	Fair	Excellent	45.11
P6	Fair	Excellent	Excellent	Fair	Excellent	46.44
P7	Fair	Excellent	Excellent	Low	Excellent	46.20
P8	Unacceptable	Fair	Fair	Low	Good	31.17
P9	Excellent	Good	Fair	Good	Good	42.69
P10	Fair	Fair	Fair	Fair	Excellent	38.55
P11	Fair	Excellent	Excellent	Fair	Good	49.33
P12	Unacceptable	Fair	Good	Low	Excellent	33.66
P13	Fair	Fair	Good	Fair	Good	36.49
P14	Excellent	Excellent	Excellent	Good	Excellent	51.02
P15	Low	Fair	Good	Low	Good	33.70
P16	Excellent	Excellent	Excellent	Good	Excellent	52.13
P17	Fair	Excellent	Excellent	Low	Good	37.82
P18	Excellent	Excellent	Excellent	Good	Excellent	49.94

To evaluate the distribution of irrigation water in the tested drip irrigation systems, the Christiansen uniformity coefficient (*CU*) was determined for the tested irrigations. The Christiansen uniformity coefficient (*CU*) values of the test plots varied between 70 and 97% and are given in Table 4.

For the evaluation of *CU*, *CU* > 90% was considered excellent, *CU* = 80–90% was good, *CU* = 70–80% was medium, *CU* = 60–70% was low, and CU < 60% was unacceptable (Table 3). The classifications for the evaluation of select performance criteria applied to the nectarine orchards are given in Table 4. As shown in Table 4, the *CU* in four orchards was classified as excellent, it was good in ten orchards, and it was fair in four orchards. Therefore, the *CU* values observed in the tested drip systems were all at acceptable levels.

The distribution uniformity (*DU*) values of the test plots varied between 71 and 95% and are given in Table 4. The classification evaluation of select performance criteria for the nectarine orchards is given in Table 5. As shown in Table 5, the *DU* in five orchards was classified as excellent, it was good in twelve orchards, and it was fair in one orchard. Accordingly, it was observed that an acceptable level of uniform irrigation was applied. It was observed that the *DU* values for irrigation were always lower than the *CU* values, as expected.

The emission uniformity (EU) of the test orchards varied between 61.0 and 89.0%, as shown in Table 4. The classification evaluation of the performance criteria for the selected nectarine orchards is given in Table 5. As shown in Table 5, the EU values in six orchards

were classified as good, in nine orchards as fair, and in three orchards as low. Considering the obtained values for EU, the low water emission uniformity values in orchards P7, P8, P12, P15, and P17 were not acceptable and were outside the recommended limit values. This non-uniformity of emitter discharge is the result of several factors. The hydraulic variation along the lateral line, submain, or manifold is a function of slope, pipe length and diameter, and emitter–discharge relations.

The statistical uniformity (Us) values for the tested drip systems varied between 85 and 97% and are given in Table 4. The classification evaluation of select performance criteria for the nectarine orchards is given in Table 5. When the Us values given in Table 4 are examined, drip systems in 13 orchards are in the excellent class and 5 orchards are in the good class.

In order to compare the hydraulic performance of the drip irrigation systems in the selected nectarine orchards, yield values were obtained, as given in Table 5. The lowest yield values were obtained from orchards P8 and P12 as 31.17 and 33.66 kg ha^{-1}, respectively. The *Cv* values of these orchards were classified as unacceptable, while their CU values were classified as fair. In the orchards with low CU values, it was observed that irrigation water was not efficiently distributed in the field. This situation prohibited the plant root zone from receiving water and decreased the yield. Also, the emitter types used in the nectarine orchards where the lowest yield values were obtained were non-pressure-regulated (P8–P12). The lowest emission uniformity (EU) values were obtained as 61 and 63% for orchards P8 and P12, respectively.

3.2. Evaluation of Irrigation Management

In this study, the drip systems in the selected nectarine orchards were operated by the farmers, and irrigation was scheduled based on their experience without using any sensors for soil water content or other factors. In general, the growers irrigated their orchards at 5- to 7-day intervals, adjusting irrigation duration by experience, using a short duration during the early season and longer durations during the flowering and fruit set and maturation stage. It was observed that none of the growers utilized scientific irrigation scheduling techniques.

The measured wetting percentages (P) of the parcels tested within the scope of the project varied between 18.3 and 37.3% and are given in Table 4. The lowest wetting area ratios were measured as 21.7%, 20%, and 18.3% in orchards P7, P10, and P11, respectively, where deficit irrigations were applied. This ratio generally varies between 30 and 37% of the total area, especially in orchards.

The storage efficiencies of the tested parcels varied between 45 and 87% (Es) depending on full irrigation, incomplete irrigation, and excessive irrigation conditions and are given in Table 4. Es values greater than 80% were found in three orchards (P10, P11, and P14); Es values between 70 and 80% were observed in two orchards (P16, and P18); Es values between 60 and 70% were found in five orchards (P1, P3, P5, P7, and P9); and Es values less than 60% were recorded in eight orchards.

The application efficiency (*Ea*) of an irrigation system is defined as the percentage of total applied water accumulated in the plant root zone. The application efficiency (*Ea*) values for the tested drip systems varied between 40% and 79% and are given in Table 4. In general, the Ea values were found to be low for the systems; in seven orchards, the *Ea* values were between 70 and 79%; in six orchards, the *Ea* values ranged from 60 to70%; and in five orchards, the *Ea* values were lower than 60%. These results revealed that there were serious irrigation management problems in the systems tested. When the *Es* and *Ea* values are considered together, the growers applied less irrigation than soil water deficit in the 90 cm root zone depth, which means that insufficient water was

applied to the trees in the selected orchards. The duration of the irrigation should be increased in most of the systems tested to satisfy the soil water deficit in the root zone depth. The potential application efficiency of the low quarter (*PELQ*) values varied between 55 and 80%. When Table 4 is examined, the *PELQ* value was highest at 80% in the P14 orchard; in eight orchards, the *PELQ* values ranged between 70 and 80%; in six orchards, the *PELQ* values changed between 60 and 70%, and in three orchards, the *PELQ* values were lower than 60%.

The low-quarter application efficiency (*AELQ*) varied between 45 and 87%. Table 4 shows that the *AELQ* values were higher than 80% in orchards P10, P11, and P14, and the rest of the orchards remained below this value. The *AELQ* is the ratio of the water infiltrated and stored in the root zone in the least-watered quarter of the land to the average depth of irrigation water applied, expressed as a percentage. Although most of the systems' performance was lower than the expected norms, they were within the range of what is normally found for in-field evaluations.

4. Discussion

According to the results of this research, lateral pressure variations were found to be above the allowable value of 20% [9]. The reason for greater pressure variations is due to using longer lateral lengths (>150 m) and partial clogging of emitters. Also, possible clogging in filtration may have reduced the optimum operating pressure of the systems, which can cause variations in pressure. The farmers did not use any chemicals (acid treatment) to prevent emitter clogging in their systems. Although the farmers used hydrocyclone and disk filters, the use of automatic filters and mesh numbers, selected according to the sediment sizes in the water source, will prevent possible clogging.

Only five orchards had excellent *Cv* values and, three of them were low. Farmers of orchards with low *Cv* values should consider design changes in their system to reduce the *Cv* values to acceptable levels. Emitter variation at a given operating pressure is caused by manufacturing variability, emitter plugging (complete or partial), water temperature changes, and emitter wear [24]. Therefore, the orchards with flow variations greater than 20% (P12, P13, and P15) should undergo modification of their system design in order to reduce flow variations.

Özer et al. [25] reported *CU* values between 80 and 96% and *DU* values ranging between 68 and 94% for 11 drip systems in corn fields and walnut orchards in the Thrace region of Türkiye. A similar result was also found in our research. The reason for this is that while the mean of deviations from the means is used in the calculation of the *CU* value, the lower quarter average is used in the calculation of the *DU* value.

The reason why the rate of wetting area varies across such a wide range is due to differences in lateral intervals and the amount of irrigation water applied. In drip irrigation system planning, it is extremely important to determine the wetting area percentage (P) correctly. For this reason, the wetting area percentage should be at least 30% in project designs. However, this value can be taken as the lower limit of 25% in humid regions and 35% in very arid regions [1].

Ashiri et al. [26] evaluated a drip system in Pakistan, and they found that the water application uniformity was above 80%, which indicates that the drip irrigation was designed with proper scale and dimensions. None of the orchards tested in this study were classified as having excellent EU values. Also, five orchards were not acceptable and were outside the recommended limit of EU values. System uniformity is important in terms of system performance and even distribution of water over a field. Additionally, in drip irrigation systems, EU directly affects the yield of the crops [27]. In some instances, the drip irrigation systems were installed with little concern for basic engineering hydraulic principles, resulting

in nonuniform emitter discharges throughout the irrigated field. To overcome this lack of uniformity, researchers found it was necessary to over-irrigate [5]. Abdulhadi et al. [28] evaluated the existing drip irrigation network of Fadak Farm in Iraq, and they reported an EU value of 96.5%, a statistical uniformity coefficient of 97%, emitter flow variation of 6.85%, a coefficient of variation of 0.026, application efficiency of 96.5%, and pressure variation of 17%. They concluded that the drip irrigation system worked well and efficiently over the entire study region. Additionally Alaç et al. [29] stated that the water emission uniformity (EU) of the drip irrigation system of a ridge-planted citrus garden changed between 92 and 95%.

In general, *Us* values are at acceptable levels in tested drip systems. Soccol et al. [30] determined the performance of a drip system in an apple orchard, and they found an EU value of 74% and a *Us* value of 77.7%.

Although the uniformity parameters showed that the system performance was acceptable, the efficiency parameters (*Es* and *Ea*) indicated that irrigation management requires alterations to increase these values to acceptable levels. The most important factors affecting field water application efficiency are the irrigation method, soil type, and the amount of irrigation water applied. Soccol et al. [30] found an *Ea* value of 100% and an Es value of 47.8%. They concluded that increasing irrigation duration resulted in increased storage and application efficiency.

PELQ is an indication of how well a system can deliver water under optimum operating conditions. The *PELQ* values are generally good, but only three orchards were determined to be lower than 60%. A low *PELQ* is a sign of planning problems [10]. Alaç et al. [29] evaluated the drip performance in a citrus orchard and reported that the lower quarter potential application efficiency (*PELQ*) was 85%, the lower quarter actual application efficiency (*AELQ*) was 94%, and the wetted area percentage was 20%. Three orchards had an *AELQ* value higher than 80% in this research. A significant difference between *AELQ* and *PELQ* values has been identified as an indicator of poor operation of irrigation systems. Özer et al. [25] reported *Ea* values between 45 and 94%, *AELQ* values ranging between 54 and 86%, and PELQ values between 52 and 84% for 11 drip systems in corn fields and walnut orchards.

5. Conclusions

The performance of drip systems in young nectarine orchards in a Mediterranean environment was evaluated based on hydraulic performance parameters like average emitter discharge (*Qavg*), Christiansen uniformity coefficient (*CU*), and distribution uniformity (*DU*), emission uniformity (*EU*), as well as irrigation management performance parameters such as system application efficiency (*Ea*), storage efficiency, *AELQ*, and *PELQ*. Although the *CU*, *DU*, and *EU* values were at acceptable levels, the variations in emitter flow rates and pressure were not at acceptable levels. The results revealed that although hydraulic performance parameters were found to be at acceptable levels in general, in the tested drip systems, the irrigation efficiency parameters were lower than expected norms, indicating that the main problem with these systems was not the design but the management and operation of these systems. Thus, the lower performances might be attributed to clogging and/or lack of system design and application practices by the farmers. Regarding the pressure variations in the laterals that were generally greater than 20%, the farmers should alter their system design and use acid injection for the prevention of clogging to reduce pressure variations in their systems. A major problem encountered in drip irrigation is the plugging or clogging of emitters. In particular, physical clogging in drippers can be obvious depending on the type of water source. We recommend farmers use hydrocyclone and disk filters in their filtration systems. Also, a disk filter placed before the fertigation equipment will be a useful tool. In this study, the farmers generally cleaned their filters at the beginning and in the middle of the growing season.

While the drip method has great potential for high irrigation efficiencies, poor system design, management, or maintenance can lead to low efficiencies. In addition, the farmers have insufficient knowledge of drip irrigation systems and their operation, especially on irrigation scheduling. It is strongly recommended that the farmers obtain appropriate training on the operation and management of drip irrigation systems.

The success of any irrigation method, particularly drip irrigation, depends to a large degree on the management of the irrigation system. With drip irrigation, precise information on the amount of water that the crop is using is required to adequately determine the irrigation amount. Control strategies using feedback information on soil water or plant water status can be used to determine if the irrigation applications are either too large or too small.

Drip irrigation is an irrigation method that has a complex structure that can serve farmers for many years with proper design, maintenance, and repair operations performed at appropriate times. These are based on engineering calculations at every stage, from when the water is taken from the source to its delivery to the plant root zone. The selection of proper emitters depending on field and lateral length, filtration systems for the type of water sources, maintenance of fitting parts, and cleaning of the filters before and after irrigation applications are the most important applications of effective drip irrigation systems.

It is recommended that newly established drip irrigation systems be tested at various intervals throughout their operation to ensure long-lasting function and reduce maintenance costs. Performance measurements should be acquired before and during the production season and should be linked to the developing technology. Thus, possible problems in the system can be detected early, and drippers can be used for a longer period. Farmers should be trained to use the system and should maintain it at certain intervals. It is important to follow irrigation schedules, record the chemicals applied and maintenance procedures, and carry out economic analyses to improve these systems.

Author Contributions: Conceptualization, A.B. and Y.B.Ç.; methodology, A.B., Y.B.Ç. and C.K.; formal analysis, A.B., Y.B.Ç., C.K. and B.D.; resources, A.B. and Y.B.Ç.; data curation, A.B., Y.B.Ç., C.K. and B.D.; writing—original draft preparation, A.B., Y.B.Ç. and C.K., writing—review and editing, A.B., Y.B.Ç., C.K. and B.D.; supervision, A.B., Y.B.Ç. and C.K. All authors have read and agreed to the published version of the manuscript.

Funding: This research was funded by the General Directorate of Agricultural Research and Policy, project no. TAGEM/TSKAD/G/17/A9/P3/430.

Data Availability Statement: The data presented in this study are available from the corresponding author upon request.

Conflicts of Interest: The authors declare no conflicts of interest.

Abbreviations

The following abbreviations are used in this manuscript:

AELQ	Actual application efficiencies
CU	Coefficient of uniformity
CV	Coefficient of variation
DU	Distribution uniformity
Ea	Water application efficiency
Es	Storage uniformity
EU	Emitter flow uniformity
PELQ	Lower quarter potential
Pv	Pressure variations in laterals
qv	Emitter flow variation
Us	Statistical uniformity

Appendix A

Table A1. Drip irrigation system characteristics in the selected nectarine orchards and irrigation water supply and quality.

Orchard No/Properties	P1	P2	P3	P4	P5	P6	P7	P8	P9	P10
Area (ha)	1.5	3.5	2.5	2.5	5.0	5.0	2.0	9.0	9.0	1.8
Tree age (years)	8	3	6	6	7	2	4	2	2	4
Plant Row Spacing (m)	5	5	5	5	5	5	5	5	5	5
Plant Row (m)	3	3	3	3	3	3	3	3	3	3
Age of the System	7	2	5	5	6	1	3	1	1	3
Filter type	H + DF	H + MF + DF	H + MF + DF	H + MF + DF	H + MF + DF	H + MF + DF	H + DF	MF + DF	H + MF + DF	H + DF
Main Pipe Material	PVC-PE	PVC-PE	PVC-PE	PVC-PE	PVC-PE	PVC-PE	PVC-PE	PVC-PE	PVC-PE	PVC-PE
Main Pipe Diameter (mm)	75	140	110	110	110	110	90	140	140	110
Main Pipe Length (m)	226	223	172	487	168	465	135	450	400	100
Manifold Pipe Material	PE	PVC	PVC	PVC	PE	PE	PE	PE	PE	PE
Manifold Diameter (mm)	63	90–75–63	90–75–63	63	90–75–63	90–75–63	63	90–75–63	90–75–63	50
Manifold length (m)	207	385	131	120	70	103	200	140–160	150	185
Lateral Pipe Diameter (mm)	16	20	20	20	16	20	20	20	20	16
Lateral Pipe Length (m)	50	137	180	180	84	165	120	167	191	87
Lateral Spacing (m)	0.80	0.80	0.80	0.80	0.80	0.30	0.80	0.30	0.30	0.80
Emitter Flow (L h^{-1})	2	2	2	2	2	2	2	2	2	2
Measured Avg. Emitter Flow Rate (L h^{-1})	2.24	2.20	2.15	2.25	2.45	2.78	2.43	1.75	2.10	2.32
Measured Avg. Emitter Pressure (kPa)	85	125	166	118	103	173	117	87	113	75
Emitter spacing (cm)	50	50	50	50	50	50	50	40	50	50
Emitter type	PC	PC	PC	PC	PC	PC	PC	NPC	PC	PC
Operating Pressure (kPa)	110	280	350	350	150	150	300	150	180	200
System Age (years)	7	2	5	5	6	1	3	1	1	3
Water Supply	Deep well	Deep well	Canal	Canal	Canal	Canal	Deep well	Canal	Canal	Deep well
Irrigation Water (EC, dS m^{-1})	0.714	0.512	1.286	1.286	0.455	0.455	0.843	0.500	0.650	0.923
Irrigation Water (pH)	7.22	8.25	7.70	7.70	7.92	7.92	6.87	7.98	8.03	6.91

Orchard No/Properties	P11	P12	P13	P14	P15	P16	P17	P18
Area (ha)	1.3	6.3	1.2	1.8	1.1	1.3	2.0	1.7
Tree age (years)	4	6	4	4	4	4	10	5
Plant Row Spacing (m)	5	5	5	5	5	5	5	5
Plant Row (m)	3	3	3	3	3	3	3	3
Age of the System	3	8	3	3	3	3	9	4
Filter type	H + DF	H + MF + DF	H + MF + DF	H + MF + DF	H + MF + DF	H + MF + DF	MF + DF	H + MF + DF
Main Pipe Material	PVC-PE	PVC-PE	PVC-PE	PVC-PE	PVC-PE	PVC-PE	PVC-PE	PVC-PE
Main Pipe Diameter (mm)	110	110	110	90	110	90	110	125
Main Pipe Length (m)	100	210	170	147	170	147	220	200
Manifold Pipe Material	PE	PE	PE	PE	PE	PE	PE	PE
Manifold Diameter (mm)	50	75–63	75–63	90–75–63	75–63	90–75–63	75–63	90–75–63
Manifold length (m)	105	60	70	125	70	110	50	90

Table A1. *Cont.*

Lateral Pipe Diameter (mm)	16	20	20	20	20	20	20	20
Lateral Pipe Length (m)	100	140	171	110	159	120	114	75
Lateral Spacing (m)	0.80	0.80	0.80	0.80	0.80	0.80	0.80	0.80
Emitter type	PC	NPC	PC	PC	PC	PC	PC	PC
Emitter Flow (L h^{-1})	2	2	2	2	2	2	2	2
Measured Avg. Emitter Flow Rate (L h^{-1})	2.34	1.53	2.50	2.11	2.45	2.16	2.25	2.91
Measured Avg. Emitter Pressure (kPa)	163	78	91	148	125	165	207	146
Emitter spacing (cm)	50	40	33	50	33	50	50	60
Operating Pressure (kPa)	200	180	200	300	250	280	270	250
System Age (years)	3	5	3	3	3	3	9	4
Water Supply	Deep well	Canal	Canal	Canal	Canal	Canal	Deep well	Deep well
Irrigation Water (EC, dS m^{-1})	0.905	0.370	0.486	0.456	0.486	0.456	0.343	0.650
Irrigation Water (pH)	6.87	8.37	8.09	8.10	8.09	8.10	7.84	8.03

Note: H, Hydrocyclone; MF, Media filter; DF, Disk filter; PC, Pressure Compensating; NPC, Non-pressure compensating.

References

1. Wang, X.R.; Zhang, C.; Li, G.Y. Improving drip irrigation uniformity by boosting the hydraulic performance of drip lateral pressure regulators. *Int. J. Agric. Biol. Eng.* **2024**, *17*, 185–192. [CrossRef]
2. Provenzano, G.; Pumo, D.; Di Dio, P. Simplified procedure to evaluate head losses in drip irrigation laterals. *J. Irrig. Drain. Eng* **2005**, *131*, 525–532. [CrossRef]
3. Seyedzadeh, A.; Khazaee, P.; Siosemardeh, A.; Maroufpoor, E. Irrigation management evaluation of multiple irrigation methods using performance indicators. *ISH J. Hydraul. Eng.* **2021**, *28*, 303–312. [CrossRef]
4. Venot, J.P.; Zwarteveen, M.; Kuper, M.; Boesveld, H.; Bossenbroek, L.; Van Der Kooij, S.; Wanvoeke, J.; Benouniche, M.; Errahj, M.; Fraiture, C.D.; et al. Beyond the promises of technology: A review of the discourses and actors who make drip. *Irrig. Drain.* **2015**, *63*, 186–194. [CrossRef]
5. Zhou, B.; Li, Y.; Song, P.; Zhou, Y.; Yu, Y.; Bralts, V. Anti-clogging evaluation for drip irrigation emitters using reclaimed. *Water Irrig. Sci.* **2017**, *35*, 181–192. [CrossRef]
6. Playan, E.; Mateos, L. Modernization and optimization of irrigation systems to increase water productivity. *Agric. Water Manag.* **2006**, *801*, 100–116. [CrossRef]
7. Elamin, A.W.M.; Eldaiam, A.M.A.; Abdalla, N.A.; Hussain, M.E. Hydraulic performance of drip irrigation system under different emitter types and operating pressures using treated wastewater at Khartoum State. *Int. J. Dev. Sustain.* **2017**, *6*, 1086–1095.
8. Al-Mhmdy, S.H.M.; Al-Dulaimy, A.M. Performance evaluation of drip irrigation system according to the suggested standards. *Iraqi J. Agric. Sci.* **2018**, *49*, 1099–1109. [CrossRef]
9. Evans, R.G.; Wu, I.P.; Smajstrala, A.G. Microirrigation Systems. In *Design and Operation of Farm Irrigation Systems*, 2nd ed.; The American Society of Agricultural and Biological Engineers: St. Joseph, MI, USA, 2007; Chapter 17; pp. 632–677.
10. Merriam, J.L.; Keller, J. *Farm Irrigation System Evaluation: A Guide for Management*, 3rd ed.; Agricultural and Irrigation Engineering, Department of Utah State University: Logan, UT, USA, 1978; p. 276.
11. Merriam, J.L.; Shearer, M.N.; Burt, C.M. Evaluating Irrigation System and Practices. In *Design and Operation of Farm Irrigation Systems*, 3rd ed.; ASAE Monograph: St. Joseph, MI, USA, 1980; pp. 721–760.
12. Wu, I.P.; Gitlin, H.M. Drip irrigation application efficiency and schedules. *Trans. Am. Soc. Agric. Eng.* **1993**, *26*, 92–99. [CrossRef]
13. Kumar, S.; Singh, P. Evaluation of hydraulic performance of drip irrigation system. *J. Agric. Eng.* **2004**, *44*, 106–108.
14. Gil, J.; Khan, L.; Hernandez, R. Evaluation of the hydraulic performance of several imported emitters for drip irrigation. *Rev. Cient. UDO Agric.* **2002**, *2*, 64–72.
15. Chamba, D.; Zubelzu, S.; Juana, L. Energy, cost and uniformity in the design of drip irrigation systems. *Biosyst. Eng.* **2019**, *178*, 200–218. [CrossRef]
16. Bralts, V.F.; Kesner, C.D. Drip irrigation field uniformity estimation. *Trans. ASAE* **1983**, *26*, 1369–1374. [CrossRef]
17. Khalil, T.M.; Ajmal, M.; Khan, T.A.; Haq, Z.U.; Khattak, M.S.; Malik, A. Evaluating hydraulic performance of locally available drip emitters used in Pakistan. *Sarhad J. Agric.* **2020**, *36*, 185–191. [CrossRef]

18. TÜİK. Turkish Statistical Organization. Crop Production Statistics, Ankara, Türkiye. Available online: https://data.tuik.gov.tr (accessed on 15 December 2017).
19. American Society of Agricultural and Biological Engineers. *Design and Installation of Microirrigation Systems*; ASAE EP405.1, APR1988 (R2008); ASABE: St. Joseph, MI, USA, 2008; 5p.
20. MGM. General Directorate of Meteorology of Turkey. Climate Data. Ankara, Türkiye. Available online: https://www.mgm.gov.tr/veridegerlendirme/il-ve-ilceler-istatistik.aspx?k=H (accessed on 15 September 2019).
21. Keller, J.; Karmeli, D. Trickle irrigation design parameters. *Trans. ASAE* **1974**, *7*, 678–684. [CrossRef]
22. James, L.G. *Principles of Farm Irrigation System Design*; John Willey and Sons Inc.: New York, NY, USA, 1988; 543p.
23. American Society of Agricultural Engineers. *Field Evaluation of Micro-Irrigation Systems*, 45th ed.; ASAE EP458; American Society of Agricultural Engineers: St. Joseph, MI, USA, 1998.
24. Asif, M.; Ahmad, M.; Mangrio, A.G.; Akbar, G.; Memon, A. Design, evaluation and irrigation scheduling of drip irrigation system on citrus orchard. *Pak. J. Meteorol.* **2017**, *12*, 37–48.
25. Özer, S.; Öztürk, O.; Çebi, U.; Aydın, B. Technical performance evaluation of some drip systems in Kırklareli. *Turk. J. Agric. Nat. Sci.* **2020**, *7*, 112–119. [CrossRef]
26. Ashiri, M.; Boroomand-Nasab, S.; Hooshmand, A. Technical evaluation of drip irrigation systems (Case Study of Shahid Rajaayi Agro-Industry–Dezful). *World Rural Obs.* **2014**, *6*, 36–43. [CrossRef]
27. Al-Karaghouli, A.A.; Minasian, A.N. Emission uniformity of drip irrigation systems. *Plasticulture* **1992**, *94*, 33–38.
28. Abdulhadi, J.S.; Alwan, H.H. Evaluation the existing drip irrigation network of Fadak Farm. *Kerbala J. Eng. Sci.* **2020**, *1*, 1–13. [CrossRef]
29. Alaç, V. Evaluation of Drip System Installed in a Citrus Orchard Established on Raised Bed. Master's Thesis, Çukurova University Science and Technolgy Institute, Adana, Turkey, 2006.
30. Soccol, O.J.; Ullmann, M.N.; Frizzone, J.A. Performance analysis of a trickle irrigation subunit installed in an apple orchard. *Braz. Arch. Biol. Technol.* **2002**, *45*, 525–530. [CrossRef]

Disclaimer/Publisher's Note: The statements, opinions and data contained in all publications are solely those of the individual author(s) and contributor(s) and not of MDPI and/or the editor(s). MDPI and/or the editor(s) disclaim responsibility for any injury to people or property resulting from any ideas, methods, instructions or products referred to in the content.

water

MDPI

Article

Understanding Unsustainable Irrigation Practices in a Regionally Contested Large River Basin in Peninsular India Through the Lens of the Water–Energy–Food–Environment (WEFE) Nexus

Bhawana Gupta [1,2,*] and John S. Rowan [1]

[1] UNESCO Centre for Water Law, Policy and Science, School of Law, University of Dundee, Nethergate, Dundee DD1 4HN, UK; j.s.rowan@dundee.ac.uk
[2] Environmental Change Institute, University of Oxford, Oxford OX1 3QY, UK
* Correspondence: bhwnagpta@gmail.com

Abstract: Water management is a long-standing source of dispute between the riparian states of Karnataka and Tamil Nadu. Recently, these disputes have intensified due to impacts from climate change and Bangalore's rapid growth to megacity status. Despite well-defined national water governance instruments, competition between state actors and limited access to reliable hydrometric data have led to a fragmented regulatory regime, allowing unchecked exploitation of surface and groundwater resources. Meanwhile, subsidised energy for groundwater pumping incentivises the unsustainable irrigation of high-value, water-intensive crops, resulting in overextraction and harm to aquatic ecosystems. Here, we employ a water–energy–food–environment (WEFE) nexus approach to examine the socio-political, economic, and environmental factors driving unsustainable irrigation practices in the Cauvery River Basin (CRB) of Southern India. Our methodology integrates spatially explicit analysis using digitised irrigation census data, theoretical energy modelling, and crop water demand simulations to assess groundwater use patterns and energy consumption for irrigation and their links with governance and economic growth. We analyse spatio-temporal irrigation patterns across the whole basin (about 85,000 km^2) and reveal the correlation between energy access and groundwater extraction. Our study highlights four key findings. First, groundwater pumping during the Rabi (short-rain) season consumes 24 times more energy than during the Kharif (long-rain) season, despite irrigating 40% less land. Second, the increasing depth of borewells, driven by falling water table levels, is a major factor in rising energy consumption. Third, energy input is highest in regions dominated by paddy cultivation. Fourth, water pumping in the Cauvery region accounts for about 16% of India's agricultural energy use, despite covering only 4% of the country's net irrigated area. Our study reinforces the existing literature advocating for holistic, catchment-wide planning, aligned with all UN Sustainable Development Goals.

Keywords: water resources; groundwater pumping; energy consumption; water–energy–food (WEF) nexus; irrigation; Cauvery

1. Introduction

The Cauvery River Basin (CRB), a vital food-producing region in semi-arid India and a growing industrial and urban hub, exemplifies the unsustainable Water–Energy–Food (WEF) nexus. Unchecked groundwater rights for landowners [1] and intensive energy use strain limited-capacity aquifers [2], leading to declining water tables, ecosystem damage [3,4], and escalating socio-economic challenges, including increased water abstraction

costs, conflicts, and heightened climate vulnerability [5,6]. Although groundwater pumping fuelled agricultural gains during the Green Revolution, it also accelerated resource depletion and carbon emissions, creating a cycle that now threatens farming livelihoods and national food security [2,7]. Addressing this crisis requires a deep understanding of the complex interconnections within the system.

As we are facing a climate emergency, effective resource management demands anticipatory governance to navigate complex trade-offs and uncertainties [8–10]. The WEF nexus framework has emerged as a powerful analytical tool for addressing these challenges [11–13], integrating contextual and quantitative information to reveal interconnections and feedback loops within complex systems [14,15]. This approach helps identify key leverage points for intervention. Our study applies the WEF nexus to understand the drivers and water–energy trade-offs in the CRB's irrigation sector.

Recently, two studies applied the nexus approach to understand the dependency of cropping patterns on energy-intensive irrigation. While these studies [16,17] have generated valuable field-based estimates of water and energy use in agriculture through surveys, their methodologies do not offer insights on the spatial relationships between the resource use patterns. Our study offers a scalable and spatially explicit framework by leveraging national-level administrative and geospatial datasets. By using mixed methods i.e., driver assessment, estimation of irrigation energy use and associated theoretical water productivity and simulating crop water needs, we provide a more complete picture of irrigation inefficiencies and the water–energy–food–environment trade-offs across an entire basin. The highly localised focus of the recent nexus studies and absence of integrated metrics such as comparisons between theoretical and actual pumping requirements, make it difficult to connect resource-intensive irrigation practices to broader questions of policy, governance, and farmers' decision-making logic.

Since the last century, government interventions and investments have supported agricultural growth in the region through surface water harvesting, groundwater irrigation, and electricity subsidies for agricultural pumping [2,10]. Although these measures aimed to boost food productivity, they also fuelled conflicts over competing water resource claims [18–20], profoundly shaping the region's agro-economy. Studies analysing the CRB through geopolitical and governance lenses link water and energy overexploitation to resource conflicts [19,21,22], uncoordinated irrigation planning [23,24], and energy subsidies [2,25], all of which undermine long-term agricultural productivity. Meanwhile, hydrological and climate studies highlight the ecological consequences of excessive groundwater pumping for irrigation [6,26–30].

While groundwater irrigation demand is a well-recognised challenge in CRB water resource management, studies often overlook how regional socio-economic factors shape irrigation practices and intensify energy use [31,32]. Understanding these local variations is crucial for sustainable solutions. To address this gap, we use a spatially explicit approach to visualise variations in groundwater structures and energy consumption, identifying resource-intensive hotspots. By integrating village-level and basin-level data, we assess the impacts of both small-scale (farm-level irrigation practices) and large-scale (basin command areas) interventions on the WEFE nexus. Specifically, we aim to carry out the following:

1. Map the factors influencing groundwater and energy use in irrigated agriculture.
2. Quantify the spatial distribution of the energy consumed for groundwater pumping.
3. Estimate the environmental impact of irrigation-related energy use, using carbon emissions as an indicator.

2. Study Area

2.1. Cauvery River Basin

Originating in the Brahmagiri hills of the Western Ghats, the Cauvery River flows eastward for approximately 800 km before draining into the Bay of Bengal (Figure 1). Its extensive 85,626 km² basin spans Karnataka (40.9%), Tamil Nadu (55.48%), Puducherry (0.18%), and Kerala (3.44%), exhibiting significant variations in precipitation, geology, water availability, and agro-economy [33]. The basin is over 66% agricultural land, with 5.8 million ha of cultivable land, which is 3% of India's total cultivable land [34]. Its agricultural output, particularly rice and millets, plays a vital role in India's food production [35]. While India has three main cropping seasons (Rabi, Kharif, and summer), cropping patterns in the CRB vary by state due to differing agro-climatic conditions and traditional practices.

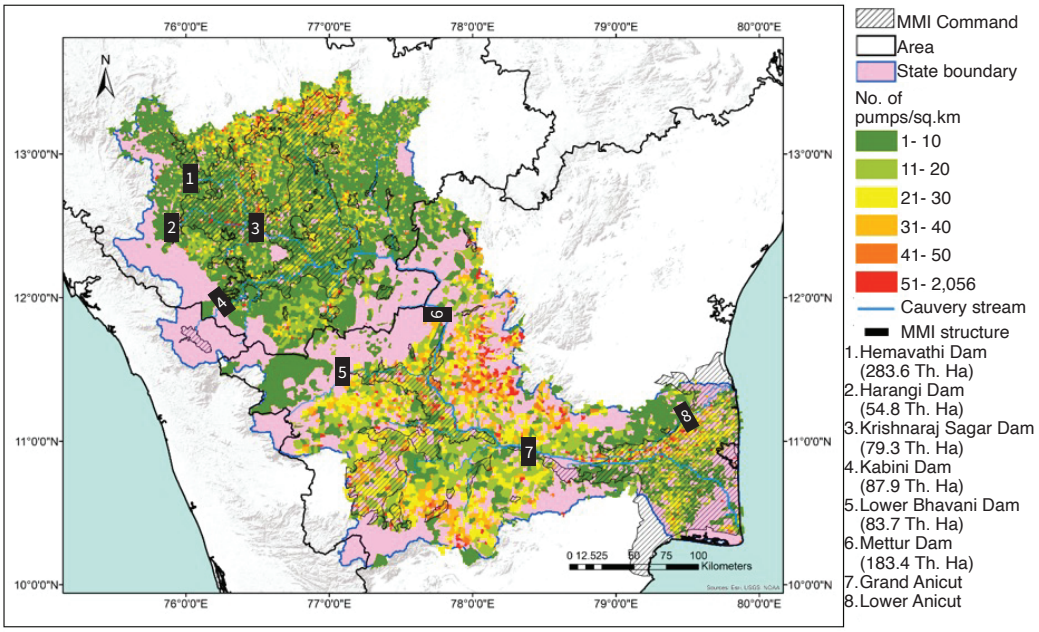


Figure 1. Density of groundwater pumps across CRB (pumps/km^2) at a village scale with major and medium irrigation (MMI) projects identified. Source: Author's elaboration based on MICD [33,36].

2.2. Water Resources Development

The CRB relies on diverse irrigation infrastructure, including river-fed canals, multi-purpose dams, traditional rain-fed tanks, and groundwater systems like dug wells and tube wells. Surface-lift systems pump water from downstream surface sources (tanks, rivers, and canals) to areas where gravity flow is not feasible. The basin contains 45 major command areas (each exceeding 10,000 ha of cultivable land) and an equal number of medium and minor command areas (2000–10,000 ha), collectively irrigating 2.4 million ha (28% of the basin) across 25 districts [33] (Figure 1). Major dams in Karnataka and Tamil Nadu, such as Krishnaraj Sagar and the Mettur Dam, play a vital role in inter-basin water-sharing, as their discharge influences crop cultivation timing in Tamil Nadu. Multiple state agencies handle water allocation, while the Cauvery Water Management Authority (CWMA), established after the 2018 Cauvery Water Disputes Tribunal (CWDT) ruling, oversees inter-state water-sharing [37].

2.3. Geopolitical Context

Decades of conflict over Cauvery River water stem from historical, political, and socio-economic factors [10,38]. Political divisions hinder national–state coordination, while fragmented state-level water administration and information sharing obstruct effective

management [10,22]. These divisions have led to fluctuating water allocations, culminating in the CWDT awards of 2007 and 2018. The dispute centres on Tamil Nadu's reliance on surface water for delta paddy cultivation and Karnataka's demand for equitable upstream irrigation rights, particularly amid monsoonal variability and growing demand from urban centres like Bangalore. While the tribunal rulings sought to balance irrigation needs, hydrological realities, and evolving demands, they have been criticised for overlooking groundwater depletion, ecosystem impacts, and inefficiencies in water distribution [19,24]. Consequently, inconsistent enforcement of water releases and decision-making delays have disrupted cropping patterns, increased groundwater reliance, intensified basin tensions, and left tail-end farmers in Tamil Nadu with unreliable supplies [22].

3. Methods and Data

3.1. Methodology

Using a spatially explicit approach, our study followed five steps (Figure 2). First, we digitised Minor Irrigation Census Data (MICD) in ArcGIS version 10.6 to map irrigation regimes using a grid cell of $0.125^\circ \times 0.125^\circ$ (192.5 km^2), capturing energy sources, borewell depths, seasonal groundwater levels, and urban/industrial water demand hotspots. Second, we estimated theoretical energy consumption for groundwater pumping using MICD data on pump efficiency, pumping hours, and pump power. Third, we calculated theoretical water productivity under conditions of unconstrained water availability. Fourth, we compared the theoretical water volume with crop water requirements simulated by the GWAVA crop model [28] to assess the gap between energy needs and actual consumption. Finally, we estimated CO_2 emissions associated with groundwater pumping.

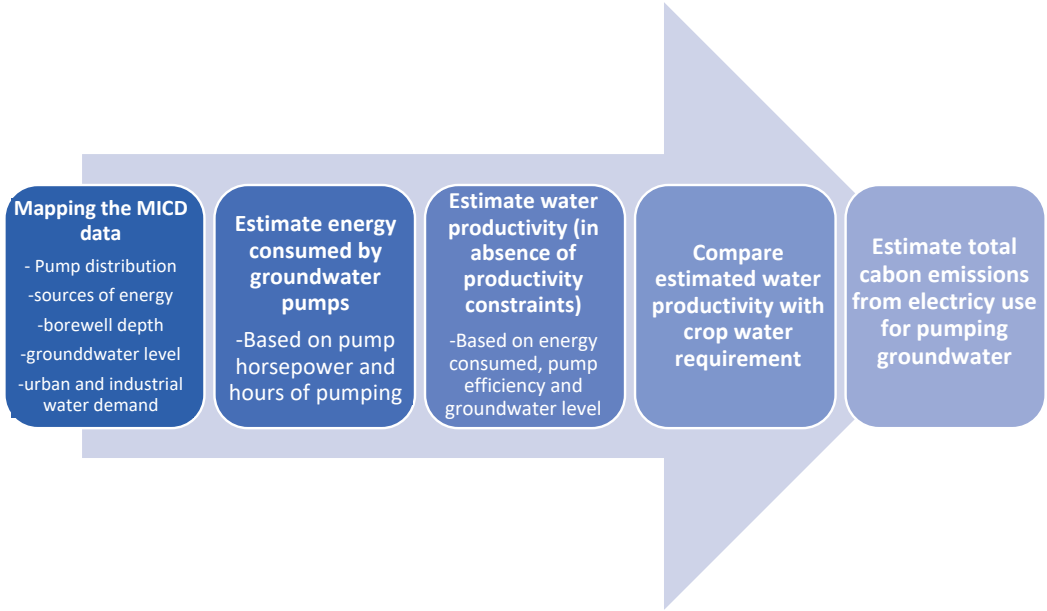


Figure 2. The five steps of research design elucidating WEFE nexus issues in the CRB, India.

3.2. Data

The core analysis including the estimation of irrigation energy use and the spatial variability of pumpset distribution focuses on the year 2013–14, which corresponds to the most recent year for which detailed Minor Irrigation Census data were available. However, to provide important contextual insights such as average seasonal groundwater depths and the long-term correlation between groundwater availability and crop production, we analysed extended time series data from 1996 to 2016. A summary of the data used is provided in Table 1.

Table 1. Data used in this chapter and data sources.

Data	Spatial scale	Period	Used for	Source
Number of pumpsets under different irrigation sources	Village scale	2013–2014	Spatial mapping of irrigation systems and estimating energy consumed	[36]
Rice production	District scale	1997–2014	Estimating correlation between rice production and groundwater availability	[39]
Groundwater table	CGWB borewells	1997–2014	Estimating correlation between rice production and groundwater availability, estimating groundwater abstraction	[33]
Hours of pumping and pump horsepower	Village scale	2013–2014	Estimating energy consumed	[36]
Irrigation potential under different irrigation sources and water distribution methods	Village scale	2013–2014	Estimating irrigation efficiency	[36]
Pumpsets under different sources of energy and depth of borewells	Village scale	2013–2014	Spatial mapping of irrigation systems	[36]
Pumpset efficiency of 30%	-	-	Estimating groundwater abstraction	[3]
Irrigation source per farmers' economic class	District scale	2014	Assessing economic factor in access to irrigation equipment	[39]

i Farmer status data—We classified district-wide pumpset ownership data by farmer type according to their economic status in the agriculture census [39]. These data were aggregated for the whole basin and used to analyse the relationships between irrigation sources, access to groundwater pumping equipment, farmers' economic status, and farm size.

ii Groundwater table data—We obtained groundwater table data from the Central Groundwater Board (CGWB) portal (India-WRIS) [33] for all observation wells in basin districts from 1996 to 2016. Since the number of wells increased annually and seasonal data gaps were common, we calculated district-level averages to analyse 20-year groundwater trends. To approximate missing values, we used observations from the previous or following year for the same season.

iii Rice Production data—We obtained district-scale rice production data from the National Agriculture Statistics archives [39] for the years 1997–2014 to estimate the correlation between rice production and groundwater availability.

iv Minor irrigation data—We obtained village-wise groundwater irrigation data for the year 2013–14 from the Minor Irrigation (MI) Census database, available through the Indian Statistical Data Dissemination Portal. This dataset included information on groundwater irrigation structures such as deep , medium and, shallow tube wells, dug wells, and minor surface water irrigation systems including surface-lift pumps and surface flow schemes. For each MI structure type, the dataset provided the number of structures, their operational status, average daily pumping hours during Rabi and Kharif seasons, the distribution of structures by pump horsepower, energy sources, and water distribution system (Table 1). The data were manually resampled for villages within the basin boundary and converted to geospatial format by joining tabular data with village shapefiles in ArcGIS 10.6 software.

v Major and medium irrigation projects—We obtained data on the area of major and medium irrigation projects from India-WRIS web-map services [33]. To analyse the correlation between groundwater pumping and the availability of surface irrigation sources, we manually digitised the command areas of these projects in ArcGIS software.

3.3. Estimating Energy Consumption and Groundwater Productivity of Pumps

The irrigation energy consumption can be estimated using the following equation [40]:

$$\begin{aligned}\text{Energy [kWh]} = 0.7457 &\times \text{Average pump horsepower } (HP) \\ &\times \text{Daily average pumping hours } (PH) \\ &\times \text{Number of pumps in use } (N)\end{aligned} \quad (1)$$

Alternatively, the energy consumption can be estimated from the physical principles governing pump power, groundwater hydraulics, pump efficiency, and discharge [8,41–45]:

$$\begin{aligned}\text{Energy [kWh]} &= \frac{9.8\ \text{ms}^{-2} \times \text{Lift [m]} \times 1000\ \text{kgm}^{-3} \times Q\ [\text{m}^3]}{3.6 \times 10^6 \times PE\ [\%]} \\ &= \frac{2.73 \times \text{Lift} \times Q}{1000 \times PE}\end{aligned} \quad (2)$$

where Energy [kWh] is the electricity drawn from the grid, Lift [m] is the vertical distance from the water table to the pump, Q [m^3] is the volume of water extracted, and PE [%] is the pump efficiency. Due to limited public data, we adopted the widely used estimate of 30% for electric pumpset efficiency in India [3].

We used Equation (2) to estimate the theoretical volume of groundwater Q that can be abstracted based on the estimated energy consumption from Equation (1), assuming no geological constraints. Estimating the groundwater depth accurately is essential for this approach, because lift head directly affects energy input (a 1 m decline in the water table increases energy input by 0.0091 kWh per m^3 of water lifted). Our calculations assumed a stable intra-seasonal groundwater table but allowed for inter-seasonal variability. We extracted the groundwater table values for each village during Kharif and Rabi seasons by interpolating the groundwater table contour maps generated in ArcGIS using Central Ground Water Board (CGWB) well data.

4. Results

4.1. Spatial Mapping of Irrigation Regimes

Figure 1 gives an overview of the density of active groundwater pumps, state boundaries, the major irrigation project command areas, key dams, and data gaps.

4.1.1. Density of Minor Irrigation Pumpsets

As of 2014, CRB housed approximately 1.4 million groundwater pumpsets, accounting for about 3% of the global total [46]. Spatial maps of active groundwater sources reveal significant variation in pump density, ranging from 1 to over 50 pumps per km^2 (Figure 3). Among 14,260 villages in the CRB, the majority (4915) have fewer than 10 pumps/km^2, while 3069 have 10–20 pumps/km^2. However, a small fraction of villages (113) show extremely high densities, exceeding 100 pumps/km^2, indicating localised hotspots of intense pump activity.

Pump density differs based on water availability and land use. Tamil Nadu has a higher average pump density than Karnataka (26 vs. 15 pumps/km^2), and a higher standard deviation (53.7 vs. 21.6), which we attribute to its larger village areas, averaging 8.9 km^2 compared to 3.5 km^2 in Karnataka. Within irrigation command areas, Tamil Nadu has a mean density of 23 pumps/km^2 and Karnataka has 16 pumps/km^2. Outside command areas, pump density rises to 29 pumps/km^2 in Tamil Nadu, driven by unreliable upstream water discharge and lower surface water productivity, whereas Karnataka's decreases to 14 pumps/km^2.

Groundwater reliance is particularly pronounced in the Cauvery Delta region, where pump density averages 23 pumps/km^2, indicating its critical role in paddy irrigation amid surface water scarcity (Figure 3). In contrast, pump density remains low in high-altitude regions like the Mahadeswaramalai and Biligirirangan Ranges, and across the Western Ghats, although data coverage is limited, but the recorded pump density is generally low.

By 2013–14, there were 660,714 active groundwater pumps, with 45.8% in Karnataka, 43.4% in Tamil Nadu (excluding the delta), and 10.8% in the Cauvery Delta (Figure 3). Additionally, 5259 pumps were used for surface water lifting under MI schemes. The data highlight Tamil Nadu's intensive groundwater, particularly in the delta region, while surface-lift pumps are more common than in Karnataka's northern sub-catchments.

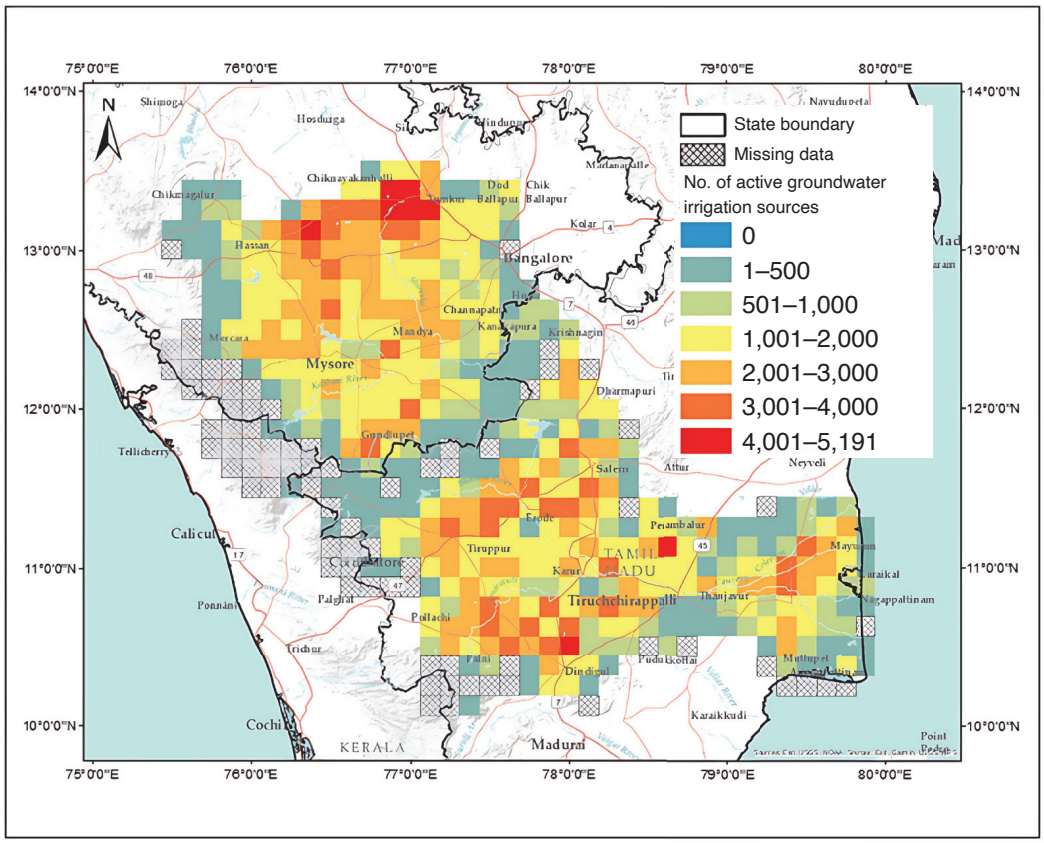


Figure 3. Number of groundwater pumps in use during the 5th Minor Irrigation Census (2013–14). Source: Author's elaboration based on [36].

4.1.2. Seasonality of Pumpset Use

In 2013–14, groundwater pumps irrigated 1.16 million hectares, accounting for 93% of the total irrigated area in the CRB. Surface water sources, including lift and flow schemes, covered only 88,000 hectares (7%), mostly in the upper catchments of Karnataka's Chikmagalur district. Seasonally, groundwater pump use peaked in the Kharif season, irrigating 47% of the total groundwater-irrigated area, followed by Rabi (29.3%) and summer (5.1%). This trend aligns with paddy cultivation, particularly in Karnataka and Tamil Nadu [47].

In Karnataka, 89.6% of the 284,000 hectares irrigated during Kharif relied on groundwater. In Rabi season, the irrigated area dropped by 57% to 122,000 hectares, with 93.5% of this area irrigated with groundwater. The decline in irrigated area during Rabi is linked to cooler temperatures, a shift to less water-intensive crops like wheat, and soil moisture retention from the monsoon [48]. In Tamil Nadu, the irrigation patterns during Kharif are similar to those in Karnataka, but the irrigated area increases in the Rabi season, particularly

in the Cauvery Delta, where year-round paddy cultivation persists as the saline soils are unsuitable for other crops.

Groundwater plays a crucial role in the delta, where it irrigates nearly all cultivated land. Delays in Mettur Dam's water release for Kuruvai crops often force heavy groundwater use during Kharif. Additionally, 18.3% of perennial crops area, such as areas with dryland fruits in higher altitudes, depends on groundwater.

Spatially, groundwater reliance intensifies from the middle catchment to the delta, particularly where canal water is insufficient. Groundwater use is lower in canal-irrigated zones in central Karnataka and the delta but rises sharply outside these zones. In northeastern and northwestern Karnataka, over 50% of irrigated land during Kharif relies on groundwater pumps, highlighting the importance of timely and adequate irrigation projects.

4.2. Drivers Influencing Water–Energy Dynamics in Irrigation Sector

4.2.1. Sources of Energy for Irrigation Pumps

In 1993–94, irrigation pumps in the CRB were powered by electricity (72%), diesel (15%), or animal labour (11%) [36]. By 2014, the basin had around 700,000 groundwater pumpsets and 5602 surface-lift pumps, together accounting for about 3% India's total [46]. The majority of these pumps were electrified (89%), followed by mixed-energy pumps (7%), diesel pumps (3%), wind (0.03%), manual/animal (0.03%) and solar (0.01%). The negligible adoption of solar pumps highlights the challenges in scaling up this irrigation technology.

Spatial mapping confirms that electricity is the dominant pump energy source in the Cauvery region, indicating nearly all agriculture villages are connected to the grid. Diesel pumps are concentrated in the delta region and areas reliant on dug wells, such as parts of Nagapattinum, Thriruvarur, and Chikmaglur. Wind- and solar-powered pumps are scattered across the basin with no significant spatial clustering (Figure 4).

Expanding the use of solar pumps from 0.01% to 1% would require installing approximately 7000 solar pumps, each linked to a 20 kW photovoltaic panel system, adding up to 70 MW of solar capacity to the grid. However, widespread adoption faces significant barriers, including subsidised electricity, inadequate groundwater regulations, and high upfront and maintenance costs. While solar pumping can reduce carbon emissions and fossil fuels dependency, it may accelerate groundwater depletion if not integrated with water-saving technologies like micro-irrigation. The shift to solar-powered irrigation pumps must be accompanied by policies that ensure efficient water use, preventing the risk of groundwater overextraction as energy becomes more accessible and affordable. Integrating energy and water management strategies—such as Morocco's approach, which links solar subsidies with micro-irrigation—could provide a model for balancing the energy–water nexus [49].

A major challenge for irrigation is the unreliable electricity supply. In 2013, 10% of wells were inactive due to power shortages. Pumping patterns have remained spatially consistent during the last 20 years, but average pump use has declined uniformly by 2–5 h a day since 1993 (see district-level data in Figure 5). This reduction may stem from the shift from diesel to electric pumps, as power companies use outages to manage electricity consumption, counterproductive to energy subsidies. Our field visits found that unannounced power cuts often force farmers to leave their pumps running continuously to secure water for irrigation, leading to an overconsumption of electricity. Additionally, deepening borewells due to declining water tables require more energy for pumping, further straining electricity supply [50].

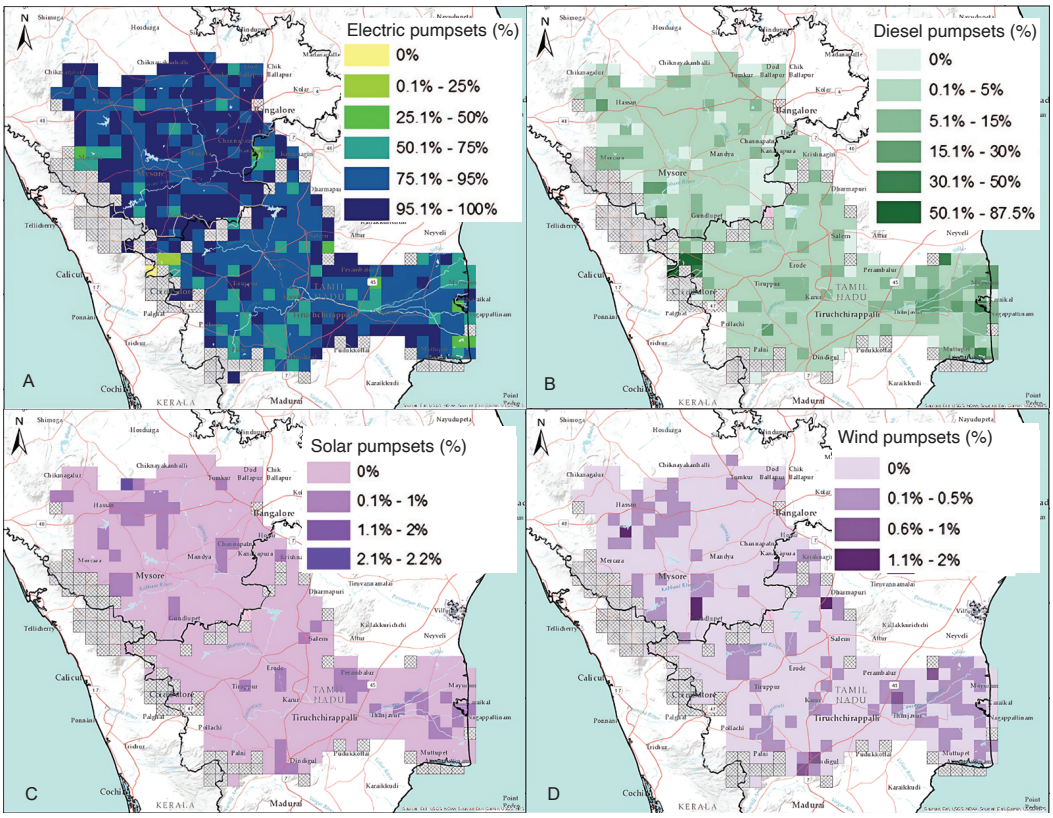


Figure 4. Energy sources for pumps (under MI schemes 2013–14). (**A**) Percentage of pumpsets powered by electricity. (**B**) Percentage of pumpsets powered by diesel. (**C**) Percentage of pumpsets powered by solar energy. (**D**) Percentage of pumpsets powered by wind energy. Source: Author's elaboration based on [36].

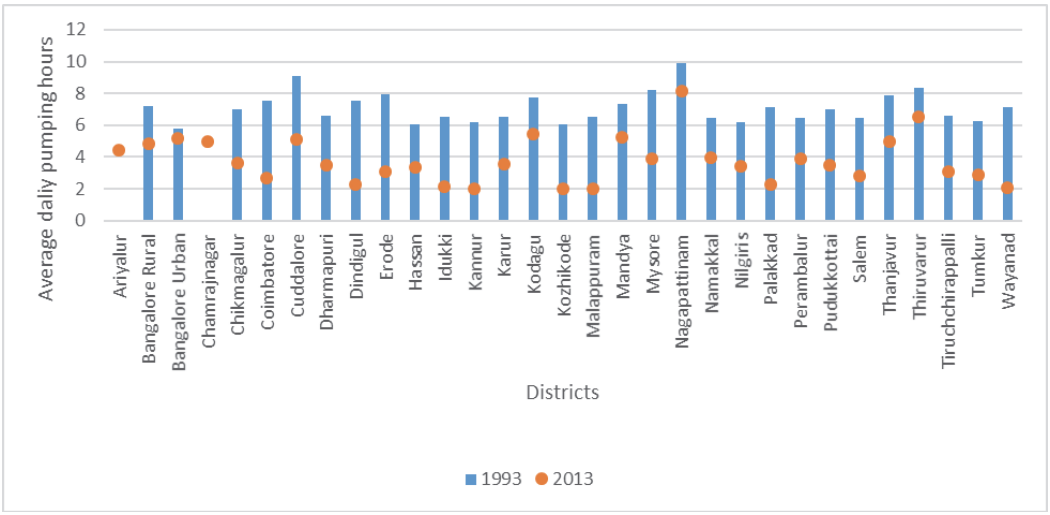


Figure 5. District-wise average pumping hours during peak irrigation season as recorded in 2nd and 5th MI census. Source: Author's elaboration based on [36].

4.2.2. Deepening Borewells and Groundwater Level

Groundwater ownership in India is tied to land ownership under the Indian Easement Act of 1882, granting landowners rights to access groundwater [1,51,52]. Across the CRB, farmers use a variety of groundwater structures of varying depth. We analysed the spatial variability of these structures to explore borewell depth and its correlation with external factors. The spatial distribution of the average groundwater structure depth is shown in Figure 6, and its relationship to groundwater table depths from CGWB is mapped in

Figure 7. Figure 8 shows the proportion of gross irrigated area that uses tube wells of depth < 35 m, 35 to 70 m, 80 to 150 m; dug wells; surface-lift schemes; and surface flow schemes.

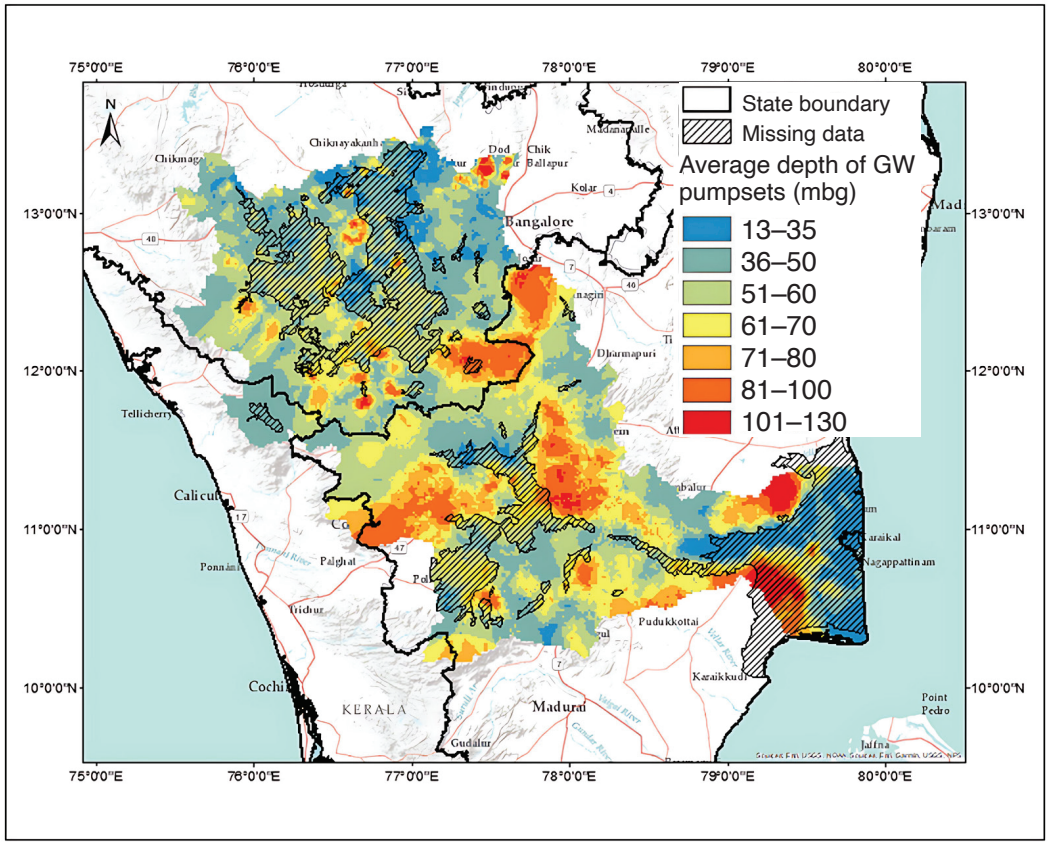


Figure 6. Average depth of groundwater structures as recorded during the 2013–14 MIC and command areas under MMI Projects. Source: Author's elaboration based on Central Ground Water Board dataset [33].

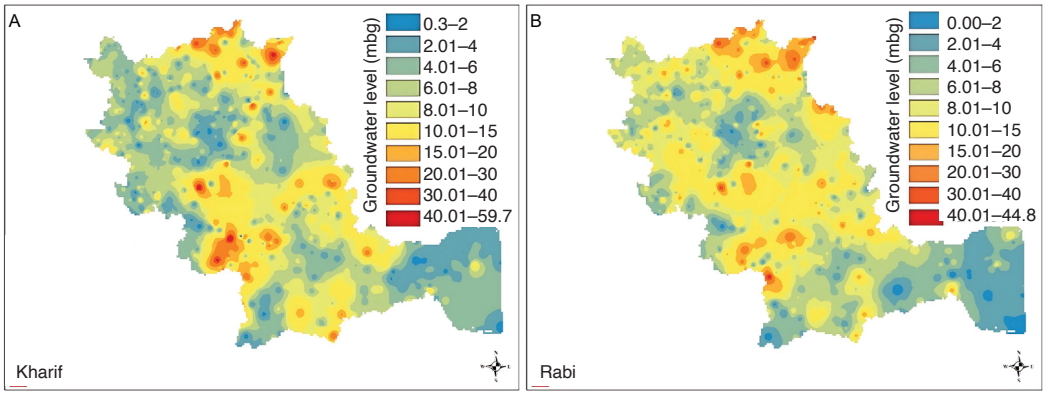


Figure 7. Groundwater level during (**A**) Kharif (Sept–Nov) and (**B**) Rabi (Nov–Feb) cropping seasons in year 2013–14. Source: Author's elaboration based on [36].

According to CGWB data (Figure 7), groundwater tables are deeper (up to 64 m) in the upper catchments, yet the average well depth remains relatively shallow (Figure 6). The use of shallow wells in the upper catchments is likely influenced by the major and medium irrigation (MMI) command area, which should result in augmentation of groundwater. We noticed a similar discrepancy in the Dharmapuri district (Tamil Nadu) near the Mahadeswaramalai–Biligirirangan ranges along the Karnataka–Tamil Nadu border, where the groundwater table is shallow (up to 15 m), yet irrigation wells extend to depths of around 100 m. These discrepancies highlight the variability and uncertainty of groundwa-

ter availability, suggesting that farmers' decisions to deepen wells are influenced by factors including economic ability and access to reliable surface water like canals. The deepest wells are prominently located outside the MMI command areas.

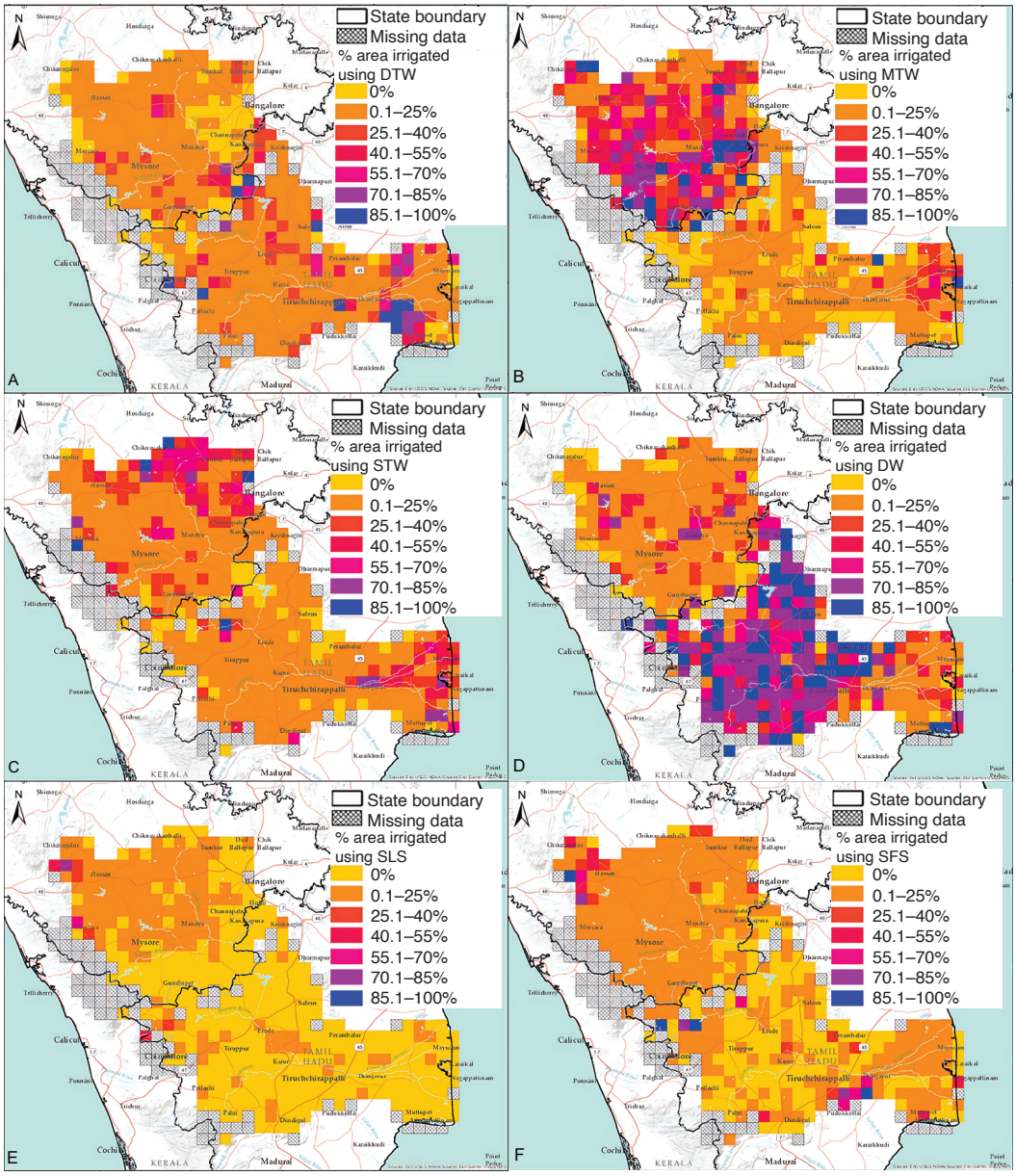


Figure 8. Percentage of gross irrigated area (under MI schemes) irrigated using different irrigation sources (2013–14). (**A**) Deep tubewells DTW (80–150 m). (**B**) Medium tubewells MTW (35–70 m). (**C**) Shallow tubewells STW (<35 m). (**D**) Dugwells DW (<30 m). (**E**) Surface-lift pumpsets SLS. (**F**) Surface flow schemes SFS. Source: Author's elaboration based on [36].

The spatial distribution of irrigation structures shows distinct patterns across the basin (Figure 8). Deep tubewells are widespread, but are particularly concentrated in parts of Chamarajnagar (Karnataka) and Dharmapuri (Tamil Nadu) near the Mahadeswaramalai–Biligirirangan ranges, as well as the Thanjavur and Ariyalur districts in the delta. Medium tubewells, machine-drilled borewells 35 to 70 m deep, are mainly used in Karnataka and in the command areas of the delta. Dug wells, hand-dug wells typically less than 30 m deep, predate the invention of drilled boreholes but remain common in Tamil Nadu due to lithological challenges that limit deeper drilling. Nonetheless, farmers are investing

regularly in deepening these wells (as noted during our field trips). Shallow tubewells are mostly used in the upper catchments and the delta region.

Groundwater remains the most reliable source of irrigation in the CRB. Despite the expansion of tube well irrigation, reports of well failures and groundwater depletion have risen since the 2000s, often linked to the low storage capacity of the region's hard rock aquifers [53]. By 2013, poor water yields had rendered 71% of total wells inactive, contributing to widespread abandonment of dug wells and deepening of borewells (Figure 9).

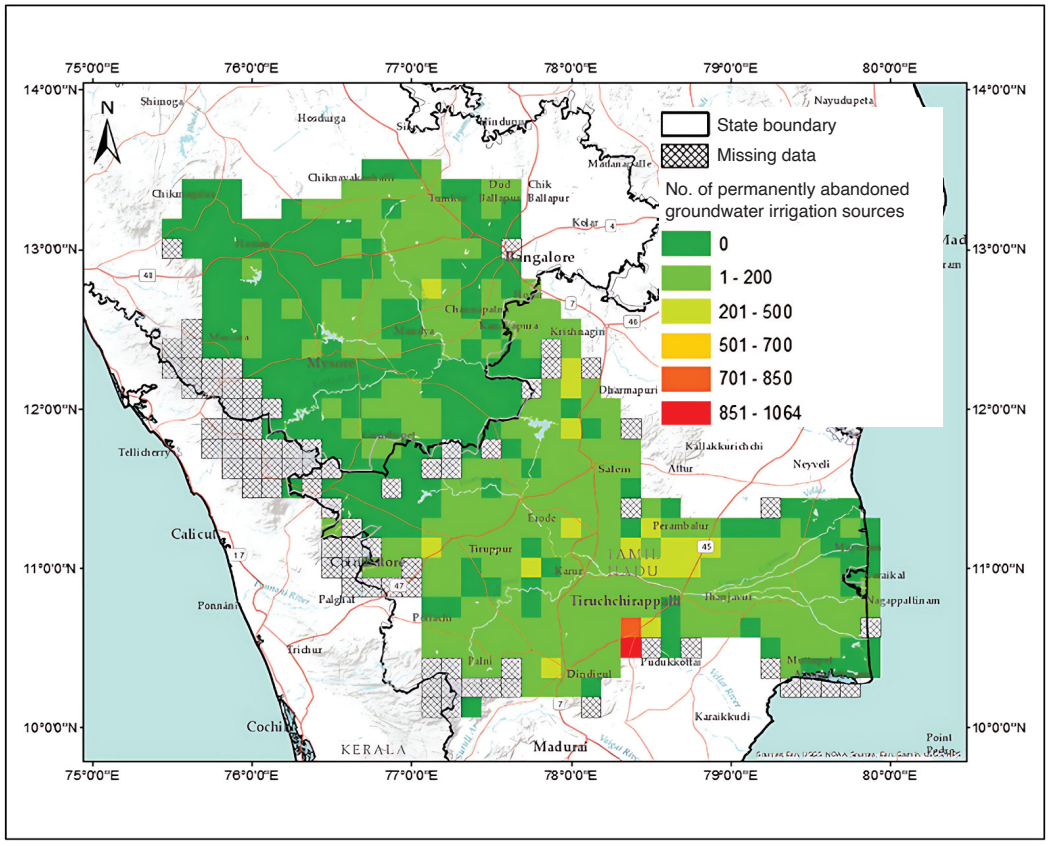


Figure 9. Number of abandoned groundwater irrigation sources in 2013–14. Source: Author's elaboration based on [36].

4.2.3. Competition for Water and Crop Production

Urban expansion in cities like Bangalore, coupled with the growth of industrial clusters and agricultural demands, has intensified competition for water resources (Figure 10). This competition is a major driver of the Cauvery conflict, exacerbating the WEF nexus challenges [54,55]. Overabstraction of groundwater in economic development zones has disrupted catchment water balance, contributing to well failure, reduced crop production, and declining farmer livelihoods downstream [7,28,53].

In groundwater-irrigated districts like Bangalore Rural and Bangalore Urban, rice production during the Rabi season is notably low. In Bangalore Rural, Rabi rice cultivation declined from over 200 ha in 2004 to below 20 ha in 2014, while Kharif rice production fell from 14,828 ha in 2000 to 598 ha. Similar trends are seen in Bangalore Urban, where Kharif rice reduced from 4,483 ha in 2000 to 950 ha, with a Rabi crop appearing only in 2012 and 2013. These declines reflect increasing water demand for urban and industrial growth, as well as shifts in employment preferences.

Across much of the basin, Rabi rice has been replaced by less water-intensive crops, like millets and non-food crops [39]. In Tumkur, a key groundwater-irrigated district and the basin's largest rice producer, we found that while the Kharif and summer production

remained stable, Rabi rice production has declined. In fully canal-irrigated districts, rice cultivation is confined to the Kharif season, aligning with scheduled dams releases in late June. In Mysuru and Mandya, where both groundwater and canal irrigation are common, the Kharif and summer crops are more productive than the Rabi crop, with no clear link to groundwater levels. In Pudukkottai, an arid district where tank irrigation is prevalent, rice cultivation is similarly limited to the Kharif season.

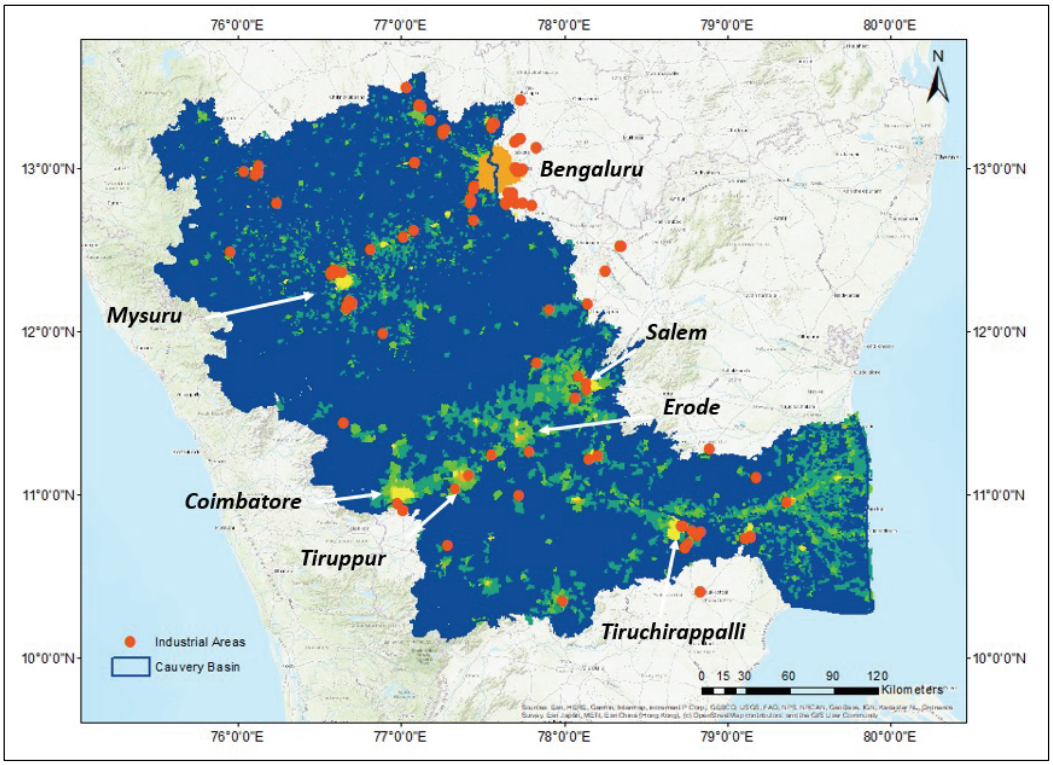


Figure 10. Major industrial areas and urban hubs as of 2020. Source: Author's elaboration based on (Census of India, 2011; Karnataka Industrial Areas Development Board, 2020; Tamil Nadu Industrial Development Corporation Ltd., 2020).

Access to reliable irrigation sources strongly influences cropping patterns across the Cauvery region. We observed a strong linear relationship between groundwater levels and rice production in Bangalore Rural, and a weaker but similar trend in Bangalore Urban, where rice production has gradually declined since 2001 due to socio-economic shifts driven by industrialisation. In Tumkur, Mandya, and Mysore, where surface water is the primary irrigation source, no significant relationship was found. In Erode, where surface and groundwater-irrigated areas are comparable, rice production shows a weak negative relationship with groundwater levels. In the delta, Pudukkottai relies on tanks and groundwater pumps for irrigation, whereas Thiruvarur falls under the delta irrigation project command area. Both districts exhibit a strong correlation between rice production and groundwater levels, reflecting their reliance on groundwater in a semi-arid climate with less than 1000 mm annual rainfall.

4.3. Spatial Analysis of Estimated Energy Consumption

In this section, we use energy consumption data to map groundwater withdrawal using Equation (2). We then compare our estimated withdrawal with actual crop water demand. If the estimated water withdrawal exceeds demand, it indicates a local overconsumption of energy.

4.3.1. Verification of Estimated Energy Consumption

To validate our energy consumption estimates, we performed a linear regression analysis using district-scale data for energy consumption data and groundwater draft data from the CGWB. Our analysis showed a strong positive correlation (p-value < 0.05, $r^2 = 0.74$) between estimated energy consumption (MWh) and groundwater draft (MCM) (Figure 11), verifying the reliability of census data in capturing irrigation-related energy demand. Uncertainties may stem from standardising pumping hours and horsepower values, as we used village-level averages.

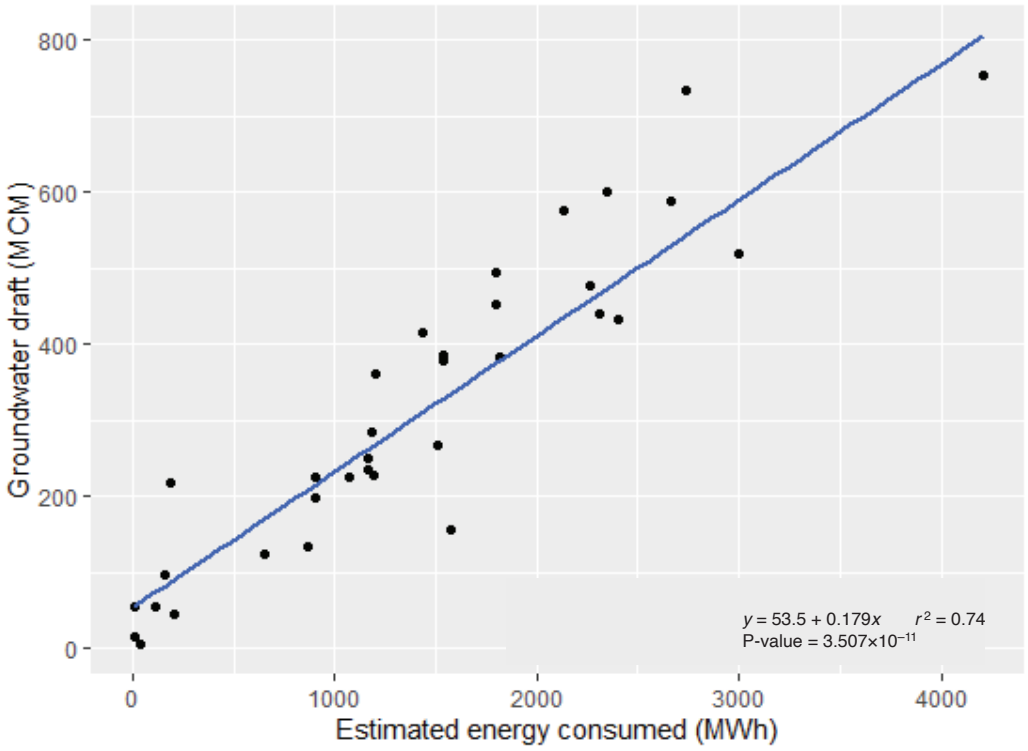


Figure 11. Estimated energy consumption for groundwater irrigation and government documented groundwater draft (2013–14) in CRB districts .

4.3.2. Energy Consumption in Irrigated Agriculture

To analyse spatial patterns of agricultural energy use, we mapped the average daily energy consumed by groundwater pumps and surface-lift schemes during peak Kharif and Rabi seasons. We found that the spatial distribution of both groundwater and surface water energy consumption remained broadly consistent across seasons (Figure 12). Interestingly, the upper catchments of Karnataka's Hassan district accounted for a significant proportion of surface water energy consumption, likely due to the region's higher altitude and the need to transport water to elevated agricultural areas.

However, a contrast emerged in the overall groundwater energy consumption. Although the spatial distribution was similar, Rabi consumption reached 349.9 GWh per day, an approximately 2400% increase compared to Kharif's 9.6 GWh per day. This substantial rise in Rabi energy consumption occurs despite a 40% reduction in irrigated land and significantly lower pumping hours, as confirmed by a two-sample t-test (Table 2). The key driver is the significant decline in the groundwater table during Rabi, which increases the energy required per pump (Equation (2)), ultimately leading to greater overall energy consumption. Energy consumption by pumpsets is highly sensitive to the depth of the groundwater table and the energy efficiency of the pumpsets. Our estimates indicate that a one-meter drop in the groundwater table can increase energy cost for lifting 1000 m^3

of groundwater by 15.36 ± 0.17% during Kharif and by 14.07 ± 0.21% during Rabi. Conversely, a 10% increase in pump efficiency could reduce energy demand by 25% during both seasons.

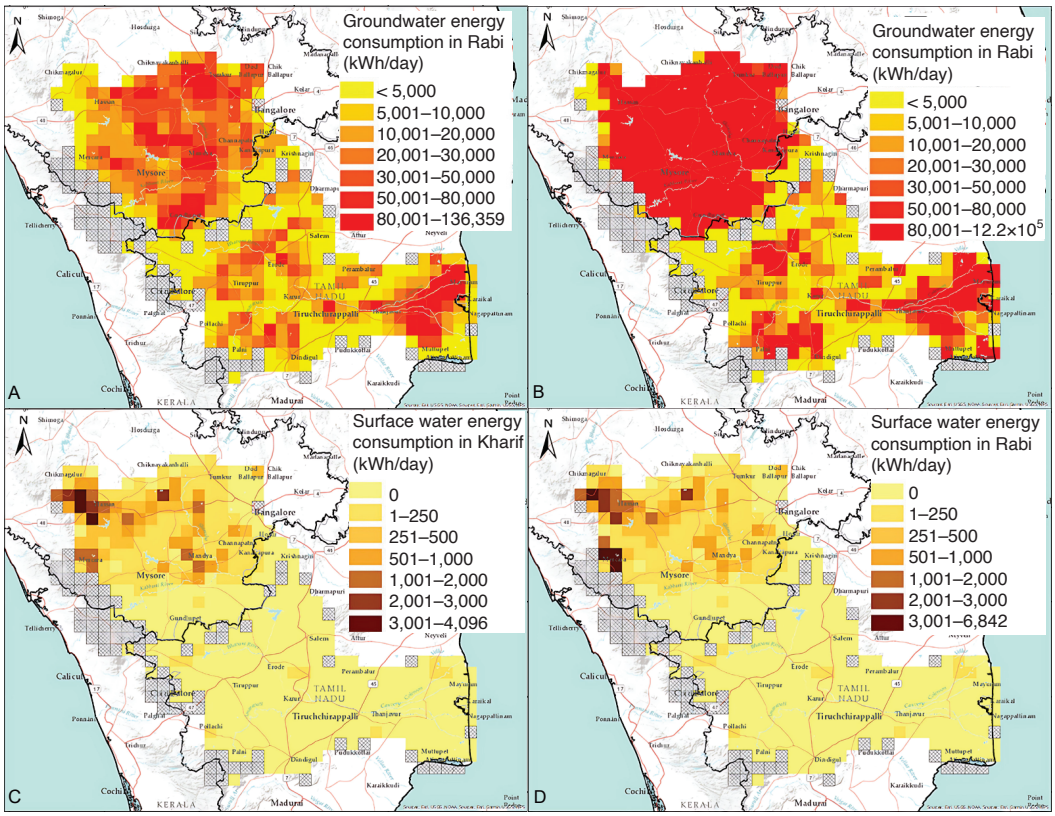


Figure 12. Average daily energy consumption by groundwater pumps during (**A**) peak Kharif season, and (**B**) peak Rabi season. Average daily energy consumption by surface-lift pumps during (**C**) peak Kharif season, and (**D**) peak Rabi season. Source: Author's calculations.

Table 2. Average daily pumping hours of pumpsets associated with different irrigation sources during peak Kharif and Rabi seasons within CRB (2013–14).

	Pumping Hours/Day (Kharif)			Pumping Hours/Day (Rabi)			
G.W Source	**Mean**	**Standard Error** [1]	**Maximum**	**Mean**	**Standard Error** [1]	**Maximum**	***p* Value**
Deep tubewells	4	±0.68	22	3.6	±0.47	22	$\ll 0.05$
Medium tubewells	4.4	±0.69	22	3.7	±0.5	22	$\ll 0.05$
Shallow tubewells	3.9	±0.46	22	3.4	±0.33	22	$\ll 0.05$
Dug wells	4	±0.4	22	3.5	±0.35	14	$\ll 0.05$
Surface-lift schemes	3	±0.48	22	2.7	±0.35	22	$\ll 0.05$

Note: [1] 95% confidence interval.

Contrary to expectations, pumpset use remained consistent inside and outside MMI command areas, despite their additional surface water supply. Seemingly, groundwater availability, pump access, and farmers' economic status play a larger role than surface water supply. This pattern aligns with broader trends in India, where agricultural energy consumption does not directly follow monsoon patterns [54]. In the CRB, surface water availability varies significantly between upstream and downstream regions. Upstream in Karnataka, farmers prefer groundwater pumping despite stable irrigation systems and high annual rainfall, likely due to its convenience and reliability. Conversely, Tamil Nadu's irrigation is heavily influenced by uncertain upstream reservoir discharges, driving farmers to rely more on groundwater pumps for traditional rice crops.

We also found that energy consumption increased as annual rainfall fell. During Kharif, the median daily energy consumption was 213.7 kWh/ha in the highest rainfall zone (3000–2000 mm), 745.7 kWh/ha in the moderate zone (2000–1000 mm), and 914.4 kWh/ha in the lowest zone (<1000 mm). During Rabi, these medians increased to 2237 kWh/ha, 6271 kWh/ha, and 2117 kWh/ha, respectively.

4.3.3. Estimating Groundwater Withdrawal

Using Equation (2) and CGWB ground level data, we estimated the groundwater withdrawal during peak Kharif and Rabi seasons (Figure 13). These calculations assumed unlimited groundwater availability and unrestricted tubewell yield, providing a theoretical maximum. Under these conditions, the estimated average daily water abstraction was 12,775 m^3/ha during Kharif and 311,753 m^3/ha during Rabi.

The estimated 2400% increase in Rabi groundwater pumping energy, despite a 40% reduction in irrigated land highlights the complex and interlinked drivers within the WEF nexus, with broader implications for national and state resource security. The Rabi energy surge creates power deficits in non-agricultural sectors, resulting in power cuts that further disrupt farmers' operations (e.g., pumpset failure). This situation raises a critical question: do farmers truly require free electricity?

To address this question, we compared our estimated groundwater withdrawals with irrigation water demand simulated by the Global Water Availability (GWAVA) model, a semi-distributed hydrological model that estimates irrigation demand by considering irrigation efficiency and crop water requirements based on physical variables such as precipitation, temperature, land use, and soil characteristics [56]. We calculated the total irrigation water demand for the basin, excluding the delta, setting the irrigation efficiency parameter at 44.11%, the India average estimated by FAO. Remarkably, we found that crop water demand is less than 1% of the theoretical water withdrawal shown in Figure 13, indicating significant overconsumption of energy for groundwater pumping. This discrepancy can be attributed to factors such as poor pump efficiency, declining groundwater tables, inefficient irrigation practices, inadequate regulatory oversight, and the absence of comprehensive water and energy accounting systems.

The spatial overlay of urban hubs, industrial zones, and high pumping intensity areas like Bangalore Rural and Urban underscores the growing pressure on local aquifers. These trends reflect a shift in surface water allocation driven by socio-economic priorities rather than agricultural suitability, leading to reduced resilience in food production. The spatial heterogeneity observed also illustrates how water competition manifests differently across the basin suggesting the need for geographically tailored but coordinated policies.

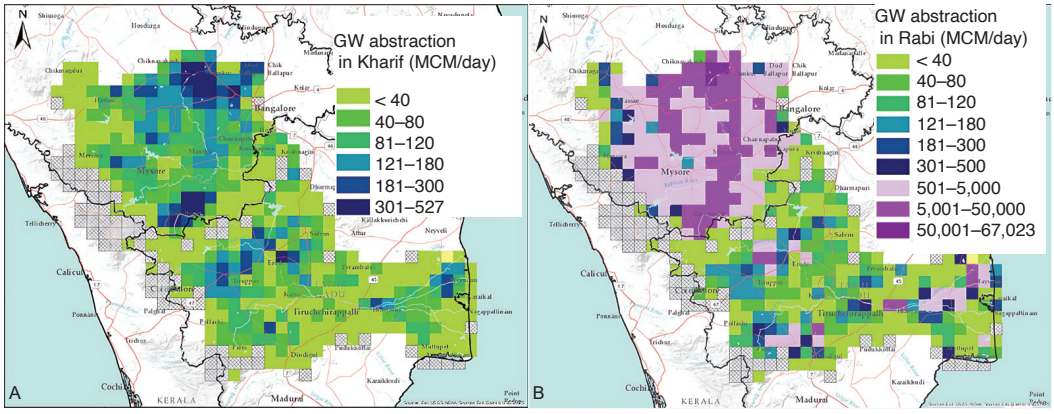


Figure 13. Average daily groundwater (GW) abstraction (theoretical) in million cubic meters (MCM) during (**A**) peak Kharif season and (**B**) peak Rabi season. Estimated using pumpset energy consumption estimates. Source: Author's calculations.

5. Discussion

5.1. The Nexus in Irrigated Agriculture

Within the WEFE framework, the intricate interdependencies between water use, energy for extraction and distribution, and agricultural productivity create complex feedback loops that influence resource availability and sustainability [13,16,17,57–61] (Figure 14). Insights generated in this paper contribute to the understanding that the WEFE nexus is not just a technical challenge, but a political and institutional one rooted in competing land and water use regimes [62–65].

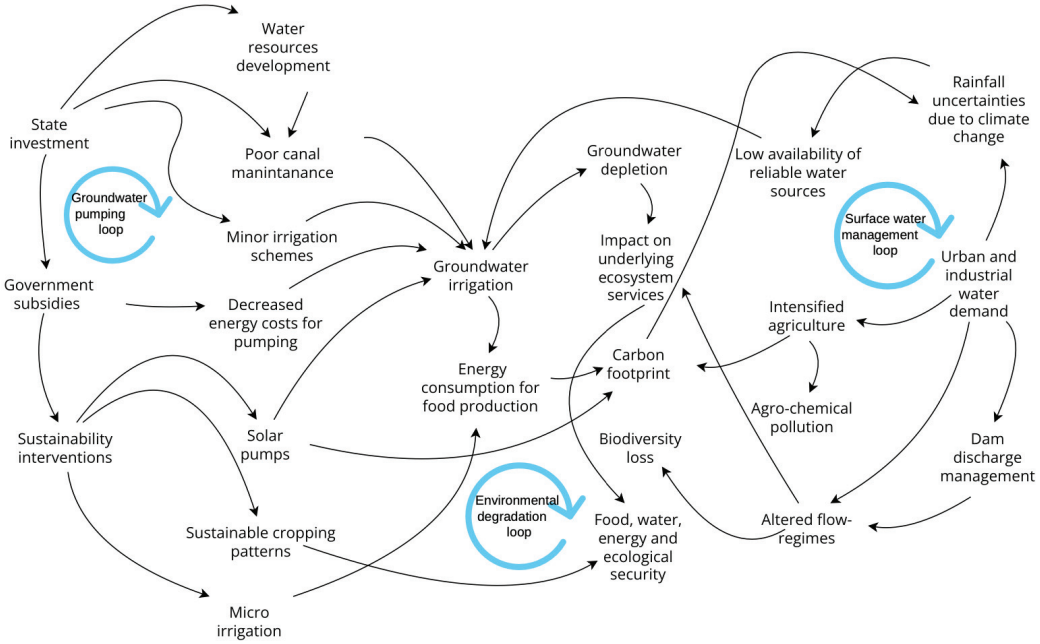


Figure 14. Causal loop diagram representing the dynamics in the WEFE nexus of the irrigation sector in CRB. Source: Author.

In the CRB, the nexus is driven by factors such as groundwater regulations and free electricity policies, which have incentivised deeper borewell drilling and accelerated groundwater depletion [25,55]. Despite this depletion, irrigation pumping hours have remained consistent, indicating a continued reliance on groundwater. Yet, deeper groundwater extraction has not improved agricultural productivity, as rice production has declined, potentially due to competing industrial water demands amongst other bio-physical and socio-economic factors.

Policies intended to ease the energy burden, such as promoting solar energy pumps and drip irrigation systems, have seen limited adoption, likely due to economic, cultural, or operational barriers surrounding new technology [66,67]. These interdependencies highlight how changes in one sector, such as energy subsidies, can cascade across the nexus, amplifying resource stresses [12]. Addressing these challenges requires integrated policy interventions that align incentives across water, energy, and agriculture.

5.2. Challenges and Uncertainties in the Nexus

The CRB faces significant challenges related to both surface and subsurface water depletion, leading to inter-sectoral competition over scarce water resources [68,69]. These challenges are exacerbated by trans-boundary water-sharing disputes and spatial variations in rainfall. Within irrigated agriculture, surface water scarcity and poor management have increased reliance on groundwater pumping. A major obstacle is the lack of reliable, spatially resolved data on groundwater and energy consumption. Inconsistent and fragmented

government data hinders comprehensive nexus assessments, making it difficult to quantify trade-offs, identify resource-intensive systems, and design region-specific management strategies [70].

Our study represents an effort to quantify the nexus within India's agricultural sector by analysing socio-economic factors and policy drivers. Our findings reveal significant spatial variability in irrigation sources, with the delta region emerging as a hotspot for energy-intensive irrigation due to its year-round paddy cultivation and unreliable canal irrigation. The basin's history of water conflicts, particularly the Cauvery water dispute, has compelled farmers to rely heavily on groundwater, especially for paddy cultivation [69]. This increased reliance has worsened inequality in water resource access, especially for farmers outside MMI command areas, who must deepen borewells up to 130 m to access groundwater, compared to 70 m required inside MMI command areas.

Historically, dam water releases are scheduled for June 12th to support the cultivation of Kuruvai (June–Sept) and Taladi (Oct–Jan) paddy crops. However, delays in these releases have compelled farmers below the Lower Anicut (major and ancient water control structure directing water through canals into the delta, Figure 1) to cultivate only the longer-duration, less productive, and less economically preferred Samba crop (Aug–Jan). Previous research revealed a strong correlation between the delay of dam releases and harvested crop area [71], confirmed by our stakeholder interactions. Consequently, a policy initially designed to enhance irrigation resources has paradoxically increased farmers' reliance on groundwater even further.

Groundwater access poses a significant economic challenge, particularly for marginal farmers. Despite free electricity, marginal farmers face substantial costs related to pump purchase and maintenance and well deepening. Our analysis of pump ownership reveals a stark disparity in access to electrified pumpsets: only 41% of marginal farmers' wells and 82% of their tubewells are electrified, compared to 83%, 86%, and 81% of wells, and 96%, 98%, and 98% of tubewells owned by semi-medium, medium, and large farmers. This economic disadvantage is further underscored by the 51% abandonment rate of wells owned by marginal farmers (see Supplementary Materials).

Although reliance on electrified groundwater pumps has grown substantially over the past two decades, their use has not improved food crop production. In Tumkur, for instance, annual Kharif production halved in the last decade, from an average of 42 million kg between 1997 and 2002 to 21 million kg between 2010 and 2014, with similar declines for Rabi (33 to 16 million kg) and summer (43 to 16 million kg) production. These statistics suggest that free electricity policies have failed to enhance food or water security and have instead complicated the challenges of the WEF security nexus. The financial burden of groundwater pumps, driven by poor management, unequal surface water distribution, and declining groundwater productivity, remains a primary cause of distress for farmers in the region [58,72].

The water–energy nexus in the CRB also has significant environmental impacts, particularly concerning greenhouse gas (GHG) emissions. The estimated daily energy consumption for water pumping during peak Kharif (9.65 GWh) and Rabi (345.9 GWh) results in substantial CO_2-eq emissions of 8 million kg in Kharif and 294 million kg in Rabi, based on an emission factor of 0.85 kg CO_2-eq per kWh [73]. Alarmingly, the Cauvery region accounts for 16% of India's agricultural energy consumption, despite representing only 4% of the country's net irrigated area. This disproportionate energy use underscores the urgent need to reassess free electricity policies and strengthen groundwater governance. While efforts have been made to mitigate these challenges, including the introduction of solar pumps and water-efficient irrigation technologies, such as drip and sprinkler systems,

the limited reach and low adoption rate of these resource-efficient solutions continue to pose significant obstacles.

The major water withdrawals as comprehensively explained in this article have made far-reaching alterations—not only to the water quantity in the river channels but also to other essential river flow and quality dynamics that are essential to support the ecosystem services. These changes have disrupted ecological regimes, degraded habitats, and affected migratory species due to altered flow from large and check dams. Inadequate consideration of biodiversity in water management has led to depleted flows, particularly in hyporheic zones, impacting both aquatic and riparian ecosystems. Additional pressures from the agriculture sector such as discharge of agrochemicals and pesticides have further contributed to the decline in fish stocks and overall biodiversity [74].

5.3. Limitations of This Study

While our spatially explicit nexus approach generates basin-wide insights into irrigation energy use and its underlying drivers and consequences, there are a few limitations. First, the theoretical estimates rely on assumptions around pump efficiency and pump yield; consequently, the results do not capture the variability in equipment performance. Second, assuming stable groundwater tables and uniform pump operations within cropping seasons may oversimplify the temporal dynamics of groundwater use, introducing uncertainties into energy and abstraction estimates. Third, extrapolating groundwater table data using observation well data underestimates the effect of 'cone-of-depression' on groundwater level in irrigation pumps. Fourth, although the influence of industrial and urban growth is clear from our analysis, lack of high-resolution sector-specific groundwater withdrawal data limits the deeper analysis of these dynamics. Finally, the lack of primary data on farmers' decision-making processes limits the ability to contextualise irrigation patterns as adaptive responses to socio-economic or institutional triggers. These limitations present important opportunities for future research that can integrate high-resolution behavioural, institutional, and bio-physical data.

6. Conclusions

The CRB exemplifies the intricate and often conflicting dynamics between economic growth, water governance, resource sustainability, and food productivity. The unsustainable practices of free electricity provision, poor surface water management, and the escalating water demands of urban and industrial centres like Bangalore have driven energy inefficiency and groundwater depletion, exacerbating socio-economic distress. Although the immediate removal of subsidies is impractical since millions of farmers depend on them, there is an urgent need to transition from traditional flood irrigation to more efficient methods like drip irrigation and expand on-farm rainwater storage. Integrated policies that provide financial and technical support to farmers could create widespread benefits, improving agricultural resilience while alleviating pressure on power utilities, state resources, and the environment.

Addressing these challenges requires a multifaceted approach. At the village scale, practices like aligning irrigation schedules with electricity supply, investing in pipeline infrastructure to reduce water loss, and developing strategic water allocation systems are essential for optimising crop yields and generating revenue from water resources. With climate change expected to increased intense rainfall events, leading to greater run-off and further strain on water resources, there is a critical need for region-specific resource management strategies. Robust monitoring of groundwater abstractions and energy consumption is crucial for understanding the groundwater–energy nexus and developing predictive models for future demand. Furthermore, metering groundwater abstraction

can enhance the economic value of groundwater, curb over abstraction, and improve energy management.

Therefore, we propose a comprehensive strategy including the following:

1. Accelerating the adoption of water-efficient irrigation methods by promoting drip irrigation and rainwater harvesting.
2. Reforming electricity subsidies to reduce energy consumption while maintaining support for farmers.
3. Strengthening water governance by improving inter-state water-sharing agreements and promoting integrated basin-level management.
4. Investing in data-driven decision-making by building a robust data.
5. Empowering farmers by providing financial and technical support for adopting sustainable agricultural practices.

By implementing these strategies, the CRB can move towards a more sustainable and resilient future. Continued research, monitoring, and adaptive management are essential to ensure the long-term effectiveness of these interventions in the face of evolving environmental and socio-economic challenges.

Supplementary Materials: The following supporting information can be downloaded at: https://www.mdpi.com/article/10.3390/w17111644/s1, Table S1: Groundwater structures owned by different farmers' class, Cauvery basin districts (2013–14).

Author Contributions: Conceptualisation, methodology, data curation, analysis, validation, writing, B.G.; supervision, project administration, funding acquisition, J.S.R. All authors have read and agreed to the published version of the manuscript.

Funding: Bhawana Gupta was funded by the Scottish Government through Hydro Nation Scholarship Program. John S. Rowan was funded through the UPSCAPE project of the Newton-Bhabha programme "Sustaining Water Resources for Food, Energy and Ecosystem Services", funded by the UK Natural Environment Research Council (NERC-UKRI) and the India Ministry of Earth Sciences (MoES), grant number NE/N016475/1.

Data Availability Statement: Data generated for this research is available from the corresponding author.

Conflicts of Interest: The authors declare no conflicts of interest. The funders had no role in the design of the study; in the collection, analyses, or interpretation of data; in the writing of the manuscript; or in the decision to publish the results.

References

1. Cullet, P.; Koonan, S. *Water Law in India: An Introduction to Legal Instruments*, 2nd ed.; Oxford University Press: Oxford, UK, 2017.
2. Badiani, R.; Jessoe, K.K.; Plant, S. Development and the Environment. *J. Environ. Dev.* **2012**, *21*, 244–262. [CrossRef]
3. Dubash, N. The Electricity-Groundwater Conundrum: Case for a Political Solution to a Political Problem. *Econ. Polit. Wkly.* **2007**, *42*, 45–55. [CrossRef]
4. Dhawan, V. *Water and Agriculture in India: Background Paper for the South Asia Expert Panel During the Global Forum for Food and Agriculture (GFFA) 2017*; OAV German Asia-Pacific Business Association: Hamburg, Germany, 2017.
5. Ragab, R.; Prudhomme, C. SW—Soil and Water: Climate Change and Water Resources Management in Arid and Semi-arid Regions: Prospective and Challenges for the 21st Century. *Biosyst. Eng.* **2002**, *81*, 3–34. [CrossRef]
6. Prayag, A.G.; Zhou, Y.; Srinivasan, V.; Stigter, T.; Verzijl, A. Assessing the impact of groundwater abstractions on aquifer depletion in the Cauvery Delta, India. *Agric. Water Manag.* **2023**, *279*, 108191. [CrossRef]
7. Brugere, C.; Lingard, J. Irrigation deficits and farmers' vulnerability in Southern India. *Agric. Syst.* **2003**, *77*, 65–88. [CrossRef]
8. Bhave, A.G.; Conway, D.; Dessai, S.; Stainforth, D.A. Water resource planning under future climate and socioeconomic uncertainty in the Cauvery River Basin in Karnataka, India. *Water Resour. Res.* **2018**, *54*, 708–728. [CrossRef]
9. Guston, D.H. Understanding 'anticipatory governance'. *Soc. Stud. Sci.* **2014**, *44*, 218–242. [CrossRef]
10. Vanham, D.; Weingartner, R.; Rauch, W. The Cauvery river basin in Southern India: Major challenges and possible solutions in the 21st century. *Water Sci. Technol.* **2011**, *64*, 122–131. [CrossRef]

11. Mukherji, A.; Verma, T.S..S., Electricity reforms and its impact on groundwater use: Evidence from India. In *Re-Thinking Water and Food Security*; CRC Press: Boca Raton, FL, USA, 2010.
12. Howells, M.; Hermann, S.; Welsch, M.; Bazilian, M.; Segerström, R.; Alfstad, T.; Gielen, D.; Rogner, H.; Fischer, G.; Velthuizen, H.V. Integrated analysis of climate change, land-use, energy and water strategies. *Nat. Clim. Chang.* **2013**, *3*, 621–626. [CrossRef]
13. Biggs, R.; Schlüter, M.; Schoon, M.L. *Principles for Building Resilience: Sustaining Ecosystem Services in Social-Ecological Systems*; Cambridge University Press: Cambridge, UK, 2015.
14. Akinsete, E.; Koundouri, P.; Kartala, X.; Englezos, N.; Lautze, J.; Yihdego, Z.; Gibson, J.; Scholz, G.; van Bers, C.; Sodoge, J. Sustainable WEF nexus management: A conceptual framework to integrate models of social, economic, policy, and institutional developments. *Front. Water* **2022**, *4*, 727772. [CrossRef]
15. Simpson, G.; Jewitt, G.; Becker, W.; Badenhorst, J.; Neves, A.; Rovira, P.; Pascual, V. The Water-Energy-Food Nexus Index: A Tool to Support Integrated Resource Planning, Management and Security. *Front. Water* **2022**, *4*, 825854. [CrossRef]
16. Sawant, N.; Kulkarni, S.; Sharma, P.; Doval, A.; Jadhav, P.J. Methodology to quantify crop, irrigation water, and energy linkages in small-holder irrigation systems. *Energy Sustain. Dev.* **2025**, *86*, 101719. [CrossRef]
17. Chand, J.B.; Bimali, S. Exploration of the cropping pattern based on the irrigation water–energy–food and carbon emission nexus. *Irrig. Drain.* **2024**, *73*, 944–960. [CrossRef]
18. Folke, S. Conflicts over Water and Land in South Indian Agriculture: A Political Economy Perspective. *Econ. Polit. Wkly.* **1998**, *33*, 341–349. Available online: http://www.jstor.org/stable/4406406 (accessed on 3 May 2025).
19. Gurumurthy, R.; Xavier, S. The Cauvery Conundrum: Historical Roots of A Modern Dispute. *J. Namib. Stud. Hist. Polit. Cult.* **2023**, *33*, 4492–4505. [CrossRef]
20. Ghosh, N.; Bandyopadhyay, J.; Thakur, J. *Conflict over Cauvery Waters: Imperatives for Innovative Policy Options*; Observer Research Foundation: New Delhi, India, 2018.
21. Amjath Babu, T.S. Economic and Environmental Impacts of Political Non-Cooperative Strategies in Water Management: An Analysis of Prospective Policies in the Cauvery River Basin of India. Ph.D. Thesis, Justus-Liebig University Giessen, Giessen, Germany, 2008.
22. Ferdin, M.; Görlitz, S.; Schwörer, S. Water stress in the Cauvery basin, south India. How current water management approaches and allocation conflict constrain reform. *ASIEN Ger. J. Polit. Econ. Cult.* **2010**, *117*, 27–44. [CrossRef]
23. Sharma, A.; Hipel, K.W.; Schweizer, V. Strategic insights into the cauvery river dispute in India. *Sustainability* **2020**, *12*, 1286. [CrossRef]
24. Garg, N.K.; Azad, S. Analysis of Cauvery water-sharing award using an analytical framework model. *J. Hydrol.* **2019**, *579*, 124214. [CrossRef]
25. Shah, T. *Taming the Anarchy: Groundwater Governance in South Asia*; Routledge: Abingdon, UK, 2010.
26. Kitterød, N.O. Hydrological challenges in the Cauvery River basin, South India. *Siècles. Cahiers du Centre d'histoire «Espaces et Cultures»* **2022**, *53*, 1–20. [CrossRef]
27. Gowri, R.; Dey, P.; Mujumdar, P.P. A hydro-climatological outlook on the long-term availability of water resources in Cauvery river basin. *Water Secur.* **2021**, *14*, 100102. [CrossRef]
28. Horan, R.; Gowri, R.; Wable, P.S.; Baron, H.; Keller, V.D.; Garg, K.K.; Mujumdar, P.P.; Houghton-Carr, H.; Rees, G. A comparative assessment of hydrological models in the Upper Cauvery catchment. *Water* **2021**, *13*, 151. [CrossRef]
29. Sreelash, K.; Mathew, M.M.; Nisha, N.; Arulbalaji, P.; Bindu, A.G.; Sharma, R.K. Changes in the Hydrological Characteristics of Cauvery River draining the eastern side of southern Western Ghats, India. *Int. J. River Basin Manag.* **2020**, *18*, 153–166. [CrossRef]
30. Wable, P.S.; Garg, K.K.; Nune, R.; Venkataradha, A.; KH, A.; Srinivasan, V.; Ragab, R.; Rowan, J.; Keller, V.; Majumdar, P. Impact of agricultural water management interventions on upstream–downstream trade-offs in the upper Cauvery catchment, southern India: A modelling study. *Irrig. Drain.* **2022**, *71*, 472–494. [CrossRef]
31. Fishman, R.M.; Siegfried, T.; Raj, P.; Modi, V.; Lall, U. Over-extraction from shallow bedrock versus deep alluvial aquifers: Reliability versus sustainability considerations for India's groundwater irrigation. *Water Resour. Res.* **2011**, *47*, 20. [CrossRef]
32. Robert, M.; Thomas, A.; Sekhar, M.; Badiger, S.; Ruiz, L.; Willaume, M.; Leenhardt, D.; Bergez, J.E. Farm Typology in the Berambadi Watershed (India): Farming Systems Are Determined by Farm Size and Access to Groundwater. *Water* **2017**, *9*, 51. [CrossRef]
33. Department of Water Resources. *India-WRIS (Water Resource Information System)*; Department of Water Resources, River Development & Ganga Rejuvenation: New Delhi, India, 2020. Available online: https://nwic.in/wris/#/ (accessed on 3 May 2025).
34. Ramesh, R.; Purvaja, R.; Lakshmi, A.; Newton, A.; Kremer, H.H.; Weichselgartner, J. *South Asia Basins: LOICZ Global Change Assessment and Synthesis of River Catchment Coastal Sea Interaction and Human Dimensions:[land-ocean Interactions in the Coastal Zone (LOICZ), Core Project of the International Geosphere-biosphere Programme (IGBP) and International Human Dimensions Programme on Global Environmental Change (IHDP)]*; LOICZ Research and Studies No. 32; GKSS Research Center: Geesthacht, Germany, 2009; 121p. [CrossRef]

35. Subramani, T.; Badrinarayanan, S.; Prasath, K.; Sridhar, S. Performanance Evaluation of the Cauvery Irrigation System, India, Using Remote Sensing and Gis Technology. *Int. J. Eng. Res. Appl.* **2014**, *4*, 191–197.
36. Ministry of Jal Shakti, Government of India. *Fifth Vensus of Minor Irrigation Schemes Report*; Department of Water Resources, River Development & Ganga Rejuvenation: New Delhi, India, 2017. Available online: https://www.data.gov.in/ (accessed on 3 May 2025).
37. Ministry of Jal Shakti, Government of India. *Cauvery Water Management Authority*; Department of Water Resources, River Development & Ganga Rejuvenation: New Delhi, India, 2024. Available online: https://www.jalshakti-dowr.gov.in/cauvery-water-management-authority (accessed on 3 May 2025).
38. Sivakumar, B. Hydropsychology: The human side of water research. *Hydrol. Sci. J.* **2011**, *56*, 719–732. [CrossRef]
39. Department of Agriculture, Co-operation and Farmers Welfare. *Agriculture Census 2015–16: All India Report on Number and Area of Operational Holdings*; Ministry of Agriculture and Farmers Welfare, Government of India: New Delhi, India, 2019. Available online: https://www.agcensus.gov.in/ (accessed on 3 May 2025).
40. Narayanamoorthy, A. Economics of drip irrigation in sugarcane cultivation: Case study of a farmer from Tamil Nadu. *Indian J. Agric. Econ.* **2005**, *60*, 235–248.
41. Jackson, T.M.; Khan, S.; Hafeez, M. A comparative analysis of water application and energy consumption at the irrigated field level. *Agric. Water Manag.* **2010**, *97*, 1477–1485. [CrossRef]
42. Karimi, P.; Qureshi, A.S.; Bahramloo, R.; Molden, D.J. Reducing carbon emissions through improved irrigation and groundwater management: A case study from Iran. *Agric. Water Manag.* **2012**, *108*, 52–60. [CrossRef]
43. Wang, J.; Rothausen, S.; Conway, D.; Zhang, L.; Xiong, W.; Holman, I.; Li, Y. China's water–energy nexus: Greenhouse-gas emissions from groundwater use for agriculture. *Environ. Res. Lett.* **2012**, *7*, 014035. [CrossRef]
44. Patle, G.; Singh, D.K.; Sarangi, A.; Khanna, M. Managing CO_2 emission from groundwater pumping for irrigating major crops in trans indo-gangetic plains of India. *Clim. Chang.* **2016**, *136*, 265–279. [CrossRef]
45. Handa, D.; Frazier, R.S.; Taghvaeian, S.; Warren, J.G. The Efficiencies, Environmental Impacts and Economics of Energy Consumption for Groundwater-Based Irrigation in Oklahoma. *Agriculture* **2019**, *9*, 27. [CrossRef]
46. Agrawal, S.; Jain, A. *Solar Pumps for Sustainable Irrigation: A Budget Neutral Opportunity*; Technical Report; Council on Energy, Environment and Water: New Delhi, India, 2015.
47. Indian Council of Agricultural Research. *Expert System for Paddy–Planting Seasons*; Tamil Nadu Agricultural University: Tamil Nadu, India, 2018. Available online: https://tnau.ac.in/expert-system/ (accessed on 3 May 2025).
48. Murari, K.; Mahato, S.; Jayaraman, T.; Swaminathan, M. Extreme Temperatures and Crop Yields in Karnataka, India. *Rev. Agrar. Stud.* **2019**, *8*, 92–114. [CrossRef]
49. Khalid, M.; Laarabi, B.; Barhdadi, A. Solar Water Pumping Applications in Morocco: State of the Art. In Proceedings of the 6th International Renewable and Sustainable Energy Conference (IRSEC), Rabat, Morocco, 5–8 December, 2018. [CrossRef]
50. Shreedhar, G.; Gupta, N.; Pullabhotla, H.; Ganesh-Kumar, A.; Gulati, A. *A Review of Input and Output Policies for Cereals Production in India*; IFPRI Discussion Paper 1159; International Food Policy Research Institute (IFPRI): Washington, DC, USA, 2012.
51. Cullet, P. Groundwater Law In India: Towards a Framework Ensuring Equitable Access and Aquifer Protection. *J. Environ. Law* **2014**, *26*, 55–81. [CrossRef]
52. Kumar, M.D. *Groundwater Management in India: Physical, Institutional and Policy Alternatives*; Sage: New Delhi, India, 2007; p. 354.
53. Hora, T.; Srinivasan, V.; Basu, N.B. The Groundwater Recovery Paradox in South India. *Geophys. Res. Lett.* **2019**, *46*, 9602–9611. [CrossRef]
54. Barik, B.; Ghosh, S.; Sahana, A.S.; Pathak, A.; Sekhar, M. Water–food–energy nexus with changing agricultural scenarios in India during recent decades. *Hydrol. Earth Syst. Sci.* **2017**, *21*, 3041–3060. [CrossRef]
55. Scott, C.A. Electricity for groundwater use: Constraints and opportunities for adaptive response to climate change. *Environ. Res. Lett.* **2013**, *8*, 035005. [CrossRef]
56. Gupta, B.; Horan, R.; Rowan, J.; Allan, A. Hydrological modelling to assess the impacts of socio-economic development and climate change on water resources in Cauvery Basin, India. *preprint* **2022**. [CrossRef]
57. Bazilian, M.; Rogner, H.; Howells, M.; Hermann, S.; Arent, D.; Gielen, D.; Steduto, P.; Müller, A.; Komor, P.; Tol, R.; et al. Considering the energy, water and food nexus: Towards an integrated modelling approach. *Energy Policy* **2011**, *39*, 7896–7906. [CrossRef]
58. Al-Saidi, M.; Elagib, N. Towards understanding the integrative approach of the water, energy and food nexus. *Sci. Total Environ.* **2017**, *574*, 1131–1139. [CrossRef] [PubMed]
59. Benson, D.; Gain, A.; Rouillard, J.; Giupponi, C. Governing for the Nexus: Empirical, Theoretical, and Normative Dimensions. In *Water-Energy-Food Nexus: Principles and Practices*; John Wiley & Sons: Hoboken, NJ, USA, 2017; pp. 77–88. [CrossRef]
60. Sadeghi, S.H.; Sharifi Moghadam, E.; Delavar, M.; Zarghami, M. Application of water-energy-food nexus approach for designating optimal agricultural management pattern at a watershed scale. *Agric. Water Manag.* **2020**, *233*, 106071. [CrossRef]

61. Mirzaei, A.; Naserin, A.; Mardani Najafabadi, M. Optimizing water-energy-food nexus index, CO2 emissions, and chemical pollutants under irrigation water salinity scenarios. *Environ. Sustain. Indic.* **2024**, *23*, 100461. [CrossRef]
62. Agrawal, A.; Bakshi, B.R.; Kodamana, H.; Ramteke, M. Multi-objective optimization of food-energy-water nexus via crops land allocation. *Comput. Chem. Eng.* **2024**, *183*, 108610. [CrossRef]
63. Albrecht, T.R.; Scott, C.A. The water-energy-food nexus: Outlook on opportunities and challenges. In *Handbook on the Governance and Politics of Water Resources*; Edward Elgar Publishing: London, UK, 2024; pp. 143–157.
64. Ali, F. The Water, Food, and Energy Nexus: The Inclusive Roles of Governance and Finance in South Asia. *Land Degrad. Dev.* **2024**, *35*, 5367–5385. [CrossRef]
65. Zahedi, R.; Yousefi, H.; Aslani, A.; Ahmadi, R. Water, energy, food and environment nexus (WEFEN): Sustainable transition, gaps and Covering approaches. *Energy Strategy Rev.* **2024**, *54*, 101496. [CrossRef]
66. Gupta, V.; Singh, S. Exploring the multiple dimensions of solar irrigation in South-Asian countries: Insights from a systematic review. *Renew. Energy Focus* **2025**, *54*, 100711. [CrossRef]
67. Mohan, G.; Perarapu, L.N.; Chapagain, S.K.; Reddy, A.A.; Melts, I.; Mishra, R.; Avtar, R.; Fukushi, K. Assessing determinants, challenges and perceptions to adopting water-saving technologies among agricultural households in semi-arid states of India. *Curr. Res. Environ. Sustain.* **2024**, *7*, 100255. [CrossRef]
68. Moharaj, P.; Rana, S.; Sahoo, D.; Kumar, K.K.; Nagaraj, G.; Borah, N.; Utagi, S. Dynamics of Water Stress in Bangalore, India: Exploring the Confluence of Geopolitical, Climatic, and Anthropogenic Factors. *J. Asian Afr. Stud.* **2025**. [CrossRef]
69. Nair, J.; Thomas, B.K.; Bahinipati, C.S. Cropping decisions under water stress: Evidence from Cauvery Delta Region, India. *World Water Policy* **2024**, *10*, 711–729. [CrossRef]
70. Mohtar, R.; Assi, A.; Daher, B. *Bridging the Water and Food Gap: The Role of the Water-Energy-Food Nexus*; United Nations University: Tokyo, Japan, 2015.
71. Bosu, S.S. Sharing of Inter-state River Water Resources: Case Studies of Two Major Irrigation Systems in Tamil Nadu, India. *Int. J. Water Resour. Dev.* **1995**, *11*, 443–456. [CrossRef]
72. Sishodia, R.P.; Shukla, S.; Graham, W.D.; Wani, S.P.; Jones, J.W.; Heaney, J. Current and future groundwater withdrawals: Effects, management and energy policy options for a semi-arid Indian watershed. *Adv. Water Resour.* **2017**, *110*, 459–475. [CrossRef]
73. Raghuvanshi, S.P.; Chandra, A.; Raghav, A.K. Carbon dioxide emissions from coal based power generation in India. *Energy Convers. Manag.* **2006**, *47*, 427–441. [CrossRef]
74. Pownkumar, V.; Ananthan, P.; Ekka, A.; Qureshi, N.W.; T, V. Fisheries as ecosystem services: A case study of the Cauvery river basin, India. *Front. Environ. Sci.* **2022**, *10*, 892012. [CrossRef]

Disclaimer/Publisher's Note: The statements, opinions and data contained in all publications are solely those of the individual author(s) and contributor(s) and not of MDPI and/or the editor(s). MDPI and/or the editor(s) disclaim responsibility for any injury to people or property resulting from any ideas, methods, instructions or products referred to in the content.

water

MDPI

Article

Patterns, Risks, and Forecasting of Irrigation Water Quality Under Drought Conditions in Mediterranean Regions

Alexandra Tomaz [1,2,3,*], Adriana Catarino [1,2], Pedro Tomaz [4], Marta Fabião [5] and Patrícia Palma [1,2,3,6]

[1] Instituto Politécnico de Beja, Escola Superior Agrária de Beja, Campus do Instituto Politécnico de Beja, 7800-295 Beja, Portugal; adriana.catarino@ipbeja.pt (A.C.); ppalma@ipbeja.pt (P.P.)
[2] Center for Sci-Tech Research in Earth System and Energy (CREATE), Instituto Politécnico de Beja, Campus do Instituto Politécnico de Beja, 7800-295 Beja, Portugal
[3] GeoBioTec, Nova School of Science and Technology, Campus da Caparica, 2829-516 Caparica, Portugal
[4] Department of Computer Science, Nova School of Science and Technology, Campus da Caparica, 2829-516 Caparica, Portugal; p.tomaz@campus.fct.unl.pt
[5] Centro Operativo e de Tecnologia de Regadio, Quinta da Saúde, Apartado 354, 7800-999 Beja, Portugal; marta.fabiao@cotr.pt
[6] Águas Publicas do Alentejo, Grupo Águas de Portugal, Rua Dr. Aresta Branco nº 51, 7800-310 Beja, Portugal
* Correspondence: atomaz@ipbeja.pt

Abstract: The seasonal and interannual irregularity of temperature and precipitation is a feature of the Mediterranean climate that is intensified by climate change and constitutes a relevant driver of water and soil degradation. This study was developed during three years in a hydro-agricultural area of the Alqueva irrigation system (Portugal) with Mediterranean climate conditions. The sampling campaigns included collecting water samples from eight irrigation hydrants, analyzed four times yearly. The analysis incorporated meteorological data and indices (precipitation, temperature, and drought conditions) alongside chemical parameters, using multivariate statistics (factor analysis and cluster analysis) to identify key water quality drivers. Additionally, machine learning models (Random Forest regression and Gradient Boosting machine) were employed to predict electrical conductivity (ECw), sodium adsorption ratio (SAR), and pH based on chemical and climatic variables. Water quality evaluation showed a prevalence of a slight to moderate soil sodification risk. The factor analysis outcome was a three-factor model related to salinity, sodicity, and climate. The cluster analysis revealed a grouping pattern led by year and followed by stage, pointing to the influence of inter-annual climate irregularity. Variations in water quality from the reservoirs to the distribution network were not substantial. The Random Forest algorithm showed superior predictive accuracy, particularly for ECw and SAR, confirming its potential for the reliable forecasting of irrigation water quality. This research emphasizes the importance of integrating time-sensitive monitoring with data-driven predictions of water quality to support sustainable water resources management in agriculture. This integrated approach offers a promising framework for early warning and informed decision-making in the context of increasing drought vulnerability across Mediterranean agro-environments.

Keywords: climate variability; hydro-agricultural areas; machine learning; multivariate statistics; salinity; sodicity

1. Introduction

Droughts are becoming more common in Mediterranean regions, with increasingly unpredictable rainfall patterns [1,2]. This variability, heightened by global climate change,

poses a serious threat to food security. Traditional farming schedules are disrupted and water scarcity during key crop-growing periods threatens crop yields [1,2].

Besides the impacts of droughts on water quantity, the quality of water for agricultural and other uses is also compromised [3,4]. The effects of erratic precipitation distribution and interannual climate variability on the deterioration of surface and groundwater quality have been widely reported and are expected to worsen with global climate change [5–11]. Extreme precipitation events can increase runoff, which subsequently causes soil erosion but also transports organic pollutants like pesticides into water bodies, thus resulting in a degradation of water quality [12,13]. Higher temperatures contribute to rising evaporative rates, concentrating dissolved salts and nutrients in water bodies [14]. Extended periods of drought reduce water flows, causing the concentration of contaminants and decreasing the dilution of pollutants [15,16].

The expansion of irrigation systems in drought-prone areas has raised concerns about soil degradation, particularly salinization and the overall loss of soil health [17,18]. In fact, soil salinization is one of the critical physical–chemical degradation processes in drought-prone regions where irrigation is adopted [19,20]. Salt-affected soils occupy more than 20% of the global irrigated area and, in some countries, they occur in more than half of the irrigated land [21]. In the Mediterranean region, 25% of the irrigated cropland is affected by moderate-to-high salinization [22].

Hillel (2000) and Hillel et al. (2008) [19,23] highlighted the importance of having early warning systems to detect salinity and sodicity in irrigated agroecosystems. Besides the routine water monitoring programs in surface or groundwater bodies that supply irrigation perimeters, the diversification of spatial and temporal monitoring could predict the onset of salinization processes, especially when usual patterns of humid and dry periods are disturbed by drought occurrence [24]. Recently, data-driven approaches such as machine learning (ML) have emerged as tools to support environmental monitoring and forecasting. Several studies have highlighted the use of ML to predict water quality based on algorithms like Artificial Neural Networks, Random Forest, Multiple Linear Regression, Gradient Boosting, Support Vector Machines, or K-Nearest Neighbors, among others [25–28]. A prediction of stream water quality based on both chemical and meteorological data was performed by [29] using the RF and Boosted regression tree (BRT) models. Some recent studies have specifically focused on modeling irrigation water quality, typically relying on datasets of physicochemical parameters to predict indices or key target variables [30–32]. Machine learning algorithms can handle complex, nonlinear relationships between large sets of variables, allowing for the prediction of key salinity indicators, the identification of the most influential parameters contributing to water degradation in irrigated systems, and the modernization of irrigation water quality management [33]. While these studies have explored the use of predictive models for irrigation water quality, to the best of our knowledge, none have integrated meteorological variables that describe cumulative dryness during drier years. In this context, the use of ML in irrigation water quality monitoring under climate uncertainty can enhance early detection of salinization risks and support more adaptive water management strategies.

This study aims to evaluate irrigation water quality at the hydrant level under drought conditions and to explore the potential of ML models in predicting key irrigation water quality parameters. Specifically, the objectives are (i) to evaluate the suitability of irrigation water for agricultural use during dry periods, (ii) to evaluate the contribution of hydrant-level water quality assessment to improve spatial monitoring, (iii) to identify the most influential factors affecting water quality variability under drought conditions, and (iv) to compare the performance of two ML algorithms, Random Forest and Gradient Boosting, in predicting salinity-related parameters from chemical and meteorological variables.

2. Materials and Methods

2.1. Study Area

This study was conducted in eight hydrants (H5, H6, H7, H16, H21, H22, H23, and H33, as identified by the water supplier company) distributing water to ten farm fields with a land use of drip-irrigated vineyards and olive orchards and sprinkler-irrigated annual field crops, forages, and pastures (Table 1), totaling 88 ha. All farm fields were located in the Brinches-Enxoé hydro-agricultural area with an equipped area of 5061 ha, part of the Alqueva irrigation system, in the Alentejo region, South Portugal (Figure 1). The conveyance networks of the Brinches-Enxoé hydro-agricultural area originate in the Laje (pressurized) and the Montinhos (gravity) reservoirs, respectively. The former is the upstream reservoir of all the studied hydrants, except for H16, supplied by Montinhos.

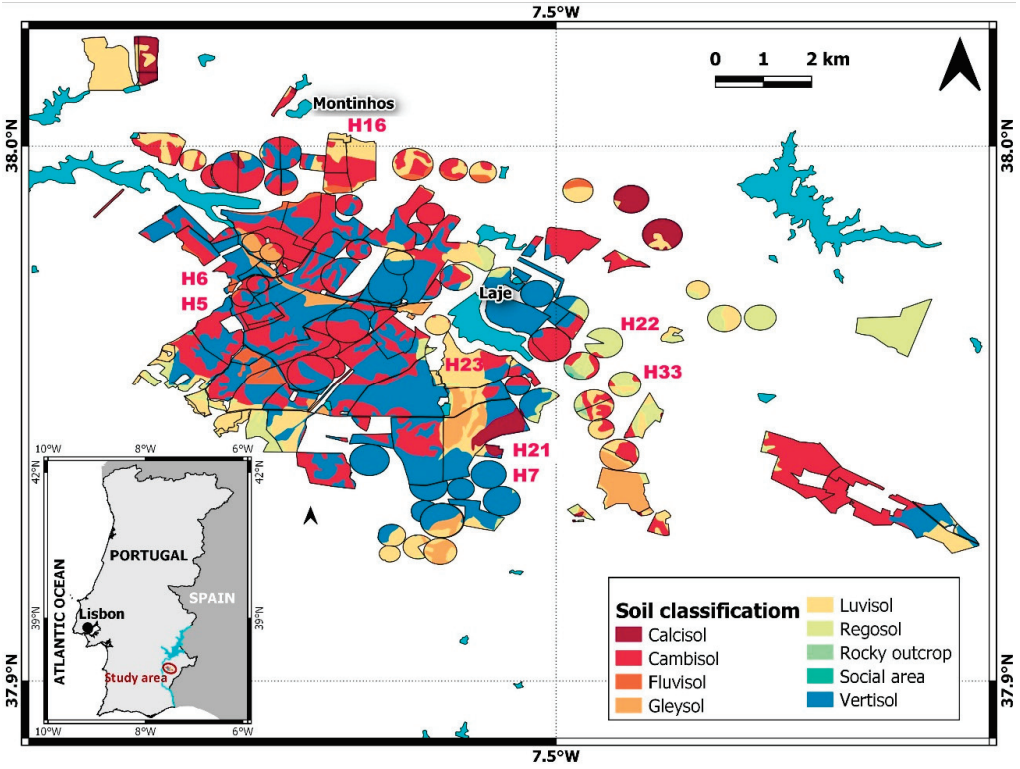


Figure 1. Location of the irrigation hydrants, Montinhos and Lage reservoirs, and predominant soil distribution in the hydro-agricultural area of Brinches-Enxoé, adapted from [20].

The predominant soil types are medium to fine-textured calcaric cambisols, chromic vertisols, and chromic luvisols [34], represented in Figure 1.

The climate in the region is temperate with a hot and dry summer (Mediterranean) with an annual precipitation and average mean monthly temperature of, respectively, 558 mm and 16.9 °C (1981–2010 climatological normal; [35]).

Table 1. Crops in the farm plots supplied by the hydrants (coordinates between brackets), integrated with the Brinches-Enxoé hydro-agricultural area, during the period of study (2018–2020).

Year	H5 (37°58′12.74″ N; 7°33′18.17″ W)	H6 (37°58′22.99″ N; 7°33′26.61″ W)	H7 (37°56′1.01″N; 7° 31′25.40″ W)	H16 (37°59′53.28″ N; 7°32′21.02″ W)	H21 (37°56′48.39″ N; 7°30′17.74″ W)	H22 (37°57′12.65″ N; 7°29′21.08″ W)	H23 (37°57′22.32″ N; 7°30′36.72″ W)	H33 (37°57′36.03″ N; 7°29′18.35″ W)
2018	Grapevine (*Vitis vinifera* L. Cv. 'Aragonez)	Maize (*Zea mays* L.)	Sunflower (*Helianthus annus* L.)	Grapevine (*Vitis vinifera* L. Cv. 'Antão Vaz) Olive (*Olea europaea* L. Cv. 'Cordovil')	Olive (*Olea europaea* L. Cv. 'Cobrançosa')	Permanent Pasture ((grasses (70%), legumes (18%) and others (12%))	Grapevine (*Vitis vinifera* L. Cv. 'Antão Vaz) Sunflower (*Helianthus annus* L.)	Alfalfa (*Medicago sativa* L.)
2019	Grapevine (*Vitis vinifera* L. Cv. 'Aragonez)	Sunflower (*Helianthus annus* L.)	Arrowleaf clover (*Trifolium vesiculosum* Savi)	Grapevine (*Vitis vinifera* L. Cv. 'Antão Vaz) Olive (*Olea europaea* L. Cv. 'Cordovil')	Olive (*Olea europaea* L. Cv. 'Cobrançosa')	Permanent Pasture ((grasses (70%), legumes (18%))	Grapevine (*Vitis vinifera* L. Cv. 'Antão Vaz) Garlic (*Allium sativum* L.) + Maize (*Zea mays* L.)	Alfalfa (*Medicago sativa* L.)
2020	Grapevine (*Vitis vinifera* L. Cv. 'Aragonez)	Maize (*Zea mays* L.)	Onion (*Allium cepa* L.)	Grapevine (*Vitis vinifera* L. Cv. 'Antão Vaz) Olive (*Olea europaea* L. Cv. 'Cordovil')	Olive (*Olea europaea* L. Cv. 'Cobrançosa')	Not sown	Grapevine (*Vitis vinifera* L. Cv. 'Antão Vaz) Sunflower (*Helianthus annus* L.)	Not sown

2.2. Meteorological Data and Drought Characterization

Meteorological data were recorded in an automatic meteorological station of the Irrigation Operating and Technology Center (Centro Operativo e de Tecnologia do Regadio—COTR) located in the area (37.97 N; 7.55 W) [36]. To characterize the meteorological trends during the study period, the monthly Standard Precipitation Index (SPI) was calculated [37]. The SPI is a statistical index that measures precipitation anomalies in a given region and time compared to historical patterns. It was obtained by fitting the long-term monthly precipitation records of the period 1981–2010 [38] to a Gamma probability distribution, which was then transformed into a normal distribution. Droughts can be classified as mild, for $-1.0 < \text{SPI} < 0$; moderate, if $-1.5 < \text{SPI} \leq -1.0$; severe, for $-2.0 < \text{SPI} \leq -1.5$; and extreme, if $\text{SPI} \leq -2.0$.

The occurrence of drought was identified according to [37] as a period in which the SPI is continuously negative and reaches a value ≤ -1.0, beginning when the SPI first falls below zero and ending with a positive value of the SPI following a value ≤ -1.0. The duration (number of months), magnitude ($\sum|\text{SPI}|$ during drought), and intensity (magnitude/duration) of droughts were also evaluated.

The values of accumulated precipitation (P_{cum}) and accumulated reference evapotranspiration ($ET0_{cum}$) until each sampling date were computed to obtain variables in the dataset that could be descriptive of the meteorological conditions when applying the multivariate statistical methods and the ML model.

2.3. Sampling Strategy

This study covered 12 water sampling campaigns, with four campaigns each year, performed in April–May, June–July, September–October, and November, corresponding to the following assigned stages of crop development/irrigation season, respectively: Initial (I); Middle (M); Late (L); and Post-cycle (P). For the assessment, 2 L water samples were collected in polyethylene bottles from the irrigation hydrants. The samples were transported to the laboratory in a cooler at 4 °C and stored, following the requisites for water conservation for each parameter [39].

Water pH was determined by potentiometry with a pH probe, and EC_W was determined by conductometry with a conductivity meter. The concentrations of ions of calcium (Ca), magnesium (Mg), sodium (Na), chloride (Cl), boron (B), and nitrate (NO_3) were determined by the ionic chromatography methodology [39].

2.4. Irrigation Water Quality Assessment

The assessment of water quality for irrigation was performed using the consensual guidelines of the Food and Agriculture Organization of the United Nations (FAO) (Table S1), which consider four types of "potential problems" that can arise from the use of poor quality irrigation water, namely (i) salinity, which can affect soil water availability; (ii) infiltration rate of water into the soil; (iii) specific ion toxicity in sensitive crops; (iv) and miscellaneous effects on susceptible crops [40].

2.5. Exploratory Statistical Analyses

Matrices of Spearman's correlation coefficients were computed for preliminary examination of the relationships between variables. Factor and cluster analyses were performed to explore data structure and case similarity using the methodology described in Tomaz et al. [41,42]. Analyses were performed with Statistica 7 [43].

2.6. Machine Learning Models

Random Forest (RF) and Gradient Boosting (GB) models were tested to forecast three key indicators of irrigation water quality (target variables), EC_W, SAR, and pH, using a dataset of the average values of continuous physicochemical and meteorological predictors: P_{cum}, $ET0_{cum}$, B, Ca, Mg, Na, Cl, and NO_3.

RF is a supervised ensemble ML model based on a collection of decision trees (estimators) [44]. Because it is an ensemble technique, it uses the best outcome given by the many decision trees, mitigating and limiting generalization mistakes as the volume of the tree architecture in the forest grows. In addition, it shows the ability to capture nonlinear relationships [28,30].

GB is also a supervised ensemble ML model that uses decision trees as base learners, but builds them sequentially, with each new tree focusing on correcting the prediction errors made by the previous ones. This boosting approach enables the model to gradually improve its accuracy by minimizing a loss function at each step [45].

Both models were developed in Visual Studio Code(version 1.100.1 Python 3.10) using Python libraries, such as scikit-learn, pandas, and matplotlib. For each target variable, the RF models were trained with 100 decision trees, which is the default configuration recommended in the library as a balance between predictive performance and computational efficiency. Similarly, the GB models were also trained using the default hyperparameters, including 100 decision trees and a learning rate of 0.1, which controls how much each new tree influences the final model. Model evaluation was performed using an 80–20% train–test split of the dataset, meaning that the RF algorithm built an input–output relationship with 80% of the dataset and subsequently generalized or predicted outputs for the 20% of unseen inputs [28,46]. For each algorithm and model, the following performance metrics were calculated: coefficient of determination (R^2), root mean square error (RMSE), mean absolute error (MAE), and relative bias (RBIAS). The final model was selected based on cross-validated performance metrics (R^2, RMSE, MAE, etc.). In addition, the mean decrease in impurity (MDI), or Gini importance, was used to rank the feature importance (of each predictor) in the RF model [47]. Measured and predicted values of each parameter were represented in scatter plots to evaluate the accuracy and goodness of fit for both models.

3. Results and Discussion

3.1. Meteorological Trends and Drought Characterization

The annual precipitation was 603 mm, 343 mm, and 615 mm in 2018, 2019, and 2020, respectively, while the mean annual temperature was 16.7 °C, 17.3 °C, and 17.8 °C. The mean temperature during the growing/irrigation season of the different crops in the study area (March to October) each year was 19.8 °C, 20.2 °C, and 20.5 °C, respectively. The year 2018 was characterized by high precipitation in the spring (March and April) and autumn (October and November); 2019 was a very dry year, characterized by high temperatures and very low precipitation; 2020 registered higher mean monthly temperatures, and despite presenting higher annual precipitation than the two previous years, rain was mostly concentrated in April and the autumn months (October and November) (Figure 2).

Calculations of the monthly SPI were made to better understand the climate's interannual and seasonal variability during the period of the study and the occurrence of drought (Figure 2).

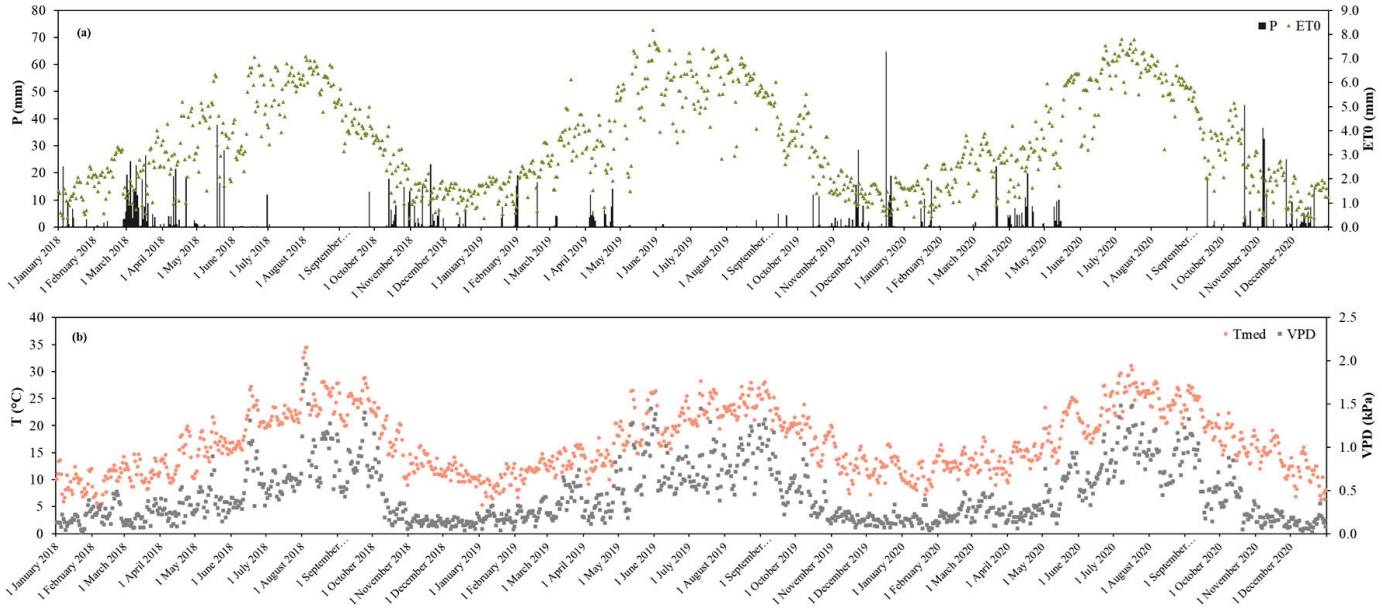


Figure 2. Daily variation of (**a**) precipitation (P) and reference evapotranspiration (ET0), and (**b**) mean temperature and vapor pressure deficit (VPD).

A continuing trend of dry conditions started from the end of 2018 through the end of 2019 and the initial months of 2020, with the occurrence of four almost consecutive droughts (Figure 3). The longest drought lasted 5 months (1 December 2018 to 1 April 2019), but the highest drought magnitude occurred from 1 May 2019 to 1 August 2019, when the minimum SPI reached −2.73, signaling extreme dry weather. These dry conditions continued until the end of 2019 (November). The drought persisted until 1 March 2020. During 2019, precipitation values were consistently lower than the climatological normal (except in April and December), which, along with the high temperatures, contributed to the year's severe dry conditions. In 2020, there was a recovery in precipitation levels, especially in March–April and October–November, but temperatures remained higher than historical records [48].

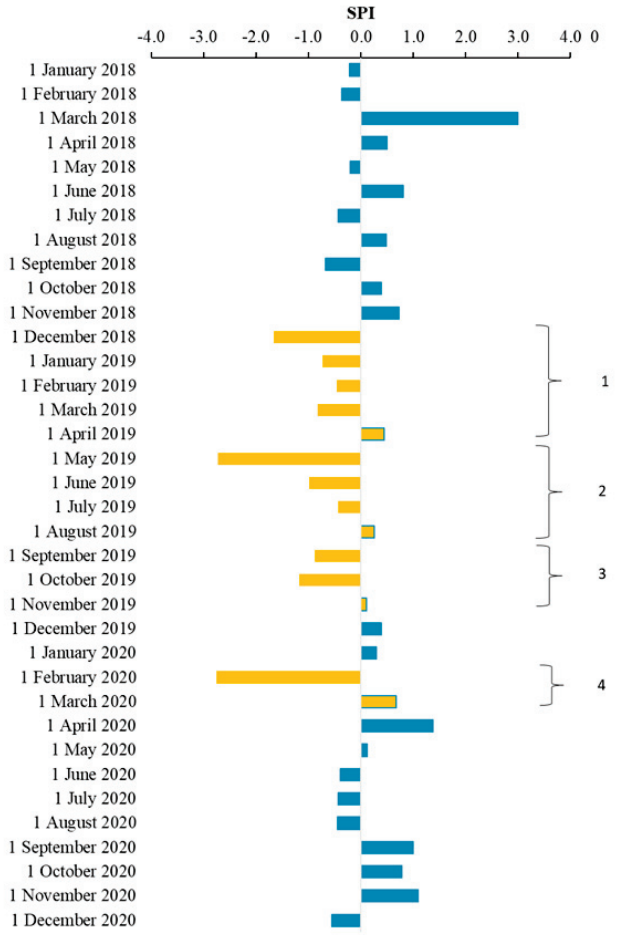
3.2. Irrigation Water Quality

The temporal and spatial variation of water physical–chemical parameters and ions was characterized by their mean and standard deviation (Figures 4 and 5).

The highest ECW value was registered in H5, at the end of 2020. In general, there was a slight increase in EC_W during the study period, more evident in 2019, which can be related to the drought conditions observed that year, as was confirmed by the Spearman negative correlation between this parameter and cumulative precipitation ($R = -0.330$; $p < 0.05$) (Table 2). The highest pH values occurred in H16 during the summer period of 2018 and 2019; the lowest value was registered in H5, at the end of 2020. The results highlighted that the increase in pH is negatively correlated with precipitation ($R = -0.371$; $p < 0.05$), indicating that higher frequency of dry periods may be negatively influencing some irrigation water quality parameters, such as pH and EC_W.

The dominant ion in most samples was Cl, followed by Na. Overall, the order of cation abundance was Na > Ca > Mg > B. Regarding nitrate, in general, all concentrations quantified in the hydrant system were within the values stipulated for good water quality for irrigation. Exceptionally high nitrate concentrations were observed in October 2019 in H23 (15.7 mg L^{-1}) and in June 2020 in H6 (26.7 mg L^{-1}), classifying the water as having mild to moderate use restrictions, according to the FAO guidelines. As these values did not occur in the Lage reservoir in the same sampling period, as reported by [49], where

maximum NO_3 concentrations were <5 mg L^{-1}, the concentrations may be correlated with contamination with some liquid formulation of nitrogen fertilizer (a common practice in the area), which could have occurred in the conveyance system. Despite the common origin of water, localized phenomena, like contamination or degradation within the pipeline infrastructure, may occasionally lead to deviations in water quality at the hydrant level. As reported in drinking water distribution systems, chemicals may be released from materials and equipment either by leaching due to contact with water or through corrosion in deteriorating pipes [50,51].



Drought	Beggining	End	Duration	SPI min	Magnitude	Average intensity
1	1 December 2018	1 April 2019	5	−1.67	4.14	0.83
2	1 May 2019	1 August 2019	4	−2.73	4.40	1.10
3	1 September 2019	1 November 2019	3	−1.18	2.17	0.72
4	1 February 2020	1 March 2020	2	−2.76	3.43	1.71

Figure 3. Monthly Standard Precipitation Index (SPI) during the study period. Droughts are identified with full yellow bars (yellow bars outlined in blue represent the end of a drought; blue bars represent monthly SPI with no drought). The table below the graph characterizes each drought for duration (months), minimum SPI value, magnitude, and intensity, according to [37].

According to the FAO guidelines, no potential salinity problem was detected, as EC_W values were persistently lower than 0.7 dS m^{-1} (Tables S2–S4). A slight to moderate risk of soil sodification prevailed, which should be carefully monitored, especially since the predominant soils in the study area are fine-textured and sprinkler-irrigated crops occupy a large area, potentially leading to adverse impacts on soil structure due to adsorbed Na [52]. This mild to moderate risk has already been observed at both the Alqueva and the Lage

reservoirs [24,49], suggesting that the irrigation conveyance network does not significantly alter these parameters, namely, potential salinity issues and the risk of soil sodification.

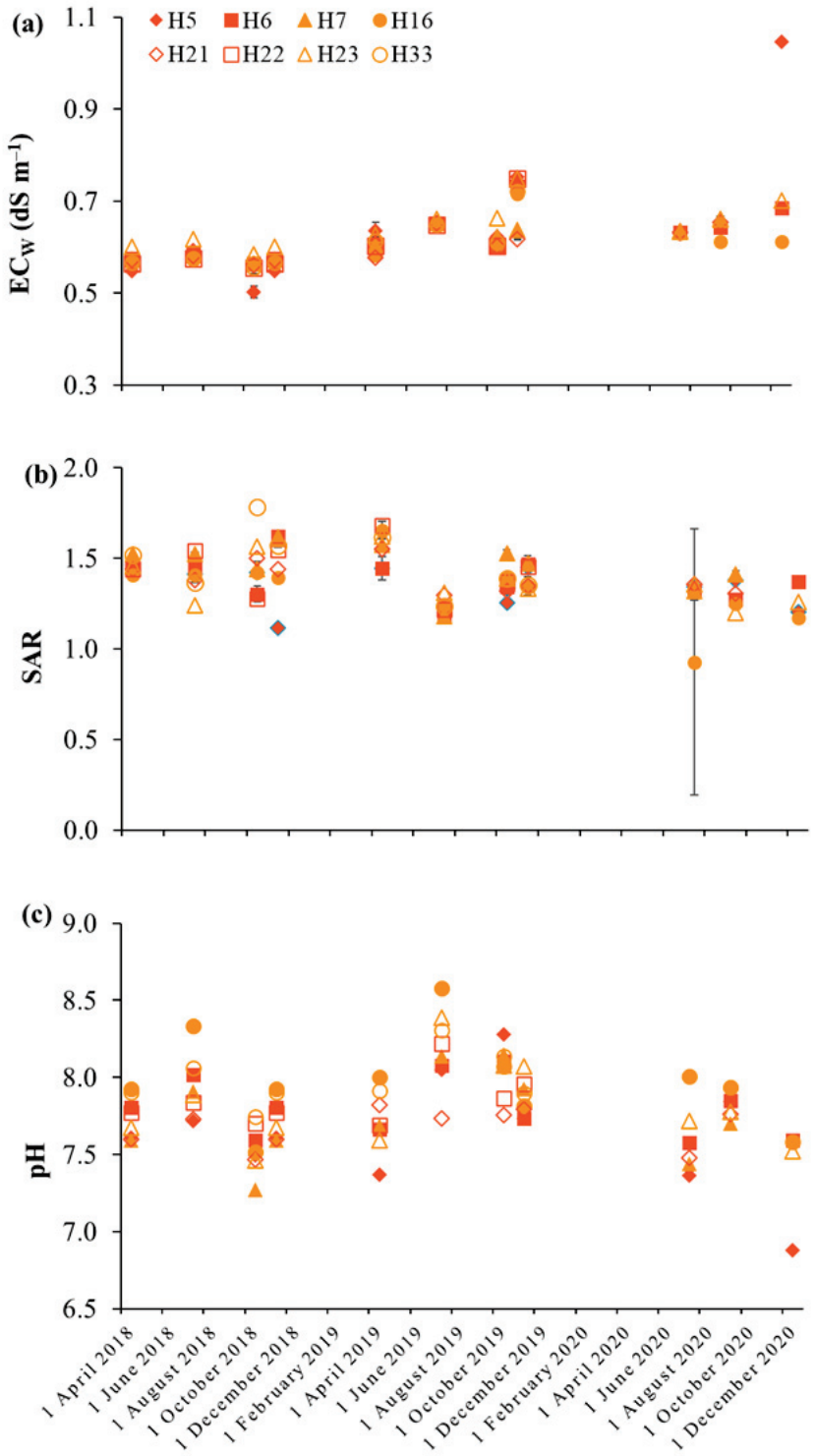


Figure 4. Temporal variation of water (**a**) EC_W, (**b**) SAR, and (**c**) pH during the period of study (12 sampling campaigns), for each hydrant. Markers represent the mean and whiskers represent the standard deviation for three repetitions.

Except for H16 (supplied by the Montinhos reservoir) in mid-season 2019, pH values remained within the normal range. In the study by [49], pH values measured in the Lage reservoir during 2019, the driest year, exceeded the upper limit (pH > 8.4). However, no

similar trend was observed in the hydrant network; in other words, no spatial decline in pH was detected. This represents the most significant difference between the reservoirs and the hydrant system in terms of irrigation water quality assessment.

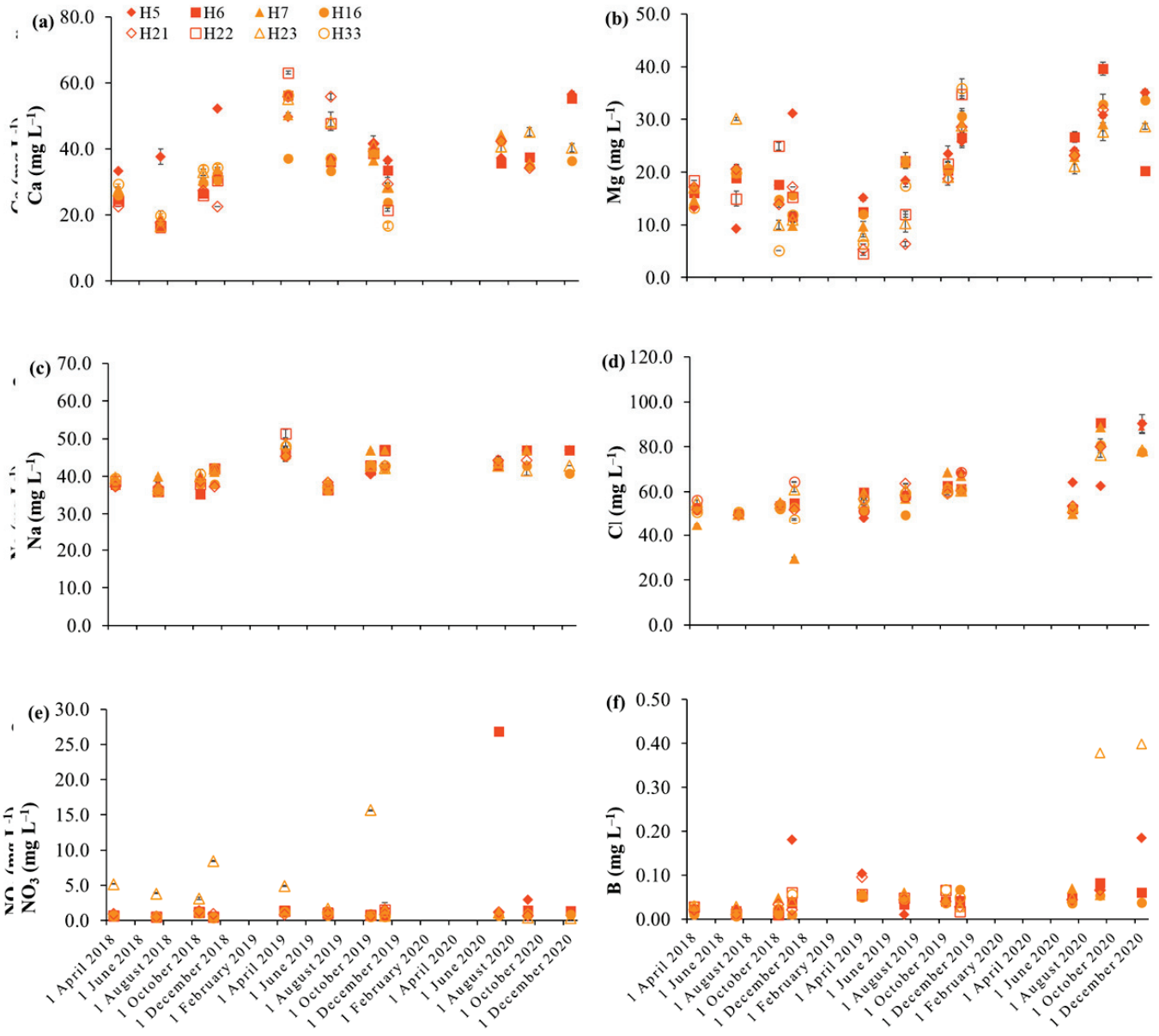


Figure 5. Temporal variation of water ion concentrations ((**a**) Ca, (**b**) Mg, (**c**) Na, (**d**) Cl, (**e**) NO_3, and (**f**) B) during the period of study (12 sampling campaigns), for each hydrant. Markers represent the mean and whiskers represent the standard deviation for three repetitions. (**a**) Ca, (**b**) Mg, (**c**) Na, (**d**) Cl, (**e**) NO_3, and (**f**) B.

3.3. Correlation, Factor Analysis, and Cluster Analysis

To better understand the interactions between chemical parameters and meteorological conditions, exploratory analyses using multivariate statistical methods were conducted. The Spearman correlation coefficient of 11 variables, including water physical-chemical parameters (EC_W, SAR, and pH), ions concentrations (Ca, Mg, Na, Cl, NO_3, and B), as well as cumulative precipitation (P_{cum}) and cumulative reference evapotranspiration ($ET0_{cum}$) until each sampling date, can be observed in Table 2.

Table 2. *Spearman* correlation matrix and heat map of water physical–chemical parameters and climate variables. Bold values are significant at $p < 0.05$.

P_{cum}	$ET0_{cum}$	pH	ECw	B	Ca	Mg	Na	Cl	NO_3	SAR	
1.000	**0.294**	**−0.371**	**−0.330**	−0.168	**−0.387**	0.105	**−0.258**	−0.076	−0.111	0.010	**P_{cum}**
	1.000	0.115	**0.401**	**0.220**	−0.040	**0.492**	**0.205**	**0.615**	−0.040	**−0.278**	**$ET0_{cum}$**
		1.000	0.193	−0.069	−0.112	0.137	−0.175	0.071	−0.183	−0.171	**pH**
	<0.200		1.000	**0.493**	**0.393**	**0.529**	**0.426**	**0.576**	**0.250**	**−0.454**	**ECw**
	0.200–0.400			1.000	**0.622**	0.190	**0.581**	**0.444**	0.126	−0.186	**B**
	0.400–0.600				1.000	−0.073	**0.485**	**0.251**	0.139	**−0.238**	**Ca**
	>0.600					1.000	**0.239**	**0.429**	−0.084	**−0.624**	**Mg**
	<−0.600						1.000	**0.425**	**0.228**	**0.220**	**Na**
	−0.600–−0.400							1.000	**0.222**	**−0.282**	**Cl**
	−0.400–−0.200								1.000	0.106	**NO_3**
	>−0.200									1.000	**SAR**

The higher significant correlation coefficients (>|0.6|) occurred between [Ca] and [B], [Cl] and $ET0_{cum}$, and SAR and [Mg], highlighting the influence of low Mg concentrations on SAR values. Other highly significant correlation coefficients (>0.5) could be found between [Mg] and EC_W, between [Na] and [B], and [Cl] and EC_W. Regarding correlations between meteorological variables and water physical-chemical parameters, $ET0_{cum}$ was significantly and positively correlated with EC_W, [B], [Mg], [Na], and [Cl], pointing to an influence of high evaporative demand conditions on water salinity, and negatively correlated with SAR; P_{cum} was significantly and positively correlated with $ET0_{cum}$, and negatively correlated with pH, EC_W, [Ca], and [Na], thereby indicating that lower precipitation induced by drought is related to a decline in water quality, as highlighted by other studies on drought impacts on agricultural water quality [24,53,54]. Furthermore, the absence of strong correlations between metals, as is the case of Mg and Na (0.239) and Mg and Ca (−0.073), suggests that these chemicals may have different sources, such as anthropogenic activities (mineral fertilizers) and geologic origins through the natural weathering of carbonate and silicate rocks [55,56].

The relationships observed among variables translated into a three-factor model accounting for around 61% of the total variance in the dataset (Table 3). Factor 1 explained 29% of the variance and presented high positive loadings of $ET0_{cum}$ (0.691), EC_W (0.703), [Cl] (0.751), and [Mg] (0.879), while a moderate positive loading was observed in [B] (0.356).

A high negative loading in Factor 1 belonged to SAR (−0.574). Therefore, Factor 1 was influenced by salinity, given the high weights of EC_W, [Cl], and [Mg]. Factor 2 was responsible for explaining approximately 19% of the total variance and represented a sodicity factor as it was mainly related to [Na] (0.759) and SAR (0.666). Factor 3 represented 14% of the total variance and was positively influenced by P_{cum} (0.887) and $ET0_{cum}$ (0.318) and negatively correlated with pH (−0.693); thus, it can be considered as a climate factor.

When analyzing the score plot of cases of the first two factors, patterns of case gatherings that were year-controlled (Figure 6a) and crop irrigation stage-controlled (Figure 6b) can be recognized. The same did not apply to the grouping of cases by location (hydrants) (Figure 6c).

Table 3. Factor loadings, eigenvalues, and percentage of total variance in a three-factor model of 11 observed variables. Bold values correspond to the higher absolute factor loadings of the variables in each factor.

	Factor 1	Factor 2	Factor 3
P_{cum}	0.099	−0.142	**0.887**
$ET0_{cum}$	**0.691**	0.090	0.318
pH	0.076	−0.289	**−0.693**
ECw	**0.703**	0.156	−0.102
B	**0.356**	−0.135	0.229
Ca	−0.052	0.203	**−0.206**
Mg	**0.879**	−0.128	0.024
Na	0.215	**0.759**	−0.096
Cl	**0.751**	0.140	0.065
NO_3	0.133	**0.511**	−0.117
SAR	**−0.574**	**0.666**	0.144
Eigenvalues	3.160	2.057	1.485
% Total variance	28.73	18.70	13.50

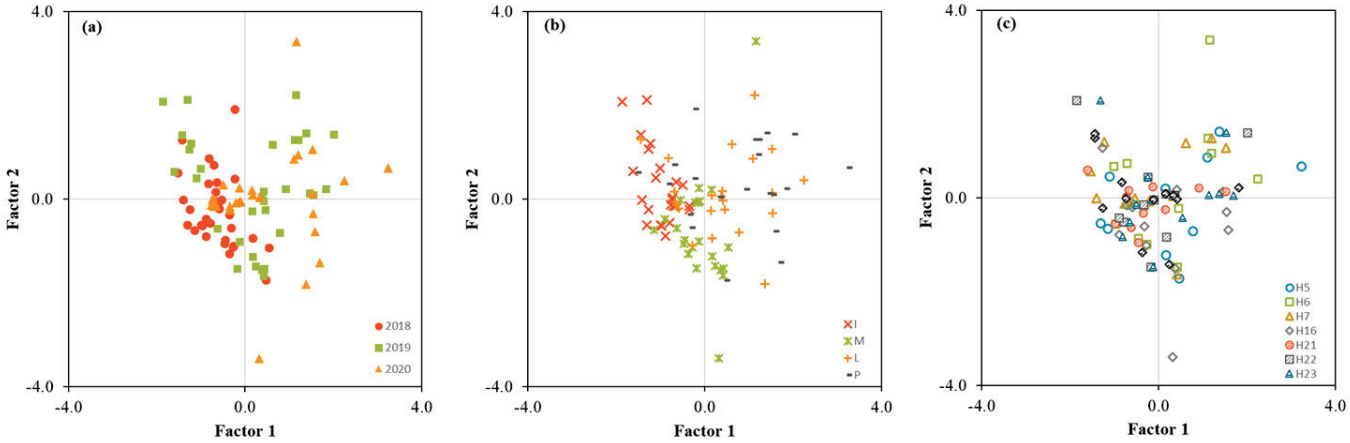


Figure 6. Score plots of cases of the first two factors. Different shapes and colors in each graphic differentiate the year (**a**), stage of irrigation season: I—Initial; M—Middle; L—Late; and P—Post-cycle (**b**), and hydrant (**c**).

To clarify these groupings of cases, a CA was performed, yielding the following cluster structure (Figure 7):

- Cluster 1, positively related to salinity (Factor 1) and sodicity (Factor 2), was composed of 16 cases, with no samples in 2018, eight cases in 2019, and eight cases in 2020; cases were mostly of the Post-cycle (P) stage (10 samples). This structure suggests a degradation of water quality following the peak water demand by crops in Mediterranean regions, that is, a pattern of salt accumulation in water sources resulting from high evapotranspiration during summer and limited water recharge due to drought occurrence and expansion of irrigation areas [57,58].
- Cluster 2, in the second quadrant, thus positively related to salinity, grouped 32 cases, mainly in 2019 (14 samples), with the remaining equally distributed between 2018 and 2020 cases; no samples belonged to the initial period, being mostly of the Middle (M) (13) and Late (L) (11) stages. This result reinforces the idea of the cumulative effects of evaporation and decreased freshwater recharge as the season progresses. A similar trend was reported by [59] in an irrigation district in southern Portugal, where the risk of salinity build-up was high to very high during very dry years in most fields.

In wetlands located in arid/semi-arid zones, periods of higher salinity can occur as a consequence of the highly evaporative conditions and water resources' depletion [60].

- Cluster 3, negatively related to both salinity and sodicity, presented 32 samples, largely of 2018 (18) and 2020 (13), from the I (16) and M (9) stages of the irrigation season.
- Cluster 4, in the 4th quadrant, grouped 13 samples of 2018 (5) and 2019 (8), the majority being of the I (8) period. Together with Cluster 4, this structure reflects the dilution effect of winter rainfall, which improves water quality at the start of the spring–summer crop cycle.

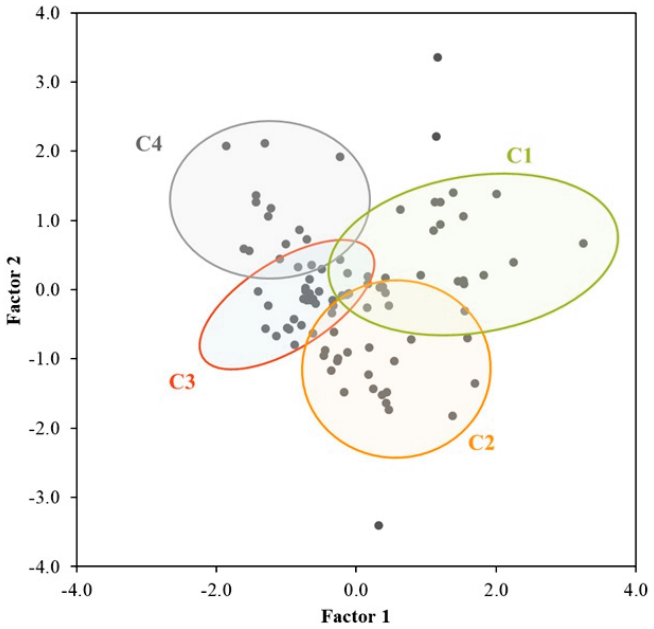


Figure 7. Score plot of cases of the first two factors with ellipses representing significant clusters with dlink/dmax ∗ 100 < 40%.

All in all, this cluster composition reveals two key effects: a drought-induced impact that intensifies salinity and sodicity levels and a seasonal influence associated with different stages of the irrigation calendar and crop cycles. Therefore, the groupings obtained confirmed the trends identified in the FA results, providing further support for the temporal patterns observed in irrigation water quality. In a study on the spatial and temporal variability of irrigation water quality in a large reservoir during a drought year, ref. [24] reported similar results, with a more time- than space-controlled pattern of sample clustering.

3.4. Random Forest and Gradient Boosting Models

All three RF models demonstrated satisfactory predictive performance, with particularly better results for SAR and EC_W (Table 4). The model predicting SAR achieved an R^2 of 0.622, a root mean square error (RMSE) of 0.106, and a mean absolute error (MAE) of 0.064, indicating a good predictive accuracy and low residual error. Similarly, the ECw model reached an R^2 of 0.605, an RMSE of 0.021, and an MAE of 0.015, which supports its applicability for forecasting. The pH model presented lower predictive capacity, with R^2 = 0.485, MAE = 0.146, and RMSE = 0.175, suggesting a more complex relationship between predictors and pH dynamics. All RF models exhibited low relative bias (RBIAS); namely, +1.27% for EC_W, +1.46% for SAR, and +0.63% for pH, demonstrating that the predictions were not affected by systematic over- or underestimation.

Table 4. Performance statistics of the Random Forest (RF) and Gradient Boosting (GB) models for the prediction of ECw, SAR, and pH.

Variable	Model	R^2	RMSE	MAE	RBIAS (%)
ECw	**RF**	0.605	0.021	0.015	1.266
	GB	0.362	0.001	0.017	2.116
SAR	**RF**	0.622	0.106	0.064	1.462
	GB	0.670	0.099	0.058	1.306
pH	**RF**	0.485	0.175	0.146	0.626
	GB	0.256	0.044	0.161	0.733

In the case of GB, the model performance for predicting SAR was slightly better than in the RF regression (R^2 = 0.670, RMSE = 0.099; MAE = 0.058, and RBIAS = 1.306%) but presented a lower predictive capacity both for ECw and pH. The RBIAS remained low but was generally higher than in the RF regression. Overall, the performance metrics showed that the RF was a better model to predict water quality parameters from chemical and meteorological data. These results follow [30,31], which found RF as one of the models with higher accuracy in the prediction of irrigation water quality indices like SAR, exchangeable sodium percentage (ESP), or total dissolved solids (TDS), making it a good model to be used in water quality forecasting in general but also, as our results show, under drier conditions by using different combinations of chemical and meteorological variables.

The feature importance in RF was assessed using the MDI. Results showed distinct variable contributions across the target variables (Figure 8). For EC_W, the most relevant predictors were $ET0_{cum}$ (23.6%), Cl (21.1%), and Ca (19.1%), pointing out the influence of evapotranspiration and ion concentrations, especially chloride and calcium, on salinity levels (Figure 8a). The SAR model was largely determined by Mg (47.3%) and Na (15.1%), which was expected given their central role in SAR calculation. P_{cum} was one of the contributors, although having a lower weight (Figure 8b).

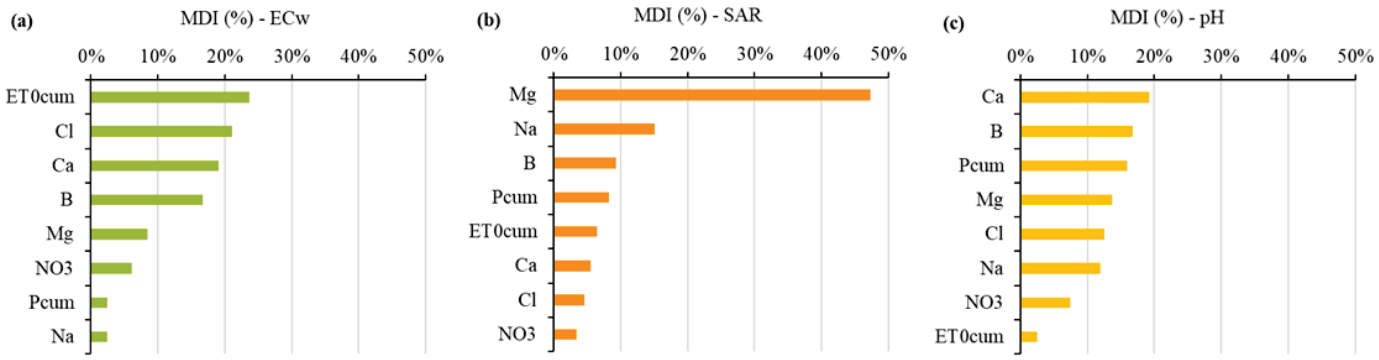


Figure 8. Feature importance of the predictor variables in the RF models, measured by the mean decrease in impurity (MDI). (**a**) EC_W; (**b**) SAR; and (**c**) pH.

In the pH model, the most influential variables were Ca (19.2%), B (16.7%), and P_{cum} (16.0%), followed by Mg and Cl. This result suggests that the acid–base balance in irrigation water is influenced by both precipitation-related dilution and the presence of alkaline earth metals (Figure 8c).

Scatterplots of observed versus predicted values confirmed the quantitative performance of the RF models (Figure 9). Both EC_W and SAR showed high correlations of 0.812 and 0.881, respectively. The pH predictions, while slightly more dispersed, are still well associated with the observed data, with a correlation of 0.772, validating the model structure for exploratory or decision support purposes.

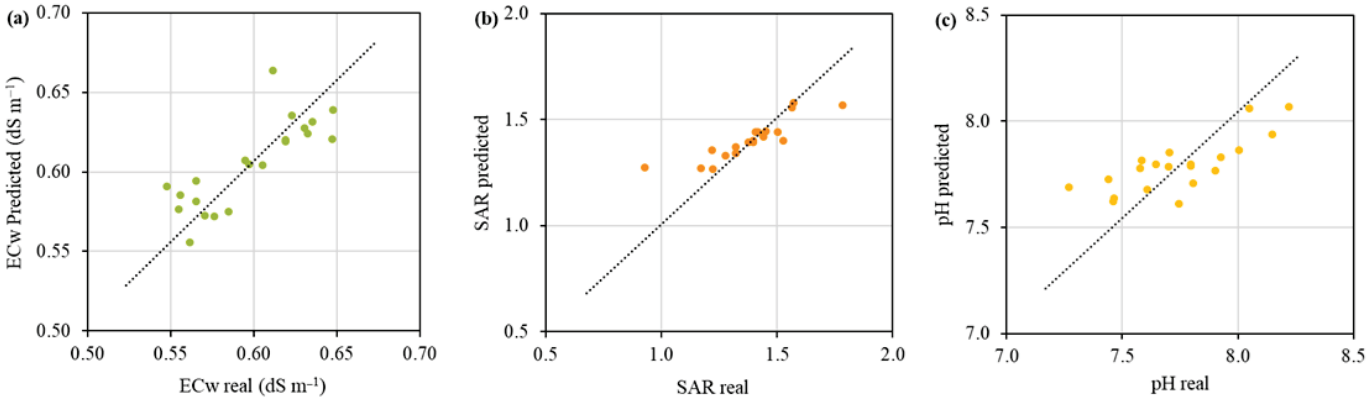


Figure 9. Scatterplots of real versus predicted values of (**a**) ECw (r = 0.812), (**b**) SAR (r = 0.881), and (**c**) pH (r = 0.772), obtained by the RF model.

These results indicate that the models may serve as early warning systems, allowing water management authorities and farmers to anticipate potential water quality deterioration, decline in crop productivity, and long-term degradation of soils due to salt accumulation [24].

To achieve a salt equilibrium in the soil, the influx of salt must be compensated for by salt removal, hence ensuring long-term salt sustainability in irrigated areas [61]. Therefore, the ability to predict irrigation water quality makes it easier to suggest suitable agricultural water management practices to mitigate negative effects, such as the following:

Preventive irrigation practices, such as the application of leaching fractions and suitably designed subsurface drainage systems [62,63];

Optimized irrigation timing to maintain favorable soil moisture levels [64,65];

Management of fertilizers to prevent excessive nutrient application rates, which contribute to soluble salt accumulation [66];

Selection of salt-tolerant crops [67];

Precision irrigation technologies, such as variable rate irrigation (VRI) to increase irrigation uniformity and efficiency [68];

Application of soil chemical amendments, e. g., gypsum, for sodicity control, facilitating the removal of Na ions and their replacement with Ca in the soil exchange complex [61,67].

4. Conclusions

The results in this study indicate that in small-scale hydro-agricultural irrigation systems, changes in irrigation water quality parameters within the conveyance network are not substantial and the water quality monitoring scheme can be focused on the reservoir, although safeguarding temporal scales that attend to the occurrence of extreme meteorological events and disruption of the regular trends typical of Mediterranean climate.

The dynamics of water quality for irrigation are linked to climate patterns. Dry weather during the crop growth cycle, corresponding to the irrigation campaigns, can exacerbate salinity and sodicity problems.

The RF and GB models show good predictive capability of water quality based on ion concentrations and meteorological data, with the RF model presenting, globally, better performance metrics in our study.

In agricultural water management under drought conditions, the application of ML algorithms to predict irrigation water quality based on chemical and meteorological variables can be a significant advancement, particularly in the implementation of early warning systems and the adoption of preventive measures to maintain soil health and crop yields.

Supplementary Materials: The following supporting information can be downloaded at: https://www.mdpi.com/article/10.3390/w17121783/s1 (containing Tables S1, S2, S3, and S4). Table S1. FAO guidelines for interpretation of water quality for irrigation (Ayers and Westcot 1985 [40]); Table S2. Irrigation water quality evaluation according to the FAO Guidelines—2018; Table S3. Irrigation water quality evaluation according to the FAO Guidelines—2019; Table S4 Irrigation water quality evaluation according to the FAO Guidelines—2020.

Author Contributions: Conceptualization, A.T. and P.P.; methodology, A.T.; software, P.T.; formal analysis, A.T. and P.T.; investigation, A.T., A.C., M.F., and P.P.; writing—original draft preparation, A.T.; writing—review and editing, A.T.; visualization, A.T.; supervision, P.P.; project administration, P.P.; funding acquisition, A.T. and P.P. All authors have read and agreed to the published version of the manuscript.

Funding: This work is a contribution to the projects CREATE (UIDB/06107/2023) and Geobiotec (UIDB/04035/2023), both funded by FCT—Fundação para a Ciência e a Tecnologia, Portugal, and for the FitoFarmGest Operational Group (PDR2020-101-030926). Adriana Catarino gratefully acknowledges funding from the Fundação para a Ciência e a Tecnologia, Portugal, under the PhD grant 2023.04004.BD.

Data Availability Statement: The raw data supporting the conclusions of this article will be made available by the authors on request.

Acknowledgments: During the preparation of this manuscript, the authors used Grammarly for grammar and spelling checking purposes and ChatGPT (OpenAI) for English phrasing and structure in some parts of the manuscript. The authors have reviewed and edited the output and take full responsibility for the content of this publication.

Conflicts of Interest: Author Patrícia Palma is currently serving on the Board of Directors of Águas Públicas do Alentejo (AgdA) under a public interest secondment. All authors declare that the research was conducted in the absence of any commercial or financial relationships that could be construed as a potential conflict of interest.

References

1. Trnka, M.; Olesen, J.E.; Kersebaum, K.C.; Skjelvåg, A.O.; Eitzinger, J.; Seguin, B.; Peltonen-Sainio, P.; Rötter, R.; Iglesias, A.; Orlandini, S.; et al. Agroclimatic Conditions in Europe under Climate Change. *Glob. Change Biol.* **2011**, *17*, 2298–2318. [CrossRef]
2. Páscoa, P.; Gouveia, C.M.; Russo, A.; Trigo, R.M. Drought Trends in the Iberian Peninsula over the Last 112 Years. *Adv. Meteorol.* **2017**, *2017*, 4653126. [CrossRef]
3. Jones, E.; van Vliet, M.T.H. Drought Impacts on River Salinity in the Southern US: Implications for Water Scarcity. *Sci. Total Environ.* **2018**, *644*, 844–853. [CrossRef]
4. de León, G.S.; Ramos-Leal, J.A.; Ramírez, J.M.; Almanza-Tovar, O.G. Drought and Water Quality in a Semi-Arid Area: Effects in Livestock Production, Agriculture and Use Urban. *Water Resour. Manag.* **2025**, *39*, 1605–1621. [CrossRef]
5. Whitehead, P.G.; Wilby, R.L.; Battarbee, R.W.; Kernan, M.; Wade, A.J. A Review of the Potential Impacts of Climate Change on Surface Water Quality. *Hydrol. Sci. J.* **2009**, *54*, 101–123. [CrossRef]
6. Delpla, I.; Jung, A.-V.; Baures, E.; Clement, M.; Thomas, O. Impacts of Climate Change on Surface Water Quality in Relation to Drinking Water Production. *Environ. Int.* **2009**, *35*, 1225–1233. [CrossRef]
7. Cañedo-Argüelles, M.; Kefford, B.J.; Piscart, C.; Prat, N.; Schäfer, R.B.; Schulz, C.-J. Salinisation of Rivers: An Urgent Ecological Issue. *Environ. Pollut.* **2013**, *173*, 157–167. [CrossRef]
8. Mosley, L.M. Drought Impacts on the Water Quality of Freshwater Systems; Review and Integration. *Earth-Sci. Rev.* **2015**, *140*, 203–214. [CrossRef]
9. Phogat, V.; Cox, J.W.; Šimůnek, J. Identifying the Future Water and Salinity Risks to Irrigated Viticulture in the Murray-Darling Basin, South Australia. *Agric. Water Manag.* **2018**, *201*, 107–117. [CrossRef]
10. Cramer, W.; Guiot, J.; Fader, M.; Garrabou, J.; Gattuso, J.-P.; Iglesias, A.; Lange, M.A.; Lionello, P.; Llasat, M.C.; Paz, S.; et al. Climate Change and Interconnected Risks to Sustainable Development in the Mediterranean. *Nat. Clim. Change* **2018**, *8*, 972–980. [CrossRef]
11. Wenng, H.; Bechmann, M.; Krogstad, T.; Skarbøvik, E. Climate Effects on Land Management and Stream Nitrogen Concentrations in Small Agricultural Catchments in Norway. *Ambio* **2020**, *49*, 1747–1758. [CrossRef] [PubMed]
12. Li, Z.; Fang, H. Impacts of Climate Change on Water Erosion: A Review. *Earth-Sci. Rev.* **2016**, *163*, 94–117. [CrossRef]

13. Ramião, J.P.; Pascoal, C.; Pinto, R.; Carvalho-Santos, C. Mitigating Water Pollution in a Portuguese River Basin under Climate Change through Agricultural Sustainable Practices. *Mitig. Adapt. Strateg. Glob. Change* **2024**, *29*, 25. [CrossRef]
14. Eswar, D.; Karuppusamy, R.; Chellamuthu, S. Drivers of Soil Salinity and Their Correlation with Climate Change. *Curr. Opin. Environ. Sustain.* **2021**, *50*, 310–318. [CrossRef]
15. Palma, P.; Köck-Schulmeyer, M.; Alvarenga, P.; Ledo, L.; Barbosa, I.R.; López de Alda, M.; Barceló, D. Risk Assessment of Pesticides Detected in Surface Water of the Alqueva Reservoir (Guadiana Basin, Southern of Portugal). *Sci. Total Environ.* **2014**, *488–489*, 208–219. [CrossRef]
16. Alves-Ferreira, J.; Vara, M.G.; Catarino, A.; Martins, I.; Mourinha, C.; Fabião, M.; Costa, M.J.; Barbieri, M.V.; de Alda, M.L.; Palma, P. Pesticide Water Variability and Prioritization: The First Steps towards Improving Water Management Strategies in Irrigation Hydro-Agriculture Areas. *Sci. Total Environ.* **2024**, *917*, 170304. [CrossRef]
17. Cerdà, A.; Daliakopoulos, I.N.; Terol, E.; Novara, A.; Fatahi, Y.; Moradi, E.; Salvati, L.; Pulido, M. Long-Term Monitoring of Soil Bulk Density and Erosion Rates in Two Prunus Persica (L) Plantations under Flood Irrigation and Glyphosate Herbicide Treatment in La Ribera District, Spain. *J. Environ. Manag.* **2021**, *282*, 111965. [CrossRef] [PubMed]
18. FAO. *The State of the World's Land and Water Resources for Food and Agriculture–Systems at Breaking Point*; Main Report; Food and Agriculture Organization of the United Nations: Rome, Italy, 2022.
19. Hillel, D.; Braimoh, A.K.; Vlek, P.L.G. Soil Degradation Under Irrigation. In *Land Use and Soil Resources*; Braimoh, A.K., Vlek, P.L.G., Eds.; Springer: Dordrecht, The Netherlands, 2008; pp. 101–119. ISBN 978-1-4020-6778-5.
20. Tomaz, A.; Costa, M.J.; Coutinho, J.; Dôres, J.; Catarino, A.; Martins, I.; Mourinha, C.; Guerreiro, I.; Pereira, M.M.; Fabião, M.; et al. Applying Risk Indices to Assess and Manage Soil Salinization and Sodification in Crop Fields within a Mediterranean Hydro-Agricultural Area. *Water* **2021**, *13*, 3070. [CrossRef]
21. Qadir, M.; Quillérou, E.; Nangia, V.; Murtaza, G.; Singh, M.; Thomas, R.J.; Drechsel, P.; Noble, A.D. Economics of Salt-Induced Land Degradation and Restoration. *Nat. Resour. Forum.* **2014**, *38*, 282–295. [CrossRef]
22. Mateo-Sagasta, J.; Burke, J. *Agriculture and Water Quality Interactions: A Global Overview*; SOLAW Background Thematic Report-TR08; Food and Agriculture Organization of the United Nations: Rome, Italy, 2010.
23. Hillel, D. *Salinity Management for Sustainable Irrigation: Integrating Science, Environment, and Economics*; The World Bank: Washington, DC, USA, 2000; ISBN 978-0-8213-4773-7.
24. Tomaz, A.; Palma, P.; Fialho, S.; Lima, A.; Alvarenga, P.; Potes, M.; Salgado, R. Spatial and Temporal Dynamics of Irrigation Water Quality under Drought Conditions in a Large Reservoir in Southern Portugal. *Environ. Monit. Assess.* **2020**, *192*, 93. [CrossRef]
25. Abbas, F.; Cai, Z.; Shoaib, M.; Iqbal, J.; Ismail, M.; Arifullah; Alrefaei, A.F.; Albeshr, M.F. Machine Learning Models for Water Quality Prediction: A Comprehensive Analysis and Uncertainty Assessment in Mirpurkhas, Sindh, Pakistan. *Water* **2024**, *16*, 941. [CrossRef]
26. Kamel Elshaarawy, M.; Eltarabily, M.G. Machine Learning Models for Predicting Water Quality Index: Optimization and Performance Analysis for El Moghra, Egypt. *Water Supply* **2024**, *24*, 3269–3294. [CrossRef]
27. Mohan, S.; Kumar, B.; Nejadhashemi, A.P. Integration of Machine Learning and Remote Sensing for Water Quality Monitoring and Prediction: A Review. *Sustainability* **2025**, *17*, 998. [CrossRef]
28. Shams, M.Y.; Elshewey, A.M.; El-kenawy, E.-S.M.; Ibrahim, A.; Talaat, F.M.; Tarek, Z. Water Quality Prediction Using Machine Learning Models Based on Grid Search Method. *Multimed. Tools Appl.* **2024**, *83*, 35307–35334. [CrossRef]
29. Alnahit, A.O.; Mishra, A.K.; Khan, A.A. Stream Water Quality Prediction Using Boosted Regression Tree and Random Forest Models. *Stoch. Environ. Res. Risk Assess.* **2022**, *36*, 2661–2680. [CrossRef]
30. El Bilali, A.; Taleb, A.; Brouziyne, Y. Groundwater Quality Forecasting Using Machine Learning Algorithms for Irrigation Purposes. *Agric. Water Manag.* **2021**, *245*, 106625. [CrossRef]
31. El Bilali, A.; Taleb, A. Prediction of Irrigation Water Quality Parameters Using Machine Learning Models in a Semi-Arid Environment. *J. Saudi Soc. Agric. Sci.* **2020**, *19*, 439–451. [CrossRef]
32. Mokhtar, A.; Elbeltagi, A.; Gyasi-Agyei, Y.; Al-Ansari, N.; Abdel-Fattah, M.K. Prediction of Irrigation Water Quality Indices Based on Machine Learning and Regression Models. *Appl. Water Sci.* **2022**, *12*, 76. [CrossRef]
33. El Bilali, A.; Taleb, A. State-of-the Art-on Irrigation Water Quality Management Using Data-Driven Methods: Practical Application, Limitations, and Prospective Directions. *Phys. Chem. Earth Parts A/B/C* **2024**, *136*, 103794. [CrossRef]
34. *IUSS Working Group WRB World Reference Base for Soil Resources 2014, Update 2015*; FAO: Rome, Italy, 2014.
35. IPMA Climate Normals-1981-2010-Beja. Available online: https://www.ipma.pt/en/oclima/normais.clima/1981-2010/#562 (accessed on 6 June 2024).
36. COTR SAGRA-Sistema Agrometeorológico Para a Gestão Da Rega No Alentejo (Agrometeorological System for Irrigation Management in Alentejo). Available online: http://www.cotr.pt/servicos/sagranet.php (accessed on 5 January 2025).
37. McKee, T.B.; Doesken, N.J.; Kleist, J. The Relationship of Drought Frequency and Duration to Time Scales. In Proceedings of the 8th Conference on Applied Climatology, American Meteorological Society, Anaheim, CA, USA, 17–22 January 1993; pp. 179–184.

38. IPMA Long Series (Beja). Available online: https://www.ipma.pt/pt/oclima/series.longas/?loc=Beja&type=raw (accessed on 2 April 2025).
39. *APHA Standard Methods for the Examination of Water and Wastewater*, 20th ed.; American Public Health Association, American Water Works Association and Water Environmental Federation: Washington, DC, USA, 1998.
40. Ayers, R.S.; Westcot, D.W. Water Quality for Agriculture. In *FAO Irrigation and Drainage Paper*; Food and Agriculture Organization of the United Nations: Rome, Italy, 1985; ISBN 978-92-5-102263-4.
41. Tomaz, A.; Palma, J.F.; Ramos, T.; Costa, M.N.; Rosa, E.; Santos, M.; Boteta, L.; Dôres, J.; Patanita, M. Yield, Technological Quality and Water Footprints of Wheat under Mediterranean Climate Conditions: A Field Experiment to Evaluate the Effects of Irrigation and Nitrogen Fertilization Strategies. *Agric. Water Manag.* **2021**, *258*, 107214. [CrossRef]
42. Tomaz, A.; Martins, I.; Catarino, A.; Mourinha, C.; Dôres, J.; Fabião, M.; Boteta, L.; Coutinho, J.; Patanita, M.; Palma, P. Insights into the Spatial and Temporal Variability of Soil Attributes in Irrigated Farm Fields and Correlations with Management Practices: A Multivariate Statistical Approach. *Water* **2022**, *14*, 3216. [CrossRef]
43. StatSoft, Inc. *STATISTICA (Data Analysis Software System)*; Scientific Research: Wuhan, China, 2004.
44. Breiman, L. Random Forests. *Mach. Learn.* **2001**, *45*, 5–32. [CrossRef]
45. Friedman, J. Greedy Function Approximation: A Gradient Boosting Machine. *Ann. Stat.* **2000**, *29*, 1189–1232. [CrossRef]
46. Sharma, A.; Jain, A.; Gupta, P.; Chowdary, V. Machine Learning Applications for Precision Agriculture: A Comprehensive Review. *IEEE Access* **2021**, *9*, 4843–4873. [CrossRef]
47. Pedregosa, F.; Varoquaux, G.; Gramfort, A.; Michel, V.; Thirion, B.; Grisel, O.; Blondel, M.; Prettenhofer, P.; Weiss, R.; Dubourg, V.; et al. Scikit-Learn: Machine Learning in Python. *J. Mach. Learn. Res.* **2012**, *12*, 2825–2830.
48. IPMA Drought Monitoring. Available online: https://www.ipma.pt/pt/oclima/observatorio.secas/ (accessed on 30 August 2023).
49. Catarino, A.; Martins, I.; Mourinha, C.; Santos, J.; Tomaz, A.; Anastácio, P.; Palma, P. Water Quality Assessment of a Hydro-Agricultural Reservoir in a Mediterranean Region (Case Study—Lage Reservoir in Southern Portugal). *Water* **2024**, *16*, 514. [CrossRef]
50. *World Health Organization Water Safety in Distribution Systems*; WHO Document Production Services: Geneva, Switzerland, 2014.
51. Tong, H.; Li, Z.; Hu, X.; Xu, W.; Li, Z. Metals in Occluded Water: A New Perspective for Pollution in Drinking Water Distribution Systems. *Int. J. Environ. Res. Public Health* **2019**, *16*, 2849. [CrossRef]
52. Tomaz, A.; Palma, P.; Fialho, S.; Lima, A.; Alvarenga, P.; Potes, M.; Costa, M.; Salgado, R. Risk Assessment of Irrigation-Related Soil Salinization and Sodification in Mediterranean Areas. *Water* **2020**, *12*, 3569. [CrossRef]
53. do Nascimento, T.V.M.; de Oliveira, R.P.; Condesso de Melo, M.T. Impacts of Large-Scale Irrigation and Climate Change on Groundwater Quality and the Hydrological Cycle: A Case Study of the Alqueva Irrigation Scheme and the Gabros de Beja Aquifer System. *Sci. Total Environ.* **2024**, *907*, 168151. [CrossRef]
54. Peña-Guerrero, M.D.; Nauditt, A.; Muñoz-Robles, C.; Ribbe, L.; Meza, F. Drought Impacts on Water Quality and Potential Implications for Agricultural Production in the Maipo River Basin, Central Chile. *Hydrol. Sci. J.* **2020**, *65*, 1005–1021. [CrossRef]
55. Liu, D.; Yu, H.; Feng, H.; Gao, H.; Zhu, Y. Revealing Heavy Metal Correlations with Water Quality and Tracking Its Latent Factors by Canonical Correlation Analysis and Structural Equation Modeling in Dongjianghu Lake. *Environ. Monit. Assess.* **2021**, *193*, 717. [CrossRef]
56. Appelo, C.A.J.; Postma, D. *Geochemistry, Groundwater and Pollution*, 2nd ed.; A.A. Balkema Publishers: Amsterdam, The Netherlands, 2005; ISBN 04-1536-421-3.
57. Chartzoulakis, K.; Bertaki, M. Sustainable Water Management in Agriculture under Climate Change. *Agric. Agric. Sci. Procedia* **2015**, *4*, 88–98. [CrossRef]
58. Huang, S.; Wortmann, M.; Duethmann, D.; Menz, C.; Shi, F.; Zhao, C.; Su, B.; Krysanova, V. Adaptation Strategies of Agriculture and Water Management to Climate Change in the Upper Tarim River Basin, NW China. *Agric. Water Manag.* **2018**, *203*, 207–224. [CrossRef]
59. Ramos, T.B.; Darouich, H.; Oliveira, A.R.; Farzamian, M.; Monteiro, T.; Castanheira, N.; Paz, A.; Alexandre, C.; Gonçalves, M.C.; Pereira, L.S. Water Use, Soil Water Balance and Soil Salinization Risks of Mediterranean Tree Orchards in Southern Portugal under Current Climate Variability: Issues for Salinity Control and Irrigation Management. *Agric. Water Manag.* **2023**, *283*, 108319. [CrossRef]
60. Jolly, I.D.; McEwan, K.L.; Holland, K.L. A Review of Groundwater–Surface Water Interactions in Arid/Semi-Arid Wetlands and the Consequences of Salinity for Wetland Ecology. *Ecohydrology* **2008**, *1*, 43–58. [CrossRef]
61. Weil, R.R.; Brady, N.C. *The Nature and Properties of Soils*, 15th ed.; Pearson: Columbus, OH, USA, 2016; ISBN 978-0-13-325448-8.
62. Corwin, D.L.; Rhoades, J.D.; Šimůnek, J. Leaching Requirement for Soil Salinity Control: Steady-State versus Transient Models. *Agric. Water Manag.* **2007**, *90*, 165–180. [CrossRef]
63. Wallender, W.W.; Tanji, K.K. *Agricultural Salinity Assessment and Management*, 2nd ed.; American Society of Civil Engineers: Reston, VA, USA, 2011; ISBN 978-0-7844-1169-8.

64. Hanson, B.R.; Grattan, S.R.; Fulton, A. Agricultural Salinity and Drainage. In *Water Management Series Publication*; University of California Irrigation Program: Davis, CA, USA, 2006.
65. Minhas, P.S.; Ramos, T.B.; Ben-Gal, A.; Pereira, L.S. Coping with Salinity in Irrigated Agriculture: Crop Evapotranspiration and Water Management Issues. *Agric. Water Manag.* **2020**, *227*, 105832. [CrossRef]
66. Machado, R.; Serralheiro, R. Soil Salinity: Effect on Vegetable Crop Growth. Management Practices to Prevent and Mitigate Soil Salinization. *Horticulturae* **2017**, *3*, 30. [CrossRef]
67. Tanji, K.K.; Kielen, N.C. *Agricultural Drainage Water Management in Arid and Semi-Arid Areas*; FAO Irrigation and Drainage Paper; Food and Agriculture Organization of the United Nations: Rome, Italy, 2002; ISBN 978-92-5-104839-9.
68. O'Shaughnessy, S.; Evett, S.; Colaizzi, P.; Andrade, M.; Marek, T.; Heeren, D.; Lamm; LaRue, J. Identifying Advantages and Disadvantages of Variable Rate Irrigation: An Updated Review. *Appl. Eng. Agric.* **2019**, *35*, 837–852. [CrossRef]

Disclaimer/Publisher's Note: The statements, opinions and data contained in all publications are solely those of the individual author(s) and contributor(s) and not of MDPI and/or the editor(s). MDPI and/or the editor(s) disclaim responsibility for any injury to people or property resulting from any ideas, methods, instructions or products referred to in the content.

MDPI AG
Grosspeteranlage 5
4052 Basel
Switzerland
Tel.: +41 61 683 77 34

Water Editorial Office
E-mail: water@mdpi.com
www.mdpi.com/journal/water



Disclaimer/Publisher's Note: The title and front matter of this reprint are at the discretion of the Guest Editors. The publisher is not responsible for their content or any associated concerns. The statements, opinions and data contained in all individual articles are solely those of the individual Editors and contributors and not of MDPI. MDPI disclaims responsibility for any injury to people or property resulting from any ideas, methods, instructions or products referred to in the content.





Academic Open
Access Publishing

mdpi.com

ISBN 978-3-7258-7371-5